National Library of Canada
Acquisitions and Bibliographic Services Branch
395 Wellington Street
Ottawa, Ontario
K1A 0N4

Bibliothèque nationale du Canada
Direction des acquisitions et des services bibliographiques
395, rue Wellington
Ottawa (Ontario)
K1A 0N4

NOTICE

The quality of this microform is heavily dependent upon the quality of the original thesis submitted for microfilming. Every effort has been made to ensure the highest quality of reproduction possible.

If pages are missing, contact the university which granted the degree.

Some pages may have indistinct print especially if the original pages were typed with a poor typewriter ribbon or if the university sent us an inferior photocopy.

Reproduction in full or in part of this microform is governed by the Canadian Copyright Act, R.S.C. 1970, c. C-30, and subsequent amendments.

AVIS

La qualité de cette microforme dépend grandement de la qualité de la thèse soumise au microfilmage. Nous avons tout fait pour assurer une qualité supérieure de reproduction.

S'il manque des pages, veuillez communiquer avec l'université qui a conféré le grade.

La qualité d'impression de certaines pages peut laisser à désirer, surtout si les pages originales ont été dactylographiées à l'aide d'un ruban usé ou si l'université nous a fait parvenir une photocopie de qualité inférieure.

La reproduction, même partielle, de cette microforme est soumise à la Loi canadienne sur le droit d'auteur, SRC 1970, c. C-30, et ses amendements subséquents.

Canada

CONCRETE PROPERTIES AND THERMAL STRESS ANALYSIS OF MEMBERS AT EARLY AGES

by

Arshad A. Khan

July 1995

Department of Civil Engineering and Applied Mechanics
McGill University
Montreal, Canada

A thesis submitted to the
Faculty of Graduate Studies and Research
in partial fulfilment of the requirements for the degree of
Doctor of Philosophy

©Arshad A. Khan, 1995

National Library of Canada
Acquisitions and Bibliographic Services Branch
395 Wellington Street
Ottawa, Ontario
K1A 0N4

Bibliothèque nationale du Canada
Direction des acquisitions et des services bibliographiques
395, rue Wellington
Ottawa (Ontario)
K1A 0N4

Your file Votre référence

Our file Notre référence

The author has granted an irrevocable non-exclusive licence allowing the National Library of Canada to reproduce, loan, distribute or sell copies of his/her thesis by any means and in any form or format, making this thesis available to interested persons.

L'auteur a accordé une licence irrévocable et non exclusive permettant à la Bibliothèque nationale du Canada de reproduire, prêter, distribuer ou vendre des copies de sa thèse de quelque manière et sous quelque forme que ce soit pour mettre des exemplaires de cette thèse à la disposition des personnes intéressées.

The author retains ownership of the copyright in his/her thesis. Neither the thesis nor substantial extracts from it may be printed or otherwise reproduced without his/her permission.

L'auteur conserve la propriété du droit d'auteur qui protège sa thèse. Ni la thèse ni des extraits substantiels de celle-ci ne doivent être imprimés ou autrement reproduits sans son autorisation.

ISBN 0-612-08120-6

Canada

In the name of God, the beneficent, the merciful

To my parents

Abstract

This research program presents an experimental study on the mechanical and thermal properties of different types of concretes at very early ages (i.e., during hydration). These properties are investigated for temperature-matched curing, sealed curing and air-dried curing. Three types of concretes are studied including normal-strength (30 MPa), medium-strength (70 MPa) and high-strength (100 MPa) concretes. About 300 cylinders and 175 flexural beams were tested to determine the early-age mechanical properties including compressive stress-strain responses, gain of compressive strength, change in elastic modulus and variation of tensile strength. Creep frames and measuring devices were built to enable the experimental determination of early-age creep, with unloaded, companion specimens giving the corresponding shrinkage strains. A temperature-matched curing bath was developed to measure the heat of hydration and to subject 15 cylinders and 12 flexural beams to temperature-matched curing. The thermal properties investigated included the heat of hydration, the thermal conductivity, the specific heat and the coefficient of thermal expansion. Expressions are proposed to predict the development of compressive strength, elastic modulus and modulus of rupture as a function of the type of concrete and the type of curing.

Sub-routines were developed for a finite element thermal analysis program "DETECT" to predict the variation of temperatures during hydration. Additional sub-routines, using the maturity concept, predicted the compressive strength, elastic modulus and tensile strength of each element, in the time domain. An experimental study was performed to observe the effect of different curing conditions and early-form stripping on the temperature and strain development in structural concrete members. Comparisons are made between the measured and predicted temperatures in large concrete columns and precast tee beams and slabs.

Sub-routines were developed to enable incremental stress analysis in the time domain to account for the rapidly changing material properties and the influence of creep. Predictions of the risk of cracking were made and compared with observations from experiments on concrete elements during hydration. Parametric analyses were carried out to determine the influence of key thermal properties, time of formwork removal, creep, and concrete strength on the thermal gradients developed and the risk of thermal cracking.

Résumé

L'auteur présente les résultats d'une recherche expérimentale sur les propriétés thermiques et mécaniques de différents types de bétons de ciment en phase d'hydratation. L'étude couvre les conditions de mûrissement adiabatiques, sous protection scellée et à l'air ambiant, et ce pour trois catégories de résistance du béton: normale (30 MPa), moyenne (70 MPa) et haute résistance (100 MPa). Environ 300 cylindres et 175 poutres de flexion ont été soumis à des essais mécaniques afin de déterminer leur comportement contrainte-déformation en compression, leur gain de résistance en compression, ainsi que la variation du module d'élasticité et de la résistance en traction. Des instruments de mesure et appareils de fluage ont été spécialement conçus pour évaluer le fluage d'échantillons en phase de mûrissement; des échantillons de référence, non chargés, ont permis d'évaluer les déformations de retrait correspondantes. Une cuve à mûrissement adiabatique à été mise au point pour mesurer la chaleur d'hydratation dégagée lors du mûrissement, pouvant accommoder 15 cylindres et 12 poutres de flexion. Les propriétés thermiques étudiées sont la chaleur d'hydratation, la conductivité thermique, la chaleur spécifique et le coefficient d'expansion thermique linéaire. L'auteur propose des expressions pour prédire l'évolution de la résistance en compression, du module d'élasticité et du module de rupture en fonction du type de béton et de la méthode de mûrissement.

En parallèle avec les études expérimentales, l'auteur a programmé des sous-routines pour un progamme d'analyse thermique par éléments finis (DETECT) afin de pouvoir prédire la variation de température dans les spécimens durant l'hydratation. D'autres sous-routines, basées sur le concept de maturité du béton, ont été développées afin de prédire l'évolution dans le temps de la résistance en compression, du module d'élasticité et de la résistance en traction. Une étude expérimentale a également été faite pour observer l'effet de différentes conditions de mûrissement et du décoffrage hâtif sur la température et les déformations dans des membrures de béton de formes (colonnes de section carrée, poutres en Té préfabriquées et dalles) et dimensions variées. Les températures mesurées ont été comparées aux prédictions du modèle numérique.

D'autres sous-routines numériques ont été développées pour permettre une analyse incrémentale des contraintes dans le temps qui tienne compte des changements rapides dans les propriétés du matériau et l'influence de fluage. Ces

calculs ont permis d'établir un indice de prédiction du risque de fissuration des spécimens mis à l'essai et de comparer ces prédictions aux résultats observés. Des analyses paramétriques avec ce modèle numérique ont permis de déterminer l'influence des propriétés thermiques importantes, du délai de décoffrage, du fluage et de la résistance du béton sur les gradients thermiques induits et le risque de fissuration qui en découle.

Acknowledgements

The author would like to express his deepest gratitude to a friend and an excellent teacher, Professor Denis Mitchell, for his continual guidance and encouragement throughout this research project. The author will remember, with pleasure, the enjoyable discussions he had with Professor Denis Mitchell during the completion of this thesis.

The author is also greatly indebted to Dr. William D. Cook for his variety of technical guidance, computer programming advice and for scientific discussions we had throughout this research project.

The assistance provided by Dr. James J. Beaudoin, Director of Construction, National Research Council, is greatly appreciated for providing the access to the laboratory facilities.

Thanks are extended to the Jamieson Structures Laboratory staff, John Bartczak, Marek Przykorski, Ron Sheppard and Damon Kiperchuk for their assistance in constructing the test setup and casting the specimens. The author also extends his thanks to Norris Lam, Homayoun H. Abrishami, Andrew Griezic, Philip E. Zeyl, Marco Di Franco, Mohammad Amjad, and to all those who encouraged and helped, in some way, during this project. The french translation of the abstract by Prof. G. McClure is greatly appreciated.

The donations of materials by Francon-Lafarge and St. Lawrence Cement are gratefully acknowledged.

The financial support provided by the Networks of Centres of Excellence Program funded by the Minister of State, Science and Technology in Canada is highly appreciated.

The author is grateful to his family, especially to his parents, for their invaluable encouragement and love without which the completion of this project would not have been possible.

Arshad A. Khan

Table of Contents

List of Figures

List of Tables

List of Symbols

$Q(t)$	= rate of heat of hydration of cement
$Q_i(t)$	= rate of heat of hydration of component "i"
w_i	= weight proportion of component "i"
i	= variable
T	= concrete temperature in °C
H(T)	= temperature function
$g(\alpha)$	= function of the degree of hydration
f(T(t))	= function of temperature, T, at time t
t_e	= equivalent age or maturity
E	= activation energy parameter
R	= gas constant
f'_c	= concrete compressive strength
E_c	= elastic modulus of concrete
w	= unit weight of concrete
γ_c	= density of concrete
α_c	= coefficient of thermal expansion
ϵ_{cth}	= unrestrained thermal strain
ΔT	= temperature change in °C
t_r	= retardation period in days
A	= a constant
$f'_c(t)$	= concrete compressive strength at time t
$E_c(t)$	= elastic modulus of concrete at time t
$f'_r(t)$	= modulus of rupture at time t
K	= a constant
ϵ_c	= total strain
ϵ_{co}	= instantaneous strain
ϵ_{creep}	= creep strain
ϵ_{sh}	= shrinkage strain
ϵ_{th}	= thermal strain

Q = heat generation rate within the body

ρ = density of concrete

λ = thermal conductivity of concrete

c = specific heat of concrete

t = time

C_α = calibration coefficient

C_β = temperature correction coefficient

ϵ_m = measured strain

t_o = age at loading in hours

t_s = age at demolding in hours

f_{co} = applied stress at t_o

f'_{co} = compressive strength at t_o

ϵ_{co} = elastic concrete strain at t_o

t_f = age at the end of test in hours

ϵ_c = total concrete strain

ϕ = creep coefficient

J = creep function at t_f

ϵ_{cf} = strain causing stress in concrete

f_c = stress in concrete

$J(t,t_o)$ = creep function representing the total stress dependent strain per unit applied stress

$E_{c,eff}$ = effective elastic modulus

ΔQ = incremental heat generated

Chapter 1

Introduction

The purpose of the research reported in this thesis is to investigate the key parameters necessary for predicting temperatures and stresses that develop in concrete structures during hydration. In order to predict these temperatures and stresses during the hydration period, an extensive experimental study was carried out to determine the thermal and mechanical properties of normal, medium and high-strength concretes at early ages. Experimental studies were also conducted to measure the developing temperatures and stresses during hydration in concrete members having different shapes and sizes. In addition, transient thermal and stress analyses were carried out to predict the temperatures and stresses as developed in concrete members at early ages.

This chapter outlines the need for the research, presents an overview of the research objectives and summarizes the organization of this thesis.

1.1 An Overview of Research Needs

The prevention and control of early-age thermal cracking of concrete is a major concern since it significantly affects the durability of structures. As early as the 1930's, considerable attention was focused on this problem during the construction of concrete dams in North America (ACI Committee 207 (1970), Bamforth (1985), Price (1982)). Various steps have been taken to minimise the problem of early age thermal cracking. These include the replacement of water with crushed ice, the use of liquid nitrogen for cooling, the development of low heat of hydration cement and early form stripping to reduce the temperature rise and the thermal gradient. Inspite of all of these preventive measures, thermal cracking remains a significant problem to overcome. Early age thermal cracking is not only associated with massive structural components, but can be significant for members such as T-shaped elements

with very thin flanges. Although there is a high rate of heat loss on the exposed surfaces of such members, resulting in reduced maximum temperatures, there can however be significant thermal gradients. This, together with the differential shrinkage on the exposed surface may aggravate the problem and can lead to surface cracking.

In the past few years, there has been a revolution in the development and use of high-strength concrete in the concrete industry. This increased use of high-strength concrete has raised a number of questions whether or not cracking will occur at early ages due to the different characteristics of this material. The use of higher-strength concrete results in increased hydration temperatures and the potential for large thermal gradients. It is interesting to note that the precast concrete industry has experienced problems with early age cracking in high-strength concrete members during early form removal. This problem can be aggravated by thermal shock and by adverse moisture effects upon stripping.

In order to predict stresses induced during hydration, it is necessary to investigate the variations of the important physical properties of different types of concrete. Because of the special characteristics of high-strength concrete, such as higher hydration temperatures and more rapid gain in both strength and modulus, there are concerns that high-strength concrete may have significantly different behaviour from normal-strength concrete. Previous research has focused almost exclusively on the properties of more mature concrete. In the past few years, interest has developed in studying the very early age behaviour of concrete due to increased use of fast-track construction. Limited information is available on properties of concrete at very early age, that is, less than 48 hours. Researchers (Byfors (1980), Lew and Reichard (1978), Oluokun et al (1991)) have studied some of the early-age properties of normal-strength concrete, including the variations in compressive strength, tensile strength and modulus of elasticity. However, information on early age creep and shrinkage of normal-strength concrete is extremely limited (Byfors (1980)). Experimental studies on the early-age properties of high-strength concrete have been carried out by LaPlante (1993). To the author's knowledge, apart from the work reported by LaPlante (1993), no other experimental studies have been done on the creep and shrinkage of high-strength concrete at very early ages.

The development of temperature with time during hydration is the most important parameter influencing the compressive strength, the elastic modulus, creep, shrinkage and the rate of hydration reaction. Temperature gradients can cause restraint stresses in hydrating

concrete which may lead to cracking of the concrete. The variation of temperature in concrete members during hydration is significant due to a number of influencing factors, such as the type and amount of cement, the member size and shape, the use of mineral admixtures, etc. In practice, temperature and curing at early ages is a key factor to both designers and contractors since it influences the speed of construction and in precast concrete the time at prestress release.

There is a need to carry out a systematic experimental program to determine the very early age properties and behaviour of different types of concretes. These properties will be helpful in predicting the temperatures and stress gradients in concrete members. Furthermore, there is a need to develop means of predicting the development of temperatures and the resulting stresses in the hydrating concrete. This is needed to assess the risk of cracking in concrete members during the hydration process.

1.2 Research Objectives

The primary objectives of this research program are:

i. To study the mechanical properties of three different types of concretes at very early ages. The experimental studies include determining the compressive stress-strain relationships, the tensile strength, the elastic modulus, creep and shrinkage at ages less than 24 hours up to 28 days. All of these properties are investigated for normal, medium and high-strength concretes subjected to different curing conditions. New testing techniques need to be developed to study some of these properties at very early ages.

ii. To study the thermal properties of three different types of concretes. Thermal properties include heat of hydration, thermal conductivity, specific heat and coefficient of thermal expansion of normal, medium and high-strength concretes at very early ages. To study the heat of hydration of concrete at early ages and to provide sufficient number of test samples subjected to adiabatic condition, an experimental testing set up needs to be developed.

iii. To develop expressions capable of predicting the development of key mechanical properties of concretes due to different curing conditions.

iv. To study the effect of curing on the temperature and stress development in different shapes and sizes of concrete members during the early period of

hydration.

v. To develop sub-routines for a two-dimensional thermal analysis program to take account of the effect of "maturity" during the hydration period and to compare predicted temperatures with temperatures measured inside structural members during hydration.

vi. To develop sub-routines for stress analysis program to take account of the changing elastic modulus and the influence of early age creep and shrinkage effects. Predicted tensile stresses need to be compared with the predicted tensile strength of the concrete in order to assess the potential of early age cracking in concrete members.

vii. To perform a parametric study to investigate the effect of different parameters on temperature development and to investigate the risk of cracking.

1.3 Organization of the Thesis

Chapter 2 will present an overview of previous research on the early age properties of different concretes. Chapter 3 describes the experimental program for determining the thermal properties of normal, medium and high-strength concretes. Chapter 4 describes the investigation carried out on the mechanical properties of normal, medium and high-strength concretes. This Chapter also includes the development of mathematical expressions describing the early age responses of different types of concretes. Chapter 5 describes the modifications made to a two-dimensional finite element program and compares the predicted time-wise temperature variations with those measured in different sizes and shapes of members subjected to different boundary conditions. Chapter 6 explains the computer analysis technique used to predict incremental stresses in the time domain for determining the risk of cracking. This approach was applied to several practical cases. Chapter 7 presents the conclusions arising from this research program.

Chapter 2

Previous Research on Thermal and Mechanical Properties of Concrete

This chapter summarizes previous research on thermal and mechanical properties of concrete. These properties are needed to predict the temperatures and the resulting induced stresses due to heat of hydration. Attention will be focused on the properties at early ages for different types of concrete. The following thermal properties of concrete are described in this chapter:

- Heat of Hydration
- Thermal Conductivity
- Specific Heat
- Thermal Diffusivity
- Coefficient of Thermal Expansion

In addition, the following mechanical properties of concrete, which are important in this research program, are discussed in this chapter:

- Compressive Stress-Strain Relationship
- Compressive Strength variation with age
- Tensile Strength Variation with age
- Modulus of Elasticity
- Shrinkage
- Creep
- Poisson's ratio

2.1 Thermal Properties of Concrete

2.1.1 Heat of Hydration

The chemical reaction between cement clinker components and water results in the formation of different hydration reaction products. The clinker components have different rates of hydration reaction with water and form products with different chemical compositions. These clinker components also bind varying amounts of water chemically and their contribution to the development of heat and strength vary in magnitude. The clinker components included in portland cement are C_3S, C_2S, C_3A, C_4AF. Their contribution to the development of heat and strength is shown in Table 2.1 (Rasmussen and Andersen (1989)) and Fig 2.1 (Byfors (1980), Bogue (1947)).

It was reported by Jawed et al (1983) that the heat of hydration of cement can be found from its major clinker components. The rate of heat of hydration, at any instant, can be obtained by summing the weighted rate of each of the components.

$$Q(t)=\sum_{i=1}^{n} w_i Q_i(t) \qquad (2.1)$$

where

$Q(t)$ = rate of heat of hydration of cement

$Q_i(t)$ = rate of heat of hydration of component "i"

w_i = weight proportion of component "i"

i = different components

For practical use and ease, it is recommended to use a single heat of hydration curve in which all the cement compositions are considered.

The chemical reaction between cement and water is highly exothermic, releasing a total amount of heat up to 150 to 350 joules per gram for ordinary portland cement (De Larrard et al (1994)). A number of factors can influence the rate and total heat of hydration of cement. The most influencing factors are:

i. Type and source of cement

ii. Total cement content

iii. Temperature

iv. Admixture

The extent to which hydration of cement paste heats the concrete depends on the size of the structural element and its environment. Heat dissipation depends on the type of formwork, amount of exposed surface area and the ambient temperature at various exposed surfaces. Because of the lower conductivity of concrete, there will be a slower rate of heat exchange between the concrete and its surroundings. Most often at early ages, heat is liberated in concrete at a higher rate than is transmitted to its surrounding, which could result in a substantial temperature rise at the centre of the concrete (Bamforth(1982), Aitcin et al (1988), Mehta and Monteiro (1993), Mukherjee and Thomas (1993), Ryell and Fasullo (1993)).

Heat of hydration of concrete can be measured by three distinct methods as explained below:

(a) Conduction Calorimeter

In this method, a small sample of cement paste is kept under isothermic conditions, that is, at constant temperature condition and the heat developed can then be determined. This method is preferable in determining the heat of hydration at very early ages, even less than 0.5 hours as reported by Danielsson (1966). One of the advantages is that it can directly measure the rate of heat of hydration at different temperatures. However, the sample size is too small to accurately achieve realistic and repeatable results.

(b) Heat of Solution Method

In this method, the heat of hydration is determined by the difference between the heat of solution of unhydrated and hydrated cement paste in acid. This method is best suited for later ages when a large amount of heat has been liberated.

(c) Adiabatic Method

The adiabatic method measures the temperature rise under perfectly insulated conditions, that is, no heat exchange occurs between the concrete sample and its surroundings. This method permits the use of a larger sample of concrete or cement paste resulting in more realistic temperatures. The adiabatic conditions simulate the curing conditions at the centre of a large mass of concrete at early ages. In order to

predict the temperature distributions in structures during hydration, this method is preferred due to its ease of measurement. The rate of heat of hydration can be obtained from the product of specific heat, density of the concrete and the rate of change of the measured adiabatic temperature curve. Some researchers have attempted to create an "adiabatic condition" by placing the concrete specimen in an insulated box. This however results in a lower rate of hydration and a lower peak temperature due to heat loss. A test setup was designed and constructed in this research program (see Chapter 3) to create adiabatic conditions for normal, medium and high-strength concretes.

2.1.2 Concept of Maturity Functions and Equivalent Age

It is well known that the rate of the hydration reaction increases with increasing temperature during hydration. This effect has a significant influence on the material properties. It has been reported by Regourd and Gautier (1980) that the rate of hydration depends on the amount of heat already developed and the current temperature. The term "maturity" or "equivalent age" is typically used to account for the combined effect of both time and temperature (Nurse (1949). The combined effect of time and temperature, including the history of temperature development, is represented by so-called maturity functions. A number of maturity functions have been proposed in the literature and are well documented by Byfors (1980). The most commonly used maturity functions are reviewed below:

(a) Nurse-Saul Temperature Function

A temperature of -10°C is widely used as a datum temperature below which there is no hydration (Byfors (1980)). In 1949, Nurse found that there exists a proportionality between the rate of heat of hydration and temperature and he assumed that hydration ceases at 0°C. In 1953, Bergstrom proposed a temperature function, H(T), based on the experimental data that hydration ceases at about -10°C, and proposed a temperature function in the following form:

$$H(T) = \frac{T+10}{20+10} \qquad (2.2)$$

where T is the concrete temperature in °C. This function gained wide spread use and was adopted in the CEB-FIP Code (1978). It has been pointed out by Byfors (1980) and Naik (1985) that this function does not fit the experimental data for very early age concrete (i.e., at lower temperatures).

(b) Rastrup Temperature Function

In 1954, Rastrup proposed a temperature function which assumes that the rate of chemical reaction doubles for each 10°C increase in temperature. This is expressed as:

$$H(T) = 2^{\left(\frac{T-20}{10}\right)} \qquad (2.3)$$

where T is the temperature in °C. This function is suitable for temperatures below 40 °C since it increases too rapidly for higher temperatures (Neville (1981)).

(c) Arrhenius' Maturity Function

The most commonly accepted maturity function is the one described by Freiesleben Hansen and Pedersen (1977), based on the Arrhenius equation for thermal activation in chemical reactions. The degree of hydration, α, is defined as the ratio between the quantity of heat developed to the quantity of heat developed at complete hydration and hence ranges from 0 to 1. The rate of hydration is expressed as:

$$F = \frac{d\alpha}{dt} \qquad (2.4)$$

Freiesleben Hansen and Pedersen (1977) expressed the rate of hydration, F, for a given cement paste at a given degree of hydration as:

$$F = \frac{d\alpha}{dt} = g(\alpha) \times f(T) \qquad (2.5)$$

where $g(\alpha)$ is a function of the degree of hydration and f(T) is a function of T at time

t. Thus, by separation of variables and integration:

$$\int_0^{\alpha} \frac{1}{g(\alpha)}\, d\alpha = G(\alpha) = \int_0^{\tau} f(T(t))\, dt \qquad (2.6)$$

The function f(T(t)) in Eq. 2.6 is often normalized with the value of the function at a reference temperature, T_o, as given by:

$$H_o = \frac{f(T(t))}{f(T_o)} \qquad (2.7)$$

where the function H_o is the temperature function. If the curing temperature development, T(t), is compared with a process occurring at a constant reference temperature, T_o, (normally 20°C) at the same degree of hydration, then $G(\alpha)$ is the same for both processes and can be written as:

$$G(\alpha) = \int_0^{\tau} f(T(t))\, dt = \int_0^{\tau_o} f(T_o)\, d\tau = f(T_o)\, \tau_o \qquad (2.8)$$

The maturity or equivalent age, t_e, at time $t = \tau$, is defined as:

$$t_e = \int_0^{\tau} \frac{f(T(t))}{f(T_o)}\, dt = \int_0^{\tau} H_o(T)\, dt \qquad (2.9)$$

For example, a maturity of 48 hours means that the concrete has reached a degree of hydration corresponding to 48 hours of curing at the reference temperature, usually taken as 20°C. Studies carried out by several researchers (Regourd and Gautier (1980), Byfors (1980), Carino (1982)) on strength development and heat of hydration of ordinary portland cement have verified the accuracy of Arrhenius' function. This function has been adopted by the CEB-FIP Code (1990) and is used in this study to account for temperatures at early ages. The function proposed by Freiesleben Hansen and Pedersen (1977), based on Arrhenius' approach, is of the following form:

$$f(T) = \exp\left[-\frac{E}{R\, T_K}\right] \qquad (2.10)$$

where

E = Activation energy parameter

T_K = Temperature of concrete in °K

R = Gas constant, 8.314 kJ/mol-°K

Arrhenius' equation is applicable for temperatures ranging from -10 to 80°C. Using Equation (2.10) and a reference temperature of 20°C, the maturity function, H(T) can be written as:

$$H(T) = \exp\left[\frac{E}{R}\left[\frac{1}{293} - \frac{1}{T+273}\right]\right] \qquad (2.11)$$

The energy activation parameter, E, depends on the chemical composition of the cement. Since the hydration reaction between cement and water involves different chemical reactions taking place simultaneously, it is difficult to determine E experimentally. Feiesleben Hansen and Pedersen (1977) have expressed the activation energy in the following form:

$$E(T) = 33.5 \text{ kJ/mol for } T \geq 20°C$$

$$E(T) = 33.5 + 1.47(20 - T) \text{ for } T < 20°C$$

In the CEB-FIP Code (1990), an average E value was chosen as 33 kJ/mol for temperature ranges from 0 to 80°C, for simplicity. For example, if the activation energy is 33.5 kJ/mol and the reference temperature is 20°C. The temperature function (Eq. (2.11)) at 25°C is:

$$H(25°C) = \exp[33500/8.314(1/293 - 1/298)] = 1.26$$

This means that the rate of hardening at a temperature of 25°C is 1.26 times that at 20°C. Therefore, a given concrete mix cured at 25°C for 1 day has the same maturity as that cured at 20°C for 1.26 days.

2.1.3 Application of "Equivalent Age" or "Maturity" of Concrete

The development of the strength of concrete with age, under different curing temperatures, has been investigated by several researchers (Byfors (1980), Carino (1982), Malhotra (1974)). The effect of varying temperatures and age has been described in terms of an "equivalent" or "mature" age, t_e, defined as;

$$t_e = \int_0^t H(T(t))\,dt \qquad (2.12)$$

Using the Arrhenius maturity function, this becomes

$$t_e = \int_o^t \exp\left\{\frac{E}{R}\left\{\frac{1}{293} - \frac{1}{T+273}\right\}\right\} dt \qquad (2.13)$$

During hydration, the temperature typically varies significantly in the concrete, being warmer at the centre of the concrete section. This results in a variation of the concrete temperature across the concrete section. Hence regions near the centre of the section will gain strength more quickly than regions near the surface. In order to predict the strength development with age, it is important to keep track of the temperature history of each element within the concrete section. The maturity or equivalent age concept, which conveniently accounts for temperature history, can be used to express the variations of the concrete material properties (i.e., compressive strength, modulus of elasticity, tensile strength, etc.) with time in each element. Figure 2.2a shows the compressive strength gain of 100 x 100 x 400 mm prisms, made with the same concrete (water/cement ratio of 0.58) but moist cured at different curing temperatures. It can be seen from this figure that different initial curing temperatures have resulted in different rates of strength gain. Figure 2.2b shows the variation of compressive strength versus the mature age calculated by Arrhenius' function for maturity. As can be seen the use of mature age can account for widely varying temperature effects, enabling the compressive strength gain to be described by a single time function.

2.1.4 Thermal Conductivity of Concrete

The thermal conductivity of concrete is one of the key parameters needed to predict the temperature variations in concrete. Concrete is a composition of different components which have very different thermal conductivity values. Very limited information is available on thermal conductivity of concrete at very early ages, and in particular no data is available on the conductivity of high-strength concrete. The different concrete components, given in decreasing order of conductivity (Neville (1981)) are:

i. Aggregate
ii. Cement paste
iii. Water
iv. Air

ACI Committee 211 (1988) reported that the thermal conductivity varies with the density of concrete, with heavier aggregates resulting in higher thermal conductivity. Since the thermal conductivity of water and air are quite different than that of the hydration product, it is expected that the thermal conductivity will change during the early period of hydration. The mineralogical composition of aggregates affect the thermal conductivity to a great extent as reported by the RILEM Technical Committee No. 42 (1981). The moisture content of the concrete strongly influences the conductivity at very early ages, because water has a lower conductivity than the aggregates, which occupy about 70% of the volume of concrete. The lower water-cement ratio and denser cement matrix in high-strength concrete could result in higher thermal conductivity than that measured in lower strength concrete. There are very few experimental methods available to measure the conductivity of fresh concrete. Contradictory results are available on the thermal conductivity of concrete at early ages (Brown and Javaid (1970), RILEM Committee No. 42 (1981), and Byfors (1980)). Brown and Javaid (1970) studied the thermal conductivity of very early age concrete, that is, from 6 hours to 7 days. For this concrete with a water-cement ratio of 0.65, the thermal conductivity varied from 2.176 W/m-°C at 6 hours to 1.515 W/m-°C at 7 days, thus resulted in a drop of 30% from its initial value during this period. Over this period, the moisture content varied from 9.3% to 1.5% and the density of the concrete varied from 2334 kg/m^3 to 2170 kg/m^3. This significant drop in moisture content would likely result in a drop of conductivity. Lofqvist (1946) did not observe any influence of age on thermal conductivity after an age of 24 hours. Byfors (1980) and RILEM Committee No. 42 (1981) concluded that there was no significant change in conductivity with age. In order to study this important parameter, thermal conductivities of different concretes were measured at very early ages, as well as for mature concrete. These results are presented in Chapter 3.

2.1.5 Specific Heat of Concrete

Specific heat is defined as the amount of heat energy required to raise the temperature of a unit mass of a material by one degree. The specific heat of concrete depends on its constituents. It is a function of the concrete composition and the type of aggregates used, but is not significantly effected by the mineralogical character of

the aggregates. Unhydrated cement and most aggregates have specific heat values of about 0.8 kJ/kg-°C, while the specific heat of water is about 5 times higher (i.e., 4.2 kJ/kg-°C). This means an increase in moisture content will increase the specific heat of concrete. Brown and Javaid (1970) reported that the specific heat for normal-strength concrete (water-cement ratio of 0.65) varied from 1.15 to 0.89 kJ/kg-°C at ages varying from 6 hours to 7 days, respectively. A significant drop of moisture content was also observed during this period which probably resulted in reducing the specific heat. Tests done by Lofqvist (1946) on cement mortar at ages from 3 days to 30 days with a water-cement ratio of 0.55 showed almost no influence of age on the specific heat. Hansen et al (1982) reported a decrease in specific heat of about 15% from a few hours after casting to an age of 5 days. These tests were conducted on rapid hardening portland cement paste with a water-cement ratio of 0.50, at a temperature of 30°C. RILEM Committee No. 42 (1981) and Mindess and Young (1981) reported results on thermal conductivity and specific heat of relatively mature concrete. They found that specific heat varies only 8% for different types of aggregates. An increase in water content from 4 to 8% resulted in a 12% increase in specific heat, while an increase in temperature from 10 to 65°C resulted in increases in specific heat of 24%. Generally, the specific heat of normal strength, mature, concrete varies from 0.8 to 1.2 kJ/kg-°C (Mindess and Young (1981)). No test data was found in the literature on the specific heat of high-strength concrete.

2.1.6 Thermal Diffusivity of Concrete

The thermal diffusivity of concrete is defined as the ratio of thermal conductivity to the product of density and specific heat of concrete, that is, $\lambda/\rho c$. ACI Committee 207 (1992) has reported the diffusivity values for different types of aggregates used in normal-strength concrete mixes.

2.1.7 Coefficient of Thermal Expansion

Factors influencing the coefficient of thermal expansion such as the type and amount of cement, type of aggregate, water-cement ratio, age and temperature have been discussed by many researchers. The cement paste of normal concrete usually has a higher coefficient of thermal expansion than the aggregate, but the aggregate has

a dominant effect because of its large volume in concrete mix (normally 70 to 80%). The coefficient of thermal expansion of concrete is approximately equal to the volumetrically weighted average of the coefficients of its ingredients (Walker et al (1952), Mitchell (1953)). Lofqvist (1946) studied the effect of heating and cooling cycles on the coefficient of thermal change (i.e., expansion during heating and contraction during cooling). They observed a linear relationship between the temperature and the coefficient of thermal change. It was reported that the coefficient of thermal expansion is slightly greater during heating than during the cooling cycle. Alexander (1972), Weigler and Karl (1974), Meyers (1950) and Miao et al (1993) observed significant age dependency of the coefficient of thermal expansion during the first few hours after casting. Miao et al (1993) reported a coefficient of thermal expansion of about 24 x 10^{-6}/°C at 7 hours after casting (water-cement ratio of 0.28, Dolomite limestone aggregates and 28 day compressive strength of 73 MPa) which stabilized to 10 x 10^{-6} at 13 hours after casting. According to ACI Committee 517 (1988) the coefficient of thermal expansion of fresh concrete is several times higher than that of hardened concrete. It decreases sharply during the first ten hours of hydration and then remains constant. At ages greater than 1 day, no effect of age on the coefficient of thermal expansion has been observed. An average value of the coefficient of thermal expansion of normal weight concrete varied from 7 x 10^{-6} to 14 x 10^{-6} depending on the type of aggregates used. It must be pointed out that the same type of aggregate from different sources may have different coefficients of thermal expansion. This is probably due to the varying mineral compositions. If the aggregate type is not known, it is customary to use 10 x 10^{-6}/°C for hardened concrete (Collins and Mitchell (1991)). More information is required on the coefficient of thermal expansion for high-strength concrete.

2.2 Mechanical Properties of Concrete

2.2.1 Compressive Stress-Strain Relationships at Early Ages

Kasai (1961) and Byfors (1980) in studying the early age stress-strain relationships of normal-strength concrete described a significant change in shape of the concrete stress-strain curves a few hours after casting. It is reported that both the strength and the modulus of elasticity of concrete increase rapidly during the first few

hours after casting due to the rapid increase in the heat of hydration reaction. Byfors (1980) did not report the complete stress-strain responses and the tests were halted at the peak compressive strength values. Oluokun et al (1991) performed compressive strength tests on 152 x 304 mm cylinders for ages ranging from 6 hours to 28 days for normal and medium-strength concretes. However, no information on the complete stress-strain relationships of these concretes was given. There is a need to investigate the complete stress-strain relationships of medium and high-strength concretes at very early age.

2.2.2 Compressive Strength Variation with Age

Figure 2.3 shows the schematic representation of strength gain with age. This figure can be divided into four stages, that is, a setting age (fresh concrete), an early age stage, an intermediate stage and a hardened concrete stage. The setting age for normal strength concrete occurs within a few hours after casting. During the "early age" period, that is, in the first three days, there is a rapid gain in strength and stiffness. At 28 days, a greater percentage of the maximum strength attainable will be reached by normal-strength concrete than by high-strength concrete. High-strength concrete will continue to gain strength after this period.

Temperature influences the hydration process, and consequently the properties of the concrete, to a considerable extent. As discussed in Section 2.1.3, concrete compressive strength development can be expressed in terms of an equivalent age to account for the combined effects of temperature and age. A number of strength functions have been suggested by different researchers to describe the strength development, as a function of age or equivalent age (e.g., Cook et al (1992), Byfors (1980), CEB-FIP Code (1990)).

High initial curing temperatures at early ages can lead to lower strength in the hardened concrete, as mentioned by several researchers (Klieger (1958), Verbeck and Helmuth (1968), Alexanderson (1972), Byfors (1980), Kjellsen and Detwiler (1993)). Figure 2.4 shows the effect of curing temperatures on the 1 day and 28 day concrete compressive strengths (Byfors (1980)). These specimens were cured at constant temperatures for 1 day and 28 days. The 1 day compressive strength of concrete increases with an increase in temperature because higher curing temperatures result

in higher rates of hydration reaction at early ages. However, Byfors observed a drop in the 28 day concrete compressive strength with increasing temperatures of curing (see Fig. 2.4).

The gain in concrete compressive strength is also affected by the curing conditions. Aitcin et al (1994) investigated the effect of curing conditions (i.e., moist, sealed and air-dried curing) on the compressive strength gain for ages varying from one day to one year. It was found that water-cured cylinders gave higher compressive strengths than sealed cylinders, which in turn gave higher compressive strengths than air-cured cylinders.

Yuan et al (1991) studied the influence of high-strength concrete on the temperature development and in situ compressive strength in large concrete columns (1.8 x 1.8 x 1.8 m high). The compressive strengths obtained from the core samples were compared to the compressive strengths obtained from standard moist and air-cured cylinders. Temperature rises of 55 and 54°C were observed at the centre of the concrete columns, which were cast at initial concrete temperatures of 33 and 40°C, respectively. The concrete contained fly ash and had average 28 day compressive strengths, obtained from moist-cured 152 x 304 mm cylinders of 81 MPa and 83 MPa. It was concluded that the core compressive strengths are about 75% and 85% of the compressive strengths of moist-cured and field-cured cylinders, respectively.

Cook et al (1992) studied the influence of concrete strength on temperature rise and restraint stresses due to high thermal gradients during hydration in large plain concrete columns, 1 x 1 x 2 m high. Miao et al (1993) reported on the compressive strength of core cylinders taken from the same concrete columns. These core strengths were compared with water-cured and air-cured cylinders for three different concrete mixes. The measured core compressive strength was found to be between the water-cured and the air-cured cylinder strengths.

It has been reported by several researchers (Lessard et al (1993), Malhotra (1976), Blick (1973), Sigvaldason (1966), Werner (1958)) that the concrete compressive strength is greatly influenced by the following factors:

i. Stiffness of the testing apparatus
ii. Specimen size and shape
iii. Bearing block diameter

iv. Specimen end preparation

v. Effect of eccentricity between the testing machine and specimen axis

vi. Type of mold and curing conditions

Recently, Lessard et al (1993) studied the effects of the above mentioned parameters on the compressive strength of high-strength concrete. The study was conducted on 378 concrete cylinders having sizes of 150 x 300 mm and 100 x 200 mm. It has been reported that the compressive strength of the high-strength concrete decreases with the increase in size. The compressive strength of the normal and high-strength concretes was not affected by the eccentricity with respect to the vertical axis of testing machine provided that the eccentricity was kept below 6 mm for normal-strength concrete and below 4 mm for high-strength concrete. Lessard et al (1993) also reported that specimens having concrete compressive strengths above 100 MPa should have their ends ground to enable a more accurate determination of the compressive strength. For the CSA A23.1 Standard (1994), Bickley (1993) proposed that end grinding of specimens, made of high-strength concrete (i.e., 28 day compressive strength of 70 MPa or greater), be mandatory.

2.2.3 Tensile Strength Variation with Age

In order to asses the potential for cracking in concrete structures, it is vital to predict the tensile strength of the concrete. The tensile strength of concrete can be determined by three distinct methods, that is, the uniaxial tension test, the splitting tensile test and the modulus of rupture test. The uniaxial tension test (or direct tension test) is seldom carried out due to the difficulty involved in the test set-up.

A significant amount of experimental data is available on the tensile strength of normal-strength concrete at ages varying from 1 day to 28 days. However, there is not much data on the tensile strength of concrete at very early ages. A brief summary of the research carried out to determine the influence of concrete compressive strength and curing conditions on the tensile strength is given below.

Gonnerman and Shuman (1928) conducted a series of tests on 178 x 254 x 965 mm plain concrete beams with average compressive strengths varying from 6.9 MPa to 62 MPa. It was concluded that moist curing resulted in higher values of modulus of rupture than air-dried specimens.

Kaplan (1959) conducted an experimental study to determine the effects of the properties of 13 different types of coarse aggregates on the flexural and compressive strength of concrete. The 28-day concrete compressive strengths varied from 19.6 MPa to 79 MPa. He reported that the elastic modulus of the aggregates was the most important factor influencing the modulus of rupture. Depending on the aggregates, a 40% difference in flexural strengths was found for the same concrete mix.

Grieb and Werner (1962) reported on flexural strengths obtained from testing 152 x 152 x 533 mm beams. It was observed that the tensile strength was more affected by a change in the curing conditions (i.e., drying vs. moist curing) than by a change in the compressive strength.

Jerome (1984) examined 12,000 individual results for direct tension, split-cylinder and modulus of rupture tests. He proposed that the modulus of rupture be taken as $0.44\ (f'_c)^{2/3}$, in MPa units, where f'_c is the concrete compressive strength. This relationship was proposed for concrete compressive strengths up to 62 MPa. The same relationship was recommended by Shah and Ahmad (1985) for predicting the modulus of rupture for concrete compressive strengths up to 83 MPa. ACI Committee 435 (1968) suggested that the modulus of rupture be taken between $0.62\sqrt{f'_c}$ and $0.99\sqrt{f'_c}$, in MPa units, for normal-weight concrete.

Carrasquillo et al (1981) suggested that the modulus of rupture, for concrete compressive strengths ranging from 21 MPa to 83 MPa, be calculated as $0.97\sqrt{f'_c}$, in MPa units. The flexural strength tests were carried out on 102 x 102 x 356 mm beams, loaded at their third points. For the high-strength concrete specimens, a maximum reduction of 26% in the 28-day modulus of rupture was observed when the specimens were subjected to drying after 7 days of moist curing. It was also reported that high-strength concrete is more sensitive to drying than normal-strength concrete.

Bakhsh et al (1990) expressed the modulus of rupture as $0.8\sqrt{f'_c}$, in MPa units, which gives a strength between the value given in the ACI Code (1983) and that proposed by Nilson (1988). This proposed expression was intended for concrete compressive strengths in the range of 40 to 90 MPa. ACI Committee 363 (1984) reported that the modulus of rupture for both light-weight and normal-weight high-strength concretes fall in the range of $0.62\sqrt{f'_c}$ to $0.99\sqrt{f'_c}$, in MPa units.

Burg and Ost (1992) conducted modulus of rupture tests at 91 days on 152 x

152 x 762 mm concrete beams, using different high-strength concrete mixes, under both moist and air-dried curing conditions. The average modulus of rupture results were plotted versus the square root of the corresponding concrete compressive strengths. It was reported that slopes of the fitted lines were similar to those recommended by ACI Committee 363 (1984), which were based on the work of Carrasquillo et al (1981).

Wafa and Ashour (1992) performed flexural strength tests on 150 x 150 x 530 mm and 100 x 100 x 350 mm plain concrete beams loaded at their third points. The modulus of rupture was expressed as $1.03\sqrt{f'_c}$, in MPa units, for beams with 100 mm square cross-sections made from high-strength concrete. In addition, Aitcin et al (1988) proposed that the modulus of rupture of high-strength concrete be taken as $1.15\sqrt{f'_c}$, in MPa units.

2.2.4 Modulus of Elasticity

The modulus of elasticity of concrete is normally expressed as a function of the concrete compressive strength. Hansen (1956), Gunzler (1970), Lew and Reichard (1978), Byfors (1980) and Oluokun et al (1991) carried out research to study the change in elastic modulus with concrete compressive strength at early ages. Most of the above mentioned studies were carried out on normal-strength concrete mixes. Limited information is available on the change of elastic modulus for high-strength concrete, at early ages, subjected to different curing conditions. The elastic modulus of concrete is affected by the water-cement ratio, temperature, cement type, properties of aggregates and curing conditions (Byfors (1980), Zia et al (1991), ACI Committee 363 (1984), Collins and Mitchell (1990)).

The ACI Code (1983) expressed the elastic modulus in terms of the concrete compressive strength as:

$$E_c = 0.043 (w)^{3/2} (f'_c)^{1/2} \quad \text{for } f'_c \leq 40\text{MPa} \tag{2.14}$$

where

w = unit weight of concrete in kg/m^3

f'_c = concrete compressive strength in MPa

ACI Committee 363 (1992) and the CSA Standard (1994) have adopted the

Carrasquillo et al (1981) expression for the elastic modulus. This is given as:

$$E_c = (3320(f'_c)^{1/2} + 6900)\left(\frac{\gamma_c}{2300}\right) \quad \text{for } 21\ \text{MPa} \le f'_c \le 83\ \text{MPa} \qquad (2.15)$$

where γ_c is the density of concrete in kg/m^3.

2.2.5 Shrinkage of Concrete

Shrinkage is defined as the decrease in concrete volume in the absence of stress and is mainly attributed to drying shrinkage due to the loss of moisture. Plastic or capillary shrinkage is a special case of drying shrinkage when the concrete is in its fresh state. It occurs as a result of capillary forces in the fresh concrete due to loss of moisture. Moisture loss can also occur during hydration due to the consumption of water, which causes a contraction of volume, referred to as autogenous, hydration or self-desiccation shrinkage. Since this type of shrinkage occurs without moisture exchange, it is measured on sealed specimens. The magnitude of autogenous shrinkage depends strongly on the water-cement ratio. For very high water-cement ratios, there is no autogenous shrinkage (van Breugel (1982)), whereas for very low water-cement ratios, autogenous shrinkage is a major part of the total shrinkage, particularly in high-strength concrete mixes (De Larrard and Roy (1992)). Baron (1971) reported the different phases involved in autogenous shrinkage as shown in Fig. 2.5. The curve is mainly defined by three major parts, that is, primary autogenous shrinkage, chemical swelling and secondary autogenous shrinkage. Primary autogenous shrinkage starts 1 to 3 hours after casting and lasts from 2 to 4 hours. The magnitude of primary autogenous shrinkage varies with the concrete mix design and the water-cement ratio (RILEM Committee No. 42 (1981)). Primary autogenous shrinkage may not cause stresses because of the low modulus in the plastic state of the concrete. As soon as the elastic modulus of concrete starts increasing, stresses build up during the temperature increase. Chemical swelling can last from 10 to 20 hours and strongly depends on the type of cement. Additional stresses may occur due to chemical swelling, while the concrete temperature is rising. Secondary autogenous shrinkage starts after the chemical swelling. If the rate of secondary shrinkage is high, the risk of cracking after setting increases due to the restraint tensile stresses in the

concrete (Baron (1971)).

Carbonation shrinkage is another type of shrinkage which is caused by the chemical reaction between hydrated cement products and carbon dioxide in the air. In practical design, autogenous and carbonation shrinkage are typically ignored.

In concrete structures, the rate of drying is affected by the size, shape of the member and the curing conditions. Pickett (1942) and Nagamatsu et al (1981) reported that drying shrinkage is basically proportional to the amount of water loss. Shrinkage of concrete is mainly affected by the following factors:

i. Composition of concrete
ii. Member size
iii. Member shape
iv. Curing conditions
v. Relative humidity
vi. Ambient temperature

It has been generally observed that an increase in water content, water-cement ratio, cement paste proportion and/or temperature will increase the shrinkage of concrete. An increase in aggregate content, relative humidity, and/or stiffness will decrease the shrinkage. Shrinkage of concrete is assumed to occur in the cement paste, with the aggregate being an inert constituent of the concrete which restrains the shrinkage. However, Neville (1981) reported that some aggregates may also shrink. Troxell et al (1958) reported that shrinkage of concrete made with sandstone aggregates can be approximately 2-3 times larger than the shrinkage of concrete made with quartz aggregates.

Due to the low moisture diffusivity of concrete, the shrinkage of concrete is greater at the surface than the interior of the member, especially at early ages. This differential shrinkage effect can cause tensile stresses at the surface and compressive stresses in the interior of the member. In addition, the concrete strength is lower at the surface than in the interior. If the developed tensile stresses exceed the tensile strength, then surface cracking will result.

2.2.6 Early-Age Shrinkage

Early-age shrinkage and swelling play an important role in the development of

early-age stresses, and hence affect the serviceability and durability of the mature concrete. Early age volume changes can be affected by the initial concrete temperature, cement content, and the type and composition of cement (Springenschmid and Breitenbucher (1991)). Shrinkage of early age concrete is different in nature from shrinkage of hardened concrete due to hydration. Plastic shrinkage cracks may develop at the surface of the concrete, under drying conditions, during the first six hours after casting (Kasai et al (1982)). The propagation of these cracks ceases due to the formation of the hydration product. Plastic shrinkage of concrete at early ages causes very little stress due to the low stiffness of the concrete during the first few hours after casting. It is very difficult to assess the stress at very early ages (Machida and Uehara (1987)). In 1982, Kasai et al (1982) reported that concrete exposed to drying at a very early age resulted in much higher shrinkage (plastic shrinkage) than concrete exposed to drying at a later age, although there was not much difference in the total water loss.

The effect of temperature is somewhat different for early age concrete than for mature concrete. It is known that the rate of hydration reaction between cement and water accelerates due to the increase in temperature, which in turn increases the rate of formation of hydration products. An increase in temperature at very early age will increase the rate of evaporation, however the shrinkage of very young concrete will actually be less due to the resistance provided by the earlier gain in strength. Kasai et al (1982) reported that concrete cured at 30°C shrinks less than the concrete cured at 20°C from 3 to 24 hours. An increase in temperature on hardened concrete results in a higher rate of shrinkage and a higher ultimate shrinkage strain (Neville (1981), Bazant (1988)). According to Bazant and Panula (1979), water diffusion is a thermal activation process. Water molecules in concrete are in a higher state of energy at higher temperatures and therefore can escape to the air more easily by breaking the various bonding forces. The CEB-FIP Code (1990) proposed a simple model which takes into account the effect of temperature on both the rate of shrinkage and the ultimate shrinkage.

Early age shrinkage is a very complex phenomenon. Shrinkage of concrete will be non-uniform within a cross-section, particularly at very early ages when the rate of shrinkage on the exposed surfaces is significant. This differential shrinkage will induce

tensile stresses at the outer surface and compressive stresses at the interior of the member. In a traditional shrinkage test, the measured average shrinkage strain is the combined effect of free shrinkage and strains induced by restraint stresses. The average shrinkage strain is typically used in structural analyses for determining deflection, restraint forces and prestress losses. Differential shrinkage of concrete can have a significant effect on the deformations of the structural members. Indirect methods were employed by Bazant and Najjar (1972) to assess the differential shrinkage in terms of water and pore humidity distributions. Sakata (1983) and Bazant et al (1987) expressed the moisture distribution or free shrinkage as a function of the drying time.

A number of models have been proposed to predict the shrinkage of concrete. The most well known models are documented in the CEB-FIP Code (1990) and by ACI Committee 209 (1992). In addition considerable analytical work was carried out by Bazant and Panula (1979, 1982). These empirical models are based on experimental data of hardened concrete. In 1989, Wang and Dilger (1989) performed a comparative study of these models. They found that the shrinkage predictions using the CEB-FIP Code (1990) expressions were the most suitable for situations encountered by many designers and practitioners. The same conclusions were presented by Muller (1992). The main drawback for predicting shrinkage strains using the ACI Committee 209 (1992) equation is the assumption that the rate of shrinkage is independent of member size. Hence, this method can significantly underestimate the shrinkage rate in thin members and can overestimate the shrinkage rate in large members (Wang and Dilger (1989)). It is important to point out that there is very limited data available on the early-age shrinkage of concrete, particularly for high-strength concrete. An experimental study was carried out in this research program to examine the early-age shrinkage behaviour of normal, medium and high-strength concretes.

2.2.7 Creep of Concrete

Early-age creep of concrete has a significant effect in reducing stresses induced during the hydration period. Creep is defined as a continuous increase in strain under constant stress. Traditionally, creep is expressed either by a creep coefficient or a creep function. The creep coefficient is defined as the ratio of creep strain to the

instantaneous strain. The ultimate creep coefficient for normal strength concrete varies from about 2 to 4. The creep function, sometimes called creep compliance, is defined as the total strain (i.e., elastic plus creep strain) per unit stress. Extensive research has been carried out to study the phenomenon of creep in mature concrete. These investigations have been summarized by Bazant and Carol (1993), ACI Committee 209 (1992), CEB-FIP (1990), Neville et al (1983), Bazant and Wittmann (1982), and Neville and Dilger (1970).

Creep of concrete is a complex problem, especially at very early ages, due to the complexity of the material (Neville et al (1983), RILEM (1981)). Aside from the non-linearity and non-homogeneity of concrete, the properties of concrete change very rapidly during the early period of hydration, which makes this phenomenon more complex and highly dependent on maturity and moisture.

To account for the influence of moisture, creep of concrete is divided into "basic creep" and "drying creep". Basic creep of concrete is defined as the creep of concrete in a perfectly sealed condition. It is interesting to note that the creep of concrete in a fully saturated condition (i.e., underwater) is not the basic creep, because there is an exchange of water.

Drying creep, sometimes called the Picket effect, is the additional creep caused by moisture loss under constant stress. It is typically assumed that creep and shrinkage are phenomena which do not interact, and hence the total strain can be obtained by summing up the individual effects of creep and shrinkage strains. Bazant (1988) has observed that this approach may underestimate the total strain.

Like shrinkage, creep can affect the serviceability and durability of concrete structures (Wang and Dilger (1989)). The deflection control criteria in design necessitate the consideration of creep. Creep can be beneficial in relieving stresses caused by thermal and shrinkage gradients, while it can also lead to significant prestress losses in prestressed concrete members.

According to ACI Committee 209 (1992) and Neville et al (1983), creep of concrete is influenced by the following factors:

i. Concrete composition

ii. Loading age

iii. Temperature

iv. Loading duration

v. Moisture condition

vi. Stress level

It is pointed out by Troxell et al (1958) that increasing the aggregate stiffness plays an important role in reducing the creep of concrete. For example, the creep of concrete made with sandstone aggregates is 2 to 3 times more than the same mix under similar conditions made with limestone aggregates. It is generally assumed that most aggregates, except sandstone, do not creep. It must be pointed out that the vast majority of studies were conducted on relatively mature concrete specimens, typically at least 7 or 28 days old.

Temperature has a two-fold effect on creep. An increase in temperature gives increased creep for mature concrete, while for hydrating concrete a temperature increase gives increased concrete strength and hence reduced creep. It has been reported that creep of mature concrete will be 2 to 3 times larger at 50°C than at room temperature (ACI Committee 209 (1992)).

2.2.8 Early-Age Creep of Concrete

During the hydration process, large thermal and shrinkage gradients can cause stresses which are significantly affected by creep of concrete. It is a well established phenomenon that creep of hydrating concrete decreases with age of loading. Earlier loading age results in higher values of elastic and creep strains due to the lower modulus of the concrete. Very early loading may also result in higher rates of creep in the mature concrete (Bazant (1988)). The behaviour and mechanism of the creep of concrete loaded at very early ages is not well understood (RILEM (1981), Neville et al (1983)).

Figure 2.6 shows a schematic representation of the factors affecting creep (Byfors (1980)). According to Neville (1981), creep in hardened concrete is proportional to the stress level for stresses up to 40% of the strength. If a constant stress is applied at very early ages, the subsequent hydration process results in a gain of concrete strength and hence reduction of the stress level.

In order to account for creep at early ages in numerical simulations, it is necessary to make some assumptions due to the complexity of the creep phenomenon.

Uniform concrete material properties are often assumed throughout the cross-section to simplify the problem of predicting stresses. However, a step-by-step analysis can be carried out to take into account the variation in the time domain of temperature, creep, shrinkage, strength and stiffness at different locations in the cross-section. Details on the analyses are presented in Chapters 5 and 6.

2.2.9 Poisson's Ratio

Very limited information is available on Poisson's ratio of concrete at early ages. Gunzler (1970) reported that there was no effect of age on Poisson's ratio at ages from 15 hours to 30 hours. Oluokun et al (1990) concluded that Poisson's ratio is not affected by age or concrete strength, as suggested by other researchers (Perenchio and Klieger (1978), Carrasquillo et al (1981), Klink (1985), NRMCA (1992)). Oluokun et al (1990) found an average Possion's ratio value of 0.19 for concrete mixes with 28-day concrete strengths of 28 MPa to 61 MPa, with ages varying from 12 hours to 28 days. However, Byfors (1980) concluded that Poisson's ratio is lower at early ages, that is, for f'_c of 1 MPa, and increases with increasing age and strength.

Table 2.1 - Total heat of hydration for four clinker components (Rasmussen and Andersen (1989))

Clinker Components	C_3S	C_2S	C_3A	C_4AF
heat of hydration* (J/g)	499	256	720	302

* Temperature of 23°C, water-cement ratio of 0.45 and cement fineness of 3,100 cm^2/g.

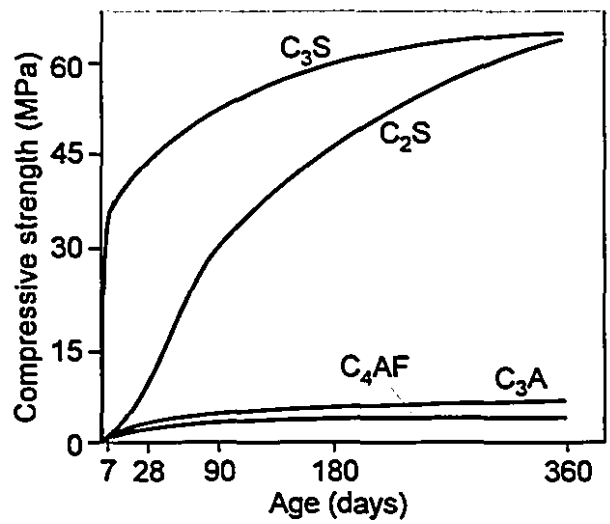

Figure 2.1 - Strength gain for different clinker components (Bogue (1947))

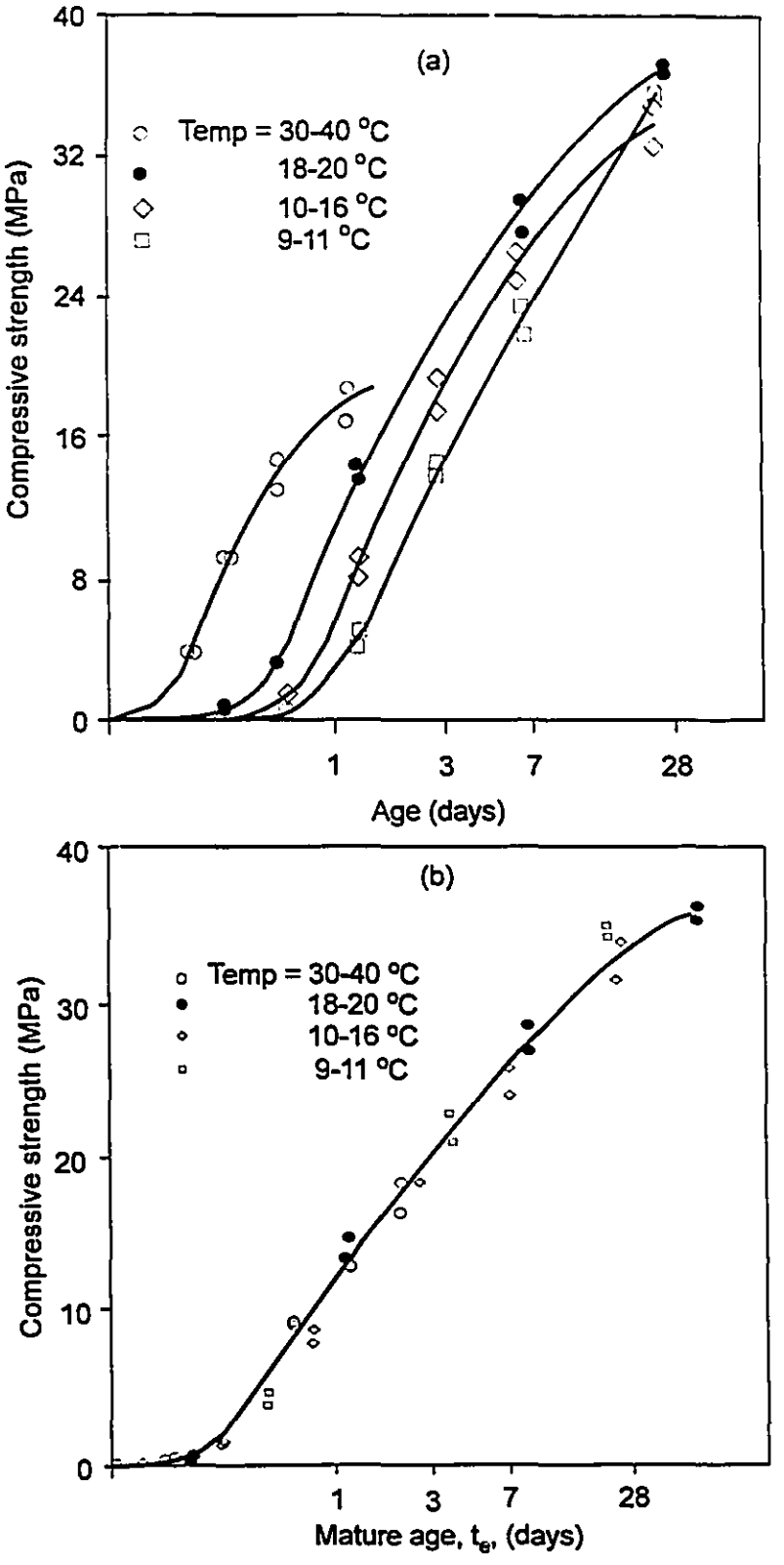

Figure 2.2 - Compressive strength gain at different curing temperatures (a) vs. real age (b) vs. mature age (Byfors (1980))

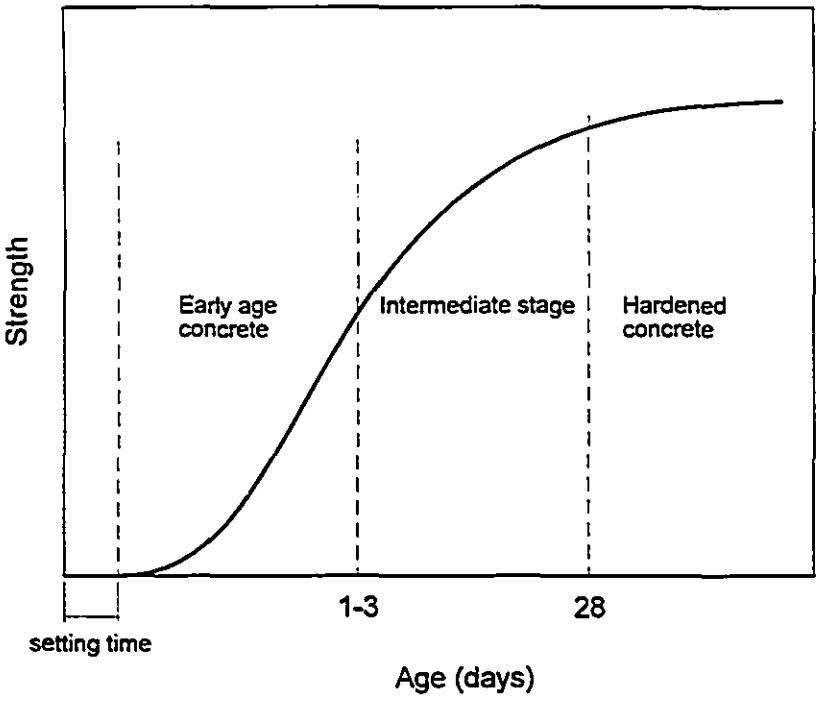

Figure 2.3 - Schematic presentation of strength gain with age

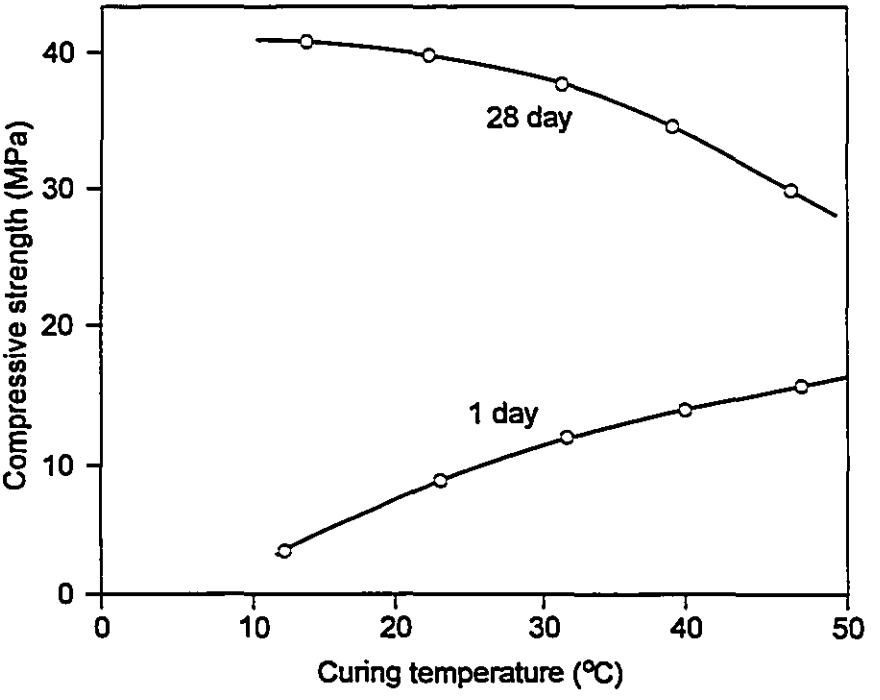

Figure 2.4 - Effect of curing temperature on 1 day and 28 day strength (Byfors (1980))

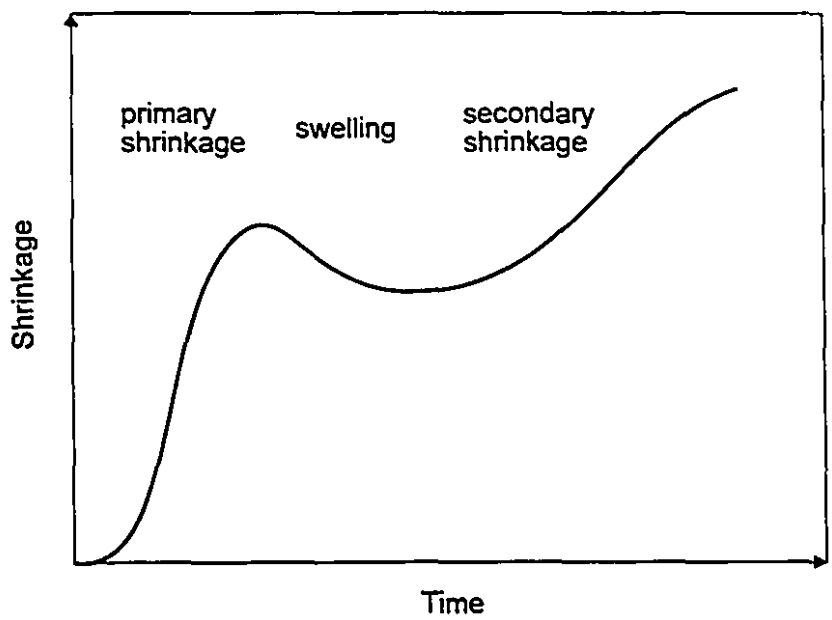

Figure 2.5 - Schematic representation of shrinakge during early hydration (Baron (1970), L'Hermite (1960))

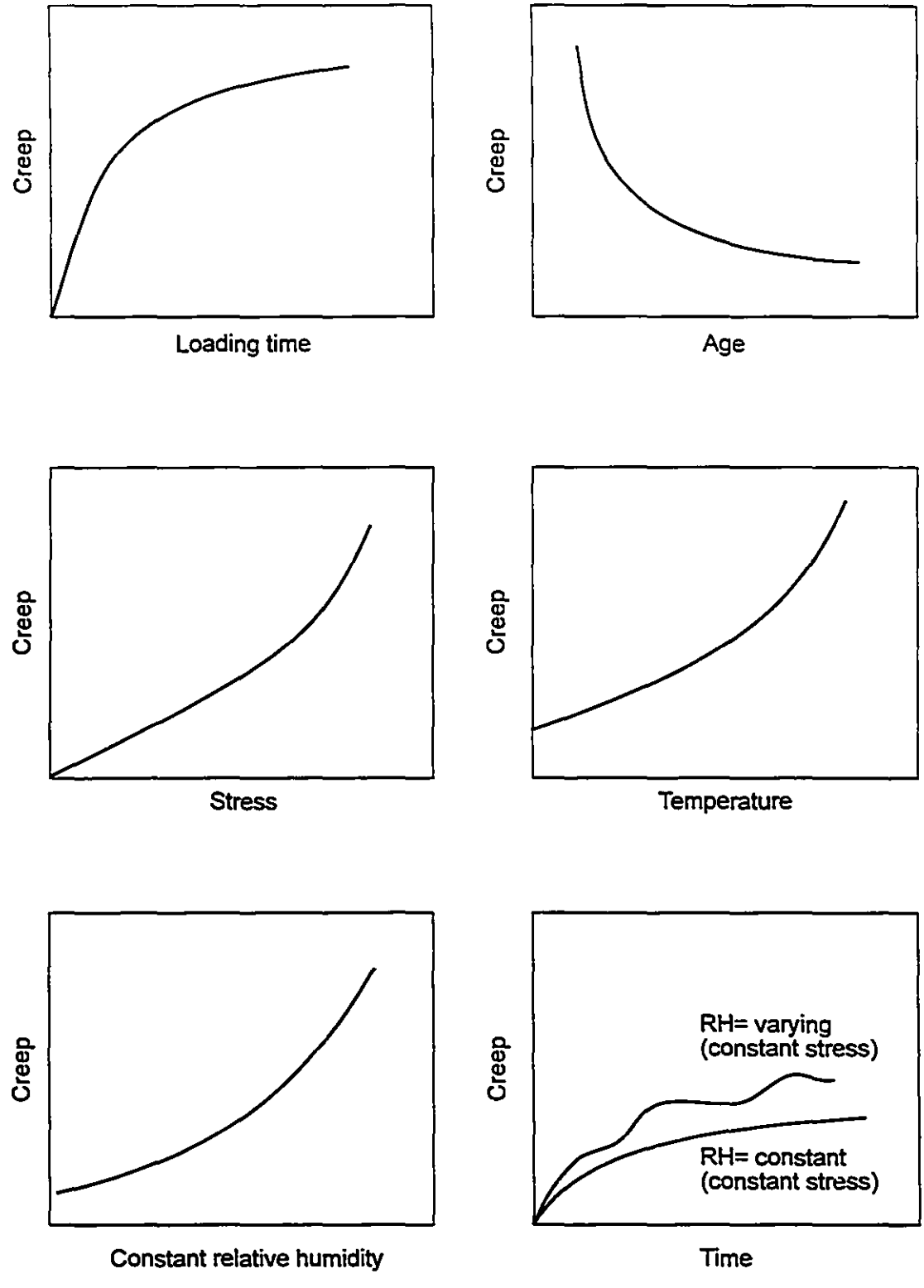

Figure 2.6 - Schematic presentation of main factors influencing creep of concrete

Chapter 3

Thermal Properties of Normal, Medium and High-Strength Concretes

In the last few years, cement characteristics have changed substantially. The strength and fineness have increased, necessitating studies on the physical properties. In predicting the temperature variations in structural members, it is necessary to determine the thermal properties of concrete. The increased use of high-strength concrete in the construction industry has accentuated the need to investigate the thermal properties of high-strength concrete mixes. It must be pointed out that the composition of normal-strength concrete varies over a wide range, and may have significant variations in thermal properties in different regions of the country. During the early period of hydration, it is expected that the thermal properties of concrete may undergo significant changes. Thus, experimental studies were carried out to investigate the thermal properties of normal, medium and high-strength concretes at both early ages and in the hardened state. The results from these studies are presented in the following sections.

3.1 Concrete Materials

In order to distinguish between the three different types of concretes, they will be referred to as the 30 (normal-strength), 70 (medium-strength) and 100 MPa (high-strength) concretes (i.e., the approximate 28-day concrete strengths).

3.1.1 Cement

Ordinary Portland Cement, CAN/CSA-A23.1-M90 Type 10 (ASTM Type I), was used for 30 MPa concrete. A blended Type 10 cement, containing 7-8% and 8-9% of silica fume by volume, was used for the 70 and 100 MPa concretes, respectively.

3.1.2 Fine and Coarse Aggregates

Limestone coarse aggregates were used for all of the concrete mixes, having maximum aggregate sizes of 20, 10 and 6 mm for the 30, 70 and 100 MPa concretes, respectively. The Coarse aggregates had a specific gravity of 2.69 and absorption of 0.6. One type of river sand, from the Lafarge St. Gabriel pit, having a fineness modulus of 2.55 and specific gravity of 2.68, was used for all the mixes in this research program. The fine and coarse aggregates were obtained from the same source.

3.1.3 Admixtures

Only the normal-strength concrete contained an air-entraining agent (see Table 3.1). Due to the low water-cement ratios in the medium and high-strength concretes, the workability was achieved by using admixtures. An aqueous solution of sulfonated naphthalene formaldehyde condensate superplasticizer (Conchem SPN) and an aqueous solution of lignosulfonates and an organic accelerator (Conchem 25 XL) were used for the medium and high-strength concretes. These admixtures contained 60% water and 40% solids. Hence in the mix design, the required amount of water was reduced to account for the presence of water in the admixtures.

3.2 Concrete Mix Proportions, Batching and Casting

Table 3.1 presents the details of the composition and the fresh concrete properties of the three types of mixes used in this testing program. The concrete was prepared in a concrete mixer in small batches. Trial batches were made to achieve the desired concrete compressive strengths and slight adjustments in the mix design were made, if necessary. Before making the concrete, the moisture content of the fine and the coarse aggregates were measured and the mix design was adjusted accordingly. In order to achieve high-strength concrete it is essential that special care be taken at

every step in the mix design, batching and casting operations. The aggregates were washed and saturated surface dry just before casting. Even the dust on crushed aggregates can significantly affect the bond between the hydration product and the aggregates, having a deleterious effect on the strength. A large number of trial batches were made to achieve the designed concrete strength and special care was taken during mixing. The concrete mixer had to be cleaned in order to prevent the absorption of water during mixing. The water temperature was 20 ± 1°C. Workability of the concrete was measured by slump test in accordance to ASTM C 143-78 (1988).

Figure 3.1 demonstrates the mixing procedure used in making the medium and high-strength concretes in the laboratory. Although the medium and high-strength concrete mixes have low water-cement ratios, the desired workability, commonly required at the construction site, was achieved by using admixtures. The superplasticizer is typically added in small quantities until the desired workability is achieved. The mix designs used in this research program were those currently used by one of the local concrete suppliers (Francon-Lafarge Canada Inc.) in Montreal.

3.3 Heat of Hydration

The heat of hydration can be obtained from the temperature rise due to adiabatic curing, the specific heat of the concrete and the density of the concrete. The adiabatic temperature rise of concrete is defined as the temperature rise due to the heat of hydration, when no heat is lost to, or gained from the surrounding environment (i.e., condition at the core of mass concrete). To achieve this condition, either the concrete has to be perfectly insulated or the temperature of the environment controlled to be the identical to that of the hydrating concrete (i.e., temperature-matched curing). Temperature-matched curing is found to be the most suitable and easiest method of obtaining the heat of hydration. A temperature-matched curing technique was developed in this research program to simulate not only the temperature rise, but also to simulate the moisture conditions at very early ages during hydration. This is discussed in section below.

3.4 Temperature-Matched Curing Apparatus

Figure 3.2 illustrates the temperature-matched curing apparatus developed in

this research program. It consists of a 1300 x 1000 x 1000 mm high-temperature resistant polyethylene tank filled with water, a submersible pump, a 1500 watt heating element, a analog-digital and digital-analog convertor and a micro-computer. The base and the sides of the tank were insulated. Temperatures of the water bath and at the centre of a control cylinder were measured using copper-constantan (Type T) thermocouples with an accuracy of 0.5°C. The thermocouple was formed by twisting two wires in a uniform manner and welding the joint. Special care was taken during welding because overheating the joint could affect the accuracy of the thermocouple. The thermocouple signals were recorded in millivolts and converted into temperatures with cold-compensation applied. A thermocouple wire was placed at the centre of a 100 x 200 mm concrete cylinder during casting and another thermocouple was placed in the water bath. The specimens were vacuum sealed to avoid water penetration and were immediately placed inside the temperature-matched curing bath to avoid loss of heat of hydration. The initial water temperature inside the bath was about the same as the mix constituents (i.e., 21 ± 1°C). The temperature-matched curing was achieved by measuring the temperature at the centre of the control cylinder and heating the surrounding water in order to match the temperature of the hydrating concrete cylinder. The water was heated using the heating element and the temperature readings and temperature adjustments were made at two second intervals. The matching of the temperatures was accomplished by using the computerised control system. The submersible pump was used to circulate the water in order to obtain a uniform heat flux inside the water bath. Computer software was developed to communicate with a data logger to measure the temperature increases with age.

The temperature-matched curing system was developed for the following reasons:

i. To determine the temperature rise during hydration of different types of concretes under adiabatic conditions.

ii. To provide a large number of samples subjected to adiabatic conditions to investigate the physical properties of different concretes .

This system could also be used to determine the effects of any other temperature history (i.e., in situ measurements).

3.5 Adiabatic Temperature-Time Responses for Normal, Medium and High-Strength Concrete

Table 3.1 presents the details of the composition and the fresh concrete properties of the three types of mixes used in this testing program. It must be pointed out that medium and high-strength concrete mixes contained 28% and 52% more cement content than the normal-strength concrete mix.

Figures 3.3, 3.4 and 3.5 show the temperature variations with age for the normal, medium and high-strength concretes, respectively, due to temperature-matched curing. The initial mix temperature was 23°C for the normal-strength, 22°C for the medium-strength and 23°C for the high-strength concrete. The peak temperature was 62°C, 64°C and 73°C for the normal, medium and high-strength concretes. In these figures, the recorded ambient temperatures are also presented.

Figure 3.6 compares the rises in temperature above initial temperature measured for the 30, 70 and 100 MPa concretes under temperature-matched curing or adiabatic conditions. Temperature increases of 39, 42 and 50°C were observed for the 30, 70 and 100 MPa concretes during hydration. The 70 and, particularly the 100 MPa, concretes displayed higher initial retardation of hydration, which resulted in a time lag in reaching the peak temperatures. This is probably due to the high dosage of superplasticizers in these mixes. After the retardation period, the slopes of the temperature rise responses and the peak temperature rises increased with increasing concrete strength. This can be attributed to the higher cement contents and the use of silica fume in these concrete mixes.

3.6 Specific Heat of Concrete

Specific heat is defined as the amount of heat energy required to raise the temperature of a unit mass of a material by one degree. The specific heat of concrete depends on its constituent materials. The specific heat of water is 4.18 J/g-°C, whereas the specific heat of cement and aggregates is 0.75 and 0.9 J/g-°C, respectively. During early period of hydration, the moisture content of the concrete significantly reduces and may result in reducing the specific heat. Tests were carried out to measure the specific heat of the concrete mixes used in this study. Due to the

changing state of concrete at very early ages, it is difficult to determine the specific heat. Tests were done using a Differential Scanning Calorimeter (DSC) at the National Research Council of Canada, to measure the specific heat of mature concrete at two extreme states, that is, for a fully saturated sample and for an oven-dried sample. The measurement is made by heating a test specimen at a fixed rate over a designated temperature range, where the specimen is held in thermal equilibrium before and after heating. Figures 3.7 and 3.8 show the variations of specific heat with temperature for saturated and oven-dried concretes. The specific heat of concrete increases with an increase in temperature. In the temperature range of 30 to 70°C, the specific heat ranged from 0.65 to 2.7 and from 0.65 to 1.1 for the saturated and oven-dried samples, respectively. By comparing the values from Fig. 3.7 and Fig. 3.8, it is evident that the moisture content has a significant effect on the specific heat. It was reported by Whiting et al (1978) that the specific heat of normal-density concrete increases with an increase in temperature and decreases with increasing concrete density. As expected, the oven-dried samples resulted in lower specific heat values than saturated samples for the same concrete strength. This can be attributed to the loss of moisture.

3.7 Thermal Conductivity of Concrete

Thermal conductivity of concrete gives the rate of heat flow through a unit area of a material under a unit temperature gradient. Very limited information is available on thermal conductivity of concrete at very early ages. Tests were carried out to measure the thermal conductivity of concretes at very early ages using a thermal probe (see Fig 3.9). This probe consists of a stainless steel tube that houses a heating element along its length and a temperature sensor at its centre. The stainless steel tube provides the necessary rigidity as well as minimizing interference with the radial heat flow. The heating element has a length of 200 mm, a diameter of 6 mm and a net electrical resistance of 4.6 ohms. The thermal probe was placed at the middle of a 100 x 200 mm cylinder before casting the concrete (see Fig. 3.9). A constant current of 0.8 amps was supplied to the heater and temperature measurements were taken at 10 second intervals over a period of 500 seconds. An initial reading was taken without supplying power to the heating element. During the measurements, the input current and the temperature from the sensor were recorded. A companion

control cylinder was instrumented with a thermocouple at its centre to measure the temperature of the hydrating concrete in order to permit compensation for the temperatures measured in the cylinder with the probe. The thermal conductivity of the concrete was determined from the slope of the temperature versus time curve (Carslaw and Jaeger (1986)). Since the conductivity is being measured, it is important that the thermal probe have good contact with the concrete along its length.

Tests were also carried out to determine the thermal conductivity of hardened concrete using a thermal conductivity meter (Model TC-31) at variable temperatures. A thin metal heating wire along with a thermocouple was placed between sliced, smooth surfaced concrete samples. The 100 x 200 mm samples were sliced and the surfaces polished with a grinder. The concrete samples were first temperature-equilibrated in a constant temperature chamber. A constant electric current was then supplied to the heating wire and the temperature increase of the heating wire was measured with time. The apparatus calculates the temperature rise of the heating wire and displays digitally the measured value of thermal conductivity. Before measurement, the thermal conductivity meter was calibrated on a standard silicone rubber sample having a thermal conductivity of 0.192 W/m-°K. The apparatus has a range of measurement from 0.05 to 5.00 W/m-°K and a reproducibility within 5%.

Table 3.2 summarizes the thermal conductivities determined for the normal, medium and high-strength concretes. These values were determined at variable temperatures for the concrete in both the hardened and maturing states. Tests were conducted during the first 48 hours for the maturing concrete. As can be seen from the results, temperature did not significantly affect the thermal conductivity. It is observed that the average thermal conductivity of the maturing normal-strength concrete is 33% higher than that of the hardened concrete. On the other hand, there is only a 2% difference in conductivity between the very early-age and hardened high-strength concrete. The lower water-cement ratio and the higher density of the high-strength concrete have contributed to a higher conductivity as well as resulting in a smaller difference in conductivities for the maturing and hardened states. The influence of type of concrete is more significant in the hardened state. For example, the thermal conductivity of the hardened medium-strength and high-strength concretes is about 36% and 50% higher than that of normal-strength concrete at 25°C.

3.8 Coefficient of Thermal Expansion

Since the thermal strains during hydration are proportional to both the temperature rise and the coefficient of thermal expansion, the magnitude of this coefficient plays an important role in the restraint stresses developed during hydration.

Due to the significant influence of the aggregates on the coefficient of thermal expansion and due to the large variation of this coefficient for different types of aggregates, it is important to measure the coefficient of thermal expansion for the particular concrete under investigation. For example, quartzite aggregates have a coefficient of thermal expansion which is about 50% higher than that of limestone aggregate.

The coefficient of thermal expansion, α_c, can be found by determining the dimensional change in a specimen for a corresponding temperature change, and is given as.

$$\alpha_c = \frac{\epsilon_{cth}}{\Delta T} \tag{3.1}$$

where ϵ_{cth} is the unrestrained thermal strain and ΔT is the temperature change.

Tests were carried out to measure the coefficient of thermal expansion of the normal, medium and the high-strength concretes at very early ages. Prisms 50 x 50 x 250 mm, were cast in specially designed plexiglass moulds with gauge studs of invar aligned at the centre of the end surfaces of the moulds, as described by ASTM C 490-86 (1988). The base and side plates of the plexiglass mould were coated with vaseline to overcome the friction. The change in the linear dimension of a test specimen was measured with a dial gage, having of precision of 0.001 mm. All of the specimens were immediately sealed after casting and kept in the sealed condition. Tests were also done to measure the coefficient of thermal expansions of hardened concrete specimens. Table 3.3 summarizes the results of the coefficients of thermal expansion of normal, medium and high-strength concretes for hardened and maturing concrete. These results show that the coefficient of thermal expansion is relatively independent of age after few hours of casting up to 28 days. Other researchers (Miao et al (1993), LaPlante (1993), ACI Committee 517 (1988)) have also observed that the coefficient of thermal expansion of concrete becomes constant a few hours after casting. An

average value of the coefficient of thermal expansion of the normal-strength (30 MPa) sealed specimens were 9.6 x 10^{-6}/°C and 9.5 x 10^{-6}/°C at 16 and 24 hours after casting, respectively. The coefficient of thermal expansion of the medium-strength hardened concrete is about 9% higher than that of the normal-strength concrete. This difference is slightly less for maturing concrete (about 7%). It must be pointed out that limestone aggregates, from the same source, were used in all these concrete mixes.

3.9 Reproducibility of Temperature-Matched Curing Results

An investigation was carried out to determine the repeatability of the test results obtained using temperature-matched curing. The repeatability of the results for the temperature rise are presented in this section, while the repeatability of the corresponding mechanical properties are discussed in Chapter 4. These investigations were performed on specimens made of normal, medium and high-strength concrete mixes with the same mix proportions, mixing procedure, and about the same initial and ambient temperatures as the initial mixes (batch 1). Figures 3.10 and 3.11 show the comparison of temperature rises for the normal and high-strength concretes. In Fig. 3.10, batch 2 represents the repeated concrete mix. For the high-strength concrete mix specimens from two repeated batches (batch 2 and batch 3) were compared with the initial results (batch 1) as shown in Fig. 3.11. These figures demonstrate that fairly reasonable repeatability of the test data was achieved. It is interesting to note that the specimens of batch 2 and 3 of the high-strength concrete specimens gave a peak temperature which was about 2°C less than the specimen from batch 1. This demonstrates the sensitivity of the temperature rise on the initial temperature of the concrete. Batches 2 and 3 had initial temperatures of 18 and 19°C, respectively, that is, about 2°C lower than that of batch 1. The importance of controlling the initial temperature of high-strength concrete mixes is recognized by the 1994 CSA Standard A23.1. This standard limits the maximum temperature reached during hydration to 70°C. An absolute maximum of 25°C (20°C preferred) at the time of delivery is recommended by the Standard based on experience with the construction of high-strength concrete structures (Ryell and Bickley (1987), Mitchell and Bickley (1993)).

Table 3.1 - Composition and properties of the 30, 70 and 100 MPa concrete mixes

Characteristics	30 MPa	70 MPa	100 MPa
cement (Type 10), kg/m^3	355	455*	540**
fine aggregates, kg/m^3	790	820	720
coarse aggregates, kg/m^3	1040	1025	1105
total water***, l/m^3	178	135	133
water-cement ratio	0.50	0.30	0.25
air-entraining agent, ml/m^3	180	-	-
water-reducing agent, ml/m^3	1110	1424	754
superplasticizer, l/m^3	-	4.5	19.5
slump, mm	146	142	185
air content, %	11.7	2.95	2.75
density, kg/m^3	2130	2419	2505
compressive strength at 28 day•, MPa	27.9	77.0	99.2

* Type 10 blended cement containing 7 - 8 % silica fume

** Type 10 blended cement containing 8 - 9 % silica fume

*** Includes the water in admixtures

• Average of 3 sealed 100 x 200 mm cylinders

Table 3.2 - Thermal conductivity of 30, 70 and 100 MPa concrete mixes for various temperatures

Concrete Type	Density (kg/m^3)	Hardened Concrete		Maturing Concrete	
		Temp. (°C)	Conductivity (W/m-°C)	Temp. (°C)	Conductivity (W/m-°C)
normal-strength (30 MPa)	2130	25	1.17	28	1.72
		37	1.14	31	1.74
medium-strength (70 MPa)	2419	27.5	1.59	-	-
high-strength (100 MPa)	2505	26	1.77	22	1.80
		73	1.77	-	-
		82	1.65	-	-

Table 3.3 - Coefficient of thermal expansion for 30, 70 and 100 MPa concrete mixes

Concrete Type	Aggregate Used	Hardened Concrete α_c (1×10^{-6}/°C)	Maturing Concrete	
			Age (Hours)	α_c (1×10^{-6}/°C)
normal-strength	limestone	10.00	16	9.60
			24	9.50
medium-strength	limestone	10.91	24	10.2
high-strength	limestone	7.35	-	-

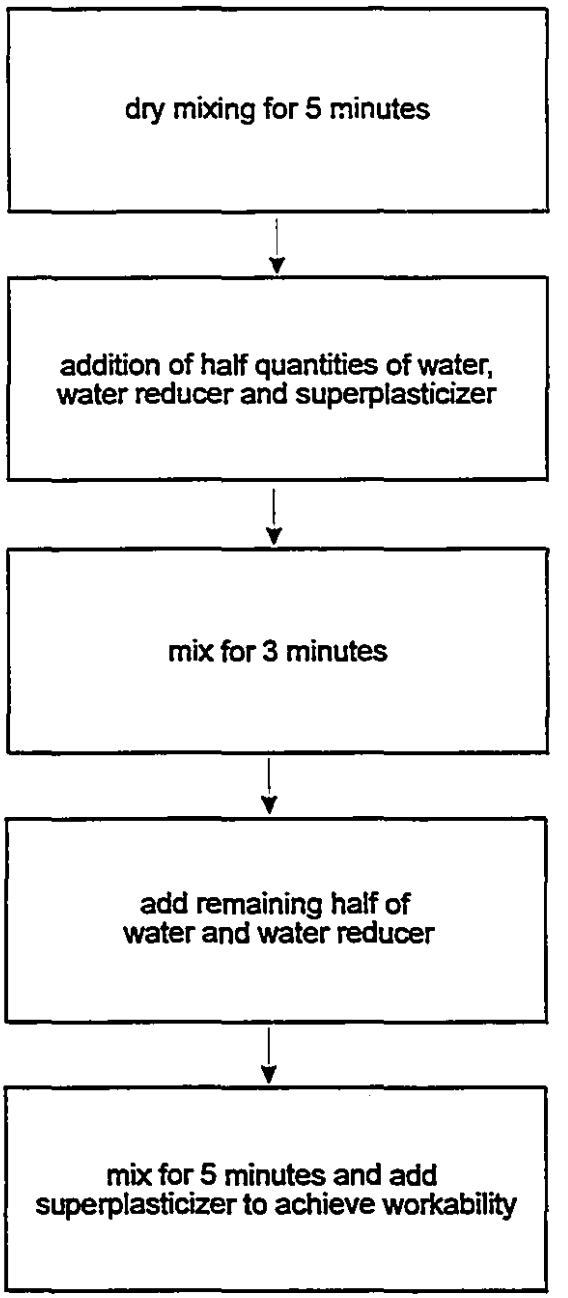

Figure 3.1 - Mixing procedure for medium and high-strength concretes

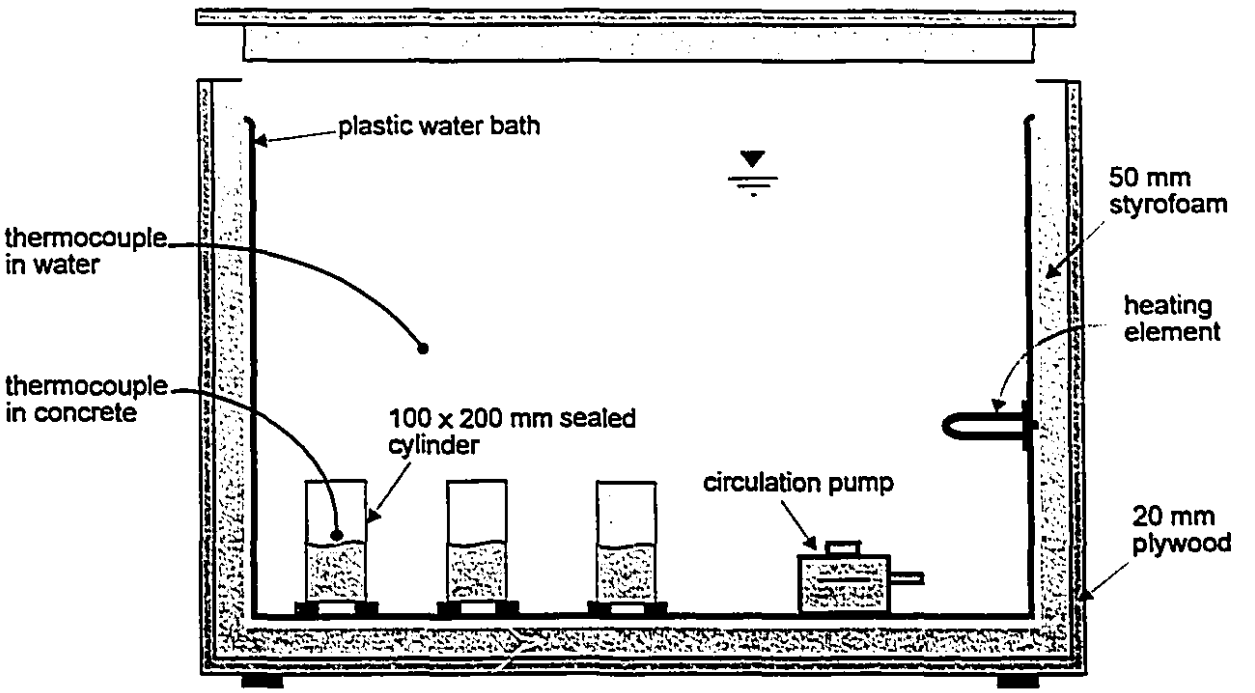

Figure 3.2 - Temperature-matched curing test setup

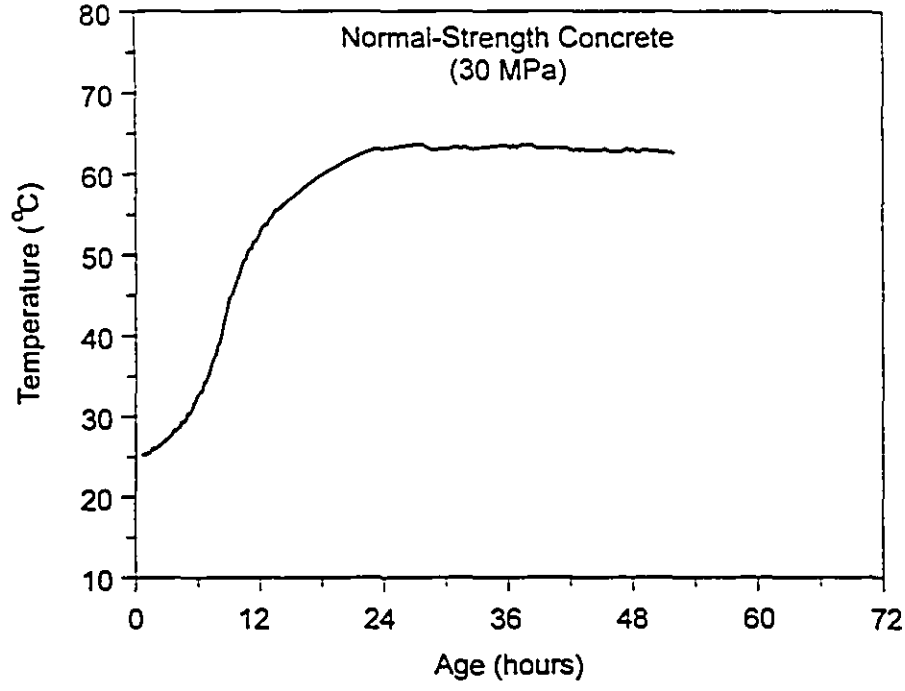

Figure 3.3 - Temperature increase of normal-strength concrete during temperature-matched curing

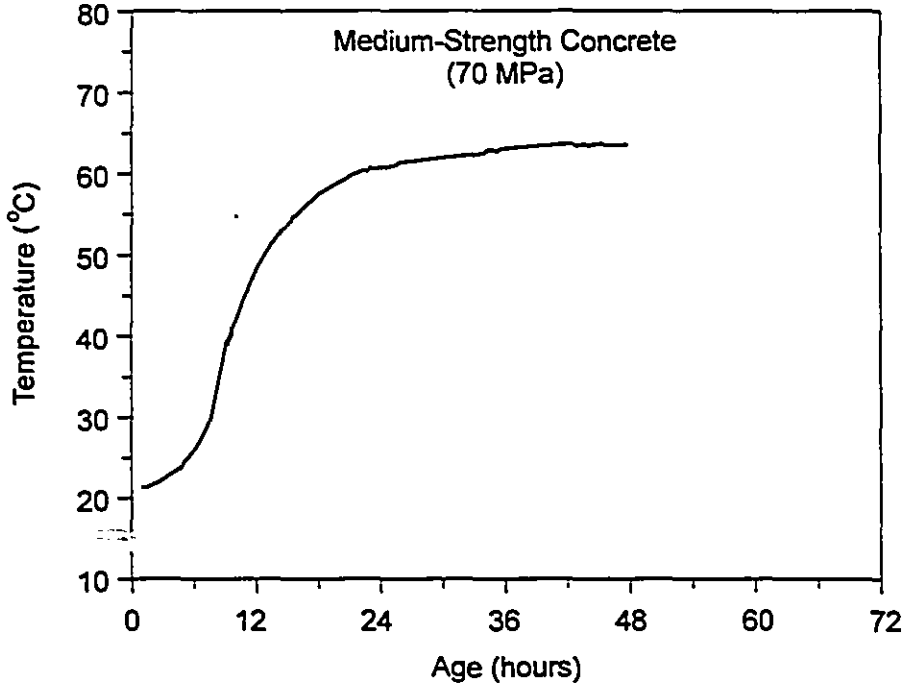

Figure 3.4 - Temperature increase of medium-strength concrete during temperature-matched curing

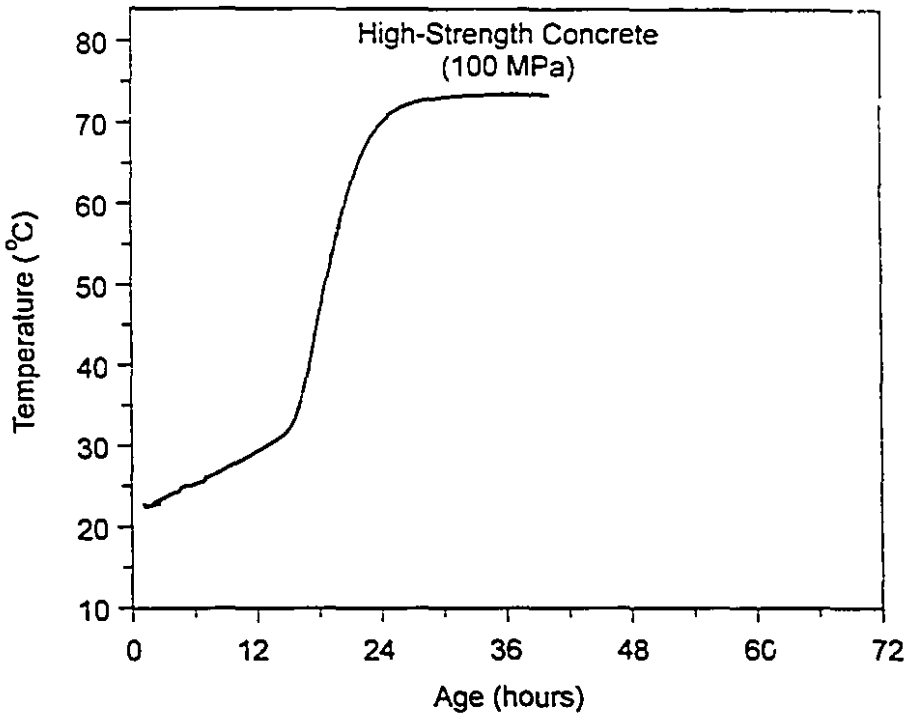

Figure 3.5 - Temperature increase of high-strength concrete during temperature-matched curing

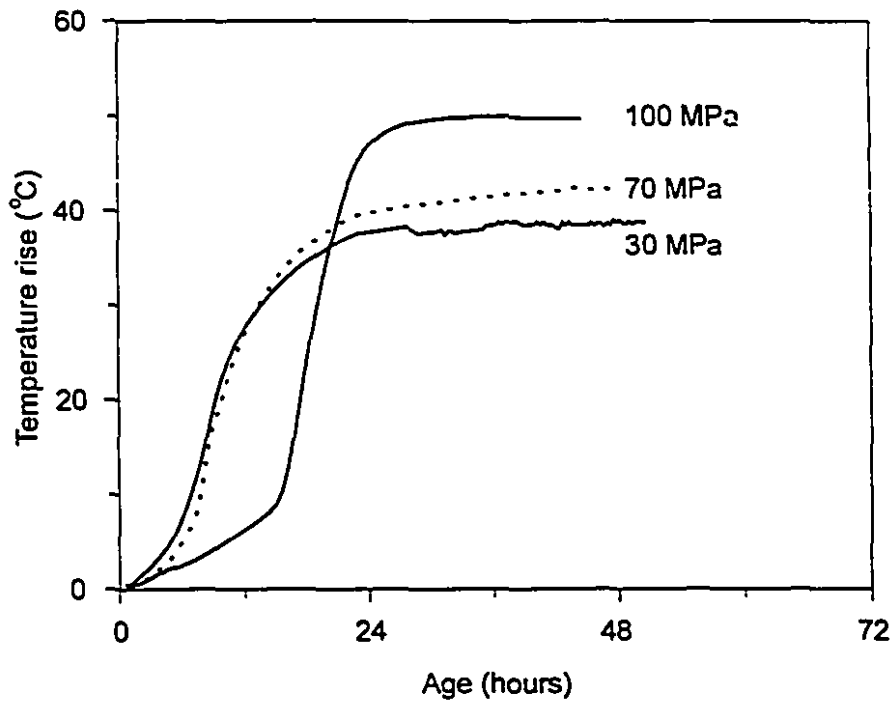

Figure 3.6 - Temperature rises of normal, medium and high-strength concretes during temperature-matched curing

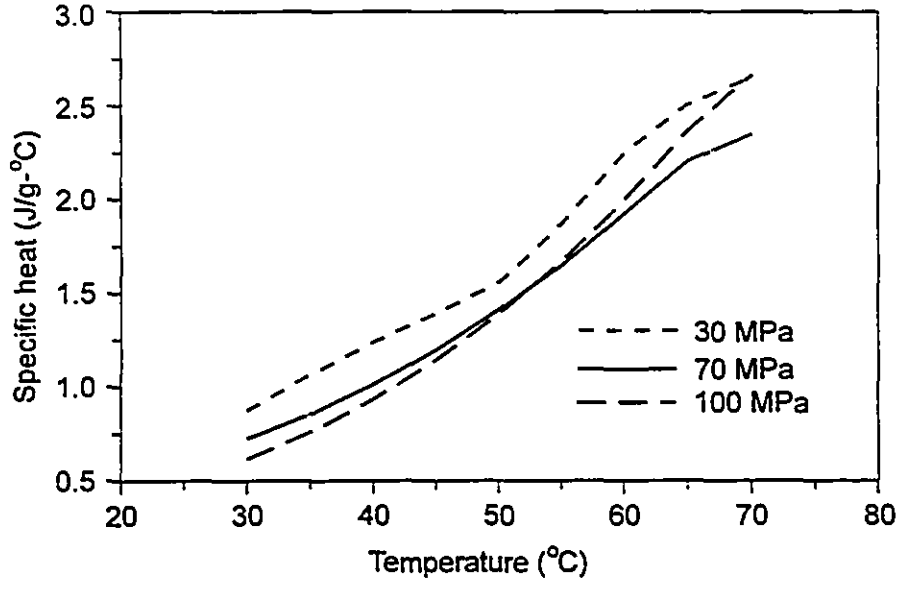

Figure 3.7 - Variation of specific heat of saturated concretes with temperature

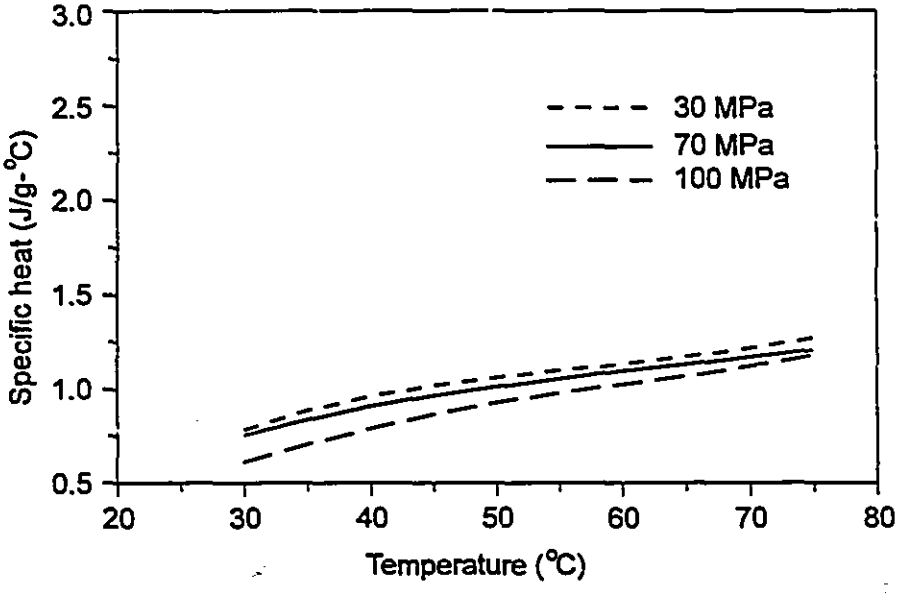

Figure 3.8 - Variation of specific heat of oven-dried concretes with temperature

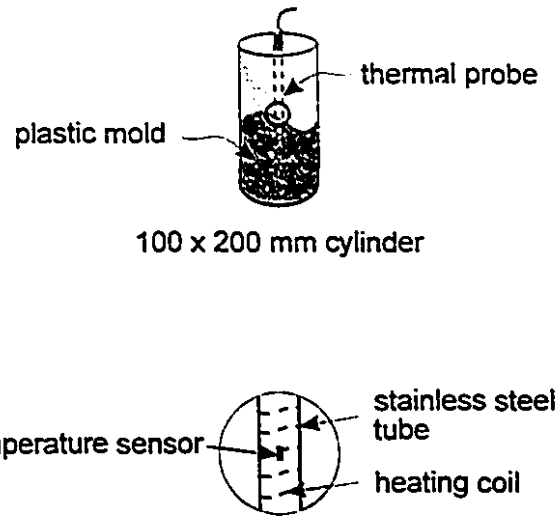

Figure 3.9 - Test set up to measure the thermal conductivity of very early-age concrete

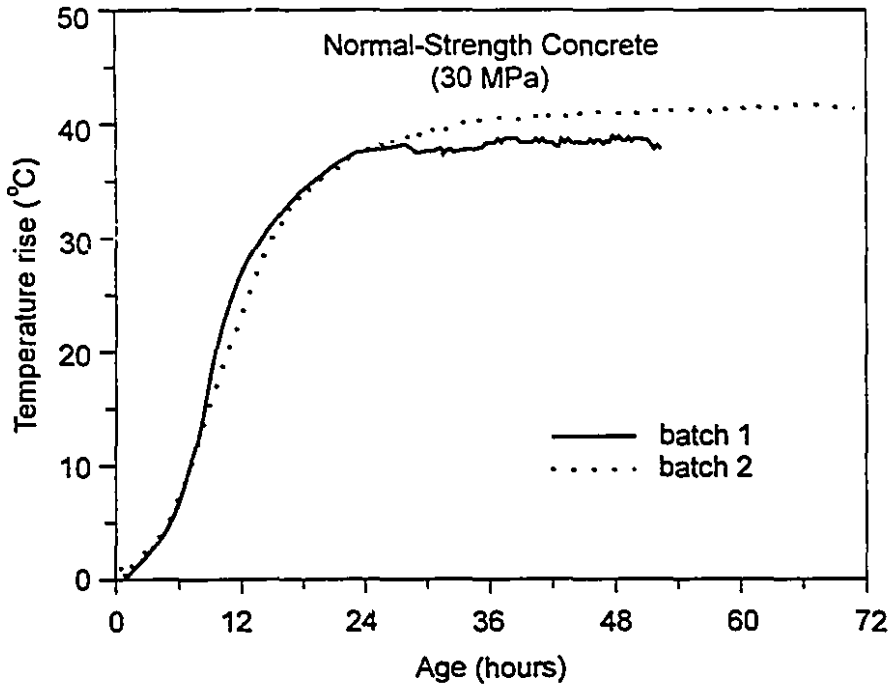

Figure 3.10 - Temperature rise of normal-strength concrete during temperature-matched curing

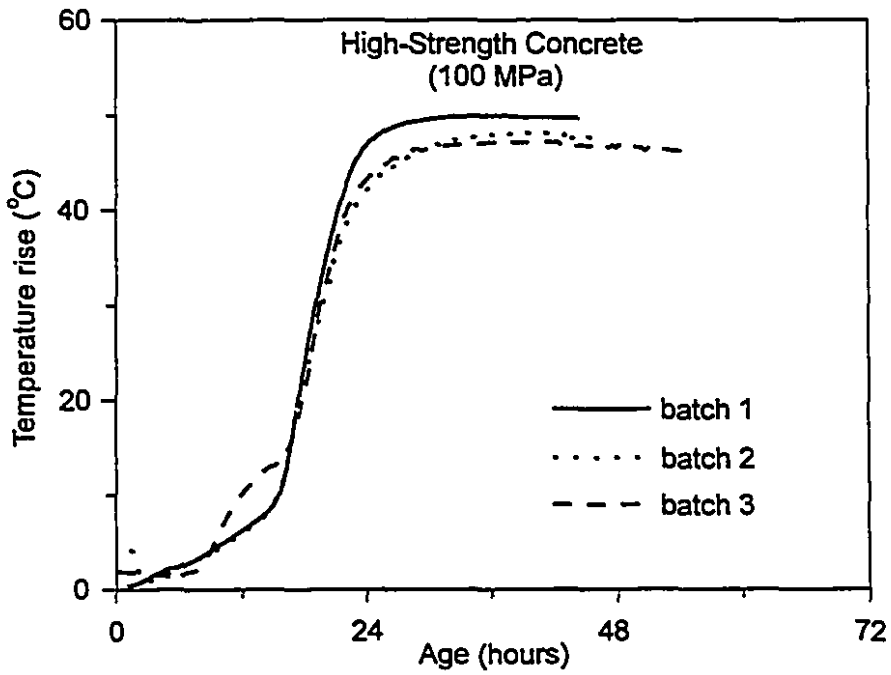

Figure 3.11 - Temperature rises of high-strength concretes during temperature-matched curing

Chapter 4

Mechanical Properties of Normal, Medium and High-Strength Concretes at Early Ages

The hydration reaction between cement and water is highly exothermic, which can result in high temperatures and significant thermal gradients in concrete members, depending on the thermal properties of the concrete and the boundary conditions. The effect of temperature and curing at very early ages can strongly influence the strength development and consequently the risk of thermal cracking and hence the long-term durability of concrete members. With the increased use of higher-strength concretes in the past few years, one of the major concerns of designers and contractors is whether or not cracking will occur at very early ages. The use of higher-strength concretes may result in higher temperatures and larger thermal gradients during hydration than normal-strength concrete. In order to understand the behaviour of concrete members at very early ages, it is necessary to determine the variations of the important mechanical properties of different concretes.

The research presented in this chapter examines the variation of the compressive stress-strain characteristics with time, the compressive strength gain, the tensile strength gain and the development of creep and shrinkage for normal, medium and high-strength concretes. In particular these characteristics are closely followed during the first 72 hours after casting.This chapter also presents mathematical expressions for the development of the key early age mechanical properties of different types of concretes. In order to distinguish between the three types of concretes, they will be referred to as the 30, 70 and 100 MPa concretes (i.e., the approximate 28 day

concrete strengths). The influence of different curing conditions on the temperature rise at early hours and its effect on the development of the mechanical properties is presented. The curing conditions investigated include temperature-matched curing, sealed curing, and air-dried curing. These conditions model the curing effects at the centre of mass concrete, close to the surface of the concrete and at the surface of a structural member, respectively.

4.1 Early Age Compressive Stress-Strain Characteristics of Normal, Medium and High-Strength Concretes

4.1.1 Experimental Program

Compressive stress-strain responses, compressive strength gain and development of elastic modulus of the normal (30 MPa), medium (70 MPa) and high-strength (100 MPa) concretes were studied. The three different curing conditions investigated were temperature-matched curing, sealed curing and air-dried curing. The apparatus used to obtain the temperature-matched curing is described in Section 3.4. Concrete cylinders, 100 x 200 mm, were cast in special plastic cylinder molds designed to enable demolding at very early ages without disturbing the concrete. All of the specimens were hand rodded in accordance with ASTM C 31 (1988). Specimens subjected to temperature-matched curing were vacuum sealed and were immediately placed inside the temperature-matched curing bath. The temperature-matched curing technique and the measured adiabatic temperature-time responses of the 30, 70 and 100 MPa concretes are discussed in Sections 3.4 and 3.5.

The sealed and air-dried curing conditions model the curing close to the surface and at the surface of a structural member, respectively. All of the specimens were covered with polyethylene sheets for 24 hours and kept in the laboratory environment (i.e., ambient temperature of 21 ± 1°C and relative humidity of 50 ± 10%). The specimens were demolded at 24 hours after casting, with the sealed conditions achieved by wrapping the cylinders with three layers of polyfilm. Special care was taken to seal the specimens in order to prevent moisture loss. Air-dried curing was achieved by leaving the specimens in a relative humidity of 50 ± 10% and an ambient temperature of 21 ± 1°C.

The compressive strength tests were carried out at frequent intervals during the

first 24 hours in order to determine the influence of early-age hydration on the stress-strain behaviour and compressive strength gain. Cylinders tested at very early ages (less than 24 hours) were end capped prior to testing using a sulphur based capping compound in accordance with ASTM C 617-87 (1988). This method of end preparation was used for all of the cylinders made with the 30 MPa concrete. After 24 hours, the cylinders made with the 70 and 100 MPa concretes were end faced by grinding since the compressive strength of these concretes is sensitive to the end conditions (Lessard et al (1993)). Due to the complexity involved in measuring the complete stress-strain responses of very early age and high-strength concrete specimens, trial compression tests were conducted using a 225 kN capacity INSTRON testing machine. This machine was not stiff enough to obtain the complete stress-strain response, including the post-peak response, of the high-strength concrete specimens. The compressive testing was repeated using a stiff testing machine (MTS Model 315.03) with a maximum loading capacity of 4600 kN. To determine the compressive strengths at very early ages (i.e., less than 24 hours), more sensitive load cells were used. These load cells had ranges of 2 kN, 22 kN, 178 kN and 335 kN based on the expected strength at the time of testing. All of the specimens were tested under strain control, as recommended by ASTM C 39-86 (1988), to obtain the post-peak responses. Axial strain was measured using MTS extensometers (Model 632.94), with 100 mm gauge lengths, placed on opposite faces of the specimen. A total of about 300, 100 x 200 mm cylinders, were tested in compression for this study.

4.1.2 Compressive Stress-Strain Responses

The effect of different curing conditions, including temperature-matched curing, sealed curing, and air-dried curing on the compressive stress-strain behaviour was studied. Cylinders were tested in compression at frequent intervals within the first 24 hours to determine the concrete compressive stress-strain responses at very early ages. At ages of 1, 2, 3, 7, 14, 21, 28 and 91 days, at least three sealed and three air-dried cylinders were tested. Figures 4.1, 4.2 and 4.3 show the measured compressive stress-strain responses for the 30, 70 and 100 MPa concretes under the three different curing conditions. During the first few hours of hydration the compressive stress-strain

responses exhibit extremely low moduli, low compressive strength and very high strains corresponding to the peak compressive stress. After about 24 hours the stress-strain responses, for all of the concretes, start to resemble the shape of the stress-strain responses at 28 days. These figures demonstrate that the strain at the peak compressive stress, that is, the peak strain, is changing with age as the concrete strength increases. Between an age of 1 day and 28 days the peak strains increased slightly with age. As the compressive strength increases both the ascending and descending portions of the compressive stress-strain responses become both steeper and more linear. It is evident that the high-strength concrete has a higher peak strain than the normal and medium strength concretes (see Fig 4.1, 4.2 and 4.3). All of the air-dried specimens had higher peak strains than companion sealed and temperature-matched cured specimens, probably due to the drying effects. Figures 4.2 and 4.3 demonstrate that once the high-strength concrete specimens have hardened, they display brittle post-peak response. The formation of microcracks in high-strength concrete occurs at much higher stress level than for normal-strength concrete. The rapid formation of microcracks close to the peak stress level results in the more brittle response (Carrasquillo et al (1981)).

4.1.3 Compressive Strength Gain

Figure 4.4 shows the variations of the average compressive strengths of the 30, 70 and 100 MPa concretes for different curing conditions. For a given mix, the temperature-matched curing typically resulted in greater compressive strengths than the sealed curing, which in turn had greater compressive strengths than the air-dried curing. The difference between the average compressive strengths of sealed and air-cured cylinders becomes greater with age. This difference becomes more significant at later ages (i.e., at 28 days) for the 30 and 70 MPa concretes. There was no significant increase in the average compressive strength of air-dried cylinders after 28 days. Figure 4.5 compares the average compressive strength gain at early ages for the three different types of concretes due to different curing conditions. The temperature-matched curing has resulted in high rates of compressive strength gain at early ages. This effect becomes more apparent with increasing compressive strength, which can be due to the higher rate of heat of hydration. The retardation in compressive strength

gain during the first few hours in the medium and high-strength concretes is due to the higher dosages of superplasticizer in these mixes. As soon as the retardation effect diminishes, there is a rapid increase in strength for the 70 and 100 MPa concretes.

4.2 Relationship Between Compressive Strength and Equivalent Age

A number of expressions have been proposed in the literature to describe the relationship between the compressive strength development, as a function of maturity or equivalent age (Laplante (1993), CEB-FIP (1990), Carino (1982), Carino and Tank (1992), Byfors (1980)). The concept of using maturity is discussed in Section 2.1.3. The use of the maturity concept enables the strength gain to be described by a single expression. The maturity concept used in this research is based on the Arrhenius' maturity function, which accounts for the combined effect of temperature histories and age. The 100 x 200 mm cylindrical specimens were cured under temperature-matched, sealed and air-dried conditions. Temperatures were recorded at the centre of these specimens using thermocouples. Figures 4.6, 4.7 and 4.8 show the temperature variation as a function of age and equivalent age (reference temperature of 20°C) for the three concretes, respectively, due to temperature-matched curing. As can be seen from these figures the use of equivalent age results in considerable "stretching-out" of the temperature-time response. Figures 4.9, 4.10 and 4.11 show the temperature variation at the centre of 100 x 200 mm sealed specimens made of normal, medium and high-strength concretes. The maximum recorded temperatures at the centre of cylinders were 25.8°C, 28.3°C and 27.4°C for the normal, medium and high-strength concretes, respectively. As can be seen from Fig. 4.9a, 4.10a and 4.11a the medium and, particularly the high-strength concrete, showed a longer retardation period of hydration reaction than the normal-strength concrete, due to the higher dosages of superplasticizers. The medium and high-strength concretes exhibited retardation periods of about 6 hours and 16 hours after casting, respectively. After the retardation period, the slope of the temperature responses increase with increasing concrete strength. Figures 4.9b, 4.10b and 4.11b compare the temperature history expressed in terms of age and equivalent age at 20°C, calculated using Arrhenius' function. These figures illustrate that, in contrast to the temperature-matched cured specimens, the smaller specimens, subjected to ambient conditions, exhibit only a small

"stretching-out" of the response when equivalent age is used.

In order to predict the compressive strength development with age, it is necessary to account for the effect of temperature history during hydration. The CEB-FIP Code (1990) proposed a relationship between the concrete compressive strength development with age, which accounts for type of cement and curing conditions. This equation does not consider the effect of retarders and admixtures, currently being used in the concrete industry. In this study, the effect of temperature during curing is accounted for by using Arrhenius' equation and the retardation effect is considered by introducing the retardation period, t_r. The following expression is a modified form of the equation recommended by the CEB-FIP Code (1990):

$$f'_c(t) = \exp\left[A\left[1-\left(\frac{28}{t_e-t_r}\right)^{0.5}\right]\right] f'_c \qquad (4.1)$$

where

A = constant depending upon the type of cement used

t_e = equivalent age in days

t_r = retardation period in days

f'_c = mean compressive strength at 28 days

Table 4.1 gives the coefficient A and the retardation period, t_r, for the three different types of concretes used in this study. The values of these terms were determined by regression analyses. The mean 28-day compressive strengths are also given in Table 4.1.

It must be pointed out that the CEB-FIP Code (1990) recommends a coefficient of 0.25 for normal and rapid-hardening concretes. The coefficient determined from this study for the normal-strength concrete is also 0.25. From Table 4.1, it is evident that as the concrete strength increases the factor A decreases and the retardation period, t_r, normally increases. Figures 4.12, 4.13 and 4.14 show the compressive strength development, at early ages, for both real age as well as equivalent age for the 30, 70 and 100 MPa concrete cylinders. From Figs 4.12b, 4.13b and 4.14b, it is evident that the use of equivalent age significantly reduces the scatter of the test results, particularly at early ages where temperature has significant influence on the rate of strength gain. The predicted strengths using the modified CEB-FIP Code (1990)

expression, Eq (4.1), are also shown for the early-age concretes. As can be seen from these figures there is good agreement between the experimental results and the predicted values, particularly for the temperature-matched and sealed specimens. It must be pointed out that the effect of drying was considered by using the 28-day strength of air-dried specimens in Equation (4.1) for ages above 1 day (i.e., time of demolding). In Figs 4.12b, 4.13b and 4.14b, the dashed lines represent the strength predictions for the air-dried specimens. These predictions demonstrate that as the concrete strength increases there is a smaller drop in the strength due to drying of the denser matrix.

4.3 Elastic Modulus of Normal, Medium and High-Strength Concretes

The chord elastic modulus was calculated from the measured stress-strain responses, in accordance with ASTM C 469-87 (1988), for the three different concretes. Figure 4.15 shows the variation of the average chord elastic modulus for the 30, 70 and 100 MPa concretes due to temperature-matched, sealed and air-dried curing conditions. As can be seen, the elastic modulus increases very rapidly at very early ages. The temperature-matched curing resulted in a higher rate of modulus gain than the sealed and air-cured cylinders at early ages. As expected, the sealed curing resulted in higher moduli than air-dried curing, particularly at later ages. The lower moduli of air-cured cylinders has been attributed to the influence of drying (Shah and Ahmad (1985) and Burg and Ost (1992)). It is also noted that the elastic moduli of specimens is more affected by drying than the compressive strength, particularly for 30 MPa concretes. This may be due to the higher permeability of the normal-strength concrete.

Figure 4.16 shows the comparison of the average modulus gain at very early ages for the three different types of concretes. The temperature-matched curing has resulted in high rates of modulus gain during the first 24 hours. This effect became more apparent with increasing compressive strength and after the effect of the retarders diminished.

4.3.1 Relationship Between Elastic Modulus and Concrete Compressive Strength

Figure 4.17 shows the variation of the average modulus versus the average

compressive strength from very early ages to an age of 91 days. Also shown in this figure are the values of the modulus predicted using the expression given in the ACI Code (1983) as well as those predicted using the expression developed by Carrasquillo et al (1981) and also recommended by ACI Committee 363 (1992). The overestimation of the modulus for the very low strength data shown in Fig 4.17 indicates that the ACI code expression may not be appropriate for very early age concrete. The ACI code expression provides a reasonable estimate of the stiffness for strengths up to about 50 MPa, but overestimates the stiffness for higher concrete strengths and for concretes at very early ages. On the other hand, the ACI 363 expression provides a conservative estimate of the average stiffness for higher concrete strengths.

The 1994 CSA A23.3 Standard points out the influence of aggregates on the modulus of elasticity and introduced two expressions for the elastic modulus. The 1994 CSA expression which applies for a wide range of concrete compressive strength is based on the equation developed by Carrasquillo et al (1981). The 1994 CSA Standard also introduced the following simplified expression for concrete compressive strengths between 20 and 40 MPa:

$$E_c = 4500\sqrt{f'_c} \quad \text{for } 20 \leq f'_c \geq 40\text{MPa} \tag{4.2}$$

where

f'_c = specified concrete compressive strength at 28 days

This simplified expression is plotted in Fig 4.17. It is clear that this expression provides a more reasonable estimate for the lower strength concretes than the ACI 363 expression or the 1983 ACI Code expression. The ACI 363 and the CSA Simplified expressions give identical results for concrete strengths equal to 36 MPa.

In order to predict the elastic modulus and accommodate a wide range of variables, the following expressions are proposed:

$$E_c(t) = 4500\sqrt{f'_c(t)} \quad \text{for } f'_c \leq 36\text{MPa} \tag{4.3a}$$

and

$$E_c(t) = (3320\sqrt{f'_c(t)} + 6900) \quad \text{for } f'_c(t) > 36\text{MPa} \tag{4.3b}$$

where

$f'_c(t)$ = concrete compressive strength at time t

$E_c(t)$ = elastic modulus of concrete at time t

Figure 4.18 shows the test data along with the prediction from Equation (4.3). It is apparent that these two expressions provide reasonable estimates of the mean chord elastic modulus over a wide range of variables including type of concrete, concrete compressive strength, curing conditions and concrete ages.

4.4 Tensile Strength of Normal, Medium and High-Strength Concretes

4.4.1 Experimental Program

The prevention and control of early-age thermal cracking of concrete is a major concern in many structures. Due to the heat of hydration, significant strain gradients are usually developed which in turn cause tensile stresses due to restraint effects. These restraint tensile stresses typically have a high gradient in structural members. Hence the modulus of rupture test, which subjects flexural specimens to a significant strain gradient, was chosen over the split-cylinder test to determine an appropriate tensile strength.

Tests were carried out on 175 beam specimens, 100 x 100 x 400 mm long, made of normal, medium and high-strength concretes. These tests enabled a study of early age tensile strength gain for the normal, medium and high-strength concretes. Tests were carried out at frequent intervals during the first 3 days after casting to observe the influence of concrete strength and curing conditions from very early age up to 91 days. The curing conditions included temperature-matched curing, sealed curing and air-dried curing.

The flexural beams were cast in specially designed molds, made of acrylic, to enable rapid demolding at very early ages without disturbing the concrete samples. For the sealed and air-dried curing, the control cylinders and flexural beams were demolded at 24 hours. All of the concrete specimens were hand rodded in accordance with

ASTM C 31-88 (1988). For temperature-matched curing the flexural beam specimens, together with a 100 x 200 mm cylinder used to control the temperature-matched curing, were vacuum sealed with thick plastic and placed in the temperature-matched curing bath immediately after casting. The sealed conditions were achieved by wrapping the specimens with three layers of polyethylene immediately after demolding, and were kept at ambient temperature of 21 ± 1°C . The air-dried specimens were cured in a relative humidity of 50 ± 10% and an ambient temperature of 21 ± 1°C after demolding. All of the specimens were covered with polyethylene until they were removed from the molds in order to minimize moisture loss. The modulus of rupture values were determined by loading each beam, over a 300 mm long span, with two-point loads producing a 100 mm long constant moment region.

4.4.2 Tensile Strength Variation with Age

All of the specimens were tested at frequent intervals during the first 24 hours. The specimens subjected to temperature-matched curing were tested over a period of about 3 days. At ages of 1, 3, 7, 14, 21, 28 and 91 days, at least two sealed and two air-dried specimens were tested. Figure 4.19 shows the variations of the average flexural strengths of the 30 MPa, 70 MPa and 100 MPa concretes under temperature-matched curing, sealed curing and air-dried curing. For a given concrete mix, specimens with temperature-matched curing typically resulted in significantly greater flexural strengths than the specimens with sealed curing and air-dried curing. This is particularly apparent during the first three days. After demolding and up to an age of about 28 days, the sealed flexural beam specimens showed higher tensile strength than companion air-dried specimens. The test data indicates that beyond 28 days this difference in tensile strength diminishes.

Figure 4.20 shows the comparison of average flexural strength gain at early ages for three different concrete mixes subjected to three different curing conditions. After an initial retardation period, the rate of flexural strength gain increases with increasing concrete compressive strength. After demolding, the specimens subjected to air-dried curing resulted in lower modulus of rupture values than the specimens subjected to sealed curing. This was particularly evident for the high-strength concrete, which may be more sensitive to drying effects due to its very low water-

cement ratio and its smaller size of aggregates. The smaller aggregate size results in a larger interfacial surface area or transition zone which may be more sensitive to drying.

4.4.3 Relationship Between Modulus of Rupture and Concrete Compressive Strength

Figure 4.21 shows the variation of the average modulus of rupture versus the average concrete compressive strength. The data includes the test results from very early ages to an age of 91 days and includes data from the three types of concrete and curing conditions. Also shown in this figure are the values of the modulus of rupture predicted using the expression given in the 1983 ACI Code as well as those values predicted using the ACI Committee 363 expression (1992). The ACI code expression is used for comparison purposes only, since it was originally intended to apply to mature concrete (i.e., 28-day concrete). Although the ACI 363 expression was intended for concrete compressive strengths ranging from 21 MPa to 83 MPa, it was used in Fig. 4.21 to predict values over a wider range. Predicted values using the ACI Code expression are also shown for a wide range of concrete compressive strengths. The ACI code expression overestimates the modulus of rupture for concrete compressive strength less than about 15 MPa at very early ages. The ACI Code expression also underestimates the modulus of rupture above about 30 MPa. It can also be seen that the empirical equation proposed by ACI Committee 363 overestimates the modulus of rupture for all types of concretes and curing conditions except for some of the specimens with temperature-matched curing. Figure 4.22 shows the relationship between the modulus of rupture values and the corresponding compressive strengths for the three different concrete mixes, all subjected to temperature-matched curing. For this particular curing condition, a linear relationship between the modulus of rupture and the concrete compressive strength provides a conservative fit to the data. This relationship for the modulus of rupture, $f_r(t)$, at a particular time t, can be expressed as:

$$f_r(t) = 0.085\, f'_c(t) \qquad (4.4)$$

Figure 4.23 presents the relationships between the modulus of rupture and the concrete compressive strength for sealed and air-dried curing conditions. Using the

form of the relationship between the modulus of rupture and compressive strength suggested by Shah and Ahmad (1985) gives:

$$f_r(t) = k\,(f'_c(t))^{2/3} \qquad (4.5)$$

From non-linear regression analyses using SAS (1985), the factor k was found to be 0.4 and 0.38 for sealed and air-dried curing conditions, respectively. The lower and upper bound 95% confidence interval limits are also presented for temperature-matched, sealed and air-dried curings (see Fig. 4.22 and Fig. 4.23).

As expected, air-dried curing resulted in lower modulus of rupture values than the sealed curing for the same value of concrete compressive strength. This reduced tensile strength for the air-dried curing is significant over a time period from demolding (i.e., an age of 1 day) up to about 28 days. This effect is more apparent for high-strength concrete, due to its very low water-cement ratio is very sensitive to drying effects.

4.5 Creep and Shrinkage of Normal, Medium and High-Strength Concretes During Hydration

During the hydration process, significant thermal and shrinkage gradients can cause stresses which could lead to cracking of concrete at early ages. The presence of creep during the hydration period, that is at very early ages, would have an effect of reducing these stresses. During hydration when temperatures are increasing, tensile stresses develop near the concrete surface where the temperature is lower and compressive stresses develop at the centre where higher temperatures exist. In addition, specimens with exposed surfaces would exhibit higher shrinkage strains at the surface, which causes tensile stresses near the surface and compressive stresses at the centre. During this phase the concrete has low strength, low elastic modulus and significant early-age creep. Although the tensile strength of the concrete is low, the combined effect of low modulus and high creep will significantly reduce the tendency for surface cracking. When the centre of the concrete starts cooling, the stresses due to thermal gradients cause the reverse effect, with reduced compressive stresses and perhaps even tensile stresses developing at the centre of the concrete. During this phase the concrete strength is higher, resulting in an increased modulus of

elasticity and lower creep. Thus it is important to study the early-age creep and shrinkage of concrete in order to accurately predict the resulting stresses due to heat of hydration. As discussed in Sections 2.2.7 and 2.2.8, extensive research on creep of mature concrete has been carried out, but very little research has been conducted on creep and shrinkage of early-age concrete and in particular for high-strength concrete.

4.5.1 Experimental Program

The details of the composition and some of the fresh concrete properties of the three concrete mixes used in this testing program are presented in Table 3.1. The coarse aggregate to cement and fine aggregate to cement proportions (by weight) were 2.93 and 2.22 for the 30 MPa concrete, 2.25 and 1.80 for the 70 MPa concrete, and 2.05 and 1.33 for the 100 MPa concrete, respectively. Two different curing methods (i.e., sealed curing and air-dried curing) were used. The cylinders were demolded just before placing in the creep frame and companion unloaded specimens were left in the same ambient conditions for shrinkage and thermal strain measurements. Specimens were tested for short-term loading using a stiff MTS rock testing machine to measure the concrete compressive strength just before loading the creep specimens. Special care was taken in handling and testing the specimens. The stress level applied to the specimens varied from 5 to 22 percent of the measured concrete compressive strength at the time of loading.

Six creep frames were made to study the creep of the 100 x 200 mm cylinders for both sealed and air-dried conditions (see Fig. 4.24). These frames used a lever system to ensure constant load on the test specimens and to enable rapid placement of the specimens in the test frame. Each frame was calibrated using a 5000 lb load cell. The pin connection was greased to reduce friction. Concrete strains were measured with a specially designed apparatus, which contained two aluminum alloy yokes, mounting points, an aluminum control rod and a very sensitive dial indicator. The apparatus was mounted on each cylinder to form a gauge length of 100 mm. The top yoke was hinged to permit rotation. The dial indicator used had a full range of 5 mm and minimum graduation of 0.001 mm. The total strain, ϵ_c, measured on the creep specimens includes the instantaneous strain, ϵ_{co}, the creep strain, ϵ_{creep}, the

shrinkage strain, ϵ_{sh}, and the thermal strain, ϵ_{th}, of the hydrating concrete. The companion unloaded specimens were subjected to the same curing conditions and were instrumented to measure the combined effects of shrinkage and thermal strains. Thus the creep strain can be determined at any time by subtracting the shrinkage, thermal and instantaneous strains from the total measured strain on the creep specimens.

4.5.2 Creep, Shrinkage and Thermal Strains Development with Age During Hydration

The time-dependent strain results are summarized in Table 4.2 for the normal, medium and high-strength concretes. The loads on the creep specimens were sustained for about 28 days.

Figure 4.25 shows the variation of shrinkage and thermal strains for the normal (30 MPa), medium (70 MPa) and high-strength (100 MPa) concretes subjected to sealed and air-dried curing. Measurements were taken on the cylinders after the concrete started to harden, several hours after casting. During the measurment of these strains, the ambient temperature was kept constant at about 20°C. Due to the heat of hydration, there would be some thermal strains, however these would be quite small after the demolding of the cylinders. The measured 28-day shrinkage and thermal strains of the specimens subjected to sealed curing were about 33%, 43% and 62% of the shrinkage and thermal strains of the air-dried specimens for the normal, medium and high-strength concrete, respectively. The test results show that the high-strength concrete exhibits greater shrinkage and thermal strains than the medium-strength concrete, which in turn shows greater strains than the normal-strength concrete for both the sealed and air-dried conditions. This may be due to the smaller aggregate-cement ratio and the addition of silica fume in the higher strength concretes. Demolding the specimens at 24 hours after casting has shown about 17% and 22% less shrinkage and thermal strains, at 20 days, than the specimens demolded at 19.5 hours (see Fig. 4.26).

Figures 4.27, 4.28 and 4.29 show the variation of the total strains (i.e., instantaneous, creep, shrinkage and thermal strains) with time for specimens loaded at very early ages for the normal (30 MPa), medium (70 MPa) and high-strength (100 MPa) concretes. The applied stress to strength ratios at the time of loading varied from

18.5% to 22% for the normal-strength concrete, 8.8% to 9% for the medium-strength concrete and 5% to 9.6% for the high-strength concrete. It can be seen from these figures that the strain rate for the normal-strength concrete, subjected to sealed curing, stabilized more quickly than the medium and high-strength concretes.

Figures 4.30, 4.31 and 4.32 show the variations of creep strains, including the initial elastic strains, with time under load, $t-t_o$, for the normal, medium and high-strength concretes. These responses are given for sealed and air-dried conditions and for different ages of loading, t_o. It can be seen from these figures that, as expected, the specimens subjected to air-dried curing had higher creep strains than the sealed specimens. In particular, this difference is significantly higher for the normal-strength and high-strength concrete specimens subjected to loading at very early ages. The medium-strength concrete did not exhibit such a large difference in creep strains between the air-dried and sealed conditions, perhaps due to a smaller amount of superplasticizer than the high-strength concrete, resulting in more rapid strength gain at very early ages. Figures 4.30, 4.31 and 4.32 also show that the creep strains decrease with an increase in the concrete compressive strength at the time of loading. It can be seen from Fig. 4.32a that the creep of the high-strength concrete is much more sensitive to the age of loading than the normal and medium-strength concretes, with very early age loading resulting in significantly higher creep. This phenomenon may be due to the large dosage of superplasticizer, the low aggregate to cement ratio and the small sized aggregates. High-strength concrete mixes which contain naphthalene-based high-range water reducers can result in higher creep of the mature concrete (Shah and Ahmad (1994)). In Figs 4.30, 4.31 and 4.32 comparisons are also made between the test results and the predicted creep functions (i.e., the sum of elastic and creep strains per unit applied stress). The creep functions were predicted using the CEB-FIP Code expressions (1990). The stress dependent strain, ϵ_{cf}, is described by CEB-FIP Code (1990) in the following form:

$$\epsilon_{cf} = f_{co}\left[\frac{1}{E_{co}} + \frac{\phi(t,t_o)}{E_c}\right] = f_{co}\,J(t,t_o) \qquad (4.6)$$

where

f_{co} = applied stress at t_o

E_{co} = elastic modulus at t_o

$\phi(t,t_o)$ = creep coefficient

t = age of concrete at the time under consideration

t_o = age at loading

E_c = elastic modulus at 28 days

$J(t,t_o)$ = creep function representing the total stress dependent strain per unit applied stress.

The creep coefficient at time t, $\phi(t,t_o)$, when the concrete is loaded at t_o can be estimated as:

$$\phi(t,t_o) = \phi(RH).\beta(f'_c).\beta(t_o).\beta_c(t-t_o) \tag{4.7}$$

where

$$\phi(RH) = 1 + \frac{1-\frac{RH}{RH_o}}{0.46(\frac{h}{h_o})^{1/3}} \tag{4.8}$$

$$\beta(f'_c) = \frac{5.3}{(f'_c/10)^{0.5}} \tag{4.9}$$

$$\beta(t_o) = \frac{1}{0.1+(t_o/t_1)^{0.2}} \tag{4.10}$$

$$\beta_c(t-t_o) = \left[\frac{(t-t_o)/t_1}{\beta_H+(t-t_o)/t_1}\right]^{0.3} \tag{4.11}$$

with

$$\beta_H = 150\left[1+(1.2\frac{RH}{RH_o})^{18}\right]\frac{h}{h_o}+250 \leq 1500 \tag{4.12}$$

where

RH = relative humidity of the ambient environment (%)

RH_o = 100%

h = $2A_c/u$; A_c is the cross sectional area (mm^2) and u is the

perimeter of the member in contact with the atmosphere (mm)

f'_c = concrete compressive strength at 28 days in MPa

t_1 = 1 day

h_o = 100 mm

It can be seen that these predictions agree reasonably well with the measured creep strains of the normal and medium-strength concretes. It is clear from Figs 4.32a and 4.32b that the measured creep strains are significantly higher than the predicted creep strains for the high-strength concrete loaded before an age of 24 hours. Figs 4.32c and 4.32d illustrate that the predictions agree well with the measured creep strains once the concrete has reached about one-third of the 28-day strength at the time of loading.

4.6 Reproducibility of Compressive Strength Development and Measured Creep and Shrinkage Strains

A series of tests were carried out to determine the reproducibility of the test results. The mix proportions, mixing procedure, testing apparatus and procedure, and curing technique were the same as the initial mixes (batch 1) and details are explained in Chapter 3. Figures 4.33 and 4.34 show the temperature variation at the centre of 100 x 200 mm cylinders made of medium and high-strength concretes, respectively. Figure 4.33 shows an excellent repeatability between the two batches. The high-strength concrete (batch 2) has shown a smaller retardation period than the batch 1 concrete, due to smaller amount of superplasticizer used (see Fig. 4.34). On the other hand, the specimens of both batches gave almost the same peak temperatures.

Figures 4.35a and 4.35b show the variations of the average compressive strength of normal-strength concrete with age due to temperature-matched and sealed curing, respectively. Figures 4.36 and 4.37 show the variations of average compressive strength and elastic modulus of high-strength concrete due to air-dried curing, respectively. These figures demonstrate that fairly good repeatability of the test data was achieved. A series of tests was also repeated for creep, shrinkage and thermal strains for the high-strength concrete specimens to substantiate the sensitivity of these strains to the amount of superplasticizer. It must be pointed out that the amount of superplasticizer used in the repeated mix (batch 2) was 35% more than that

of the original batch (batch 1, see Table 3.1). Figure 4.38 compares the variation of shrinkage and thermal strains with age for both of these batches, made of high-strength concrete. The specimens for shrinkage were demolded at 19.6 hours after casting, which was slightly higher than the original batch. Batch 2 exhibited slightly less shrinkage and thermal strains values than the original batch, particularly for the air-dried specimen. Figure 4.39 shows the variation of total strains with time for the high-strength concrete loaded at different ages. The results of the sealed specimen loaded at 23.8 hours after casting are not presented in Fig. 4.39c due to inadequate sealing. The repeated tests exhibited higher total strains than the original tests for the same age of loading. This is due to the higher dosage of superplasticizer in batch 2.

4.7 Special Consideration for Creep of High-Strength Concrete Loaded at Very Early Ages

In this study, it was observed that high-strength concrete loaded after about 24 hours exhibited creep which can be predicted well by the CEB-FIP (1990) creep expression. However, the presence of naphthalene based superplasticizer together with loading before 24 hours and subjected to air-dried curing resulted in significantly increased values of creep (see Fig. 4.32a and 4.32b) than those predicted. Although more research is required to quantify these effects on the creep. It is suggested that in the interim the values from the CEB-FIP expression be multiplied by a factor varying from 2.5 to 4.5 for ages of 22 hours and 19.5 hours, respectively, to account for the combined effects listed above. These increased values of creep at very early ages of loading would result in a reduction of restraint stresses and would therefore be beneficial in reducing the risk of cracking during hydration.

Table 4.1 - Values of terms used in Eq. (4.1) for determining the variation of concrete compressive strength with time

Concrete Type	A	t_r (days)	f'_c (sealed) (MPa)	f'_c (air-dried) (MPa)
normal-strength (30 MPa)	0.25	0.25	28.0	22.2
medium-strength (70 MPa)	0.15	0.28	77.0	65.4
high-strength (100 MPa)	0.13	0.60	99.2	95.7

Table 4.2 - Summary of time dependent strain data

t_o (hours)	f'_{co} at t_o (MPa)	f_{co}/f'_{co} at t_o	curing	ϵ_{co} at t_o (10^{-6})	t_f (hours)	ϵ_c at t_f (10^{-6})	$\epsilon_{sh} + \epsilon_{sh}$ at t_f (10^{-6})	ϵ_{creep} at t_f (10^{-6})	φ at t_f	J at t_f (10^{-6}/MPa)
Normal-Strength Concrete (30 MPa)										
16.25	9.46	0.185	sealed air-dried	115 130	451	300 735	117 400	68 205	0.59 1.58	39 117
21.25	11.17	0.223	sealed air-dried	135 150	678	395 795	132 448	128 197	0.95 1.31	51 79
25.0	12.00	0.196	sealed air-dried	115 160	674	320 1095	125 440	80 495	0.69 3.09	34 210
30.5	16.00	0.190	sealed air-dried	130 150	669	335 875	120 440	85 285	0.65 1.90	28 94
Medium-Strength Concrete (70 MPa)										
11.25	25.4	0.088	sealed air-dried	75 65	708	425 855	235 540	115 250	1.53 3.85	52 112
13.02	29.0	0.090	sealed air-dried	80 95	707	460 800	235 540	145 165	1.81 1.74	54 62
15.75	35.4	0.089	sealed air-dried	90 75	704	390 805	230 525	70 205	0.78 2.73	22 65
High-Strength Concrete (100 MPa)										
19.53	15.73	0.096	sealed air-dried	60 75	741	575 980	350 570	165 335	2.75 4.47	109 222
22.13	23.00	0.088	sealed air-dried	70 55	738	540 845	340 550	130 240	1.86 4.36	64 118
25.10	37.50	0.095	sealed air-dried	100 100	735	545 895	335 535	110 260	1.10 2.60	31 73
89.50	71.40	0.050	sealed air-dried	85 80	693	330 505	210 340	120 165	1.41 2.06	33 46

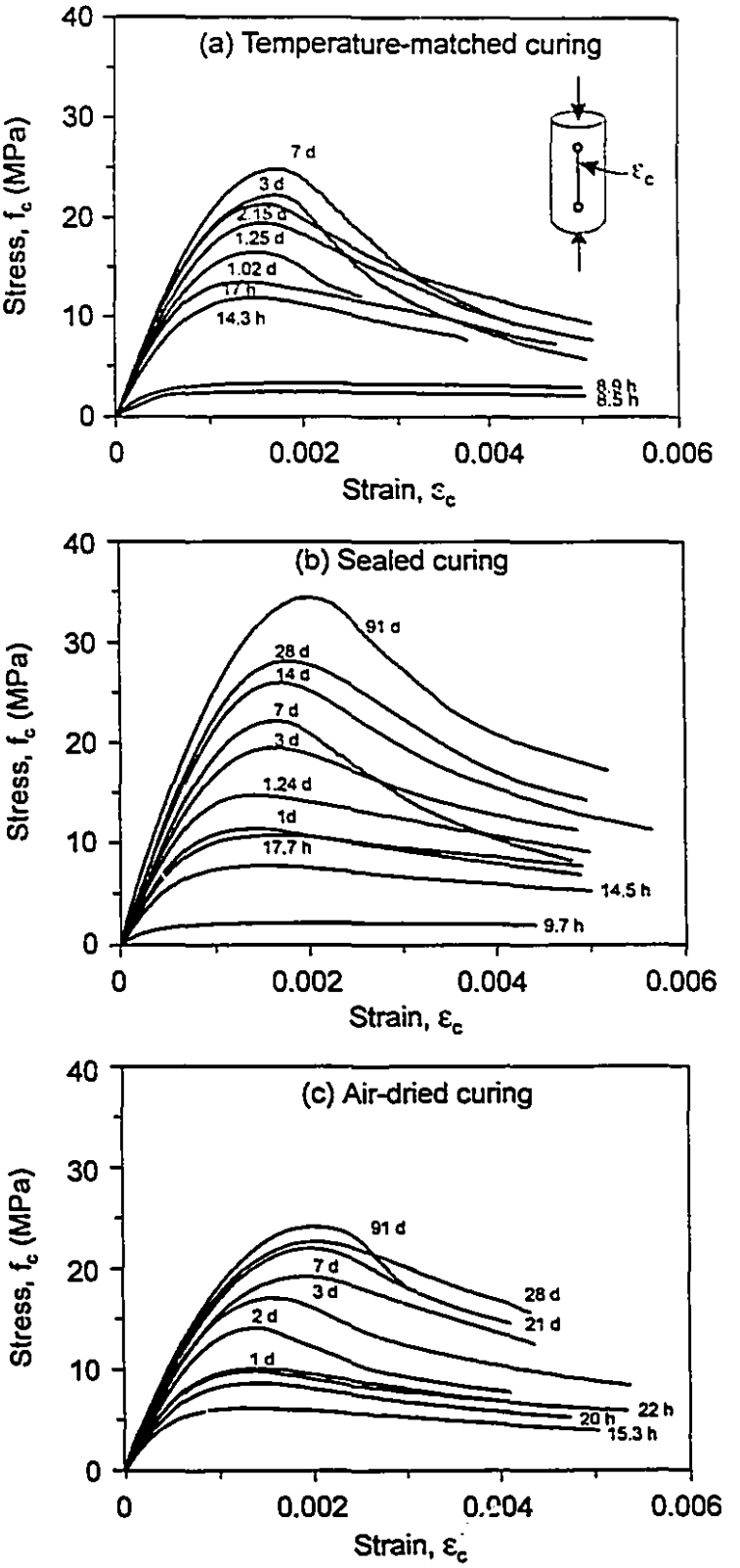

Figure 4.1 - Compressive stress-strain responses of 30 MPa concrete for three different curing conditions

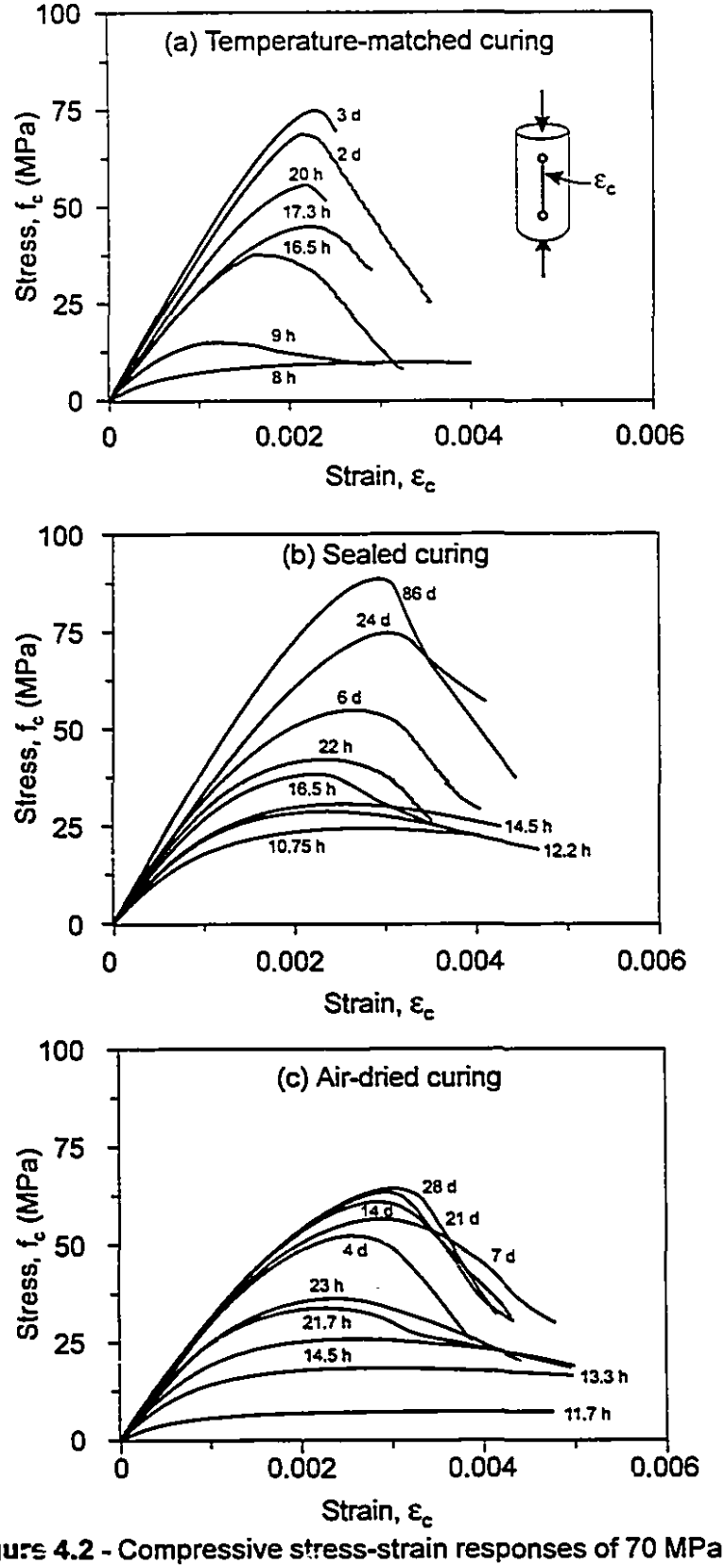

Figure 4.2 - Compressive stress-strain responses of 70 MPa concrete for three different curing conditions

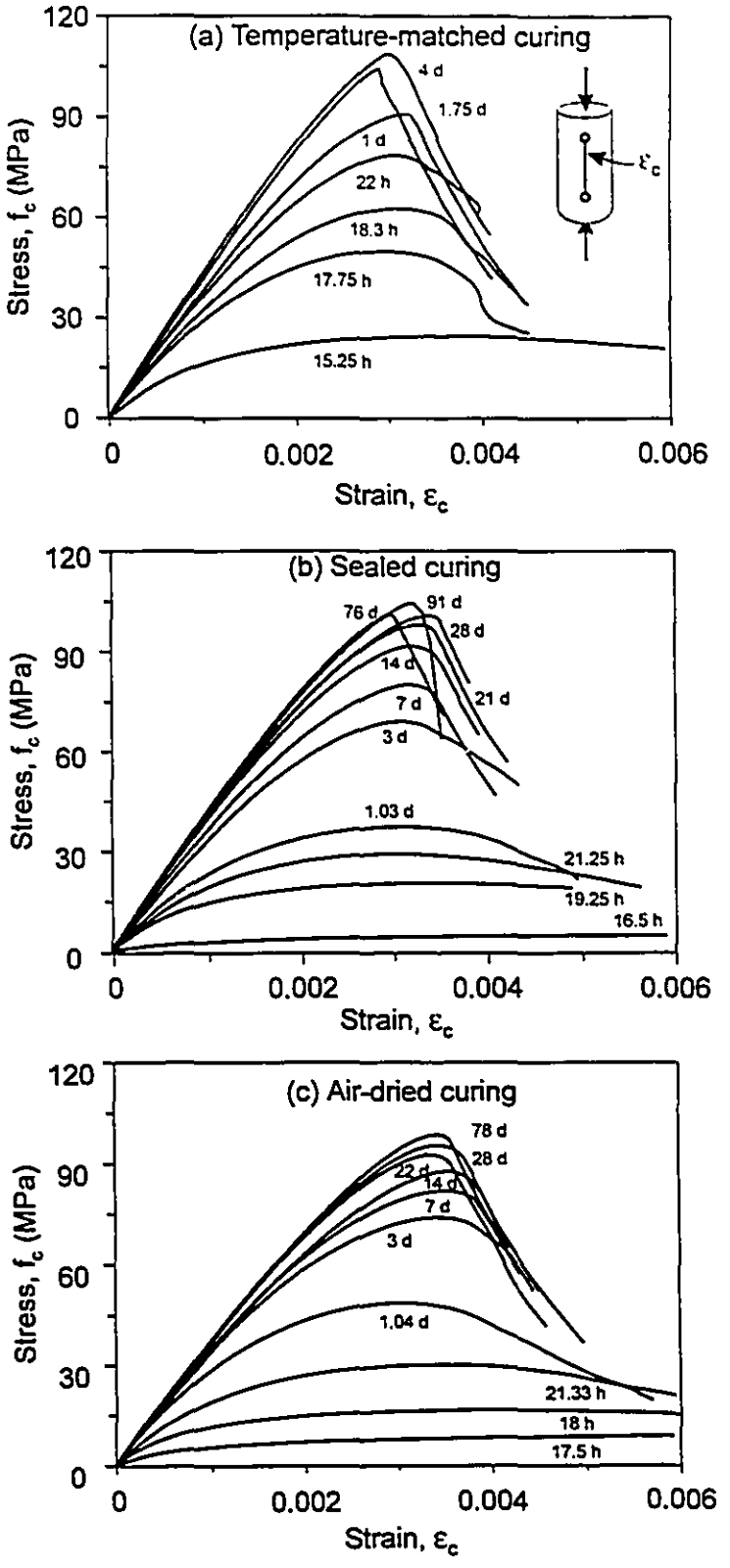

Figure 4.3 - Compressive stress-strain responses of 100 MPa concrete for three different curing conditions

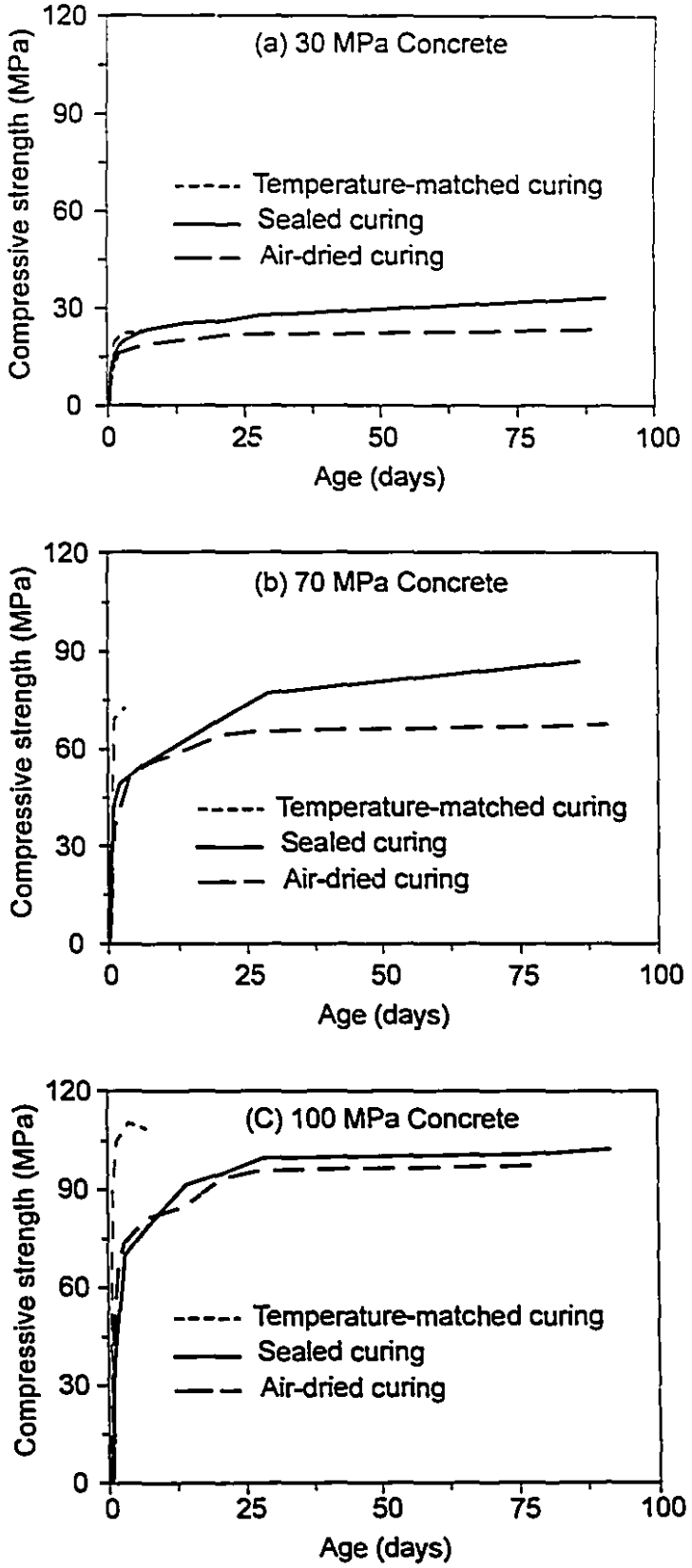

Figure 4.4 - Effect of different curing conditions on the variation of average compressive strength

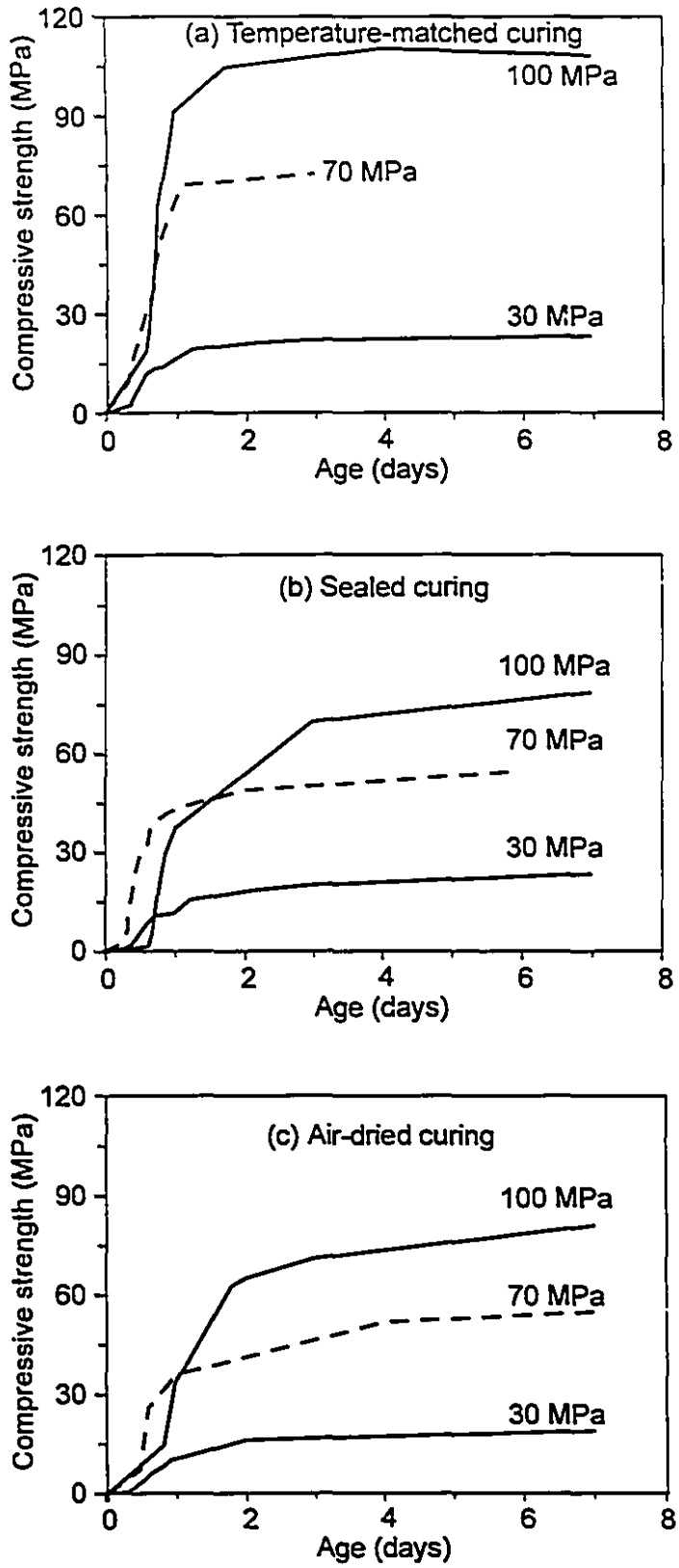

Figure 4.5 - Effect of different curing conditions on the variation of average compressive strength at early ages

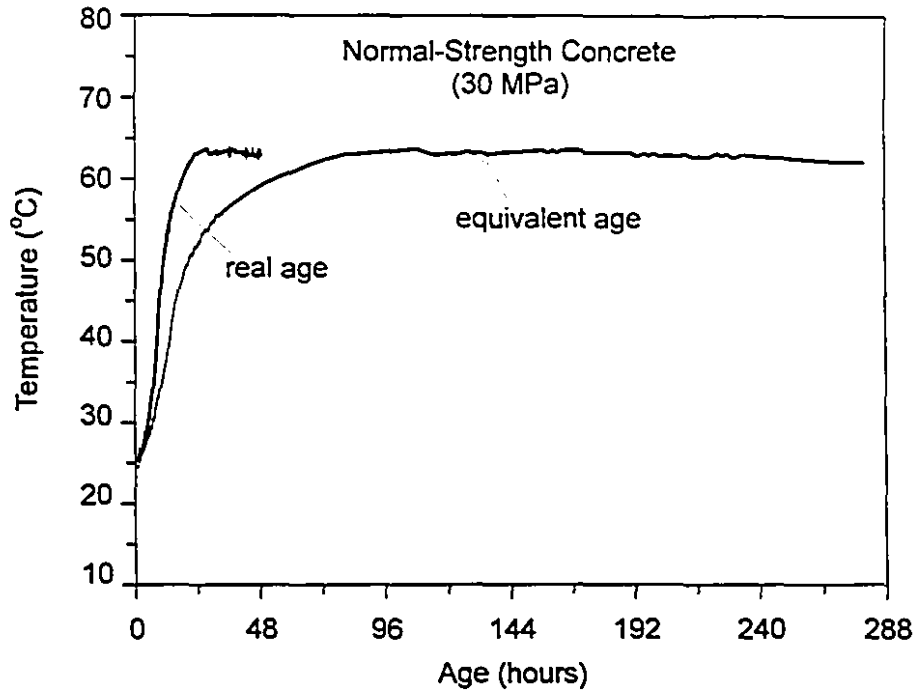

Figure 4.6 - Temperature variation in a temperature-matched cylinder of 30 MPa concrete for both real and equivalent ages

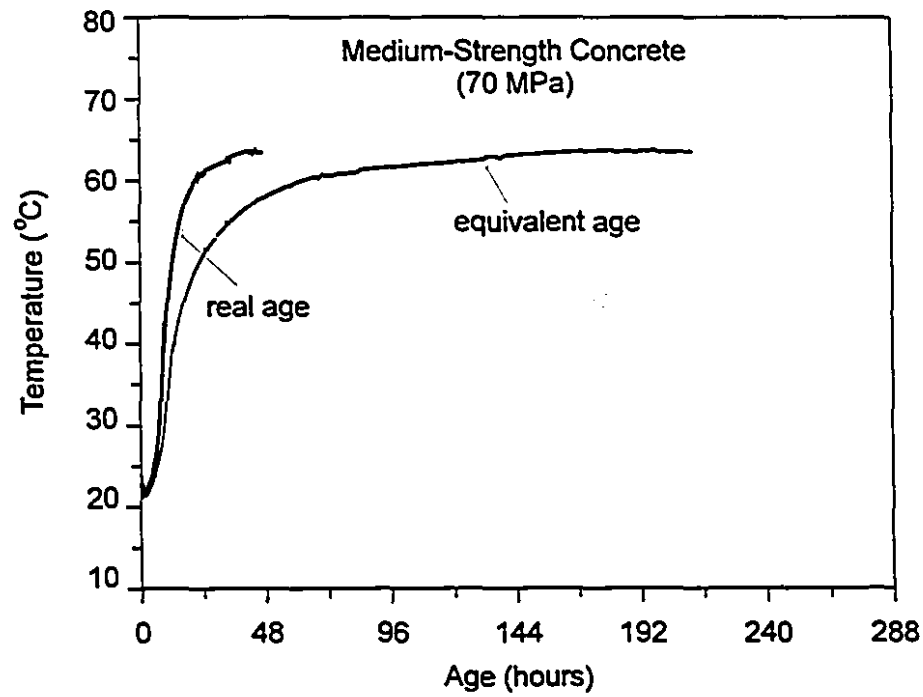

Figure 4.7 - Temperature variation in a temperature-matched cylinder of 70 MPa concrete for both real and equivalent ages

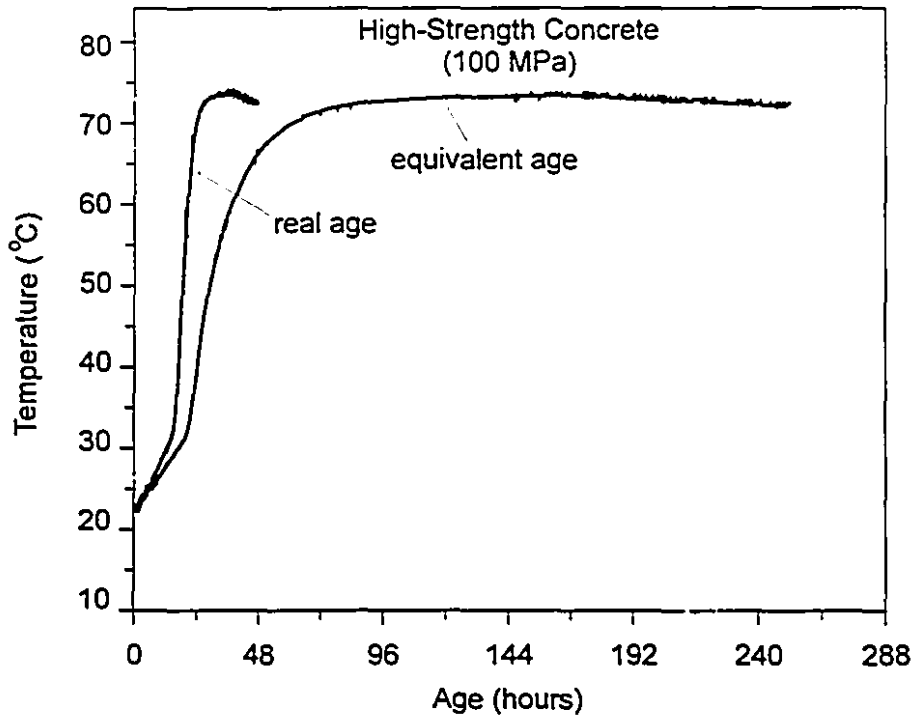

Figure 4.8 - Temperature variation in a temperature-matched cylinder of 100 MPa concrete for both real and equivalent ages

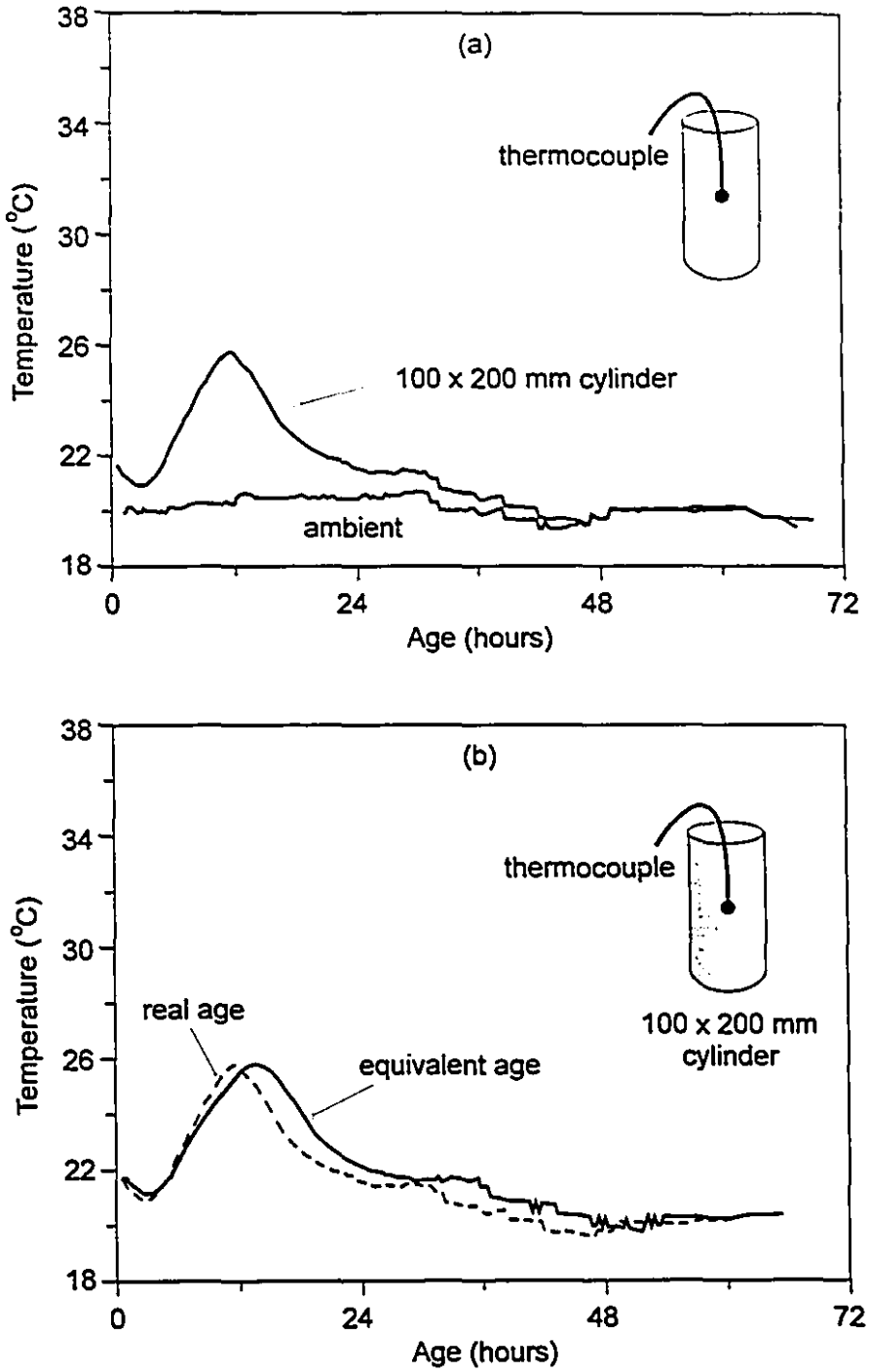

Figure 4.9 - Temperature variation in a sealed cylinder of 30 MPa concrete (a) real age (b) real age and equivalent age

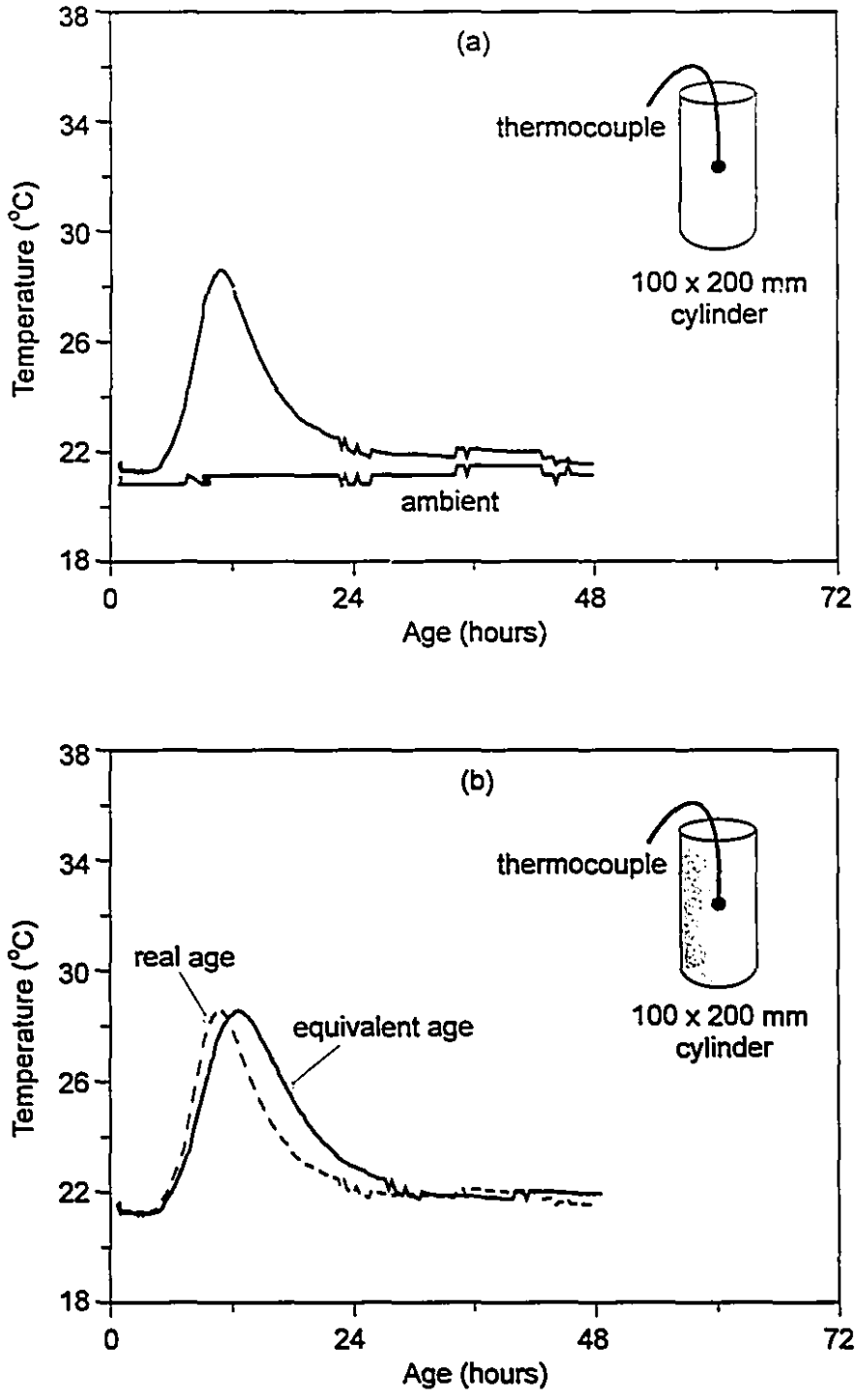

Figure 4.10 - Temperature variation in a sealed cylinder of 70 MPa concrete (a) real age (b) real age and equivalent age

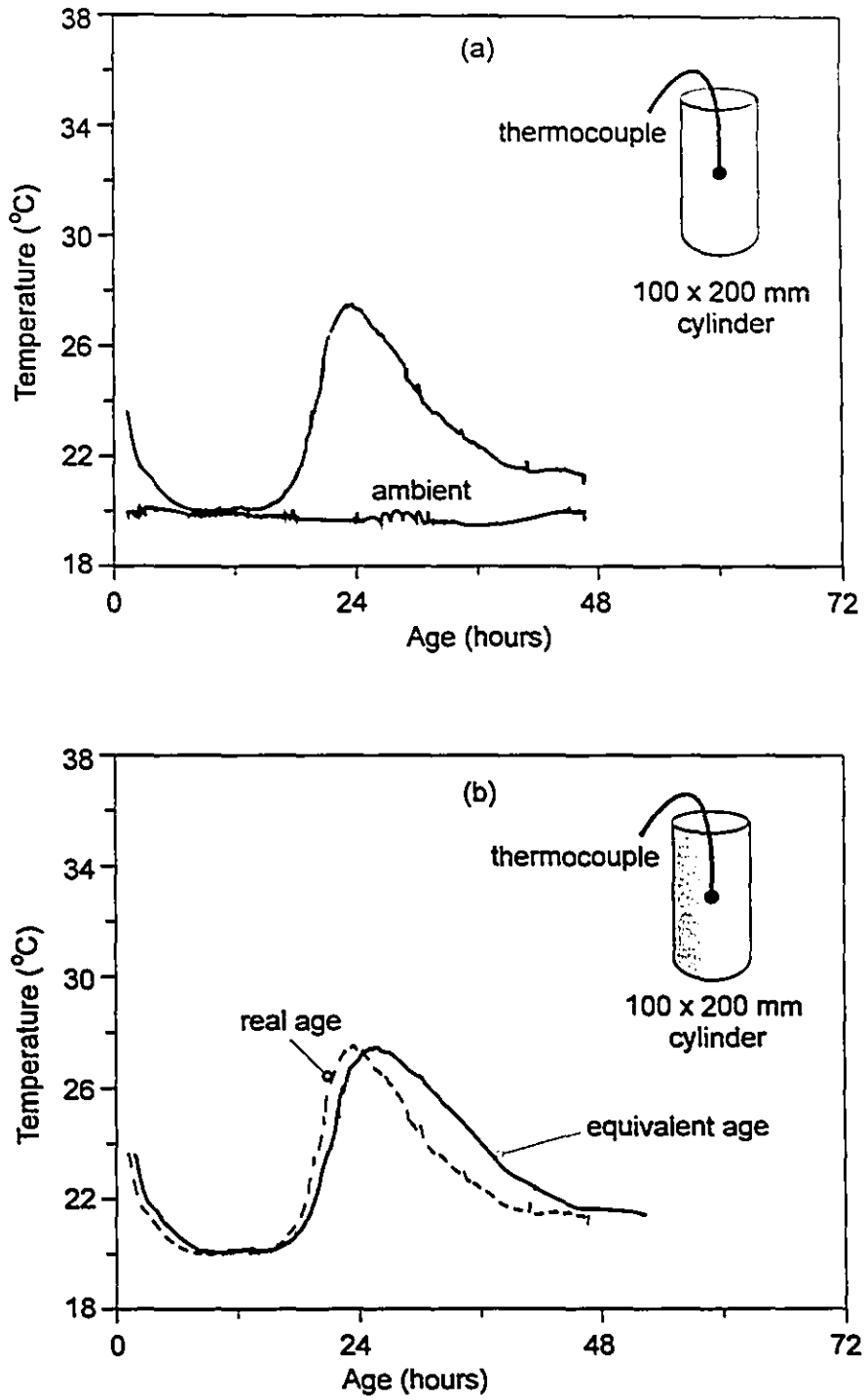

Figure 4.11 - Temperature variation in a sealed cylinder of 100 MPa concrete (a) real age (b) real age and equivalent age

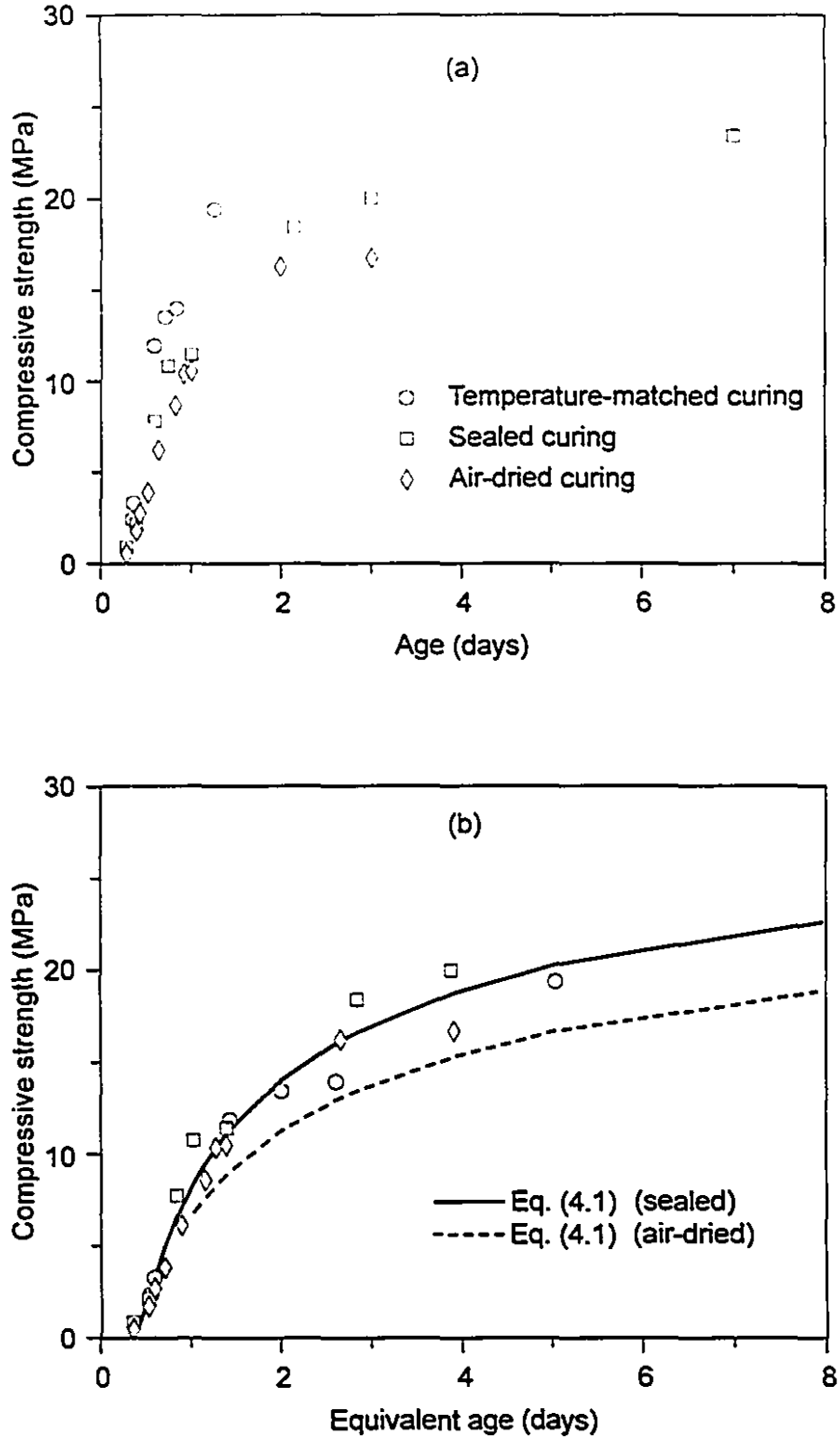

Figure 4.12 - Compressive strength development of 30 MPa concrete (a) vs. real age (b) vs. equivalent age

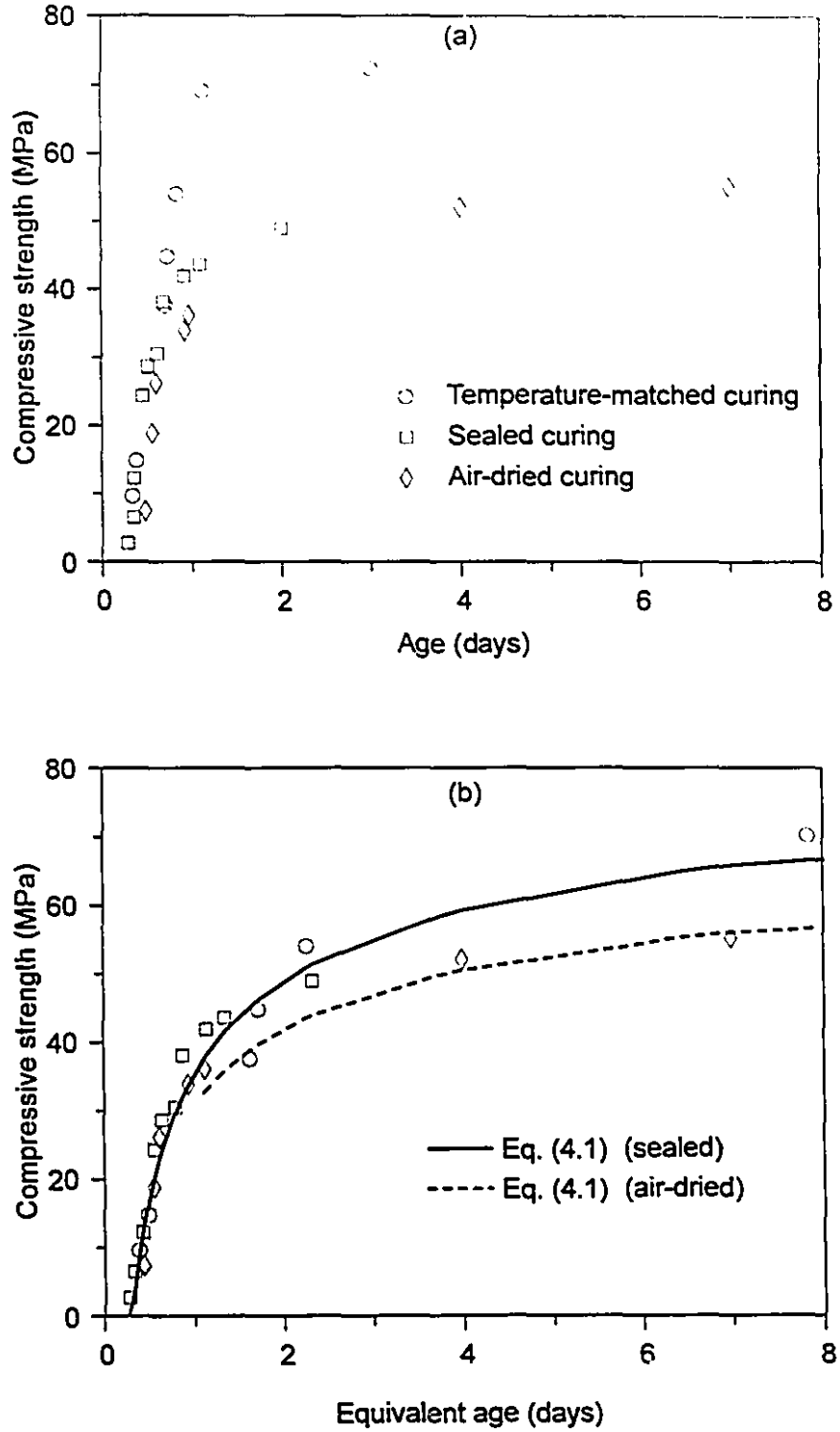

Figure 4.13 - Compressive strength development of 70 MPa concrete (a) vs. real age (b) vs. equivalent age

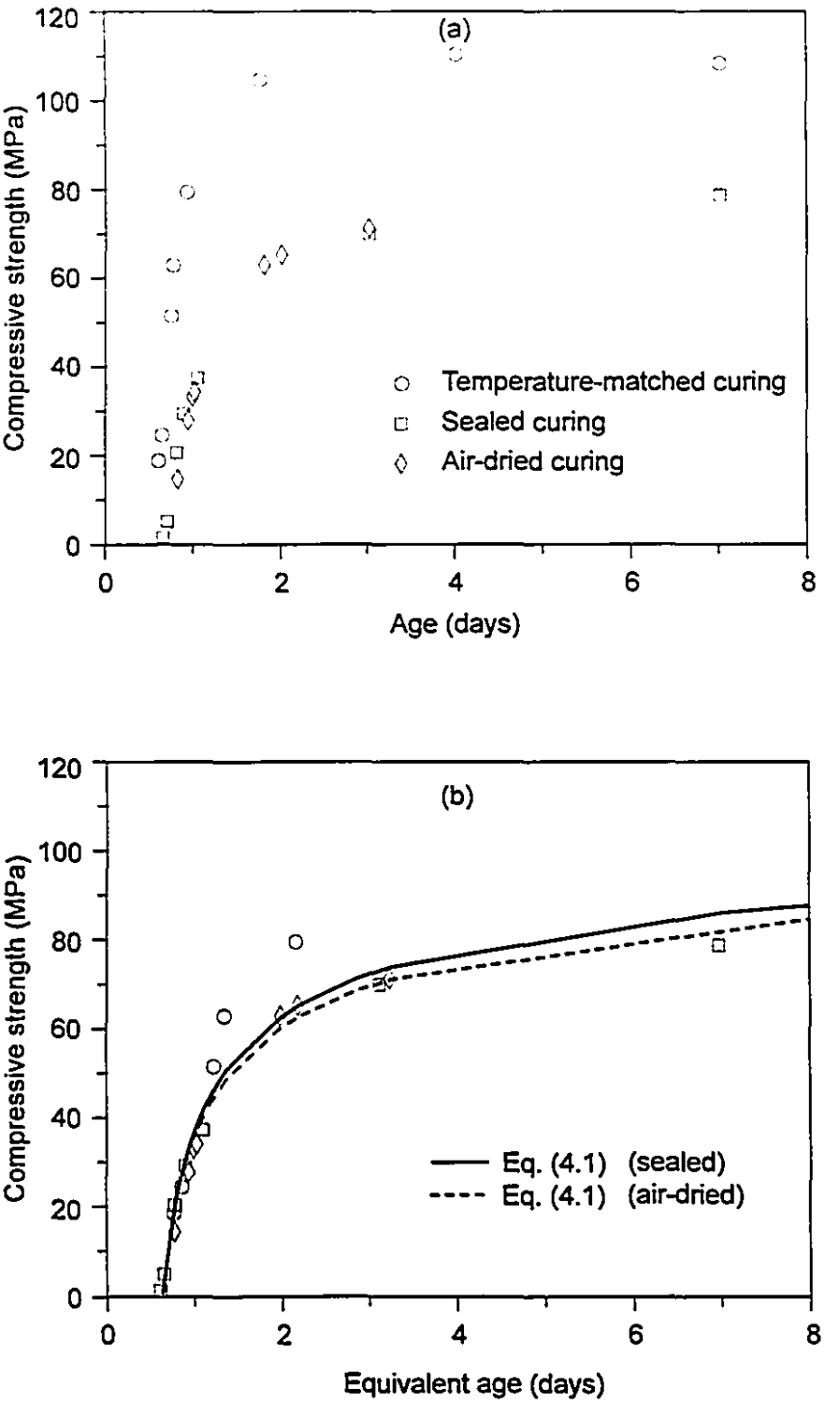

Figure 4.14 - Compressive strength development of 100 MPa concrete (a) vs. real age (b) vs. equivalent age

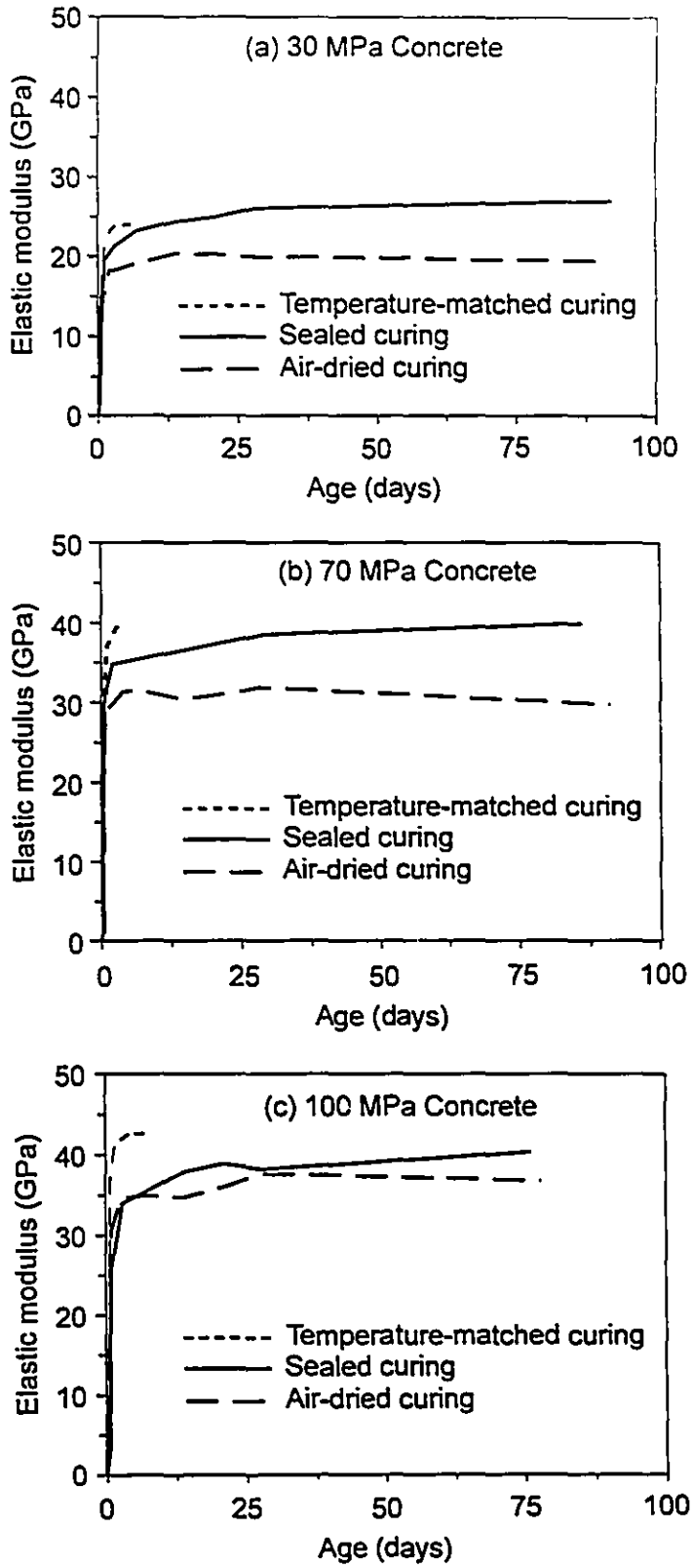

Figure 4.15 - Effect of different curing conditions on the variation of average elastic modulus

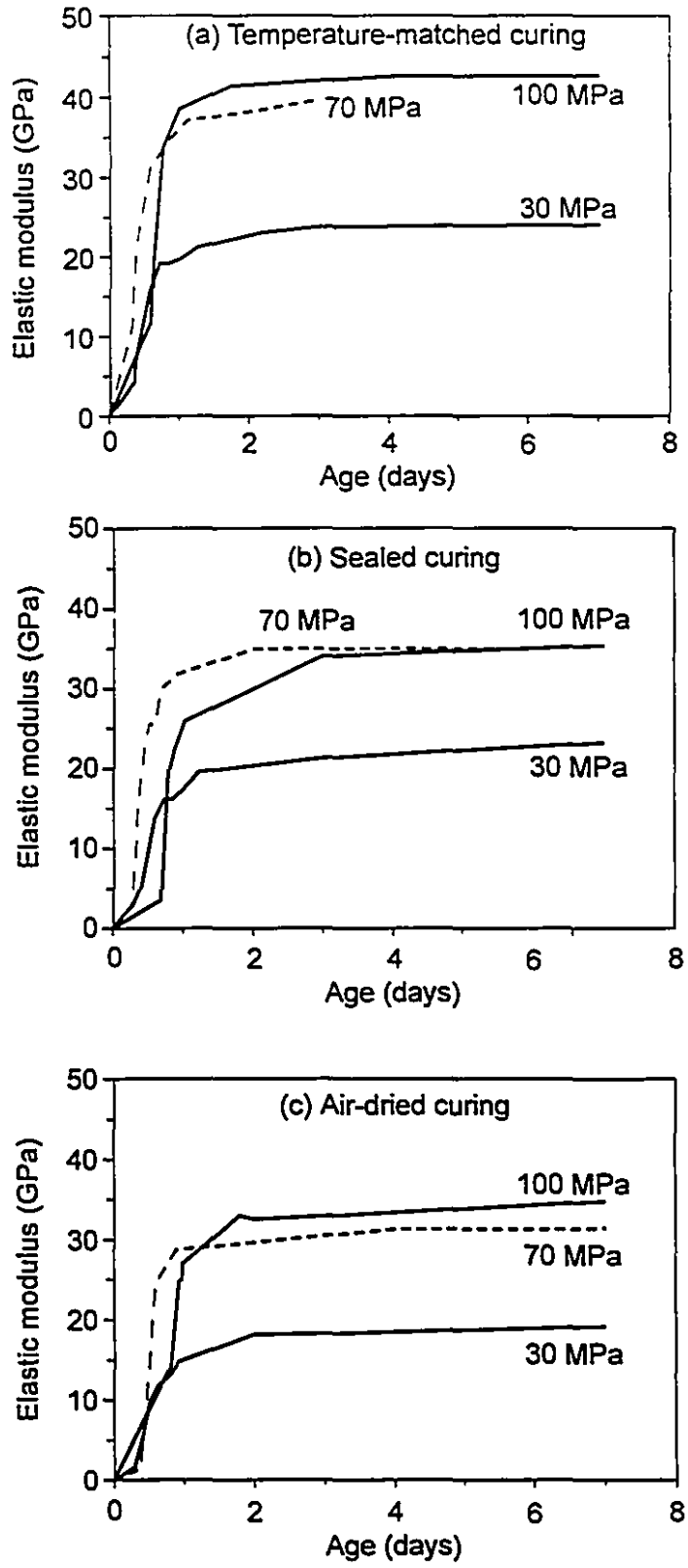

Figure 4.16 - Effect of different curing conditions on the variation of average elastic modulus at early ages

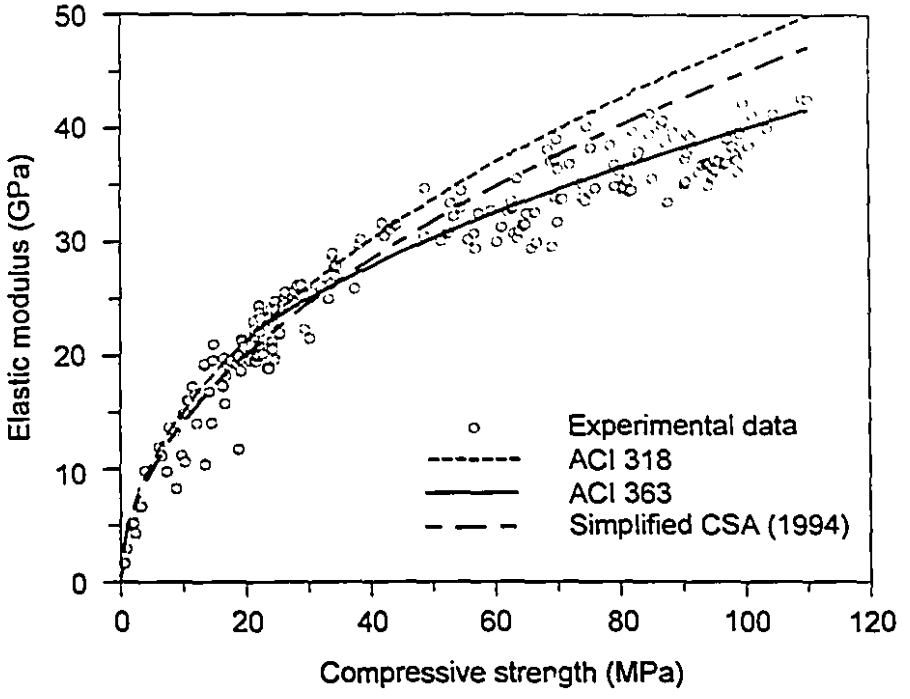

Figure 4.17 - Comparisons between the experimental data and prediction using ACI equations

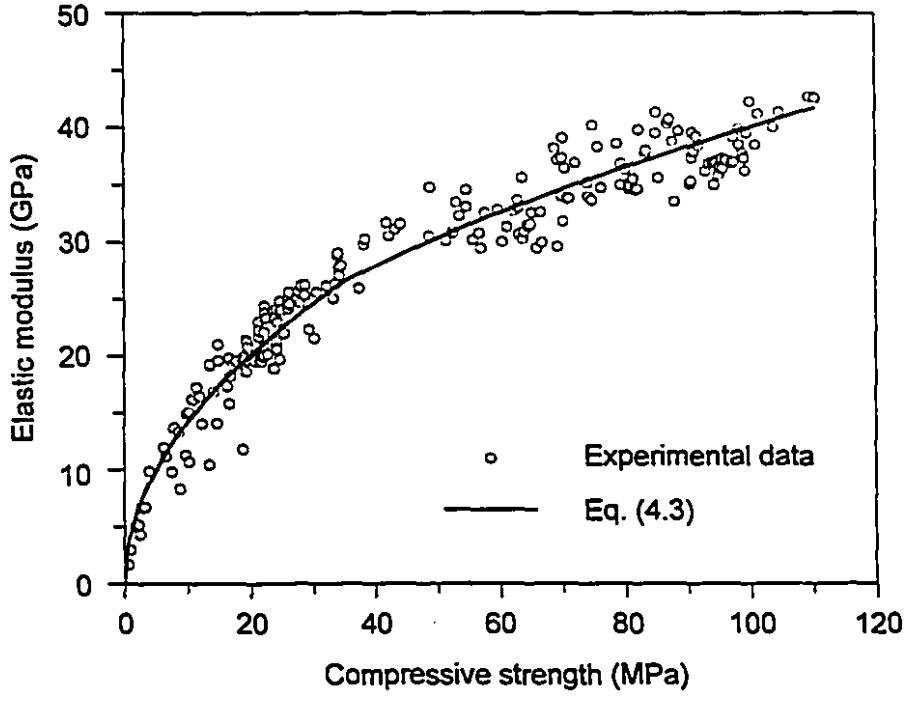

Figure 4.18 - Comparisons between the experimental data and prediction using Equation 4.3

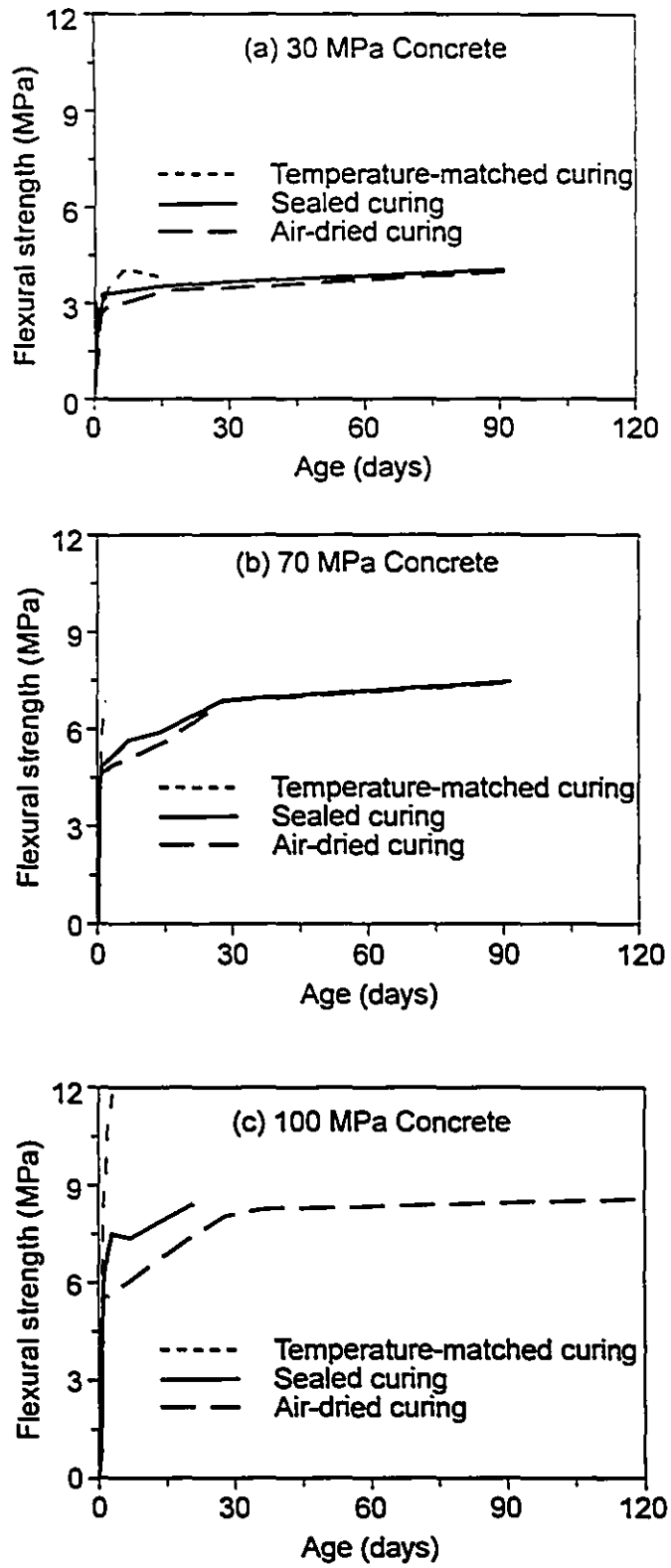

Figure 4.19 - Effect of different curing conditions on the variation of average flexural strength

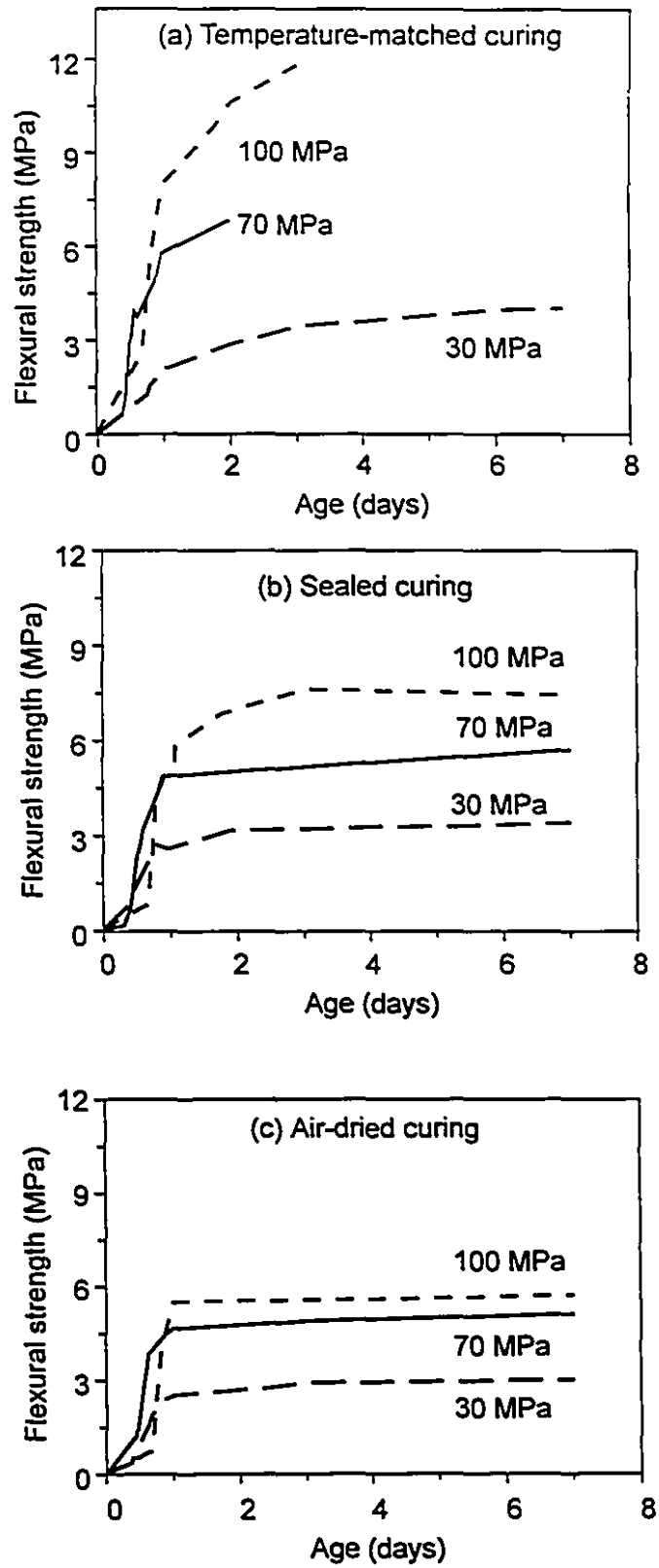

Figure 4.20 - Effect of different curing conditions on average flexural strength at early ages

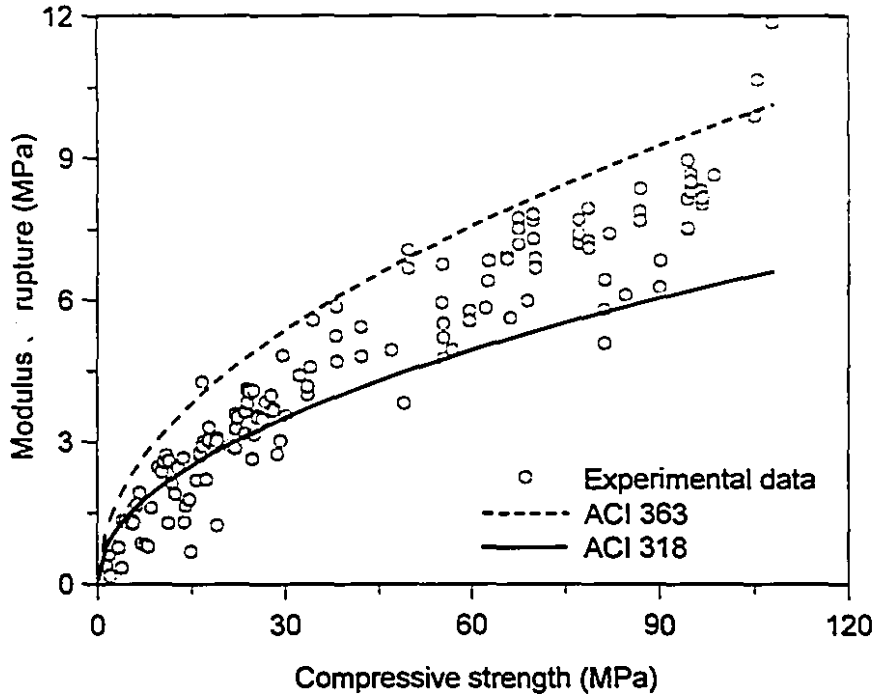

Figure 4.21 - Comparison between the experimental data and prediction using ACI equations

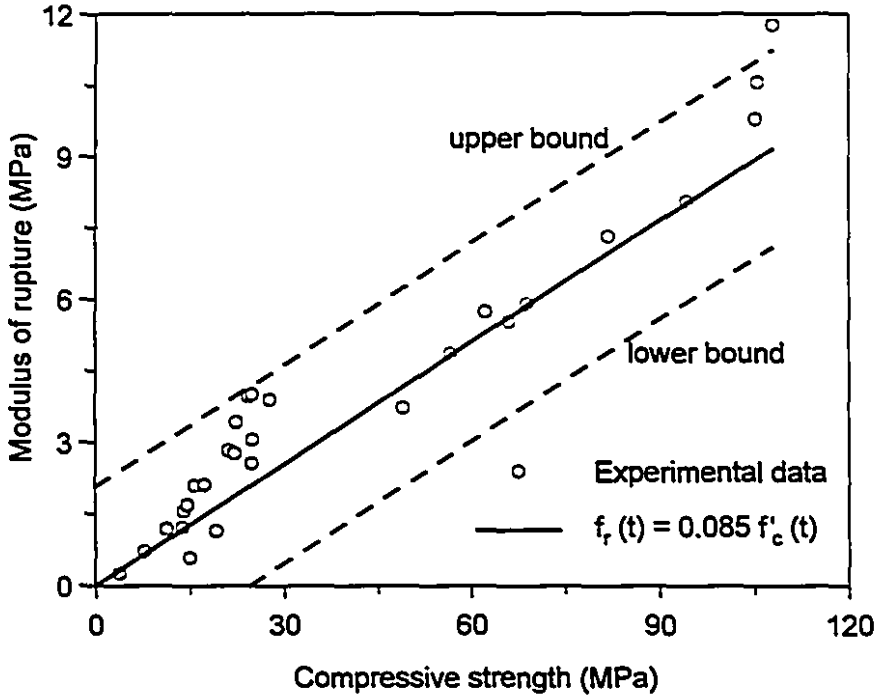

Figure 4.22 - Relationship between modulus of rupture and concrete compressive strength for temperature-matched curing

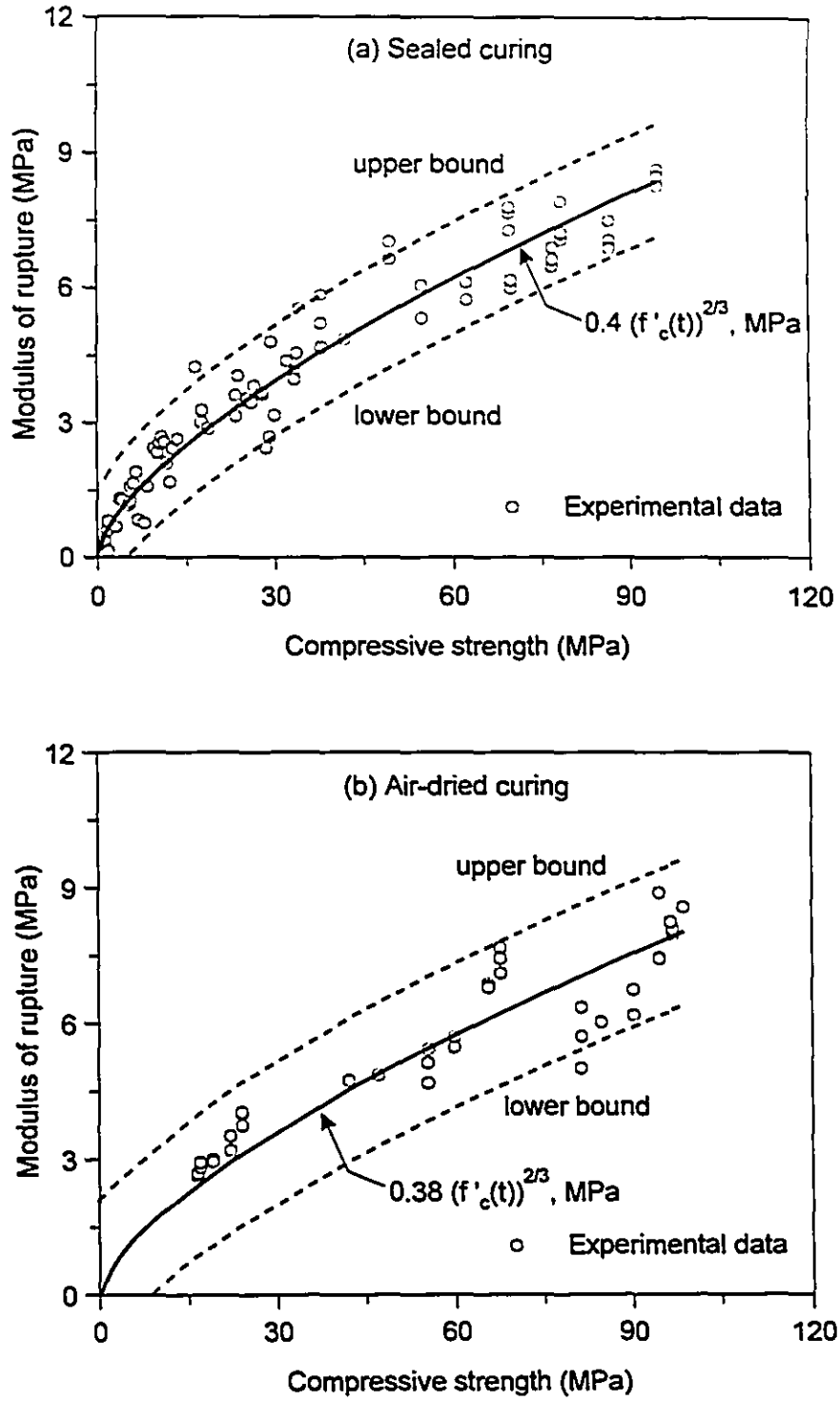

Figure 4.23 - Relationship between modulus of rupture and concrete compressive strength for sealed and air-dried curing

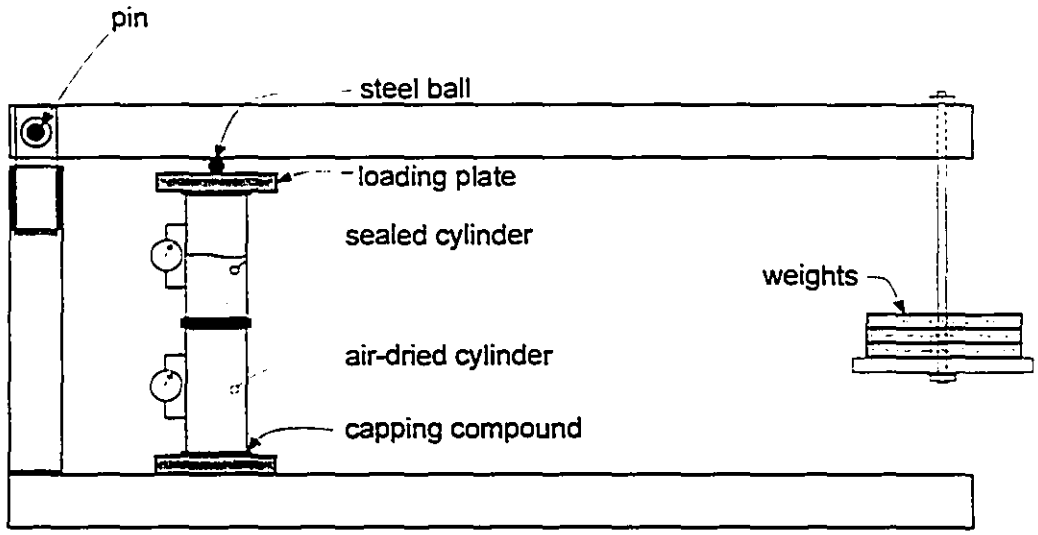

(a) Creep frame

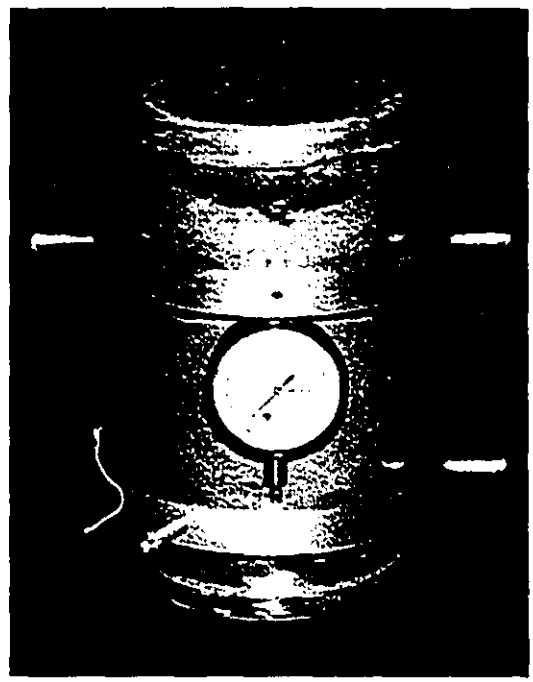

(b) Clamping device to measure the strain

Figure 4.24 - Test setup to measure the early age creep

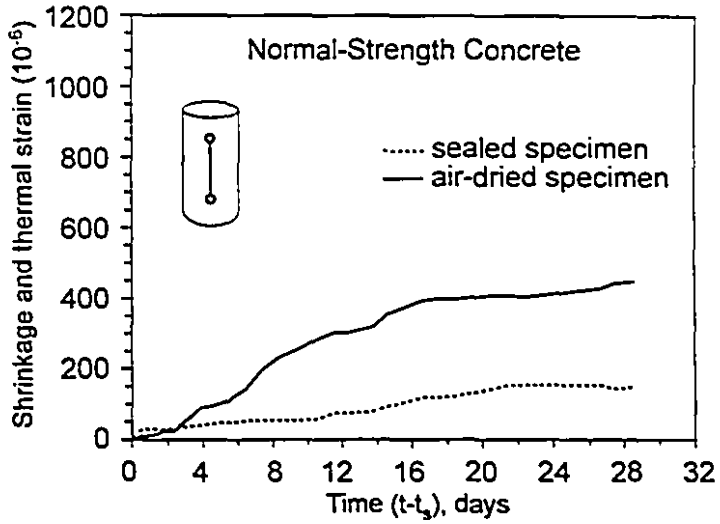

a) Age at demolding, t_s=12.7 hours

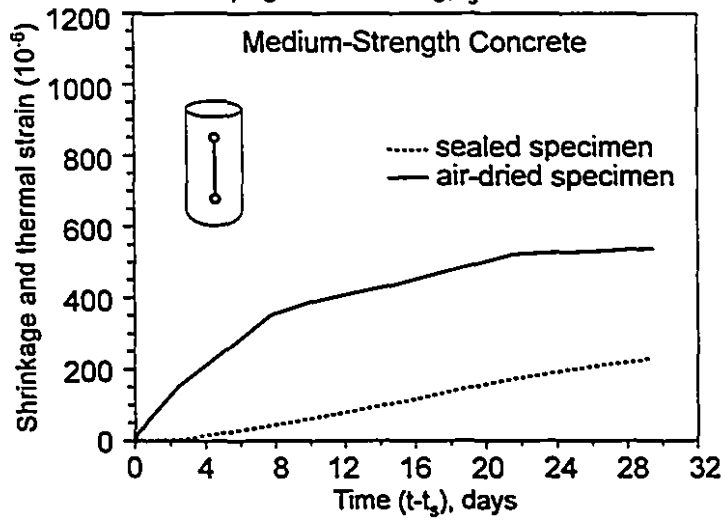

b) Age at demolding, t_s=11.25 hours

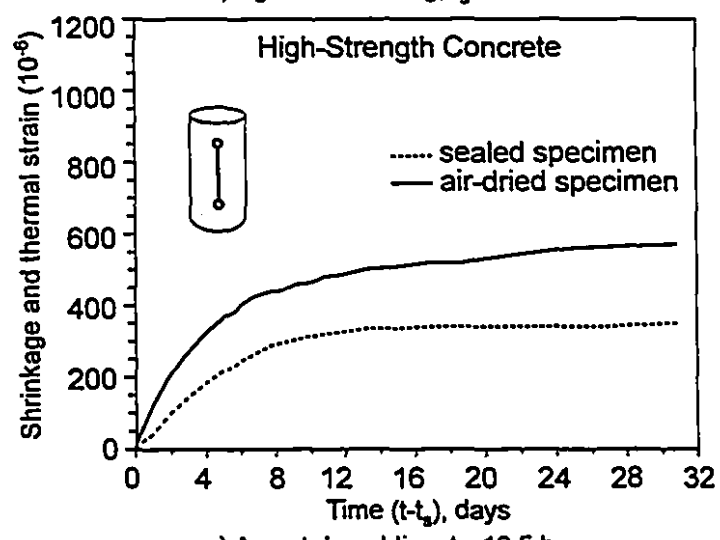

c) Age at demolding, t_s=19.5 hours

Figure 4.25 - Variation of shrinkage and thermal strains with time for normal, medium and high-strength concretes

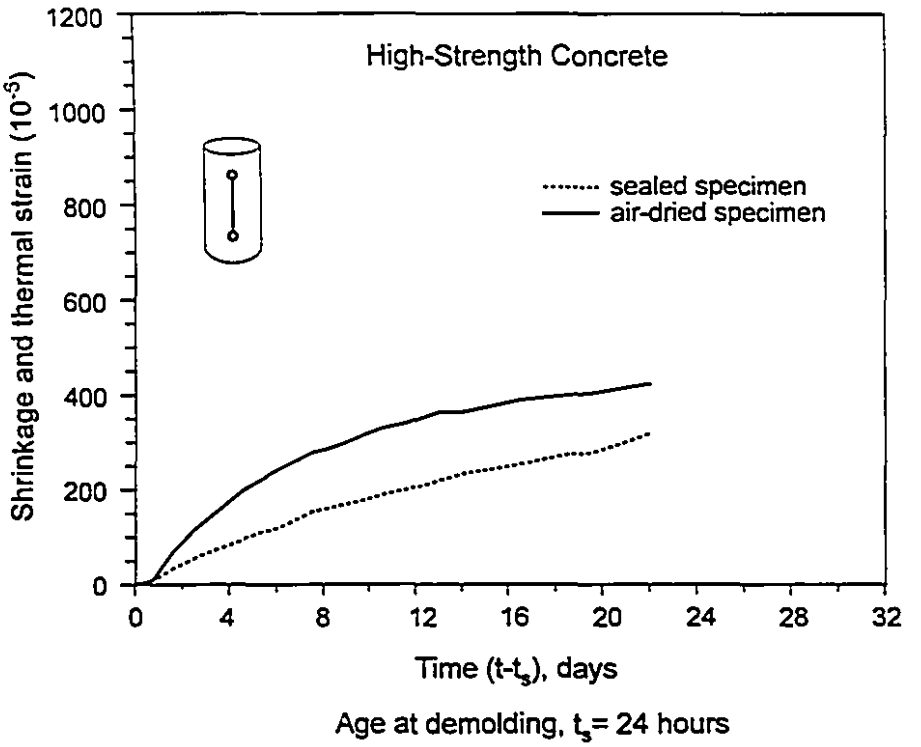

Figure 4.26 - Variation of shrinkage and thermal strains with time for high-strength concrete

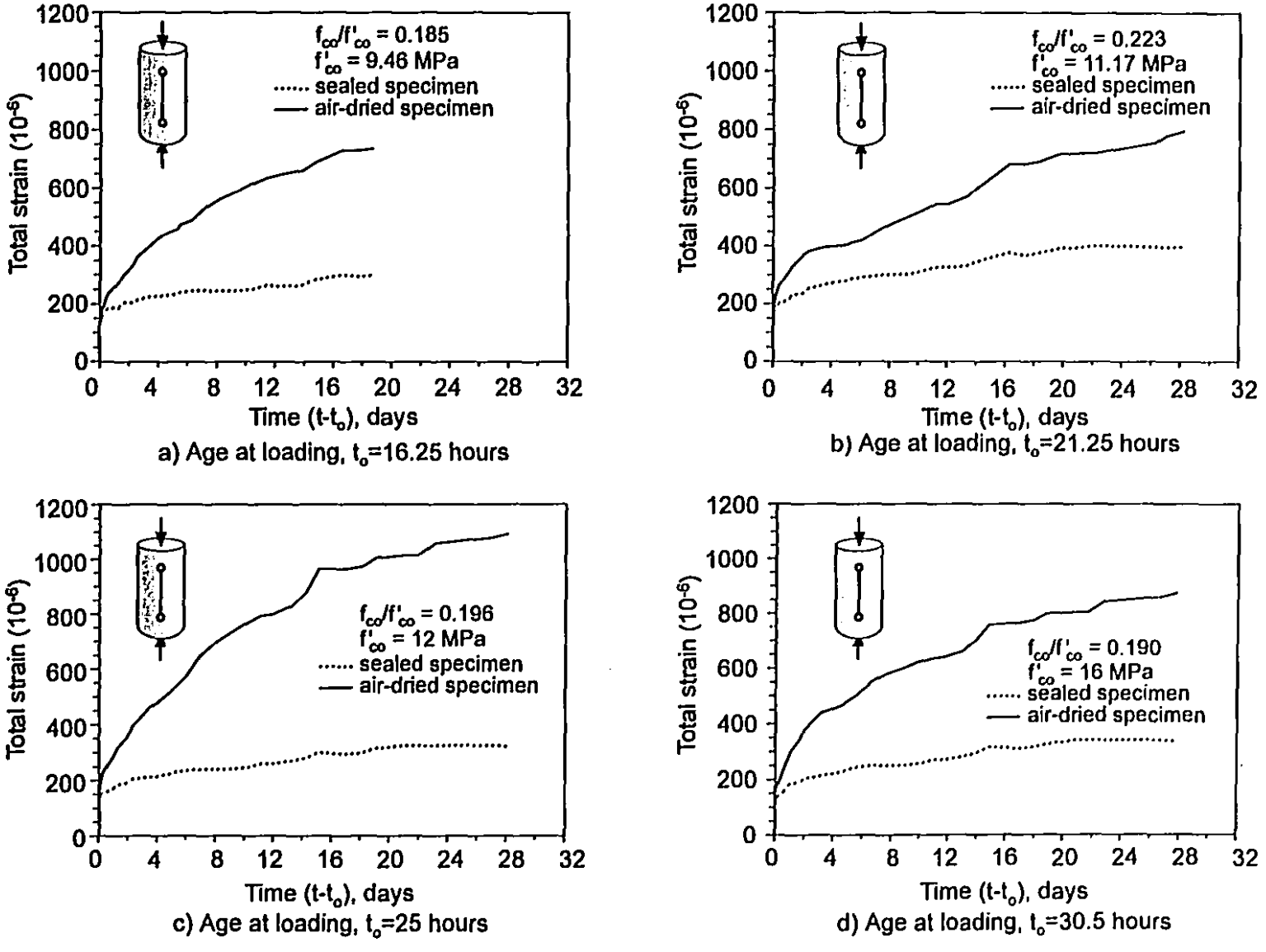

Figure 4.27 - Variation of total strain with time for normal strength concrete loaded at different ages

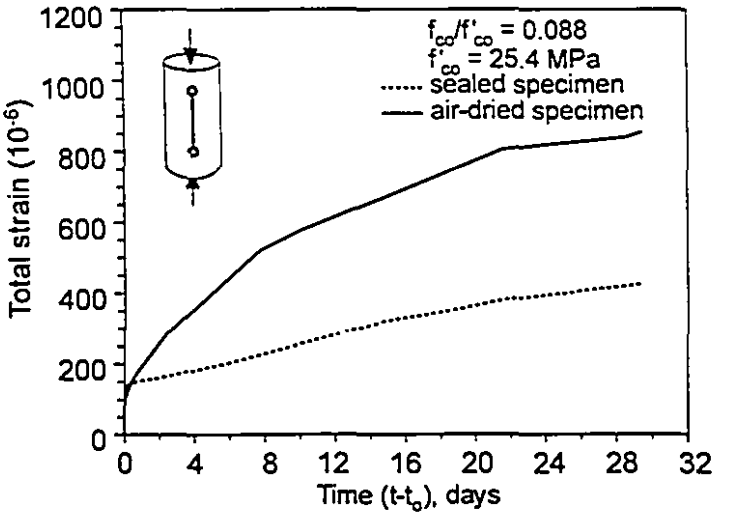

a) Age at loading, t_o=11.25 hours

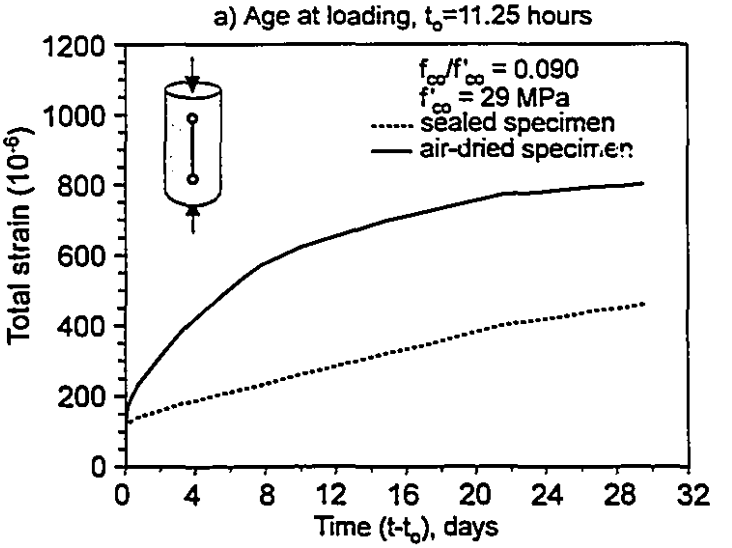

b) Age at loading, t_o=13 hours

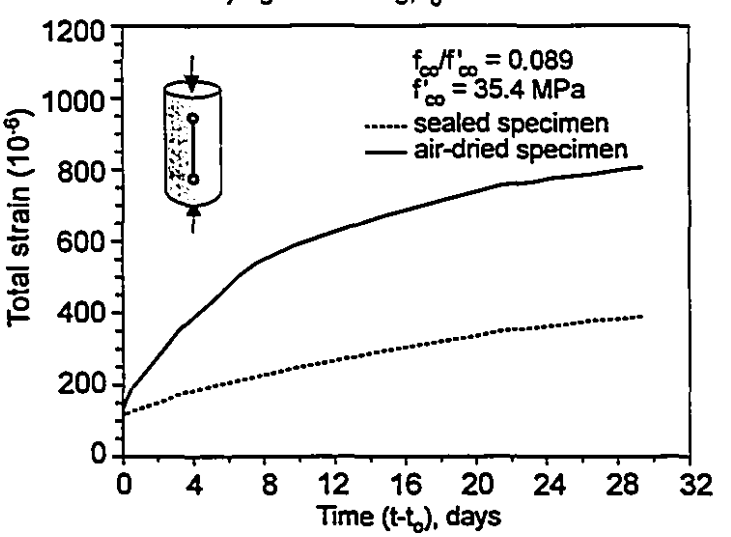

c) Age at loading, t_o=15.75 hours

Figure 4.28 - Variation of total strain with time for medium strength concrete loaded at different ages

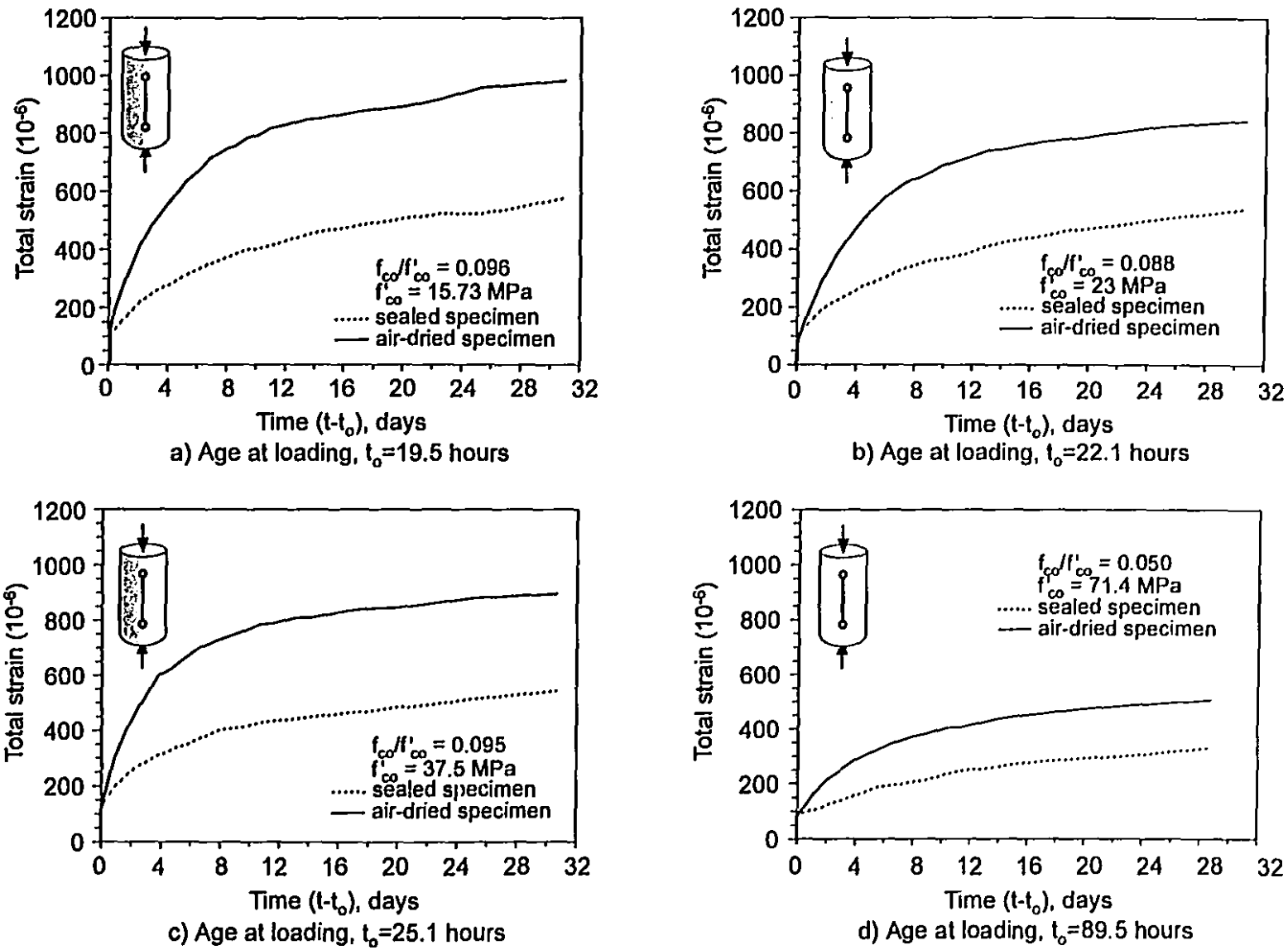

Figure 4.29 - Variation of total strain with time for high-strength concrete loaded at different ages

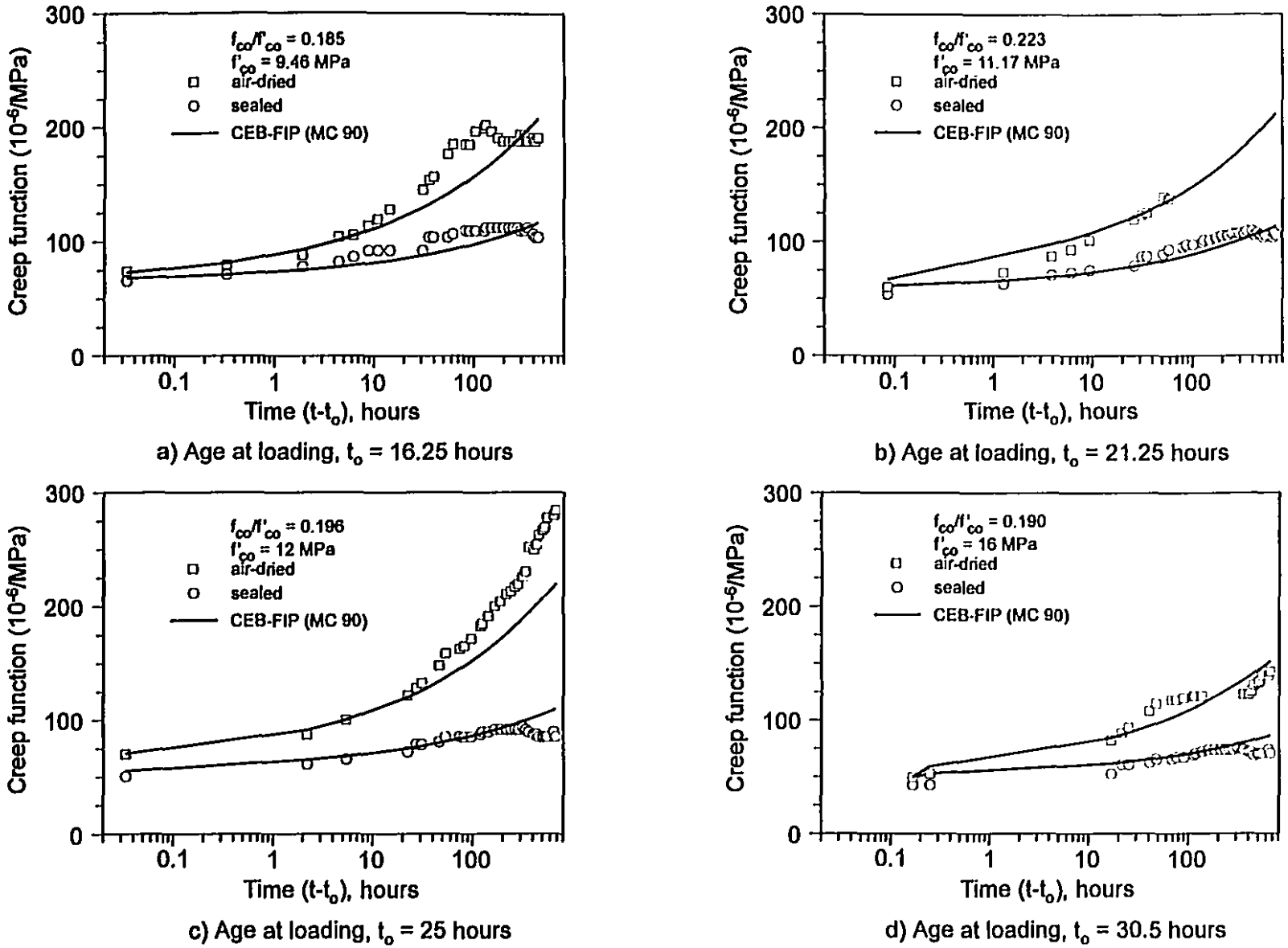

Figure 4.30 - Comparison between the measured and predicted creep of normal-strength concrete

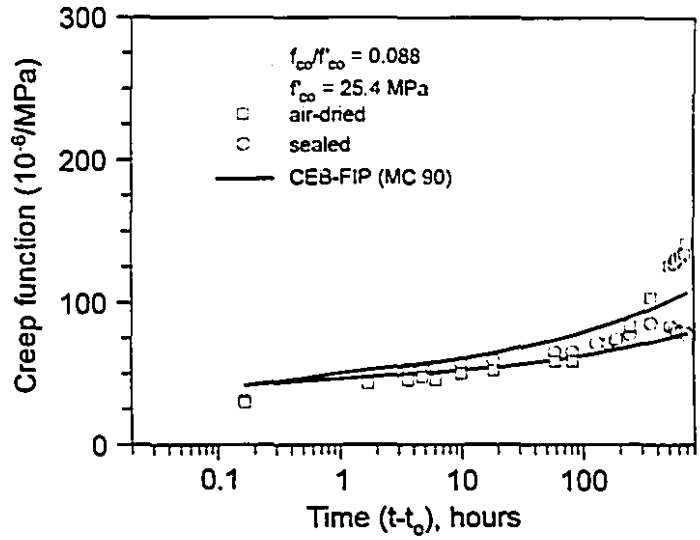

a) Age at loading, t_o = 11.25 hours

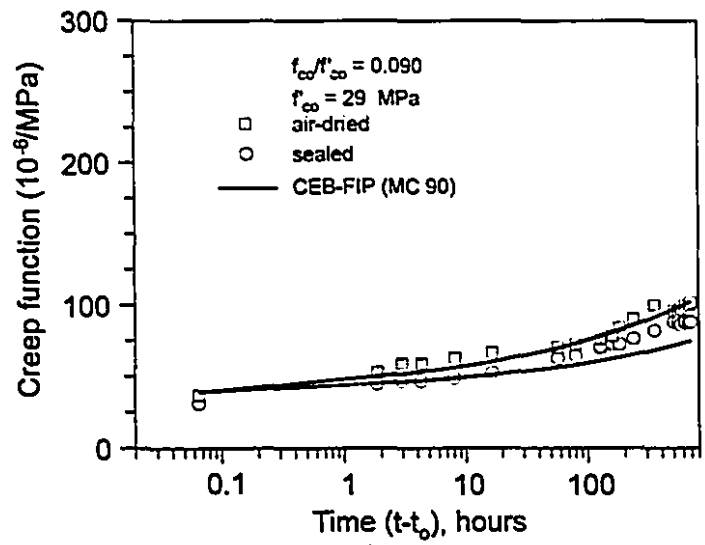

b) Age at loading, t_o = 13 hours

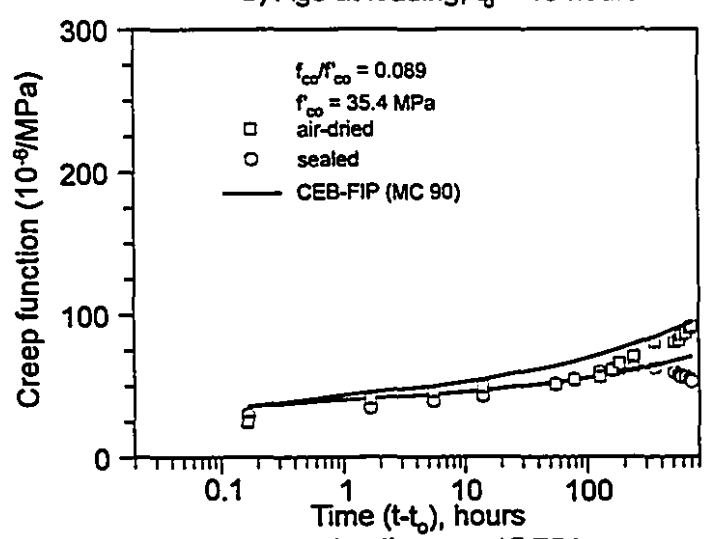

c) Age at loading, t_o = 15.75 hours

Figure 4.31 - Comparison between the measured and predicted creep of medium-strength concrete

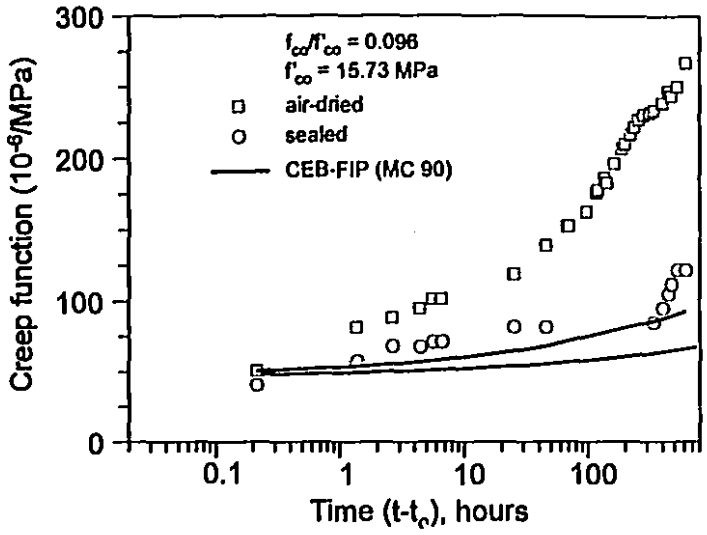

a) Age at loading, t_o = 19.5 hours

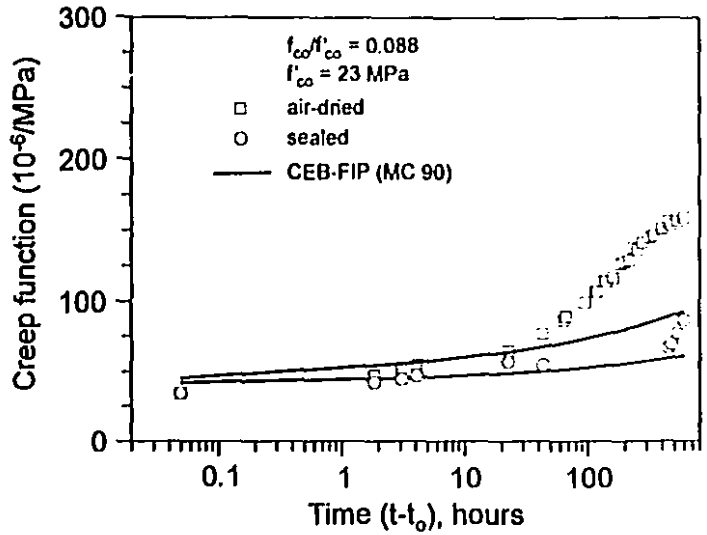

b) Age at loading, t_o = 22.1 hours

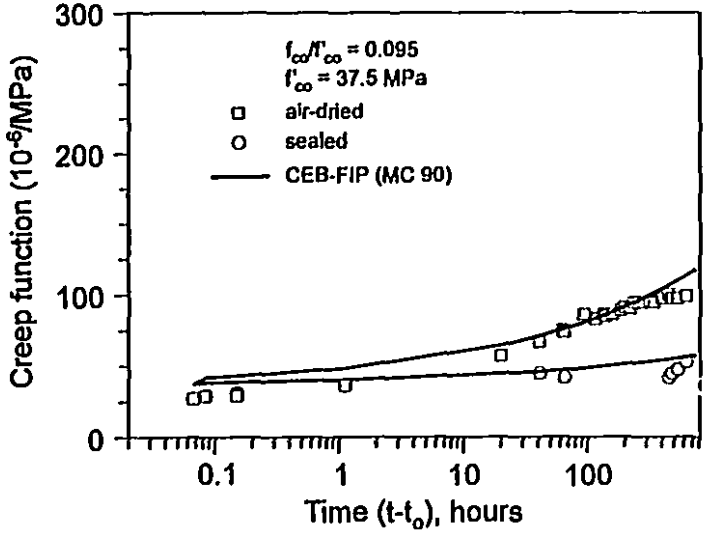

c) Age at loading, t_o = 25.1 hours

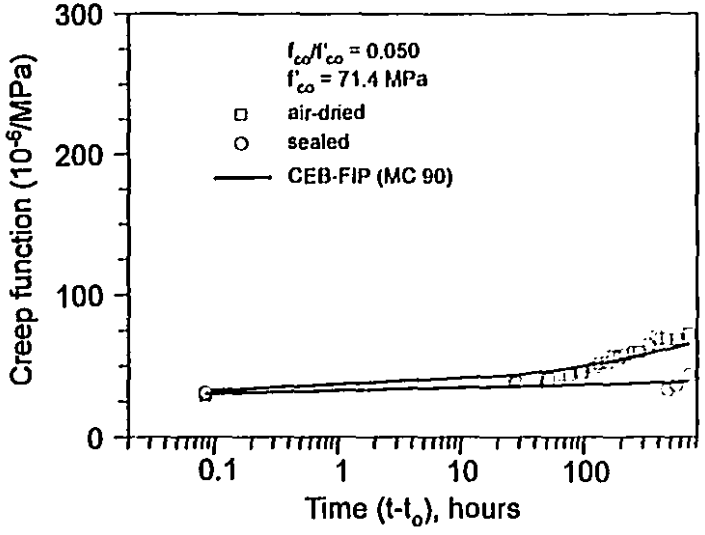

d) Age at loading, t_o = 89.5 hours

Figure 4.32 - Comparison between the measured and predicted creep of high-strength concrete

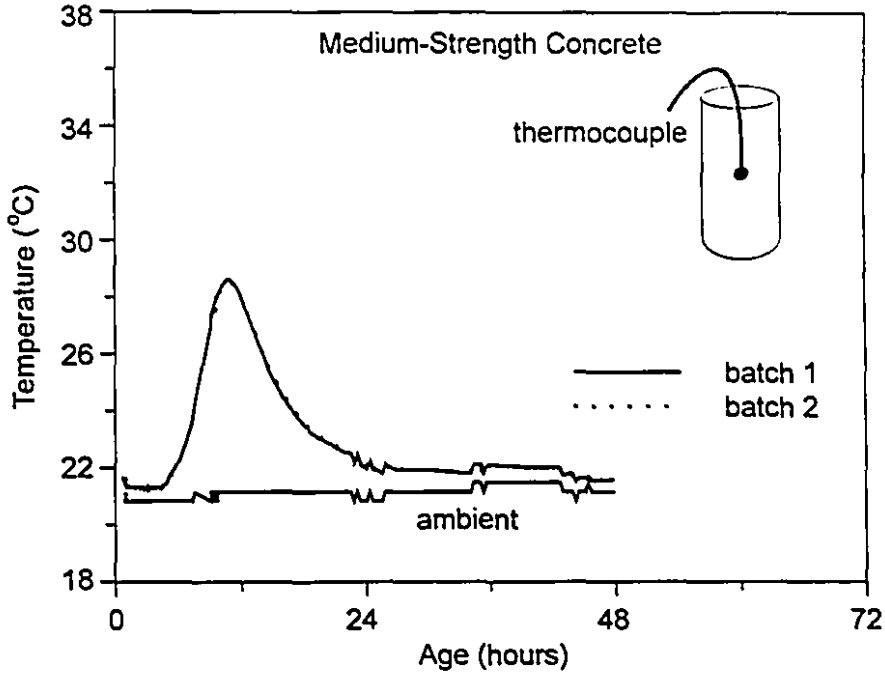

Figure 4.33 - Temperature variation in a sealed 100 x 200 mm cylinder of 70 MPa concrete

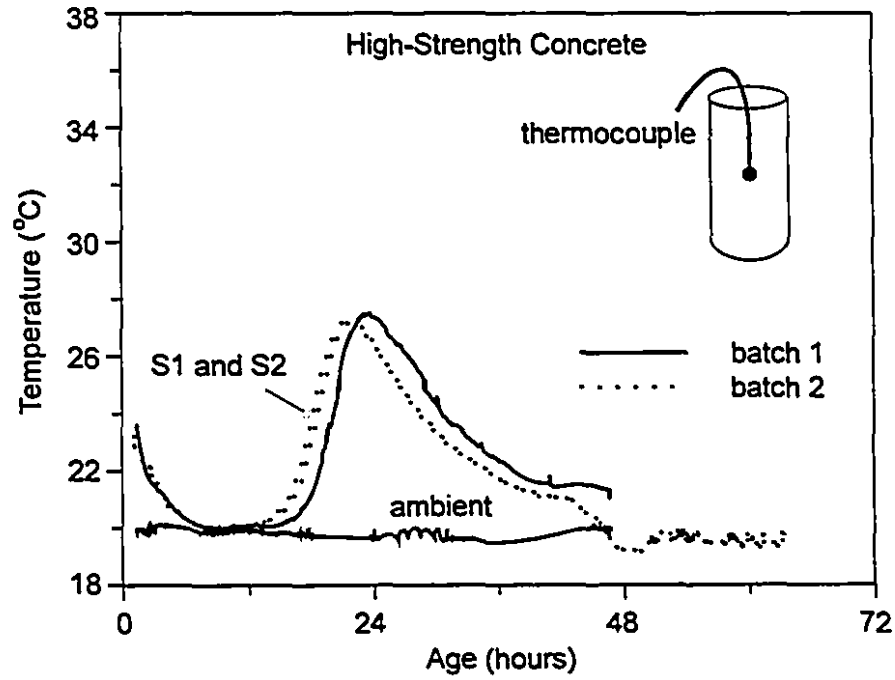

Figure 4.34 - Temperature variation in a sealed 100 x 200 mm cylinder of 100 MPa concrete

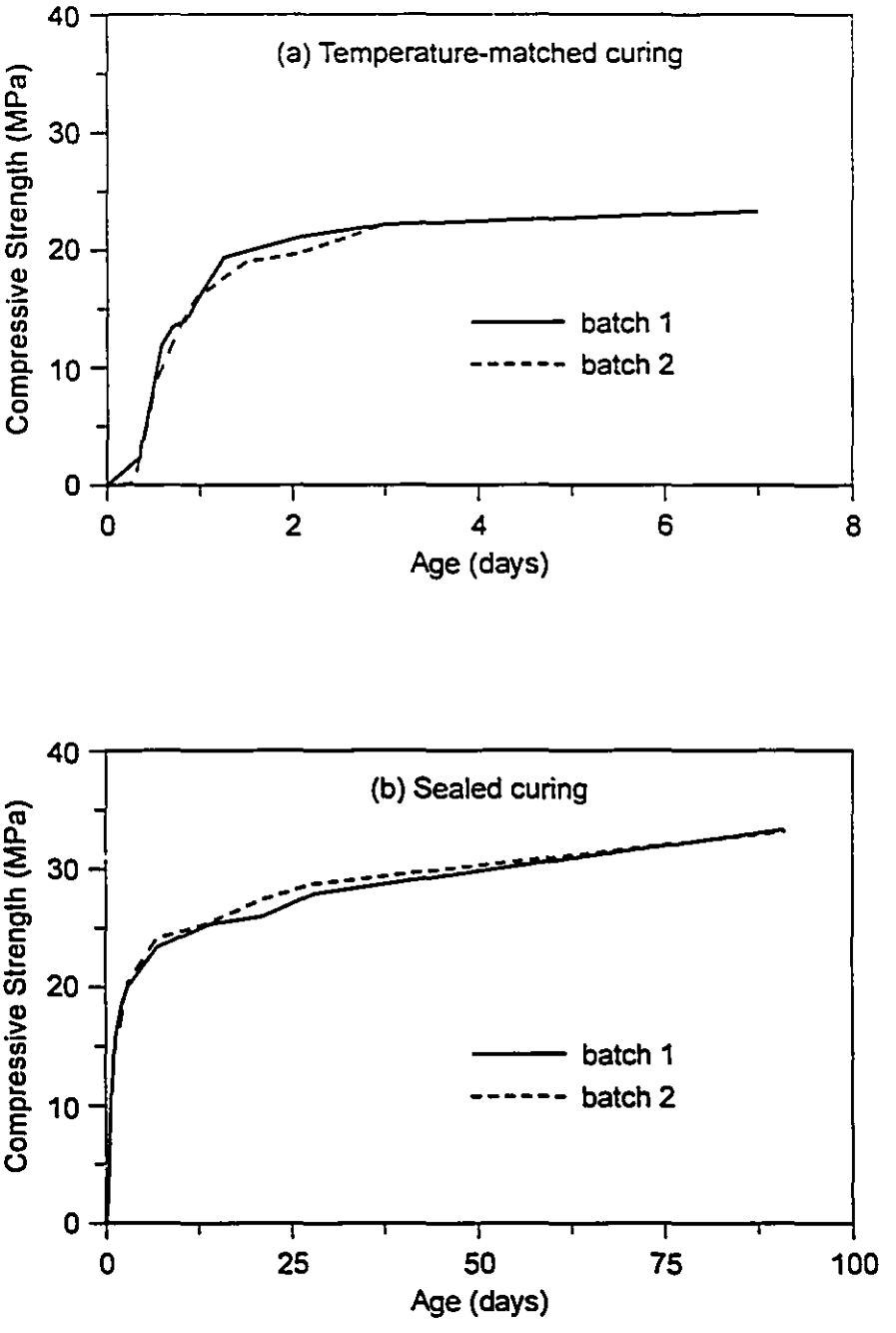

Figure 4.35 - Variation of average compressive strength of normal-strength concrete due to temperature-matched and sealed curing

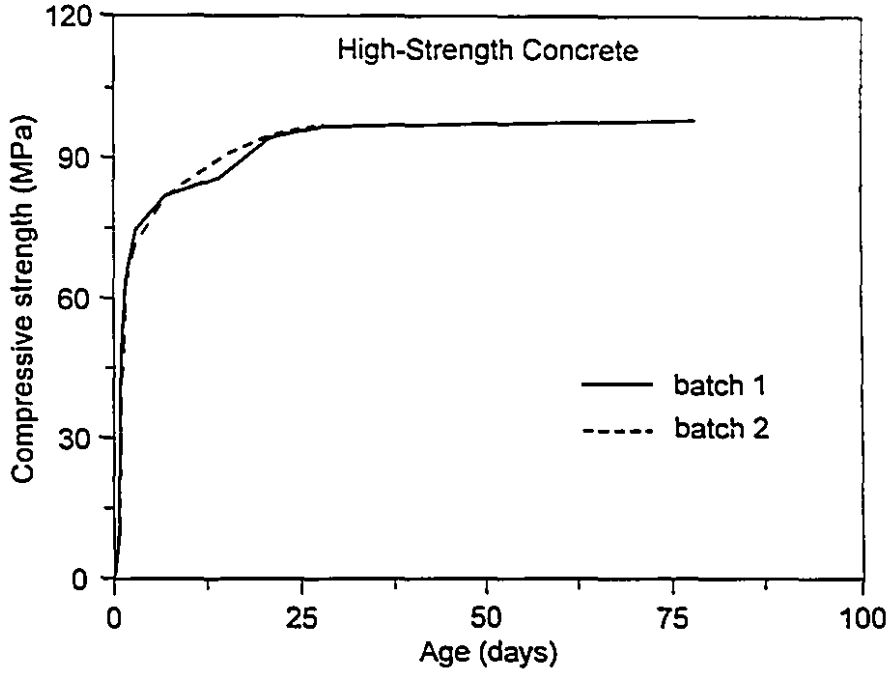

Figure 4.36 - Variation of average compressive strength of high-strength concrete with age due to air-dried curing

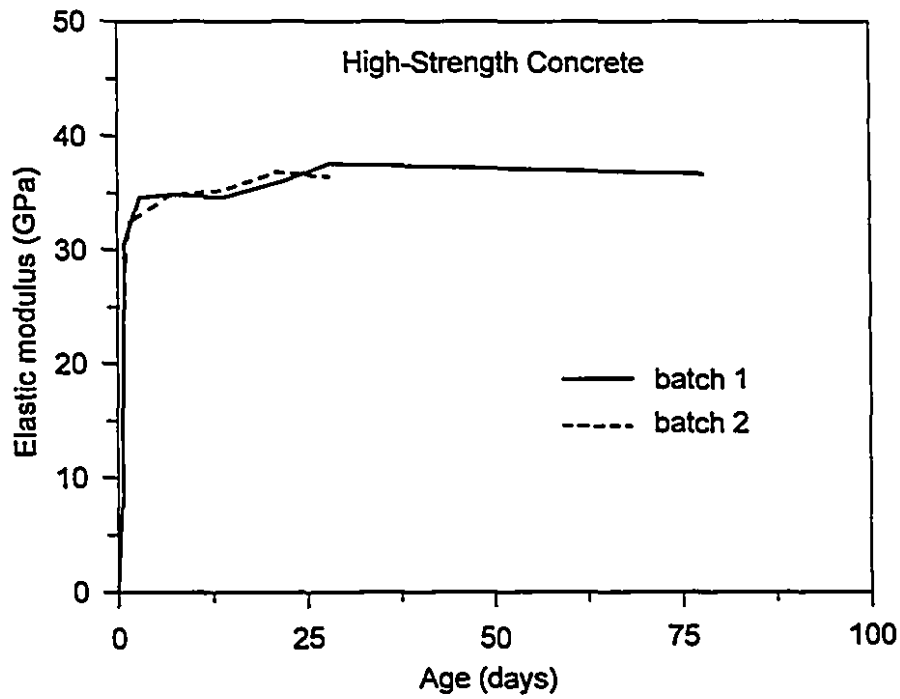

Figure 4.37 - Variation of average elastic modulus of high-strength concrete with age due to air-dried curing

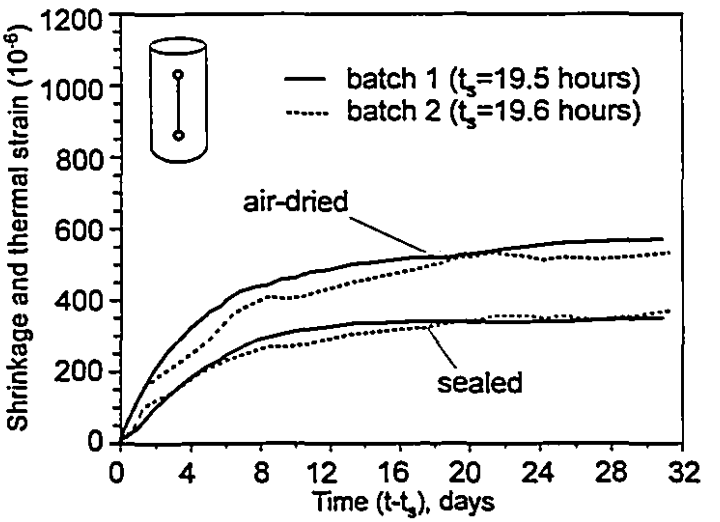

Figure 4.38 - Variation of shrinkage and thermal strains with time for high-strength concrete

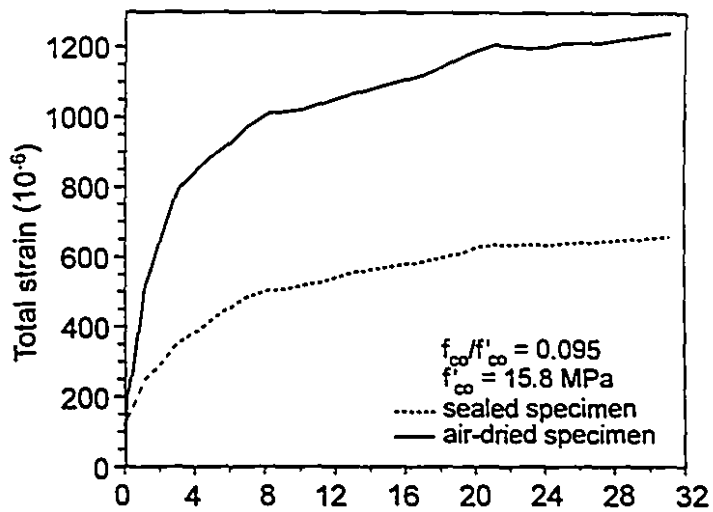

a) Age at loading, t_o=19.6 hours

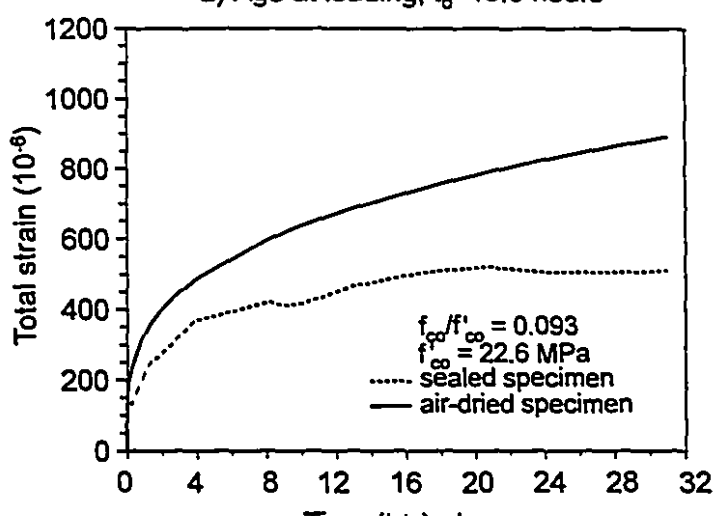

b) Age at loading, t_o=21.8 hours

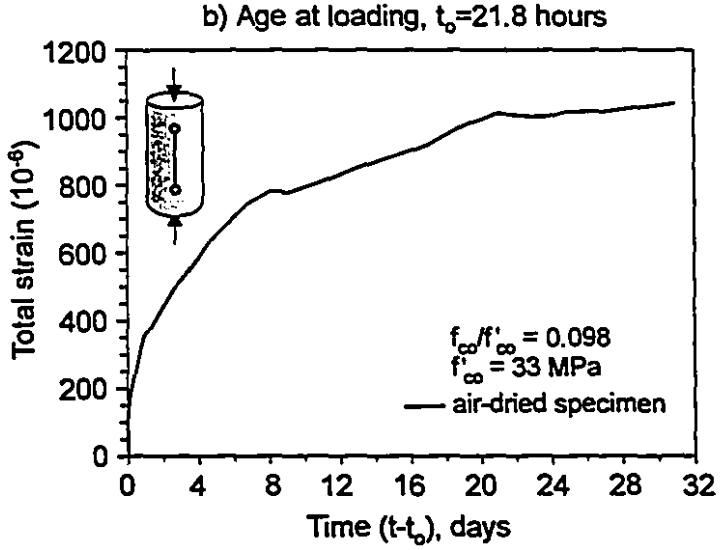

c) Age at loading, t_o=23.8 hours

Figure 4.39 - Variation of total strain with time for high-strength concrete loaded at different ages

Chapter 5

Transient Thermal Analysis and Measured Responses of Structural Members During Hydration

In order to accurately predict the risk of cracking, it is necessary to compare the thermally induced stresses with the strength at different locations in structural members. Both the induced stress and the strength are a function of the temperature history, which varies with time and location. In order to determine the temperatures during hydration, it is important to account for a number of factors such as heat of hydration, thermal properties, placing temperature and boundary conditions. This chapter deals with the measurements of temperature histories during hydration in different structural members subjected to different curing conditions. Finite element thermal analyses in the time domain are carried out to predict the temperature fields and comparisons are made between the measured and predicted responses. The extension and modifications made to a finite element computer program to account for heat of hydration are also presented.

5.1 Basic Concept of Heat Transfer

A transient two-dimensional thermal analysis can be carried out over the cross-section of a member assuming that no heat flow occurs in the longitudinal direction of the member. The basic equation governing the distribution of temperature in a solid subjected to internal heat generation was developed by Fourier (Holman (1990)). For a two-dimensional case, the fundamental heat flow Fourier Equation for an isotropic and homogeneous material is given as:

$$\lambda \left[\frac{\partial^2 T}{\partial x^2} + \frac{\partial^2 T}{\partial y^2} \right] + Q = \rho c \frac{\partial T}{\partial t} \qquad (5.1)$$

where

T = temperature at (x,y), at time t

λ = thermal conductivity of concrete

Q = heat generation rate within the body

ρ = density of concrete

c = specific heat capacity

t = time

For an anisotropic and non-homogeneous material, the thermal conductivity and specific heat is temperature and space dependent which leads to non-linearity of the heat flow equation. In order to determine a unique solution to Eq. 5.1, proper initial and boundary conditions must be specified which are compatible with the physical conditions.

The initial conditions must be defined by prescribing the temperature distribution throughout the body at time zero, as a known function of x and y;

$$T(x,y,t) = f(x,y) \text{ at } t=0 \qquad (5.2)$$

Boundary conditions must be defined by specifying the ambient conditions and the heat flow parameters at the boundary of the body. The ambient temperature can be either constant or a function of time. In many engineering problems, heat may be transferred by convection or radiation across a boundary layer and must be specified. The convection coefficient of air is given in many references (e.g., ASHRAE (1989)) and varies from 5 to 30 $W/m^2\,^oC$. It can be different for different surfaces (i.e., top, bottom and sides) of the same cross section of a member, depending on the orientation of the surface the speed and direction of the wind.

Solutions to Eq. 5.1 can be obtained using closed-form solutions, approximate analytical methods and numerical methods. The closed-form solutions are given in many classical heat transfer textbooks (e.g., Carslaw and Jaeger(1986), Holman (1990), Pitts and Sissom (1991)). In most of the cases, no closed-form solution exists and the temperature field must be determined by numerical methods. Finite difference

or finite element methods can be employed to predict the temperature distribution in the time domain by solving the differential equation of heat flow (Eq. 5.1). In order to predict the temperatures and the resulting thermal stresses in structural members, the finite element method is used. The transient thermal analysis requires knowledge about the thermal properties of the concrete, including the thermal conductivity, the rate of heat of hydration and the thermal diffusivity (i.e, $\lambda/c\rho$) of the concrete. The thermal properties are explained in Chapter 3.

5.2 Modifications to Finite Element Program "DETECT"

Heat flow is a three-dimensional phenomenon, however a two-dimensional analysis can produce reasonable results, if the structural member has a uniform cross section and has a uniform temperature distribution in the longitudinal direction. At first, commercially available software (SAP90 (1990), ADINA-T (1992)) were used to model and predict the temperatures in concrete elements due to the heat of hydration. However, these programs did not account for the complex thermal activation process during hydration captured by Arrhenius' function. It was also found that these programs were not capable of accounting for the changing boundary conditions (such as removal of formwork and insulation) nor the realistic effects such as retardation.

In this study, a 2-D finite element transient thermal analysis was carried out using a modified version of the computer program "DETECT" (Determination of Temperatures in Construction) to predict the temperatures variations both in space and time. This program was originally developed by Polivka and Wilson (1976) for the analysis of structures constructed incrementally. The program is very general with respect to geometry, material properties and boundary conditions. This program can perform steady state or transient thermal analysis of two dimensional planar or axisymmetric structures of arbitrary geometry, constructed incrementally. The program was developed for the purpose of evaluating the temperature distribution during the construction of massive structures such as dams, foundations and bridge piers. The solution is based on the finite element technique, and includes the effects of time-dependent boundary conditions, such as convection, presence of insulation, and artificial cooling by means of embedded pipes. The program includes two-dimensional 4 - to 8-node planar or axisymmetric isoparametric elements, 2-node planar or

axisymmetric solid boundary elements and linear cooling pipe elements. In this study, the program is extended to account for the development of rate of heat of hydration as a function of maturity based on Arrhenius' approach. Due to the low thermal conductivity of concrete, the centre of a concrete element will be hotter than the surface, resulting in different rates of heat of hydration at different locations in the cross section. It has been reported by Regourd and Gautier (1980) that the rate of heat of hydration, for each point at any instant, is a function of current temperature and total quantity of heat already developed. Hence the computer program was modified to keep track of the nodal temperatures, total quantity of heat developed and maturity from previous time steps. The program was also extended to predict the "mature" or "equivalent" age of any element from its temperature history. This additional information is used for the stress analyses for predicting the concrete properties as they change during hydration (see Chapter 6).

Figure 5.1 shows the flow chart for the transient thermal analysis. The steps used to carry out the incremental transient thermal analysis are briefly described below:

i. Input data

The input data required includes the geometry, thermal properties, initial conditions and boundary conditions. The cross-section of the member was modelled using finite elements. The thermal properties, such as the conductivity, specific heat, and the adiabatic temperature rise curve were provided. It is essential to properly model the boundary conditions and any changes that occur to these conditions. The initial conditions such as the initial concrete temperature of each element must be defined.

ii. Increment time, Δt

A small time increment of Δt is applied such that the new conditions at time $t+\Delta t$ can be determined. It must be pointed out that after several analyses, it was found that a time step of 30 minutes was sufficient to give accurate predictions.

iii. Update boundary conditions

In order to appropriately model the key events during the construction such as the addition or removal of formwork or insulation, a feature referred to as "the birth and death of elements" was added to enable adjustment of the changing boundary conditions.

iv. Determine equivalent age "t_e"

The equivalent age, t_e, was calculated for each element using the maturity concept described in Section 2.1.3. The adiabatic temperature rise, expressed in terms of equivalent age, was used as the reference curve for determining temperatures and the heat of hydration.

v. Determine the incremental heat generated "ΔQ

The actual rate of heat of hydration in each element is calculated as a function of the temperature and the degree of hydration. The incremental heat generated, ΔQ, during each time step is obtained from the reference adiabatic heat of hydration curve and adjusted for temperature using Arrhenius' expression.

vi. Solve heat balance equation

Using the finite element program "DETECT", the heat balance equation is solved for the incremental temperature, ΔT, for each element.

vii. Determine heat generated and temperature

The incremental heat generated, ΔQ, is used to update the total heat generated from the equation $Q = Q + \Delta Q$ and the total temperature is determined as $T = T + \Delta T$ for each element.

viii. Store nodal values of T, t_e, ΔQ and total Q

Necessary information such as nodal temperature, T, the equivalent age, t_e, the incremental heat generated, ΔQ, and the total heat generated, Q, was stored for each element. These values will be used for determining the necessary material properties for the subsequent stress analysis.

ix. Return to step ii and repeat steps iii through viii until the total analysis is complete.

A post-processor was also written to enable plotting with commercially available graphics packages. Additional modifications were made to account for changing boundary conditions, such as addition or removal of formwork and insulation. These additional changes enabled more accurate modelling of these important aspects of construction. This program can then be used to study the influence of different construction techniques enabling decisions to be made in controlling the temperature and the temperature gradients. In the computer program "DETECT", changes in the boundary conditions, that is, removal of formwork or addition of insulation, were

incorporated by removing or adding ("death" and "birth") elements for both 4 to 8 nodes isoparametric and 2 node linear elements. The program has the capability of specifying the temperature or heat flux boundary conditions at any point within the element system. The finite element approach generates heat flow equilibrium equations for the system in the form of a symmetric positive-definite matrix. This matrix is banded and equations can be solved with a minimum use of computer storage and time. The input parameters required in "DETECT" to predict the temperature variations are:

i. the adiabatic temperature rise curve of the concrete
ii. the variation of ambient temperature
iii. the thermal conductivity, specific heat and density of the concrete
iv. thermal properties of the boundary elements

For thermal analysis, 4 node isoparametric elements were used to model the concrete cross-section and 2 node linear boundary elements were used for the convection surfaces. This was felt important to carry out detailed experimental work in order to obtain the key input information that will be needed for the predictions. It is a well known fact that the thermal conductivity and specific heat of many materials can vary with temperatures. Tests were carried out to measure these properties for normal, medium and high-strength concretes and no significant difference were observed. In the present study, it is assumed that thermal conductivity and specific heat do not change with temperature and are taken as constant. It is assumed that the state of deformation in a body does not affect the temperature field. Therefore, a heat transfer analysis can be carried out initially using finite element idealization and then thermal stress analyses, including creep effects, can be performed independently.

The developed program can be used as a useful tool for the construction industry to accurately predict temperatures, design the necessary insulation, and adopt suitable measures to reduce the temperature gradients in concrete elements.

5.3 Experimental Program

Thermal cracking of precast pretensioned elements has been reported by the precast industry (see Section 1.1). In particular, cracks have been observed at the surfaces of the flanges of tee shaped elements constructed using high-strength

concrete containing silica fume. These members were cast in steel formwork and were heated externally (normally to 70°C).

An experimental study was carried out to measure the variations of temperatures and strains with time at different locations in high-strength concrete precast tee-beams and slabs. Three single tees and three slabs were constructed in the laboratory. Table 5.1 presents the details of the composition and the fresh concrete properties of the high-strength, ready-mix concrete (i.e., design 28-day compressive strength of 90 MPa). In addition to the casting of the slabs and tee-beams, a large number of control specimens (i.e., 100 x 200 mm cylinders and 100 x 100 x 400 mm long beams) were cast to determine the compressive strength and modulus of rupture of the concrete. All of the concrete cylinders and flexural beams were hand rodded in accordance with ASTM C 31-88 (1988). Dolomite limestone coarse aggregates were used with maximum aggregate size of 14 mm. River sand, having a fineness modulus of 2.65, was used for this concrete mix.

The slabs and tee beams were heavily instrumented at different locations to measure the temperatures and strains. These 1 m long specimens were subjected to three different curing conditions (i.e., fully insulated, moist curing and air-dried curing). Figures 5.2, 5.3, 5.4 and 5.5 show the specimens before casting, the curing conditions and the instrumentation at different locations in the cross sections at midspan. These curing conditions were used to study the full range of curing conditions used in construction. The effect of the length of practical members was simulated by insulating both ends of each specimen with 25 mm thick styrofoam insulation. Specimens were immediately covered with polyethylene sheets after casting, except for the air-dried specimens. Twenty five millimetre thick styrofoam sheets were used to insulate the sides of the insulated slab and beam before casting and the top surface of the specimens after the initial set (see Fig. 5.2 to 5.5). The insulated curing reduces the heat loss during hydration, and will therefore lead to higher, more uniform temperatures and hence reduced thermal gradients. For the cases where the formwork and insulation are removed during hydration, a rapid temperature drop near the surfaces will occur and may cause cracking due to thermal shock. For specimens subjected to moist and air-dried curing, the sides were not insulated. The moist-curing condition was achieved by covering the top surfaces of the specimens with wet burlap and

plastic sheets after the final set (i.e., about 8 hours after casting) to avoid moisture loss. The extreme case of air-dried curing was achieved by leaving the top surface of the specimen exposed during hydration in the laboratory environment (i.e., an average ambient temperature of 22°C and relative humidity of 50 ± 15%). The formwork and insulation were removed from the insulated specimens when their peak temperatures were achieved, between 21 to 22 hours after casting. This subjected the specimens to thermal shock, producing a large thermal gradient across the cross-section which could lead to cracking.

The temperatures in the slabs and beams were measured using Type T (i.e., copper-constantan) thermocouples with an accuracy of ± 0.5°C. These thermocouples were attached to a data acquisition system and readings were taken at frequent intervals during the first 72 hours. Ambient temperature and humidity were also recorded during the first 3 days after casting the concrete.

The adiabatic temperature rise curve was obtained by temperature-matched curing in the specially designed water bath. A thermocouple was placed at the centre of 100 x 200 mm vacuum sealed cylinder and placed in the water bath. Ten cylinders and eleven flexural beams were vacuum sealed and placed in the temperature-matched curing bath. These specimens were taken out of the water bath and tested at frequent intervals.

Due to the very low strength and stiffness of concrete at very early ages, it is difficult to measure the developing strains during the hardening of the concrete. Although Klink (1975) successfully measured the internal strains in hardened concrete cylinders under compression, there is no standard means of measuring internal strain of very early-age concrete.

Figure 5.6 shows the embedment strain gauge used in this research study to measure the early-age strains. This embedment gage (TML (type KM-100B)) is designed to account for the curing strains generated by several effects, such as thermal and shrinkage strains. TML (type KM-100B) gauges, due to their greater flexibility and higher precision, have provided reliable information for concrete having a stiffness of about 1000 MPa (Boulay and Paties (1993)). All of the gauges were calibrated prior to placing inside the concrete. The total strain can be found as:

$$\epsilon_t = C_\alpha \epsilon_m + C_\beta \Delta T \quad (5.3)$$

where

ϵ_t = total strain

C_α = calibration coefficient

ϵ_m = measured strain

C_β = temperature correction coefficient

ΔT = difference between the measured and initial temperatures

The coefficients C_α and C_β were provided by the manufacturers. The KM-100B embedment strain gage has a full range capacity of $\pm$ 5000 x 10^{-6} and a safe temperature range of -20 to 80°C.

5.4 Experimental Results

5.4.1 Adiabatic Temperature-Time Response

Figure 5.7 shows the temperature increase under temperature-matched curing of the high-strength concrete (90 MPa) control cylinder. This adiabatic response is illustrated for both real age and equivalent age. The initial mix temperature and the ambient temperature was 17 $\pm$ 1°C. The temperature in the water bath was adjusted close to the mix temperature before placing the concrete cylinders and flexural beams. There is a slight increase in temperature during the first 14 hours and a sharp increase in temperature within the next 10 hours. The curve gets fairly smooth about 24 hours after casting. A temperature increase of about 50°C was observed for this 90 MPa concrete mix during hydration. The concrete displayed retardation of hydration during the first 14 hours after casting, which resulted in a time lag in reaching the peak temperature. This is due to the high dosage of superplasticizers. After the retardation period, the slope of the temperature rise response increased very sharply. This curve will be later used as input (i.e., adiabatic temperature rise) in predicting the temperature variations in the tee beams and slabs.

5.4.2 Mechanical Properties

Figure 5.8 shows the compressive stress-strain responses of the 90 MPa concrete for four different curing conditions. These curing conditions include

temperature-matched curing, moist curing, sealed curing and air-dried curing. For the temperature-matched curing, the specimens were cast in special plastic moulds, then vacuum sealed and placed in the water bath. The moist-cured specimens were covered with wet burlap and a plastic sheet. The air-dried specimens were not covered with a plastic sheet, both before and after demoulding. The moist, sealed and air-dried specimens were demolded at about 22 hours after casting and kept in their respective curing conditions for 29 days. The compressive strength and modulus of elasticity were measured over a period of 29 days (see Table 5.2). It must be noted that early-age curing has a significant effect on the long term strength and stiffness. The air-dried specimens had 29-day average compressive strengths of 88% of the moist-cured and 92% of the sealed specimens. Figure 5.9 shows the gain in average compressive strength from very early age up to 29 days. As can be seen the temperature-matched cured specimens had a very rapid gain in compressive strength within a period of 2 days after casting, reaching 85 MPa at 2 days. Whereas, the sealed and air-cured specimens achieved only about 52% of the strength and about 77% of the stiffness of the temperature-matched values at 2 days. This demonstrates the variation of strength and stiffness that can occur in different regions of the concrete members during hydration. Table 5.3 presents the average flexural strength test results due to temperature-matched, moist and air-dried curing conditions. The influence of drying resulted lower flexural strength for the air-cured specimens than the moist-cured specimens, particularly for later ages.

5.4.3 Temperature-Time Responses of Slabs and Beams

Figures 5.10 through 5.15 show the measured temperature-time responses of the slabs and tee beams subjected to insulated, moist and air-dried curing. The temperature measurements were taken at a number of locations over the cross section. As can be seen from these figures there is not a significant time shift between the temperature responses of the specimens subjected to insulated and moist-curing. As expected, the temperature-time responses for the specimens subjected to air-dried curing, particularly the slab, are significantly affected by the curing. The insulated and moist-cured specimens show almost no increase in temperatures during the first 2 hours after casting. There is a temperature rise of about 7°C and 6°C relative to the

placement temperature at about 16 hours after casting for the insulated and moist-cured slabs, respectively. On the other hand, the air-dried slab did not show any increase in temperature during this period of hydration. This is due to the higher rate of heat loss because of the large exposed surface area. Due to the higher dosages of retarders and superplasticizers in this high-strength concrete mix, there is no substantial increase in temperatures during the first 17-18 hours after casting. After the retardation period, a sudden rise in temperature was observed during a period of 4-6 hours. As expected, the insulated specimens showed higher peak temperatures than the moist-cured and air-cured specimens at the same locations. It is also noticed that the rate of temperature increase for the insulated and moist-cured specimens is substantially higher than the air-cured specimens. All of these observations can be explained by the maturity concept (i.e., the rate of heat of hydration increases with increases in temperature). Figures 5.10 and 5.11 illustrate that the insulated and moist-cured slabs have peak temperatures of 53°C and 48.5°C at 21.5 and 21.2 hours, respectively, after casting. The centre of the air-dried slab had a peak temperature of only 35°C at 23.5 hours after casting. The large exposed surface area of the air-dried slab resulted in a lower peak temperature and a longer period to reach the peak temperature. The maximum temperatures recorded were 49°C, 50°C and 44°C in the insulated, moist and air-dried tee-beams, respectively (Fig. 5.13, 5.14 and 5.15). These maximum temperatures were observed at about 22.5, 22 and 21.7 hours after casting. Figure 5.16 shows the measured temperature responses across the flanges of the insulated and moist cured tee-beams. As expected, minimum temperature responses occurred at the tips of these flanges. The recorded maximum temperatures at the tips were 37°C and 38°C at 21.25 hours after casting. It must be pointed out that the insulation, burlap, plastic sheets and formwork were all removed at about the time when the peak temperatures were achieved. This resulted in a sudden drop of temperatures, particularly near the surfaces. This also resulted in a maximum thermal gradient in the specimens of 15.8°C for the insulated tee-beam and 17.5°C for the moist cured beam at about 23 hours after casting. This large thermal gradient in very thin flanged members may provide the potential for cracking. These figures demonstrate the significance of curing conditions on the temperature-time response.

Plastic shrinkage cracks were observed on the top of the air-dried slab. The first

crack (about 1 mm wide and 10 mm long) occurred at about 5 hours after casting near the corner of the slab. In order to study the sensitivity of surface finishing, one-half of the air-dried slab was screeded at a time of 4 hours while the other half was left undisturbed. A second crack formed 6 hours after casting. The length of the initial crack increased to 50 mm at a time of 9 hours. The combined effect of rapid drying and striking off the surface with screeds may have produced tension on the surface, resulting in surface cracking. It was observed that these cracks stopped propagating after 12 hours, and became smaller in width. No cracks were observed on the moist-cured and insulated specimens. After stripping, one crack was observed on the bottom surface of one flange of the air-dried tee beam. This may be due to the thermal shock from stripping the form-work when the peak temperature of the concrete was reached. The common practice of early stripping (18-20 hours) of precast elements may cause thermal shock and promote large thermal gradients, thus increasing the potential of thermal cracking.

Figures 5.17, 5.18 and 5.19 illustrate the influence of curing on the strains measured near the top and bottom of the precast tee beams. As expected, the difference between the top and bottom are minimal in the case of the fully insulated tee beam (see Fig. 5.17), whereas the tee beam with moist curing results in a drop in temperature near the top of the tee beam due to loss of heat near the surface (see Fig. 5.18). Air-dried curing results in a lower peak temperature, larger drop in temperatures near the top surface and a greater shrinkage strain near the surface, both of which result in smaller values of total strains near the surface (see Fig. 5.19). It is apparent from Figs. 5.18 and 5.19 that the early-age shrinkage plays a key role on the deformations. In both cases, after the formwork removal at about 22 hours, the strains are strongly affected by shrinkage with shortening strains of about -100 microstrains at an age of 78 hours.

Figure 5.20 shows the total strains measured at the centre of the insulated, moist-cured and air-dried slabs. It is apparent from this figure that the total strain measured in the air-dried slab is dominated by the early-age shrinkage. The early-age shrinkage plays such a dominant role in the air-dried slab that it totally outweighed the expansion from the thermal effects. The strains were measured at the centre of the slab and even larger shrinkage strains would be expected on the top exposed surface.

Lack of proper curing can result in significant shrinkage strains (-350 microstrains at 24 hours) which may lead to early age cracking. It is interesting to note that the air-dried slab experienced some surface cracking following the final screeding of the concrete surface. During this stage, the slab was undergoing significant plastic shrinkage.

5.5 Finite Element Temperature Predictions

Two-dimensional transient thermal analyses, with different boundary conditions, were carried out to predict the temperatures in the slab specimens. It was assumed that each slab was infinitely long such that there is no temperature variation in the longitudinal direction. The middle cross-section of the slab was idealized using two-dimensional isoparametric elements and the boundaries were modelled by convection elements. Figures 5.21 and 5.22 show the comparisons between the measured and predicted temperatures at two locations (i.e., at the centre and close to the surface) of the insulated and moist-cured slabs. In these figures, the measured ambient temperatures are also shown. Fig 5.23 shows the comparison between the measured and predicted temperatures at the centre of the air-dried slab. As can be seen from these figures the predicted values show close agreement with the measured data. It must be pointed out that the top surface of the air-dried slab was not covered, resulting in relatively low peak temperatures due to significant heat loss and the drying effect. The boundary elements representing the plywood formwork, the burlap, the plastic sheet and the insulation were included in the model up to 21.5 hours for the insulated specimens and up to 22 hours for the air-dried specimens. These boundary elements were removed to simulate the actual conditions and new surface convection elements were employed. The input parameters included the adiabatic temperature curve, the thermal conductivity, density and specific heat as well as the appropriate thermal characteristics of the boundary elements. Table 5.4 presents the parameters used for thermal analyses. It was assumed that the thermal conductivity and the specific heat (taken as average of air-dried and saturated concrete) of the concrete did not change with age and temperature. The thermal properties of the boundary elements, such as the plywood and insulation, were taken from manufacturers data and other information, such as the convection coefficient of air, were taken from

handbooks (ASHRAE (1989), CPCI (1987)). Due to the controlled laboratory conditions, the convection heat transfer coefficient of still air was used in the analyses.

Figure 5.24 shows the predicted temperature contours for the three slabs (insulated, moist cured and air-dried) using the modified version of program "DETECT". Temperatures were predicted at the time corresponding to the maximum thermal differences (i.e., about 22 hours) in the slabs. Figure 5.24 shows predicted temperature differences of 6.8, 6.4 and 4.4°C for the insulated, moist-cured and air-dried slabs, respectively. The maximum measured temperature differences between the centre and the outside surface were 7.0°C for the insulated slab and 6.5°C for the moist-cured slab occurring at about 23 hours after casting. Unlike the other two slabs, the air-dried slab did not have a thermocouple at the corner of the slab. As predicted, the insulated slab experienced the highest temperature difference after the removal of formwork, which can result in significant restraint stresses and the possibility of thermal cracking.

5.5.1 Temperature Predictions for Large Concrete Columns

Three large 1 x 1 x 2 m high plain concrete columns were cast at McGill University using ready-mix concrete (Cook et al (1992)). The mixes were designed to produce normal-strength concrete (35 MPa compressive strength at 28 days), a high-strength concrete (90 MPa compressive strength at 28 days) and a very high-strength concrete (120 MPa compressive strength at 28 days). Both the 90 and 120 MPa concrete mixes used a blended cement containing 7-8% by volume of silica fume. Thermocouples were used to measure the temperatures at a number of locations over the cross section, located at the mid-height of each column and along the centreline of each column. The locations of these thermocouples, having a precision of 0.1°C, are shown in Fig. 5.25. The initial concrete temperatures, on delivery from the ready mix plant, were 25.5, 22 and 16.5°C for the 35, 90 and 120 MPa concretes, respectively. These values were used as the initial temperature condition in the thermal analyses (see Table 5.4). It must be pointed out that the initial concrete temperature is a very important factor which can affect the rate of temperature rise and the peak temperature. The peak temperatures recorded were 68, 68 and 63°C, with corresponding temperature rises of 43, 46 and 47°C, for the 35, 90 and 120 MPa

concrete columns, respectively.

Figure 5.26 shows the comparison between the measured and predicted temperatures at the centre and midside surface of each column. In the two-dimensional analyses, only one quarter of the 1 x 1 m column cross section was modelled due to symmetry about the X and Y axes. It was assumed that the column was significantly long such that there was no temperature variation in the Z-direction, thus permitting a two-dimensional analysis to be carried out. The measured ambient temperatures are also shown in Fig. 5.26, and are used in predicting the temperatures. There is a reasonably close agreement between the measured and predicted values of temperatures. The largest difference between the predicted and measured peak temperatures was 2°C for the 35 MPa concrete column.

Figure 5.27 shows the predicted temperature contours corresponding to the maximum thermal gradient in a quadrant of 1 x 1 m cross section for the 35, 90 and 120 MPa concrete columns. As can be seen from this figure the 35 MPa and 90 MPa columns have nearly identical temperature differences (i.e., 23°C for 35 MPa and 22°C for 90 MPa), between the centre and the corner of the column. On the other hand, 120 MPa concrete column showed a significantly smaller temperature difference of 17°C. No cracks were observed at the surfaces of these columns.

It must be pointed out that although these temperature differences accurately model the actual conditions experienced in the hydrating concrete columns, they do not provide a fair comparison because of the significantly different initial temperatures of the concrete and the different ambient temperature conditions. Parametric studies of the temperatures and stresses developed in large columns, made from different concretes, having the same initial concrete temperatures and the same ambient conditions are presented in Chapter 6.

5.5.2 Temperature Predictions for a Large Precast I-Girder

Figure 5.28 shows the predicted temperature contours in a large precast pretensioned I-girder section. This cross section is a standard CPCI 2300 section with an over all depth of 2300 mm and a web thickness of 150 mm. This section is currently being used for a major project in eastern Canada. Analyses were carried out using the modified version of program "DETECT" in which the following assumptions

were made:

i. A temperature-matched curing curve consistent with that obtained for the 100 MPa high-strength concrete used in this research program.

ii. The initial concrete temperature was assumed to be 18°C and a constant ambient temperature of 22°C was used.

iii. In one case steel formwork with a thickness of 10 mm was assumed, and in the other case plywood formwork with a thickness of 20 mm was assumed (see Table 5.4, Fig's 5.30 and 5.31).

iv. It was assumed that the formwork was removed 20 hours after casting.

v. Parametric studies were carried out with different values of thermal conductivity and specific heat.

The removal of the formwork at a time of 20 hours after casting simulated normal practice in the precast concrete industry. A maximum temperature of 50°C was found at the centre of the bottom flange, and a peak temperature of 44°C was predicted at the centre of the web (see Fig. 5.28). Cracking was observed, upon form removal, in the first CPCI 2300 girder fabricated. This was accentuated by very low ambient temperatures (about 5°C) at the outdoor precast plant, during the casting of the first girder.

Figure 5.29 shows the maximum predicted temperature histories at the centre of the bottom flange of the I-girder due to the use of either plywood or steel formwork. As expected, the concrete cast in steel formwork resulted in lower peak temperature (about 4°C lower) than the concrete cast in wooden formwork. This is due to the very high thermal conductivity of steel as compared to plywood. It must be pointed out that concrete cast in wooden formwork will result in higher temperatures but lower temperature differences between the centre and surface of the member compared to that cast in steel formwork. While at first this may appear to be advantageous, the wooden formwork, however, may result in higher thermal stresses upon sudden form removal as the member cools quickly. Steel formwork is preferred in the precast industry. Another important factor affecting cracking during hydration is the presence of external restraint effects. For this case, the CPCI girder is restrained in the longitudinal direction by a large number of pretensioned strands anchored in the pretensioning bed. Hence as the member rapidly cools after form removal, the tensile

stresses arising from the restraint offered by the pretensioned strands together with the tensile stresses developed from thermal gradients as the member cools may result in cracking.

Temperature predictions have also been made for the I-girder to study the influence of thermal conductivity of the concrete. Factors such as age, composition and types of aggregates have a strong influence on the conductivity. Figure 5.30 illustrates the temperature variations due to different thermal conductivity values ranging from 1 W/m-°C to 3 W/m-°C. The other parameters, such as specific heat, density, formwork and boundary conditions were kept the same. As expected, the temperature decreases as the thermal conductivity increases. There is about a 3°C drop in peak temperature as the thermal conductivity is increased from 1 to 3 W/m-°C.

Figure 5.31 illustrates the effect of the specific heat of concrete on the temperature rise. Thermal analyses were carried using a wide range of specific heat values of concrete (i.e., from 0.5 J/g-°C to 1.0 J/g-°C). As expected, the temperature decreases with decreasing values of specific heat for a constant value of thermal conductivity and density. A range of peak temperatures from 57°C to 52°C were predicted as the specific heat varied from 1.0 J/g-°C and 0.5 J/g-°C, respectively.

Table 5.1 - Composition and properties of 90 MPa ready mix concrete

Characteristics	90 MPa
cement (Type 10), kg/m^3	570 *
fine aggregates, kg/m^3	730
coarse aggregates, kg/m^3	960
total water**, kg/m^3	143
water-Cement ratio	0.25
water-reducing agent, ml/100 kg of cement	370
superplasticizer, ml/100 kg of cement	2100
slump, mm	200
air content, %	1.5
density, kg/m^3	2417

* Type 10 blended cement containing 8 - 9 % silica fume

** Includes the water in admixtures

Table 5.2 - Compressive strength and elastic modulus for 90 MPa concrete for different curing conditions

Age (days)	f_c (t) (MPa)				E_c (t) (GPa)			
Temperature-matched curing								
	S1	S2	S3	Mean	S1	S2	S3	Mean
0.59	4.62	-	-	4.62	3.75	-	-	3.75
0.66	24.06	-	-	24.06	21.00	-	-	21.00
0.76	33.95	-	-	33.95	29.00	-	-	29.00
1.89	82.13	-	-	82.13	39.80	-	-	39.80
2.02	84.94	-	-	84.94	41.30	-	-	41.30
Moist curing								
0.71	1.60	-	-	1.60	1.70	-	-	1.70
0.81	13.41	-	-	13.41	10.40	-	-	10.40
1.03	33.59	-	-	33.59	26.30	-	-	26.30
1.84	44.16	-	-	44.16	31.60	-	-	31.60
6	63.08	62.20	-	62.60	30.70	32.70	-	31.70
7	70.23	69.80	-	70.00	36.40	37.30	-	36.80
22	87.45	85.00	-	86.20	38.80	-	-	38.80
29	87.10	87.20	90.30	88.20	39.30	-	41.00	40.10
Sealed curing								
0.68	0.79	-	-	0.79	-	-	-	-
0.85	25.99	-	-	25.99	24.10	-	-	24.10
1.05	34.14	-	-	34.14	27.80	-	-	27.80
6	60.35	61.70	-	61.05	30.00	-	-	30.00
23	83.22	83.20	86.90	84.4	38.00	37.90	40.00	38.60
29	87.25	85.30	-	86.3	37.60	39.00	-	38.30
Air-dried curing								
0.83	10.19	-	-	10.19	10.60	-	-	10.60
0.88	24.14	-	-	24.14	21.30	-	-	21.30
1.83	42.26	-	-	42.26	30.50	-	-	30.50
6	57.58	59.60	-	58.60	32.50	32.80	-	32.70
7	63.61	62.90	-	63.20	35.60	33.10	-	34.40
29	76.47	78.60	76.20	77.10	34.40	35.50	35.70	35.20

Table 5.3 - Average flexural strength test results for 90 MPa concrete due to different curing conditions

Age (days)	Temperature-matched curing $f_r(t)$, MPa	Age (days)	Moist curing $f_r(t)$, MPa	Age (days)	Air-dried curing $f_r(t)$, MPa
0.65	2.41	0.81	2.06	0.82	1.03
1.01	5.35	1.04	4.95	1.03	4.92
1.91	8.01	34	7.40	34	5.30
8	9.13	-	-	-	-
14	9.49	-	-	-	-

Table 5.4 - Parameters used for thermal analyses of columns, slabs and I-girder

Parameters	35 MPa Column	90 MPa Column	120 MPa Column
conductivity (W/m-°C)	1.40	1.68	1.80
specific heat (J/kg-°C)	1170	1050	1000
convection coefficient (W/m^2-°C)	8.3	8.3	8.3
initial T (°C)	25.5	22.0	16.5
ambient T (°C)	23.5-29.0 (see Fig. 5.25)	17.0-24.0 (see Fig. 5.25)	14.5-27.0 (see Fig. 5.25)
adiabatic ΔT (°C)	42.0	50.0	52.0
density (kg/m^3)	2300	2410	2505
formwork type	plywood* (20mm)	plywood* (20 mm)	plywood* (20 mm)
Parameters	**90 MPa Slabs**	**50 MPa I-Girder**	
conductivity (W/m-°C)	1.76	1.17	
specific heat (J/kg-°C)	770	864	
convection coefficient (W/m^2-°C)	8.3 (side) 9.3 (bottom) 6.2 (top)	8.3 (side) 9.3 (bottom) 6.2 (top)	
initial T (°C)	18.0	18.0	
ambient T (°C)	18.5-25.5 (see Fig. 5.20)	22.0	
adiabatic ΔT (°C)	50.0 (see Fig. 5.6)	50.0 (see Fig. 5.6)	
density (kg/m^3)	2480	2300	
formwork and insulation	plywood* (18 mm) styrofoam** (25mm) burlap□ (5mm)	steel● (10 mm) or plywood* (20 mm)	

* conductivity = 0.12 W/m-°C, specific heat = 1213 J/kg-°C, density = 545 kg/m^3
** conductivity = 0.03 W/m-°C, specific heat = 1213 J/kg-°C, density = 29 kg/m^3
□ conductivity = 0.02 W/m-°C, specific heat = 1280 J/kg-°C, density = 30 kg/m^3
● conductivity = 54 W/m-°C, specific heat = 465 J/kg-°C, density = 7833 kg/m^3

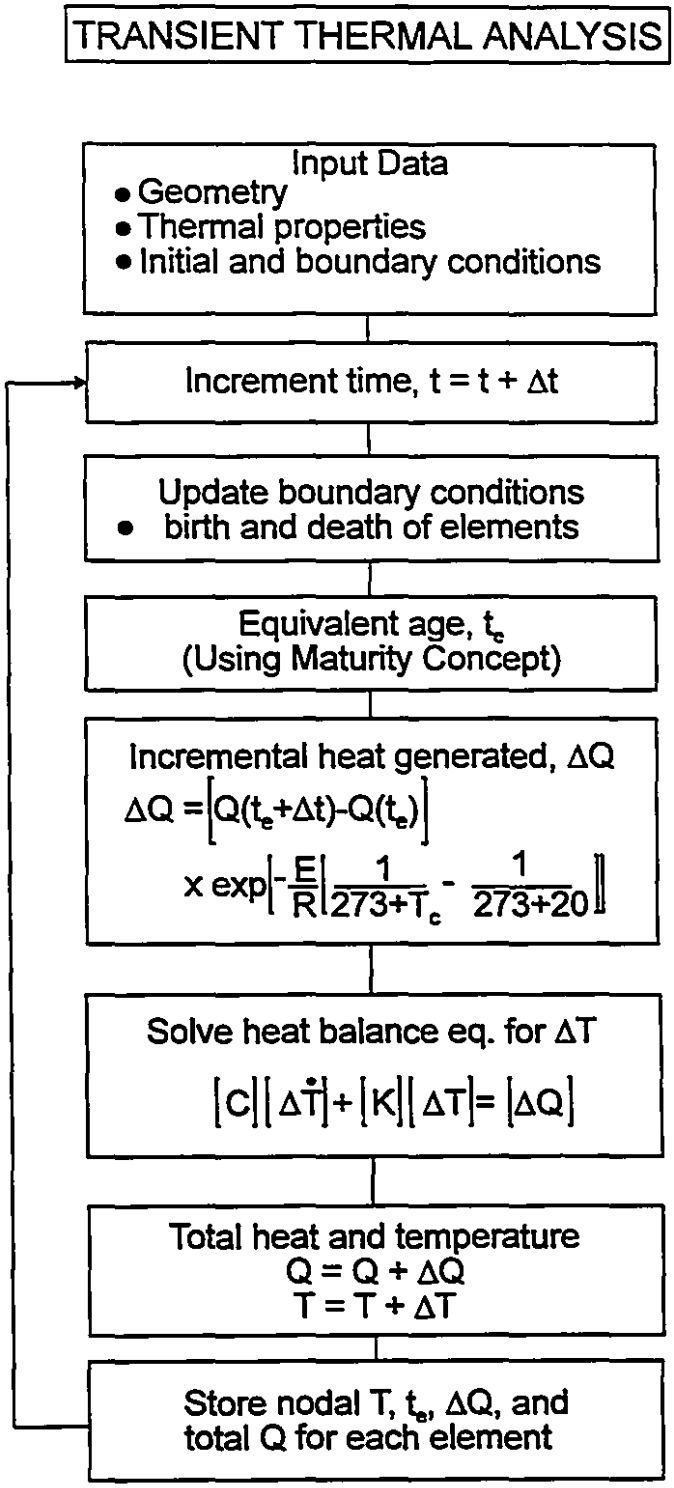

Figure 5.1- Flow chart for the transient thermal analysis

Figure 5.2 - Photograph of insulated slab and instrumentation before casting

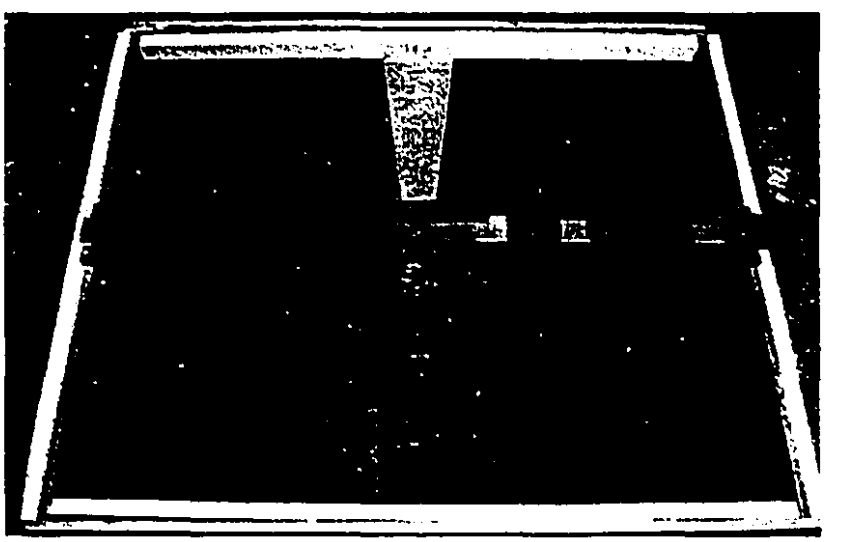

Figure 5.3 - Photograph of insulated tee beam and instrumentation before casting

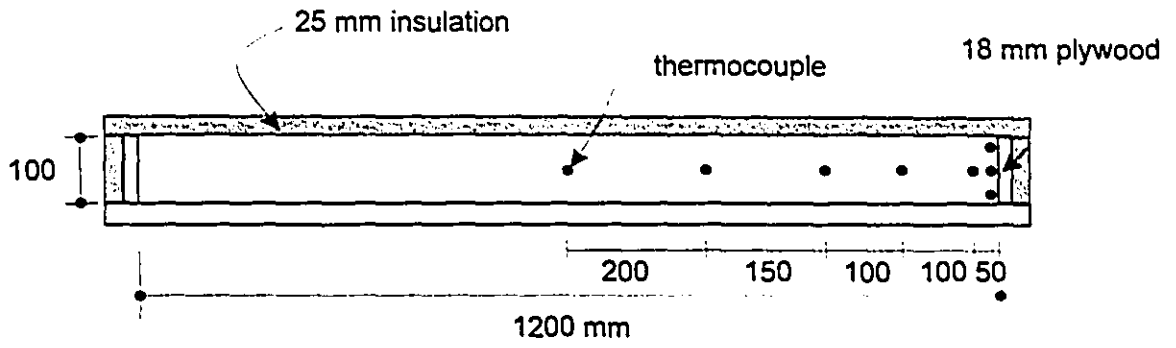

(a) Insulated slab

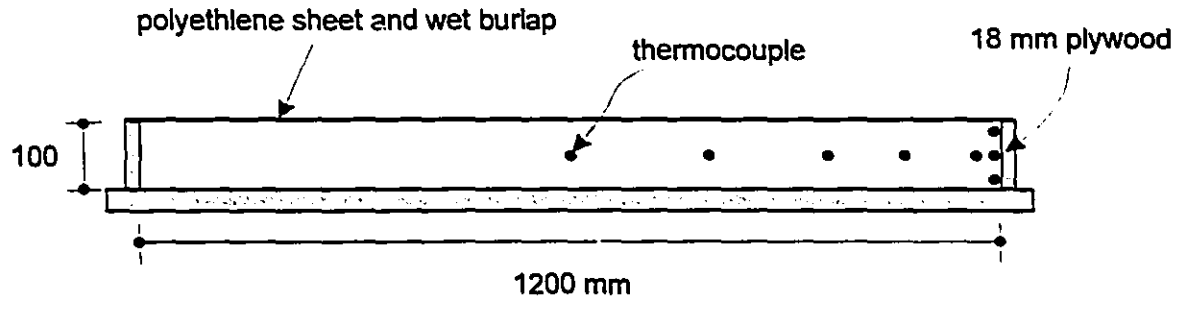

(b) Moist-cured slab

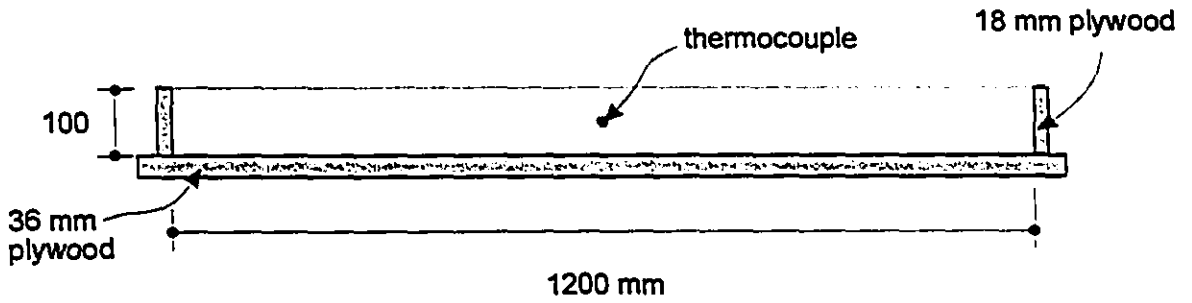

(c) Air-dried slab

Figure 5.4 - Instrumentation and curing conditions for slabs

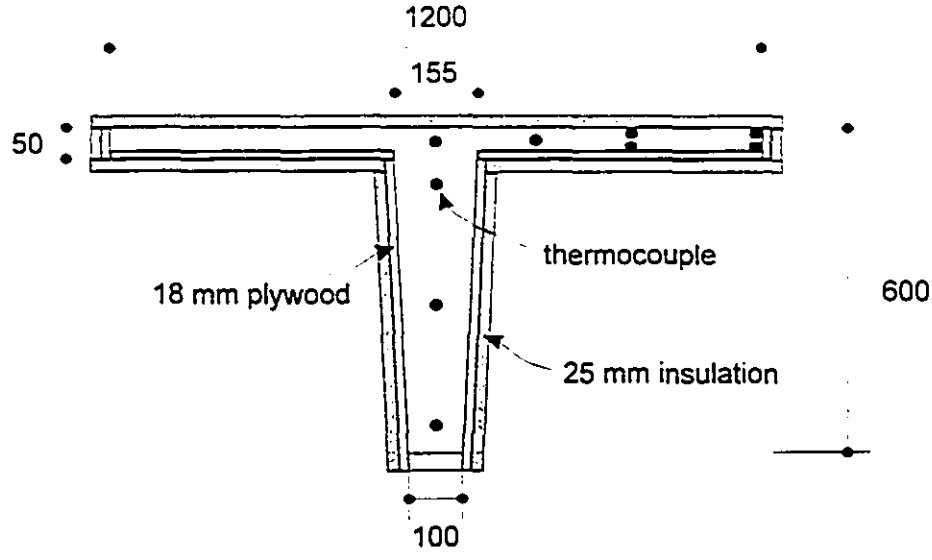

(a) Insulated tee-beam

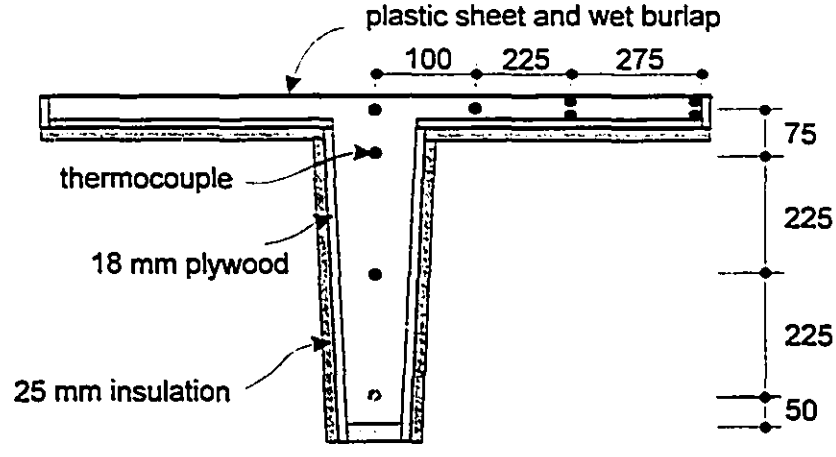

(b) Moist-cured tee-beam

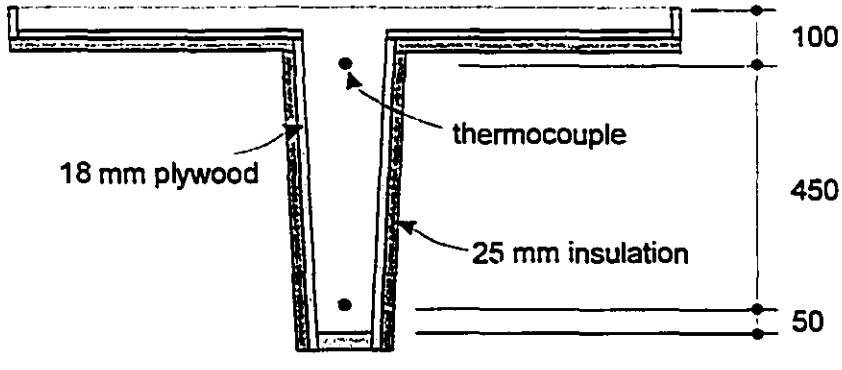

(c) Air-dried tee-beam

Figure 5.5 - Instrumentation and curing conditions for tee beams

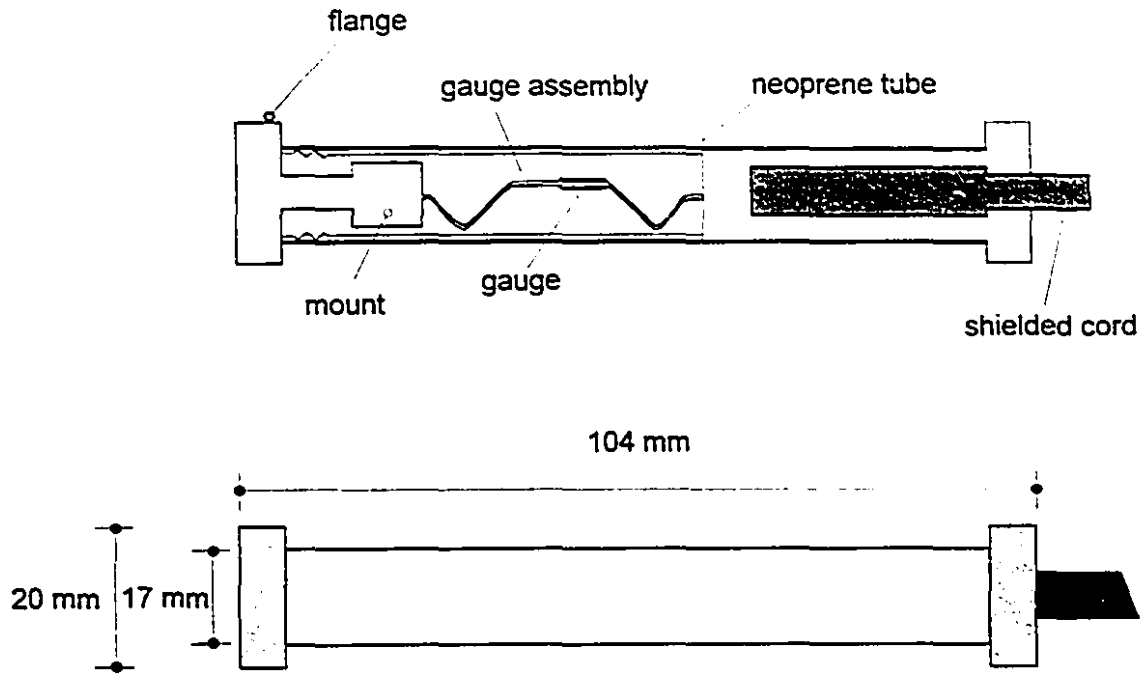

Figure 5.6 - Embedment strain gauge used for measuring early-age strain

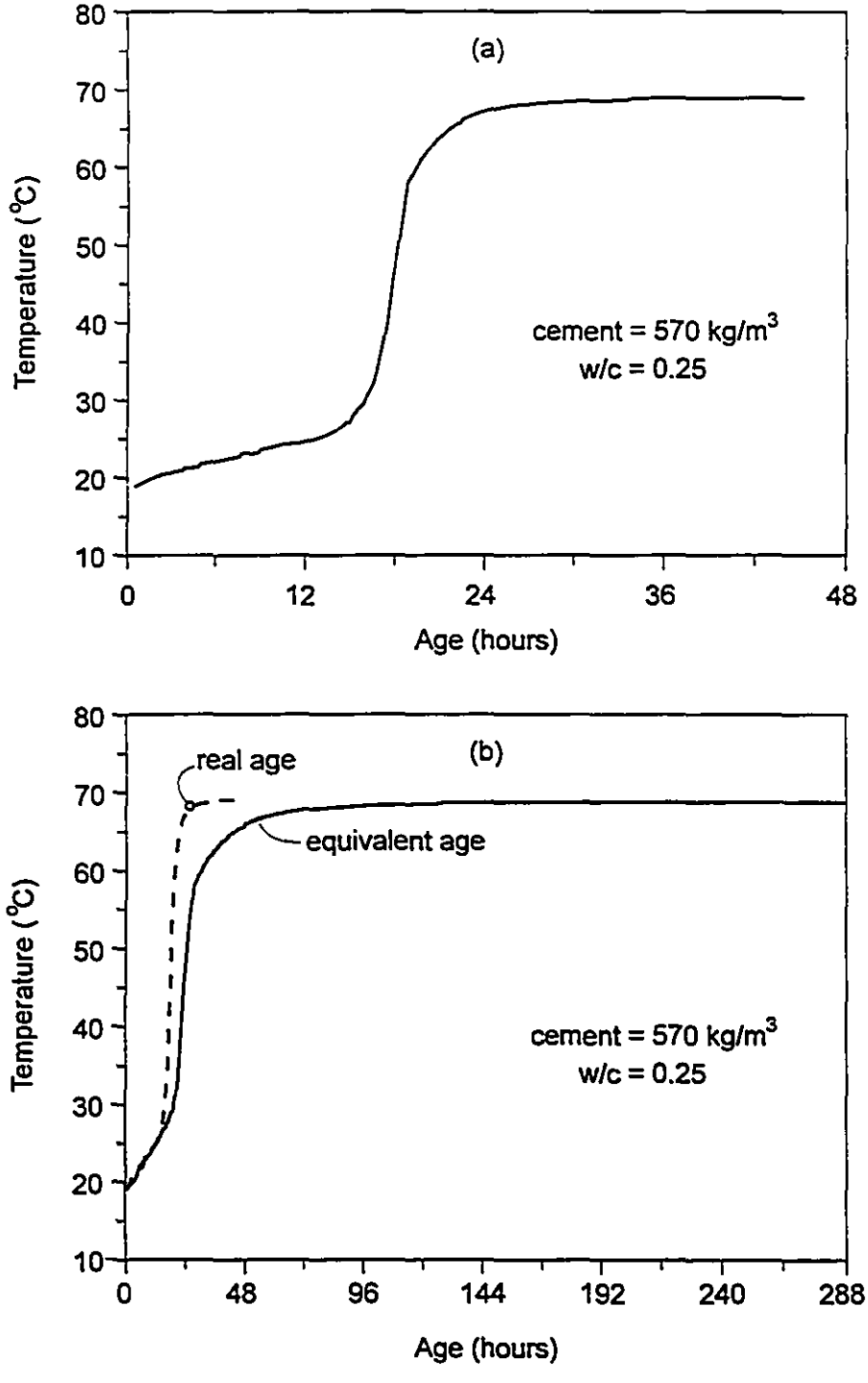

Figure 5.7 - Temperature increase of 90 MPa concrete during temperature-matched curing

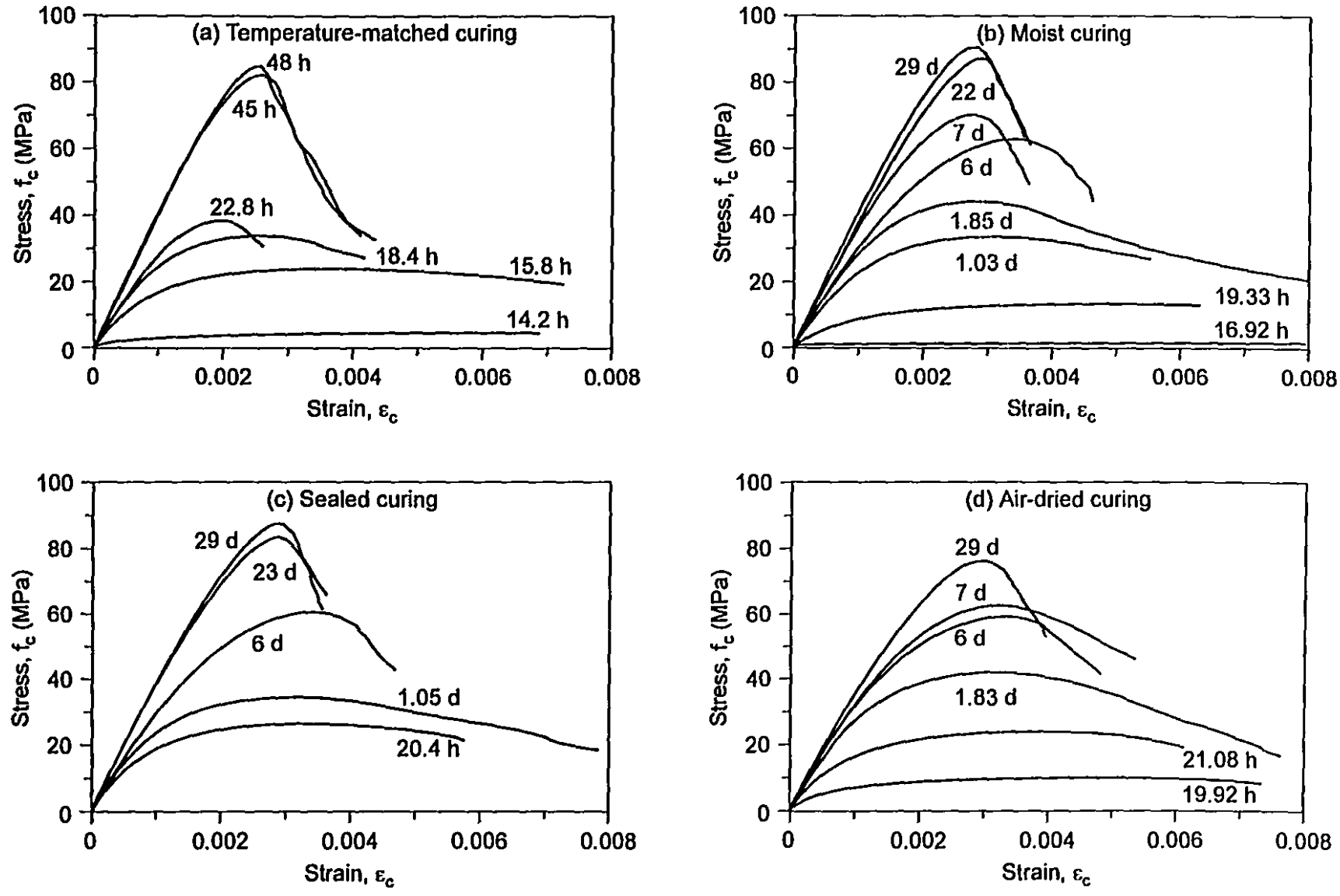

Figure 5.8 - Compressive stress-strain responses of 90 MPa concrete for four different curing conditions

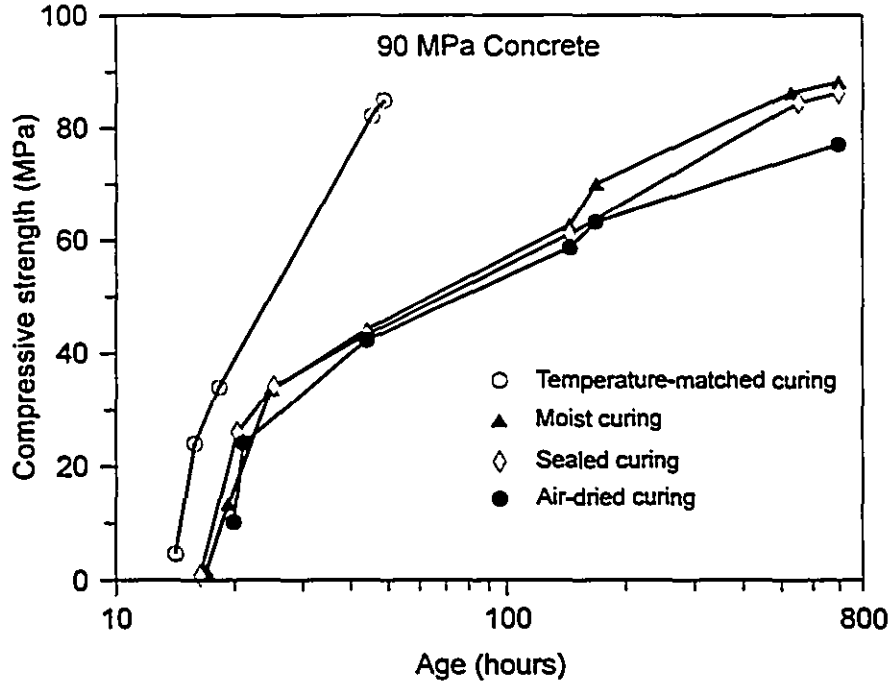

Figure 5.9 - Variation of average compressive strength with age (on log scale)

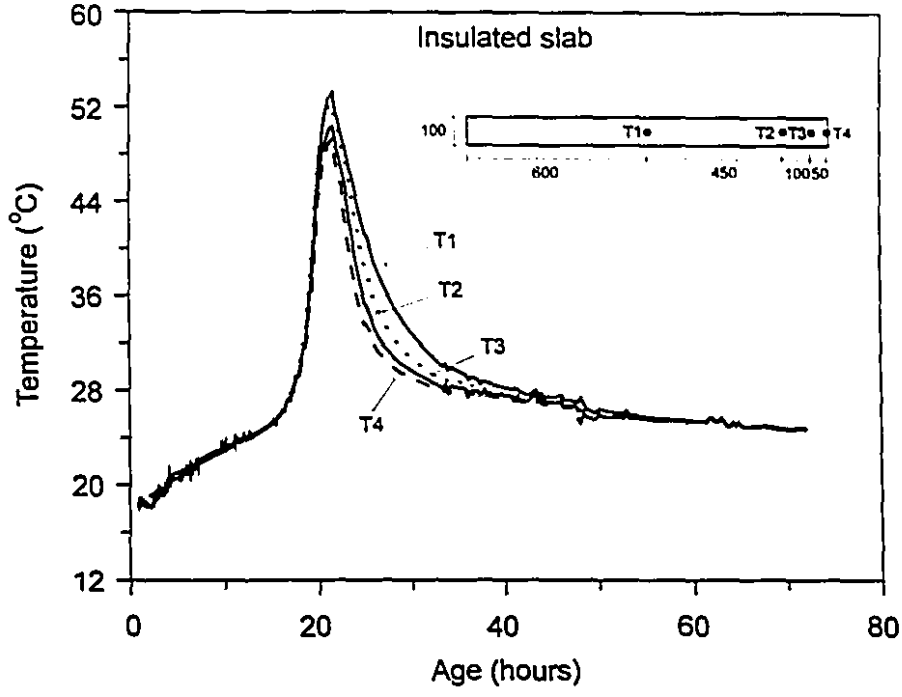

Figure 5.10 - Measured temperature variation in an insulated slab

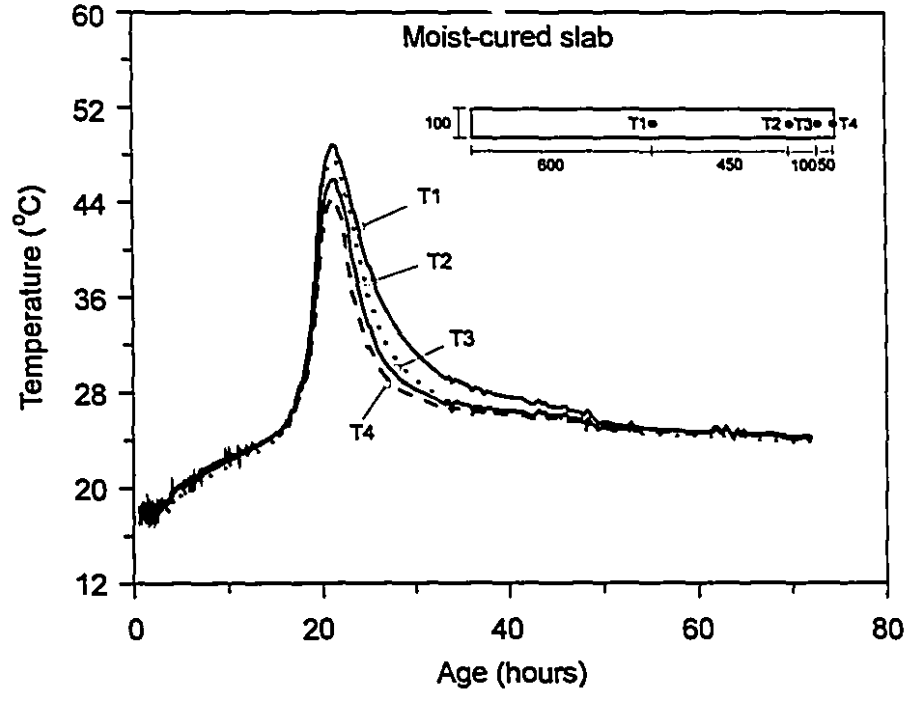

Figure 5.11 - Measured temperature variation in a moist-cured slab

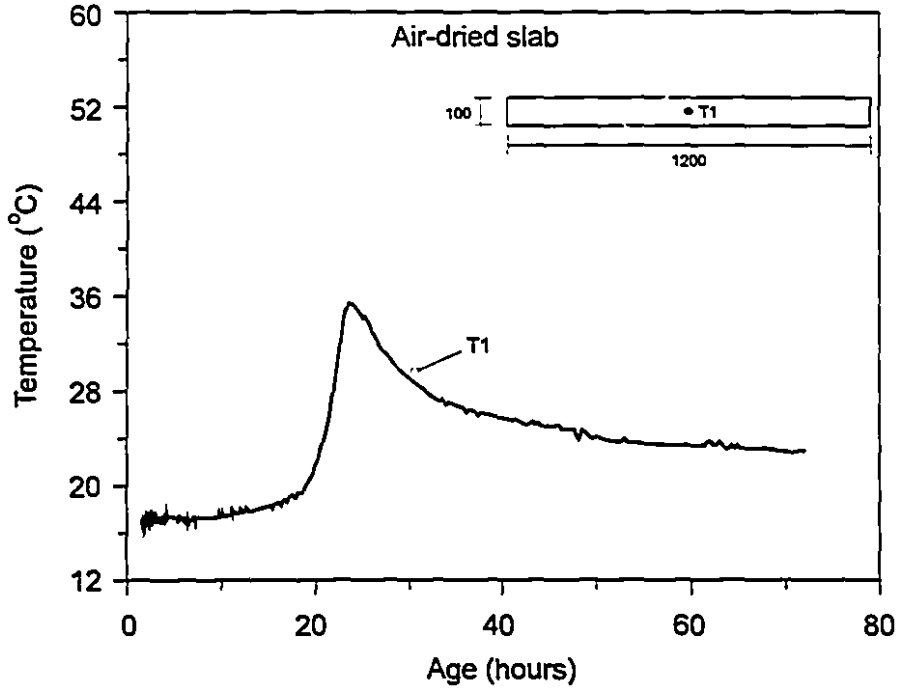

Figure 5.12 - Measured temperature variation in an air-dried slab

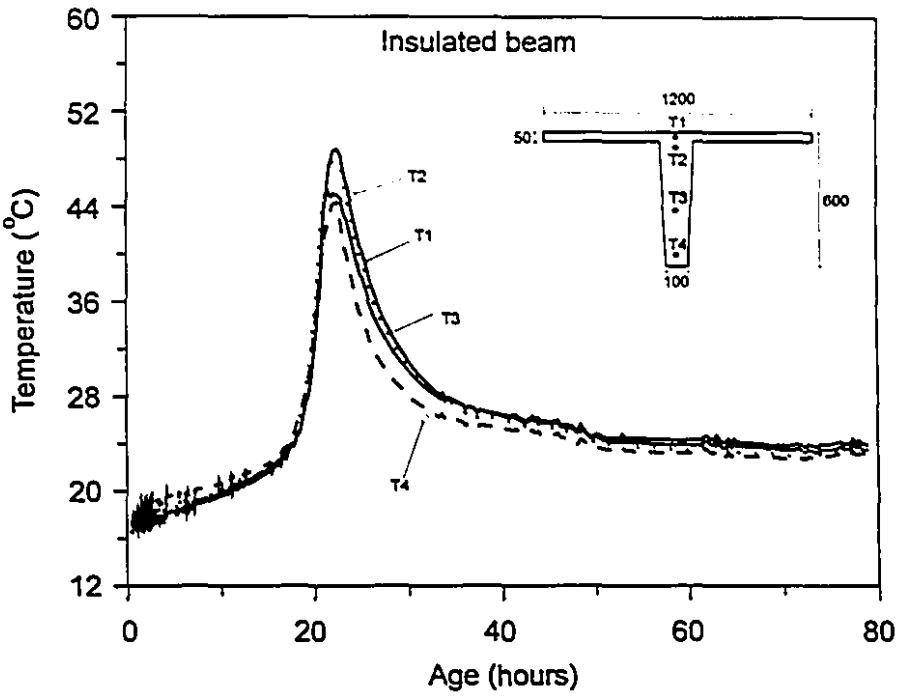

Figure 5.13 - Measured temperature variation in a tee-beam subjected to insulated curing

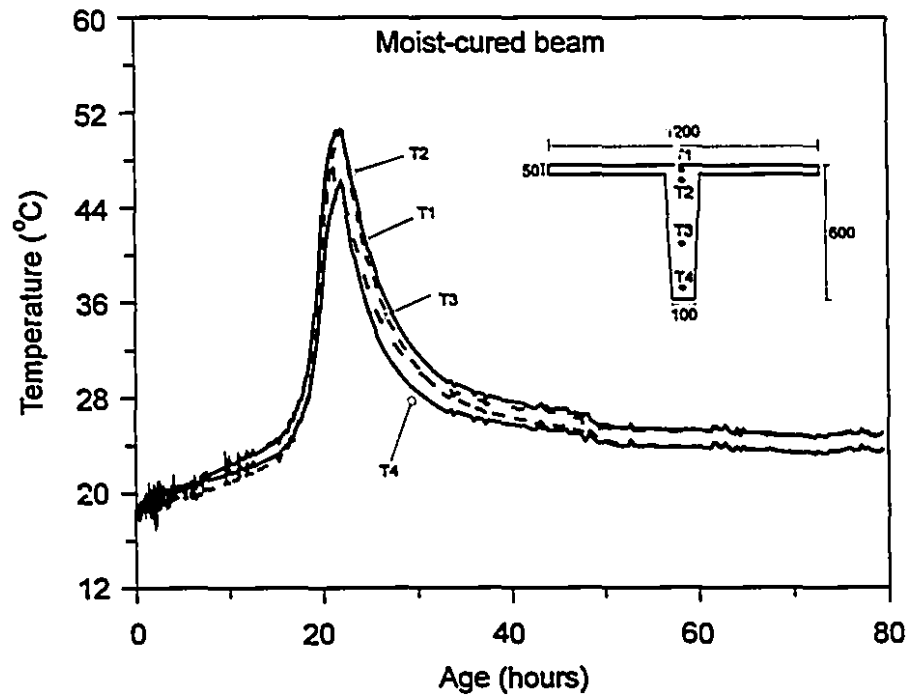

Figure 5.14 - Measured temperature variation in a tee-beam subjected to moist curing

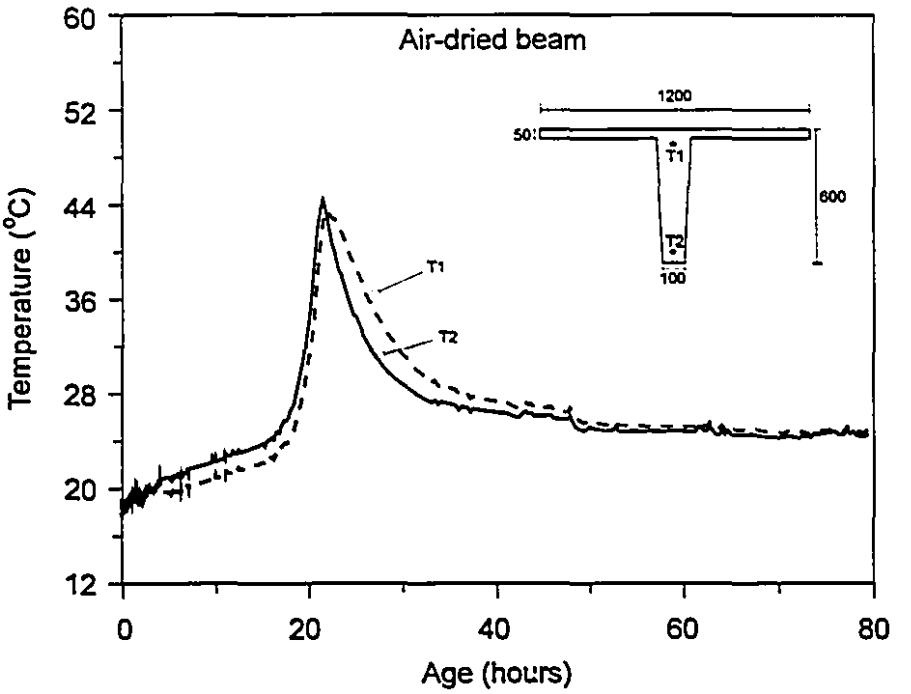

Figure 5.15 - Measured temperature variation in tee-beam subjected to air-dried curing

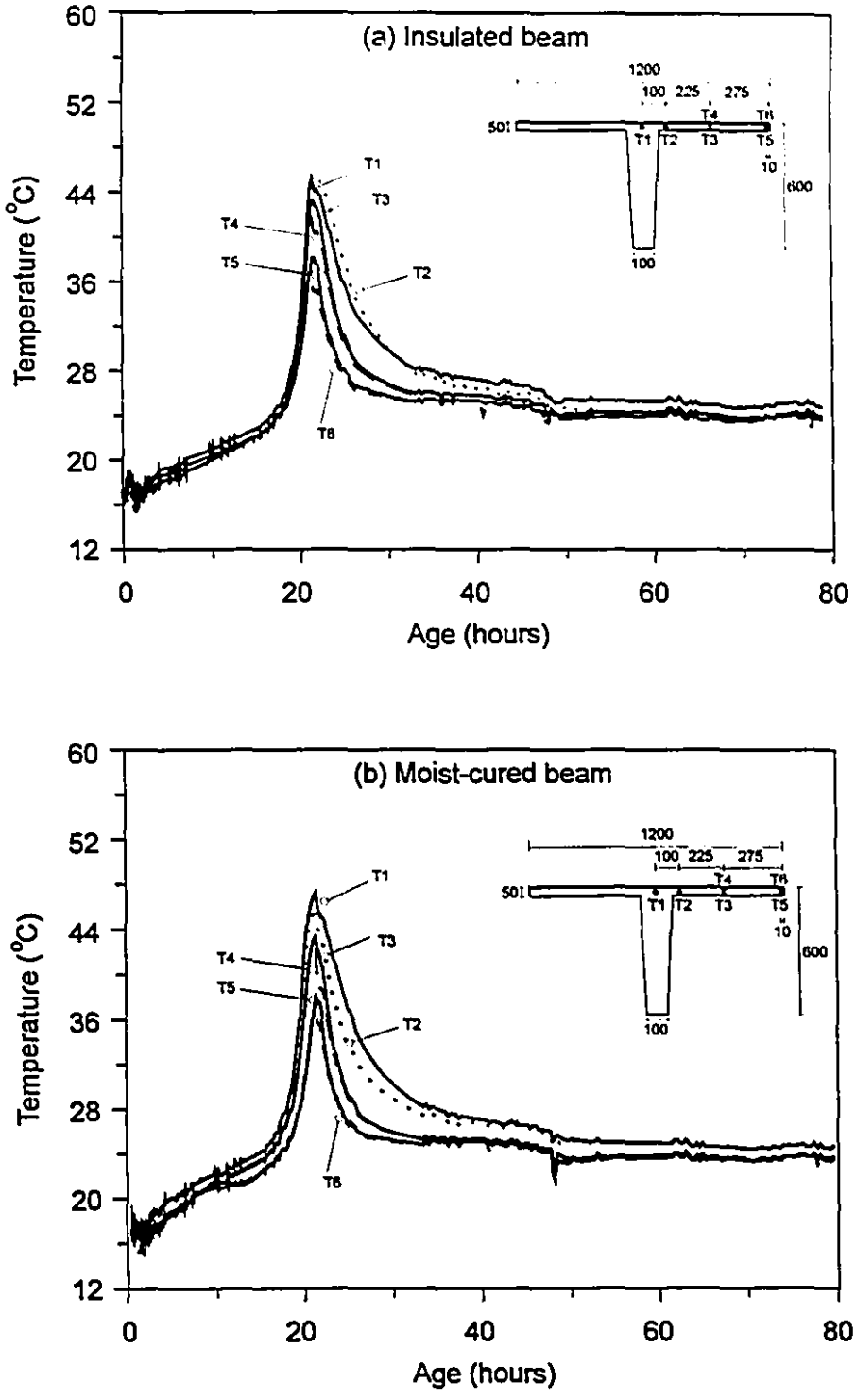

Figure 5.16 - Measured temperature variation across tee-beam flanges

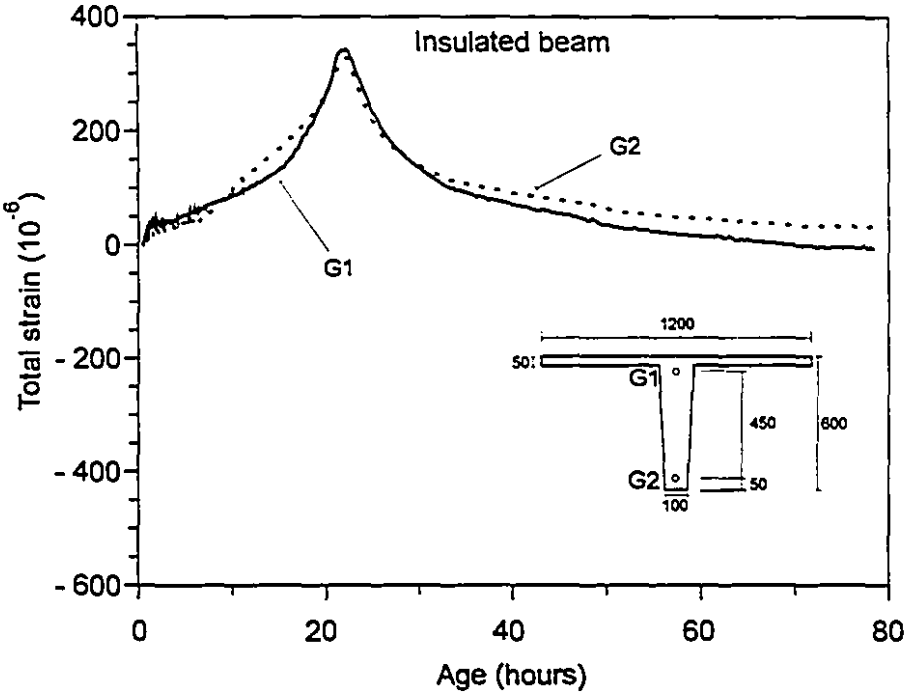

Figure 5.17 - Total strain variation with age in tee beam subjected to insulated curing

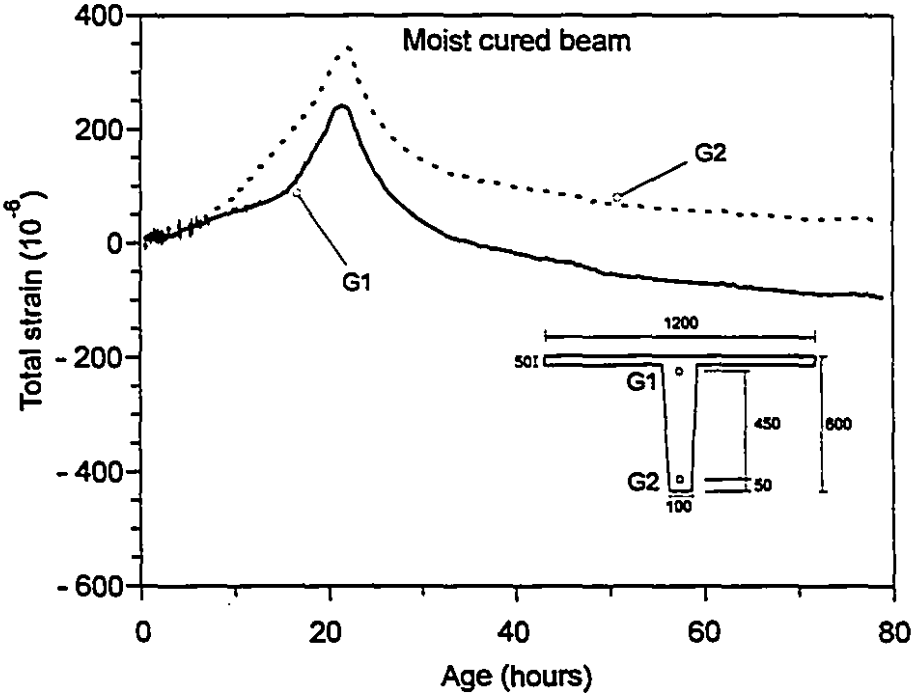

Figure 5.18 - Total strain variation with age in tee beam subjected to moist curing

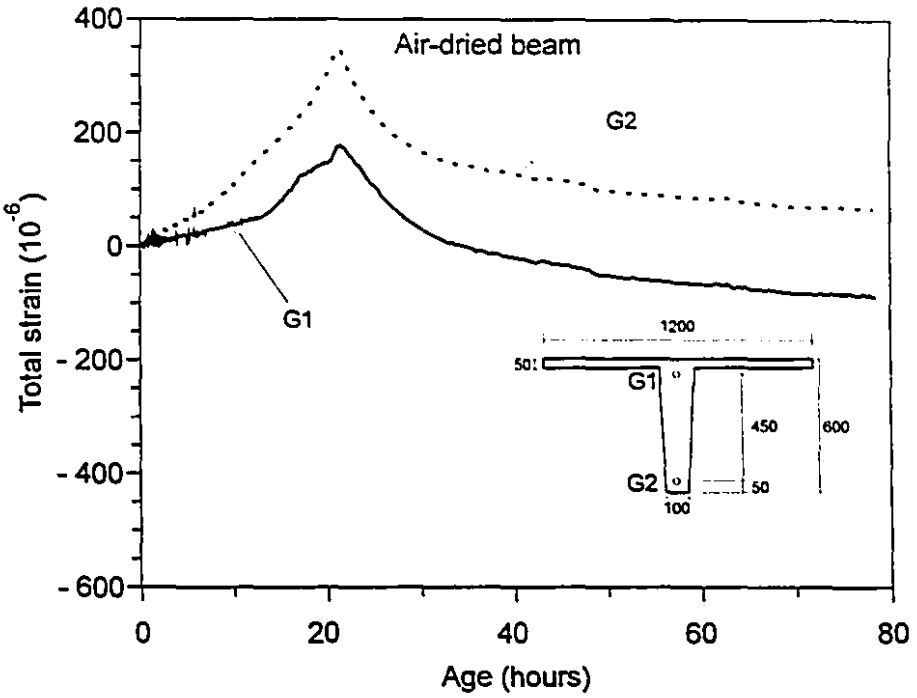

Figure 5.19 - Total strain variation with age in tee beam subjected to air-dried curing

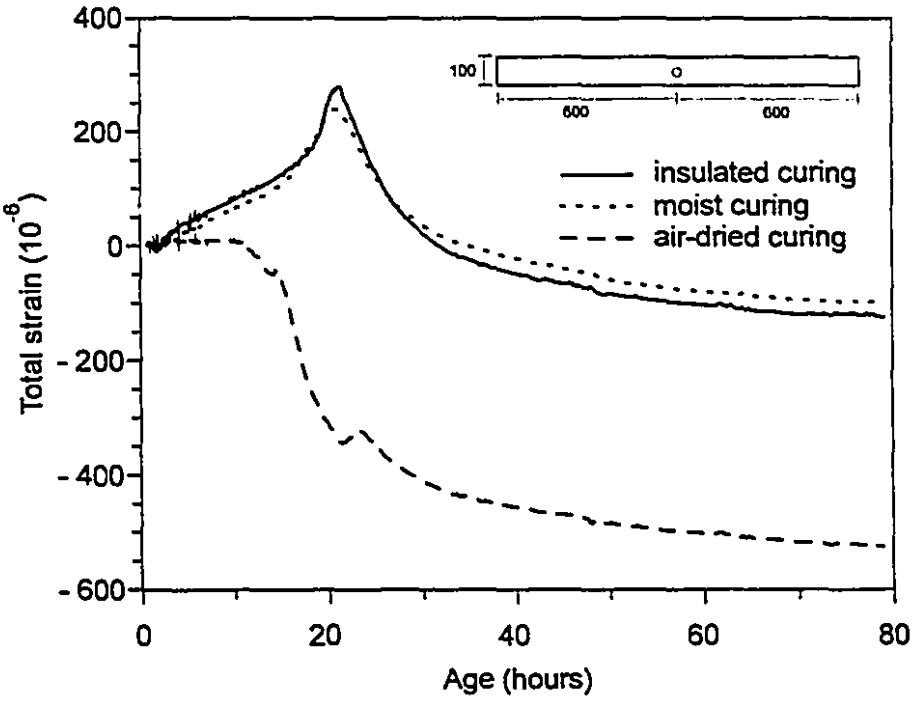

Figure 5.20 - Total strain variation with age in a slab subjected to different curing conditions

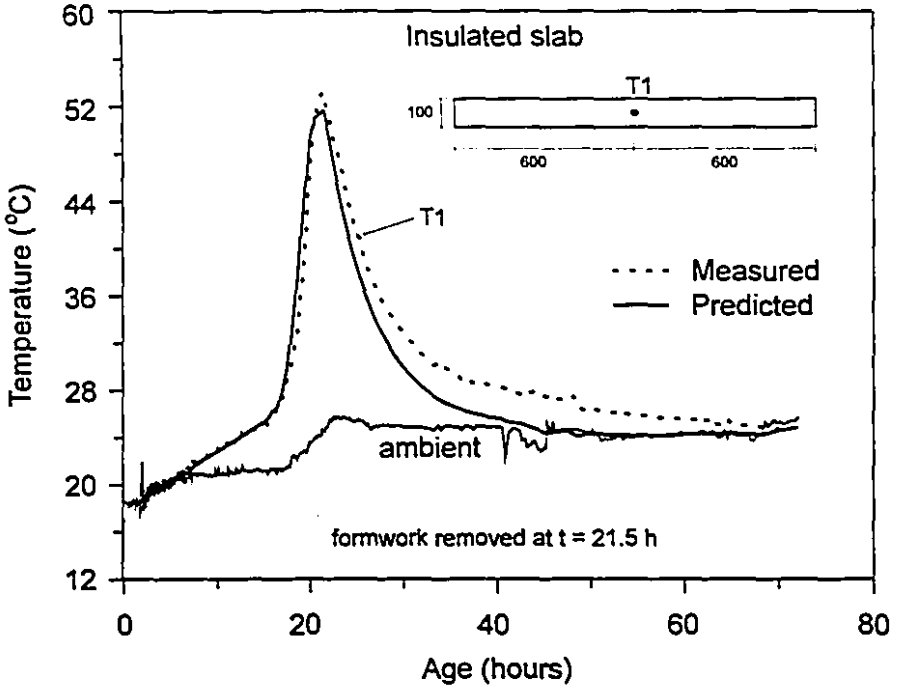

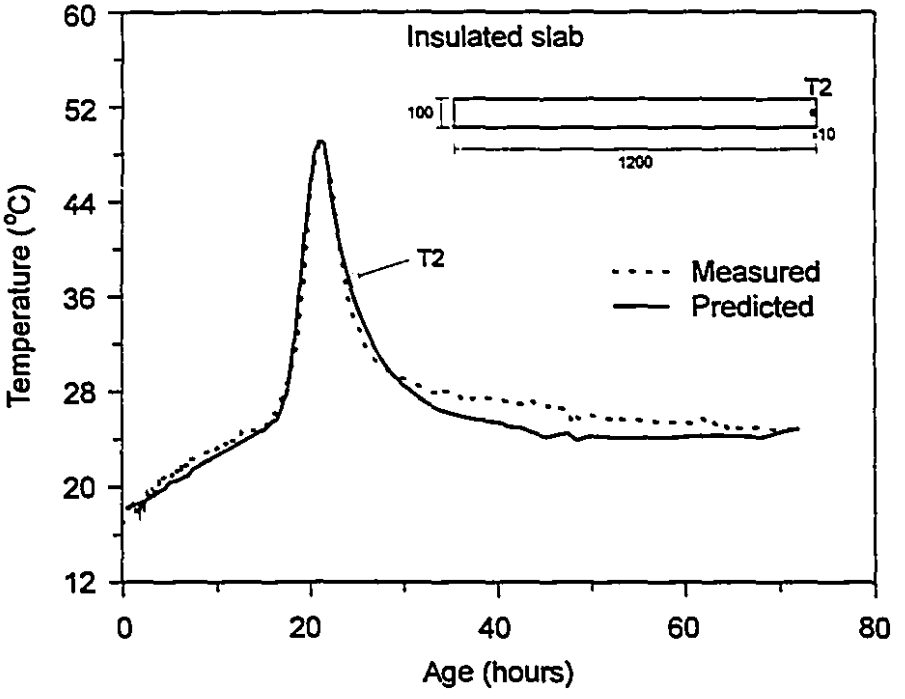

Figure 5.21 - Comparison between the measured and predicted temperature responses for insulated slab

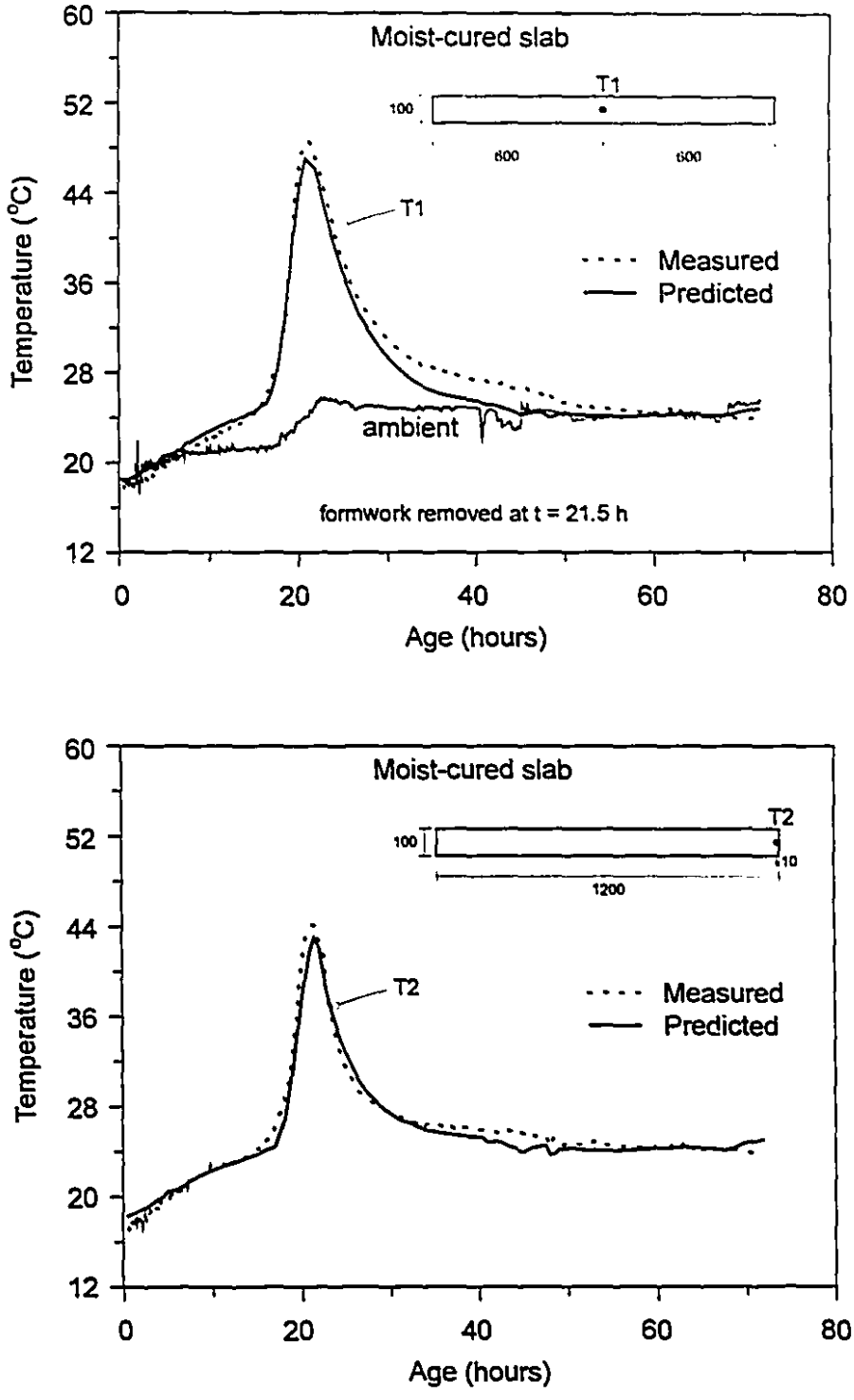

Figure 5.22 - Comparison between the measured and predicted temperature responses for moist cured slab

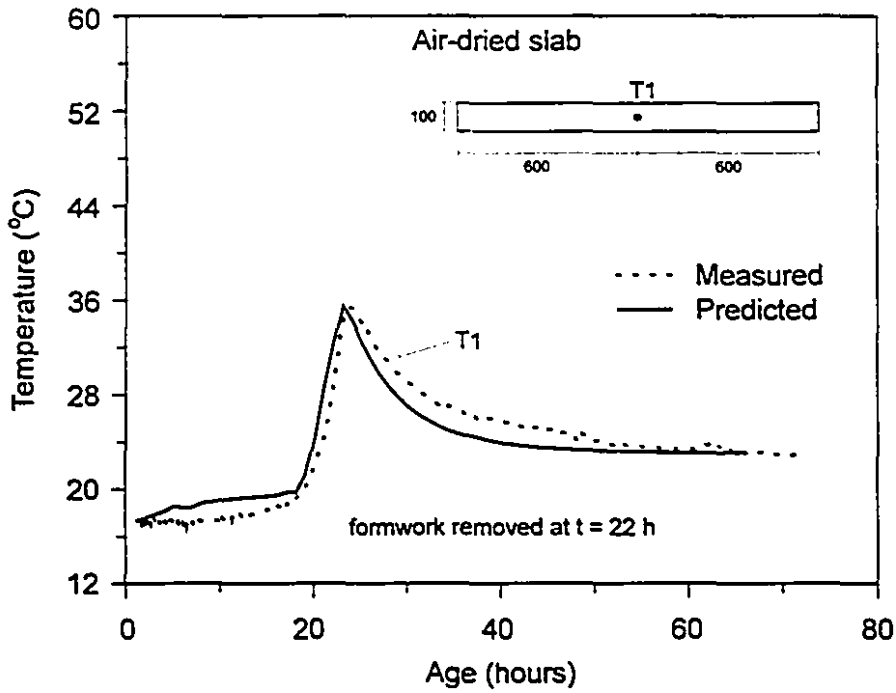

Figure 5.23 - Comparison between the measured and predicted temperature responses for air-dried slab

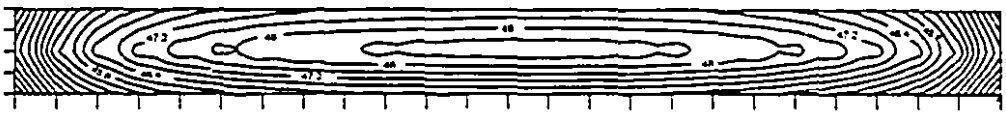

(a) Insulated slab

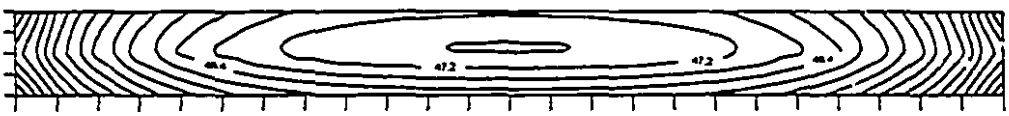

(b) Moist cured slab

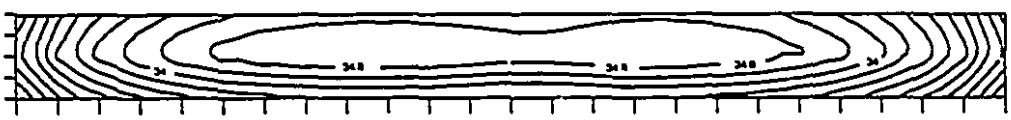

(c) Air-dried slab

Figure 5.24 - Predicted temperature contours in 100 x 1200 mm slabs
(t =22 hours)

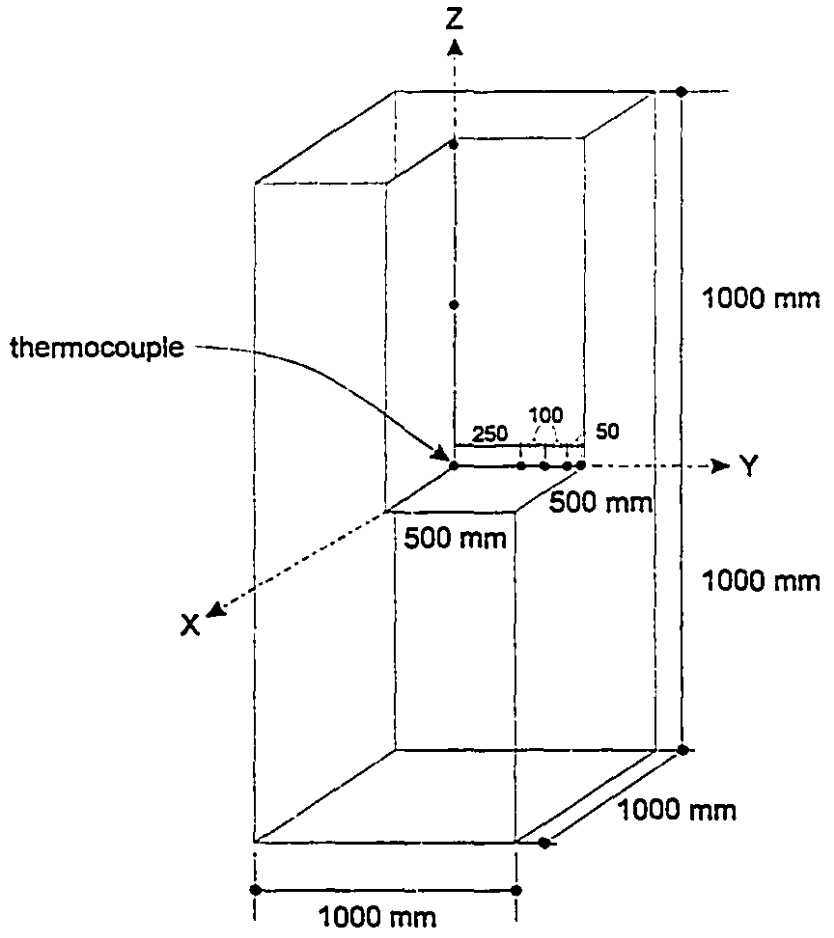

Figure 5.25 - Position of thermocouples in a concrete column

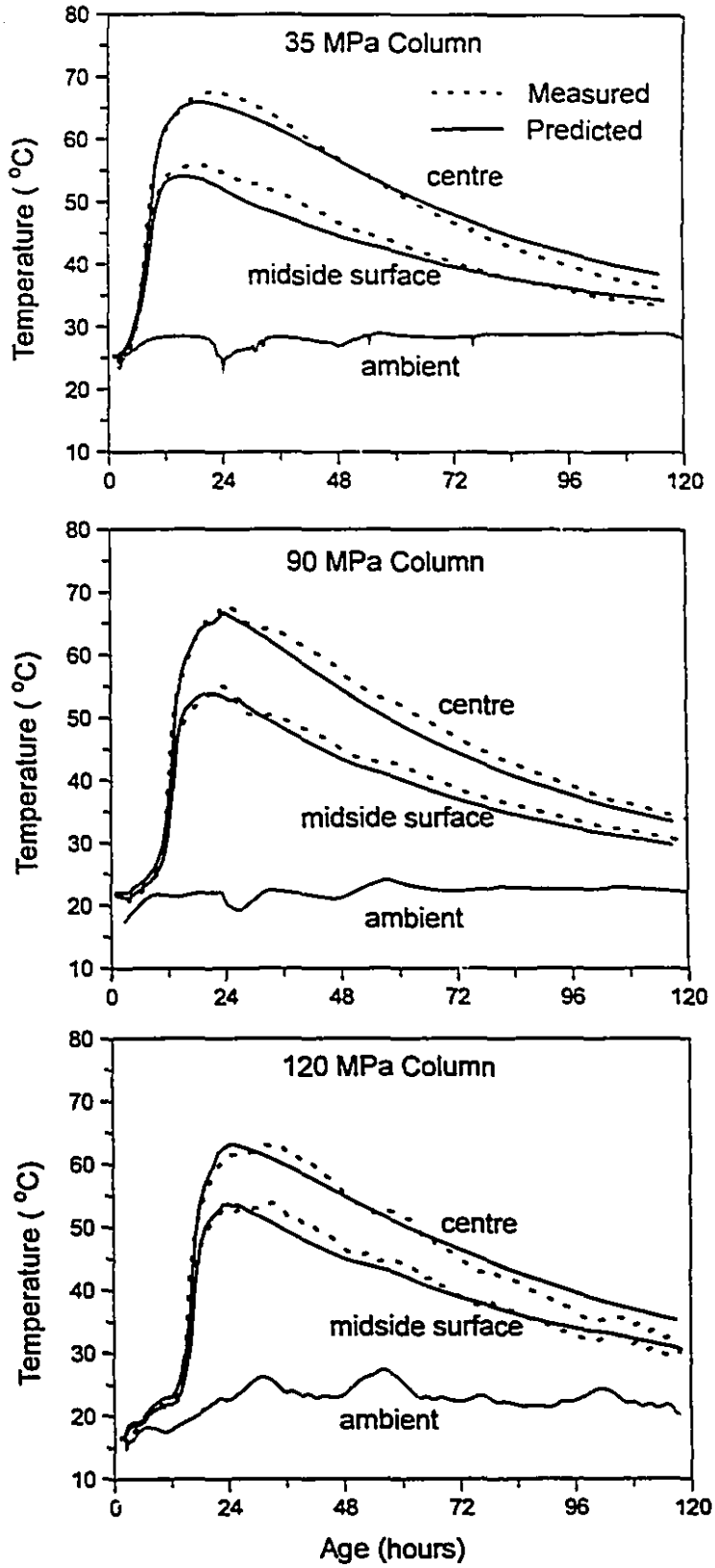

Figure 5.26 - Comparison between the measured and predicted temperatures in a 1 x 1 m concrete column

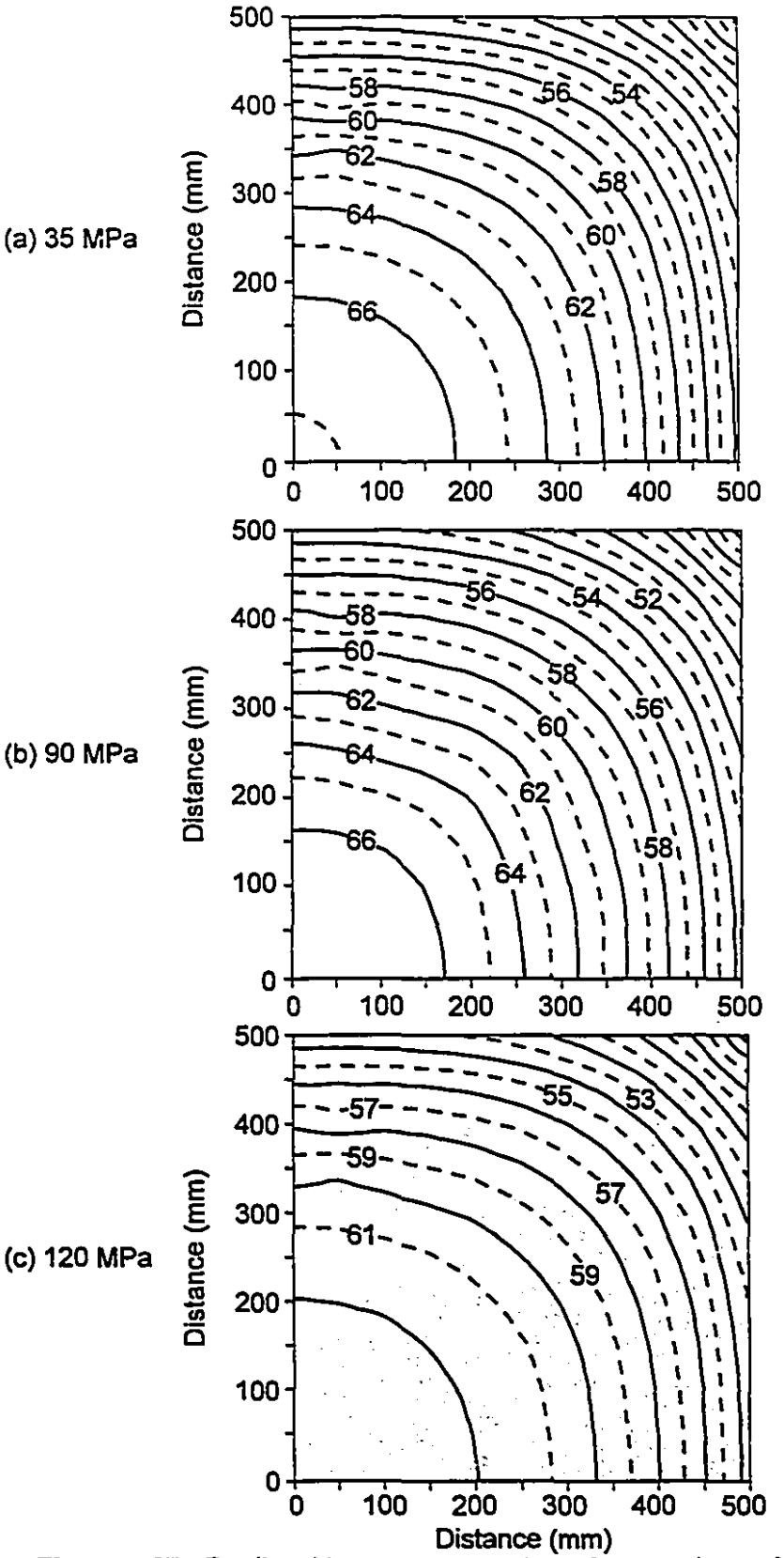

Figure 5.27 - Predicted temperature contours in a quadrant of a 1 x 1 m concrete column

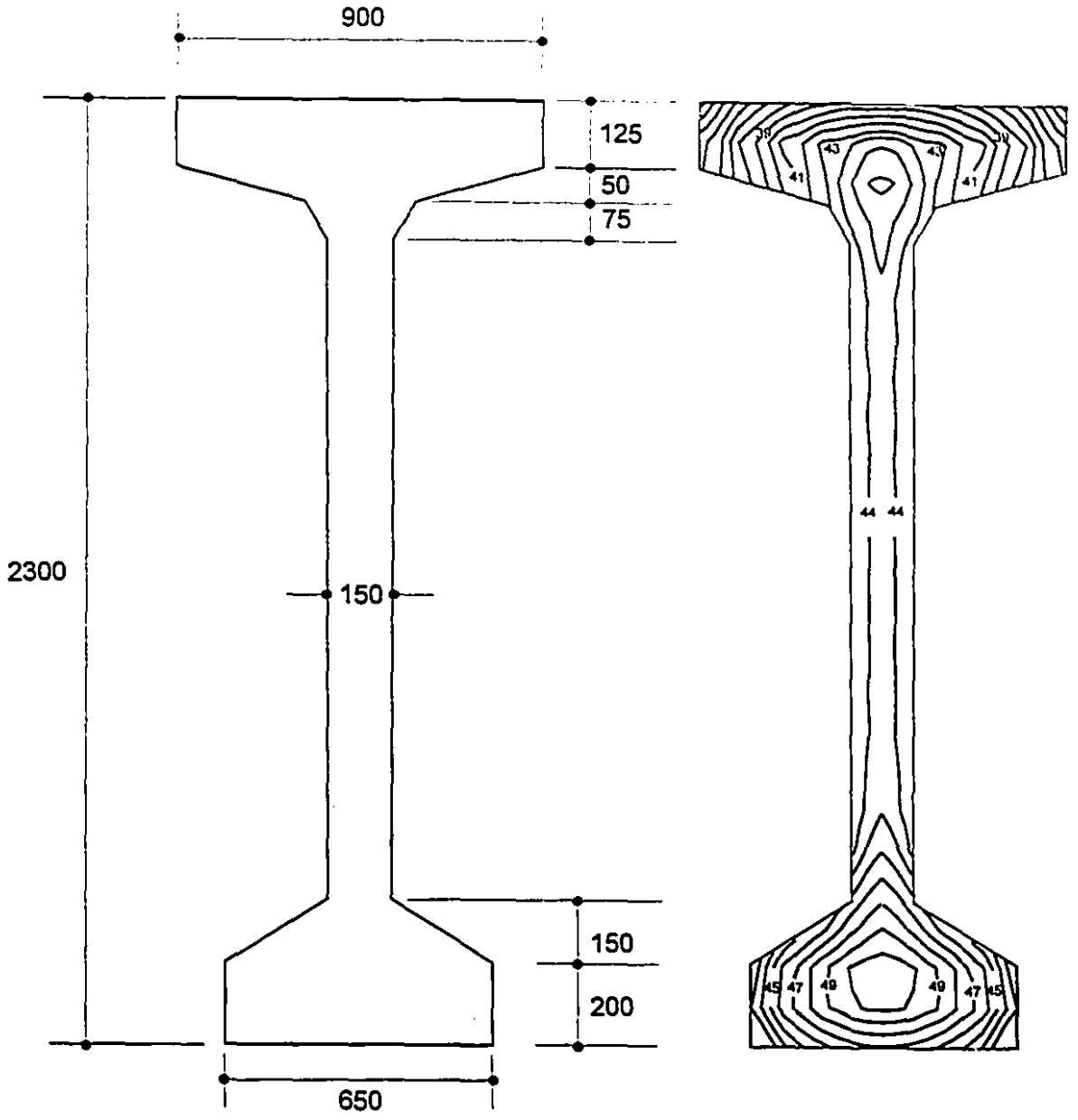

Figure 5.28 - Temperature contours in a typical precast I-girder section at t = 20 hours

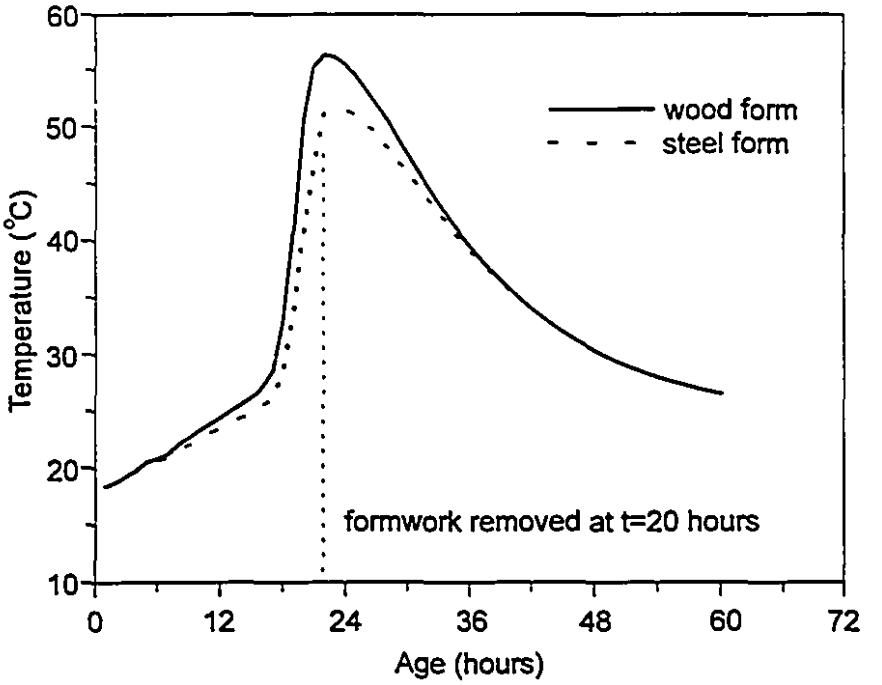

Figure 5.29 - Effect of formwork on the temperature rise in I-girder

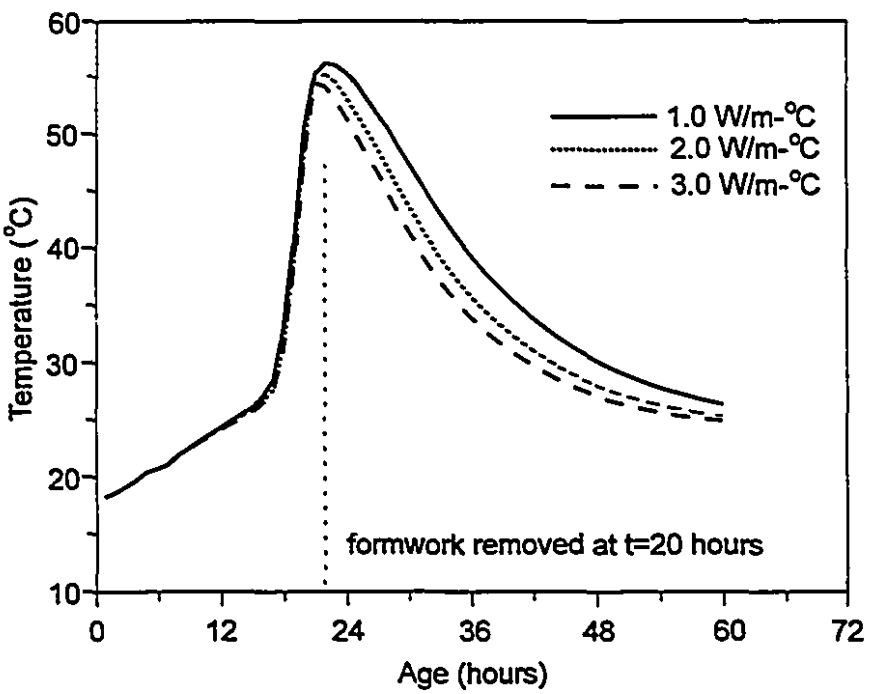

Figure 5.30 - Effect of thermal conductivity on the temperature rise of I-girder

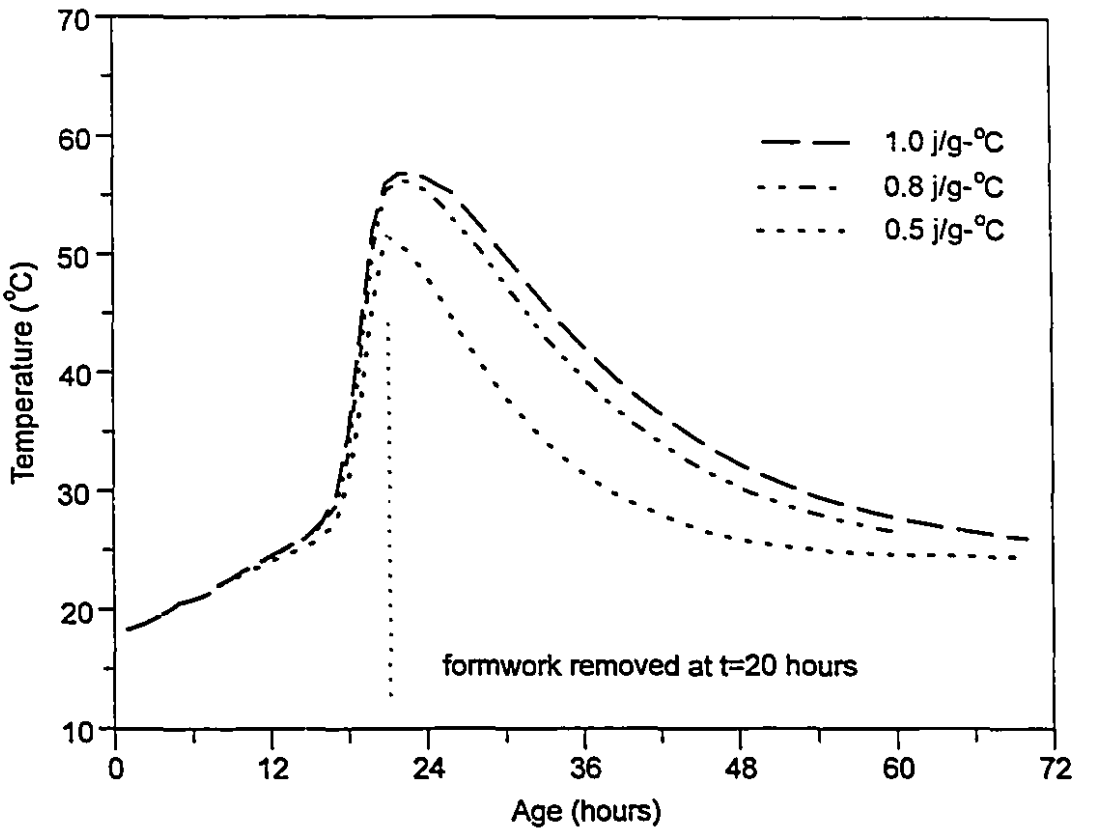

Figure 5.31 - Effect of specific heat of concrete on the temperature rise in I-girder

Chapter 6

Thermal Stress Analysis of Structural Members During Hydration

This chapter presents a method for determining thermal stresses during hydration in concrete members. In order to carry out this stress analysis it is necessary to first predict the temperature histories, using transient thermal analyses (see Chapter 5) and to predict the key mechanical properties, at different locations in the member. In order to demonstrate the capabilities of the stress analysis in the time domain the stresses developed during hydration are predicted for large concrete columns. A parametric study is carried out on the influence of concrete strength, initial and ambient temperature conditions, as well as the time of form removal on the risk of thermal cracking. The important effect of early-age creep during hydration on the development of thermal restraint stresses is also studied.

6.1 Basic Concepts of Induced Thermal Stresses

During hydration, different regions of a cross-section of a concrete member may experience induced thermal stresses due to non-linear temperature distributions in the member. Figure 6.1 shows schematically the temperature variations, and the resulting induced stresses, at the centre and at the surface of a cross-section during hydration. During hydration when temperatures are increasing, compressive stresses will develop at the centre, where higher temperatures exist, and tensile stresses develop near the surface where the temperature is lower. When the centre of the concrete starts cooling, the self-equilibrating stresses due to the thermal gradient tend to cause the reverse effect, with reduced compressive stresses and even tensile stresses developing at the centre of the concrete. It must be pointed out that the concrete has lower strength, lower elastic modulus and significant creep during the early period of

temperature rise. Although the tensile strength of the concrete is lower at this time, the combined effect of the low elastic modulus and high creep may significantly reduce the potential of surface cracking. During the cooling phase, the concrete has higher strength, resulting in an increased modulus of elasticity and reduced creep. Therefore, the stress relieving effect of creep on the resulting tensile stresses, during cooling, will be lower. If cracks appear at the surface during the temperature rise, they will tend to close during the drop of temperature due to compressive stresses developing at the surface (Neville (1981)).

6.2 Stress Analysis in the Time Domain

In order to understand the way in which concrete stresses can arise from thermal and shrinkage strain gradients it is necessary to consider the different components of strain. The total strain in the concrete, ϵ_c, can be found from:

$$\epsilon_c = \epsilon_{th} + \epsilon_{sh} + \epsilon_{cf} \tag{6.1}$$

where ϵ_{th} is the thermal strain, ϵ_{sh} is the shrinkage strain and ϵ_{cf} is the strain causing stress in the concrete.

If it is assumed that, due to compatibility, plane-sections remain plane, then the total strain, ϵ_c, must vary in a linear manner over a cross section. Hence, if both the thermal strain and the shrinkage vary uniformly or linearly over the cross section of a statically determinate beam, then no strains causing stress will be developed and the concrete stresses will be zero (see Fig. 6.2a and 6.2b). If, on the other hand, the shrinkage strains and thermal strains vary in a non-linear fashion over the section, then strains causing stress will be generated in order that compatibility is achieved (see Fig. 6.2c). If the concrete stress-strain relationship is linear and the concrete remains uncracked, the stress, f_c, in the concrete can be determined from:

$$f_c = \epsilon_{cf} E_c \tag{6.2}$$

where E_c is the modulus of elasticity of the concrete.

The simple approach for determining concrete stresses described above assumes that the strains due to shrinkage and thermal effects occurred instantaneously. That is, there was no gradual development of these strains and hence

it was not necessary to track the buildup of stresses in the time domain. However, during the hydration process the problem of finding the concrete stresses requires a more complex analysis. It is necessary to carry out a transient thermal analysis to determine the history of temperature development over the cross section due to hydration. Once the history of temperatures is determined, then the time-wise variation of thermal strains can be determined provided that the coefficient of thermal expansion, α_c, is known (i.e., $\epsilon_{th} = \alpha_c \Delta T$). The shrinkage strains will vary over the cross section and will change with time. In order to determine the shrinkage strains it is necessary to know the shrinkage strain development in the concrete for different curing conditions. Once the history of strain development has been determined then a stress analysis can be conducted. A finite element analysis can be carried out in the time domain. For each time step, j, the strains causing stress are first determined from Equation (6.1). The incremental instantaneous concrete stress, $\Delta f_c(t_j)$ for the time period t_{j-1} to t_j is calculated as:

$$\Delta f_c(t_j) = \Delta \epsilon_{cf}(t_j) E_c(t_j) \tag{6.3}$$

where $\Delta \epsilon_{cf}(t_j)$ is the incremental strain causing stress between t_{j-1} and t_j, and $E_c(t_j)$ is the instantaneous modulus of the concrete at time t_j. To determine the total stress in the concrete at time t, it is necessary to add to $\Delta f_c(t_j)$ the sum of the incremental stresses that have occurred during the previous time steps, duly adjusted to take account of the creep that has occurred. In order to account for the influence of creep, an effective modulus which accounts for the elastic modulus at the time of loading, $E_c(t_j)$, and the creep coefficient, $\phi\ (t_n, t_{j-1})$, can be derived from the creep expression given in the CEB-FIP code (1990). This effective adjusted modulus, $E_{c,eff}(t_j)$, can be derived from Eq. (4.6), as:

$$E_{c,eff}(t_j) = \frac{1}{\left[\frac{1}{E_c(t_j)} + \frac{\phi(t_j, t_{j-1})}{E_c}\right]} \tag{6.4}$$

It is interesting to note that, for mature concrete, this equation reduces to the well known relationship for the effective modulus for loading applied at t_o and held constant until time t, as:

$$E_{c,eff} = \frac{E_c(t_o)}{1+\phi(t,t_o)} \tag{6.5}$$

The incremental stress in the concrete, $\Delta f_{c,eff}(t_j)$, at time t_j including creep, can be determined by adjusting the incremental instantaneous stress, $\Delta f_c(t_j)$, by:

$$\Delta f_{c,eff}(t_j) = \Delta f_c(t_j)\ \frac{E_{c,eff}(t_j)}{E_c(t_j)} \tag{6.6}$$

The incremental stress accounting for creep can be derived from Eq. (6.4) and Eq. (6.6) as:

$$\Delta f_{c,eff}(t_j) = \Delta f_c(t_j)\ \left[\frac{1}{1+\frac{E_c(t_j)}{E_c}\phi(t_j,t_{j-1})}\right] \tag{6.7}$$

In order to determine the stress in the concrete at any time, t_n, it is necessary to sum up the incremental stresses developed in the previous time steps duly accounting for the influence of creep. Hence the total stress at time t_n is:

$$f_{c,eff}(t_n) = \sum_{j=1}^{n} \frac{\Delta f_c(t_j)}{\left[1+\frac{E_c(t_j)}{E_c}\phi(t_n,t_{j-1})\right]} \tag{6.8}$$

where $\Delta f_c(t_j)$ is the incremental instantaneous concrete stress between time t_{j-1} and t_j, and $\phi(t_n,t_{j-1})$ is the creep coefficient for loading from time t_{j-1} to time t_n. Therefore, to determine the concrete stress at a particular location in the cross section at a particular time requires information on the variation of the instantaneous modulus of the concrete as well as information on the creep coefficient.

Once the concrete stresses have been determined at different locations in the cross section as a function of time then the risk of cracking can be assessed. The risk of cracking at any location can be judged from the variation of the ratio of the maximum principal tensile stress to the tensile strength of the concrete (i.e., $\sigma_1(t)/f_r(t)$).

In 1967, Trost developed an aging coefficient to account for creep in a situation where mature concrete is subjected to incrementally applied stress and hence is useful in carrying out analyses for stage-wise construction (Ghali and Favre (1986)). Equation

(6.8) accounts for the more complex situation of incrementally applied stress on maturing concrete where the stiffness of the concrete is rapidly changing. In the procedure described above, the incremental analysis in the time domain captures the effects of the changing concrete stiffness, the changing stress in the concrete and the corresponding creep. The incremental stresses in the concrete were determined by using subroutines developed to track the changing concrete properties and to provide the input data for carrying out linear elastic stress analyses. The computer program "SAP90" (SAP90 (1989)) was used for the finite element stress analysis at each time step.

Figure 6.3 shows the flow chart for the incremental stress analysis. The steps used in the analysis are summarized below:

i. Input data

The geometry of the member was first defined using finite elements. The boundary conditions were modelled appropriately for the stress analysis.

ii. Increment time, Δt

A small time increment of Δt is applied such that the new conditions at time $t + \Delta t$ can be determined.

iii. Results from thermal analysis

Thermal analysis was carried out to determine the temperature history of each element of the cross-section, as discussed in Section 5.2. The effect of temperature was accounted for in predicting the changing mechanical properties using the maturity concept. The incremental thermal loads and the mechanical properties of each element at each time step were incorporated in the stress analysis.

iv. Solve load-displacement equation

The stiffness equations were solved for the incremental displacements, Δu.

v. Determine incremental stress

By knowing the changing stiffness of each element, the incremental stresses, Δf, were calculated for each element during each time step.

vi. Compute total stress accounting for creep

Once the incremental stresses, Δf, were determined for different locations of the cross-section, these stresses were adjusted for early age creep. The total stress was obtained by summing up the incremental stresses developed in the previous time

steps, duly accounting for the influence of creep. The risk of cracking at any location can be assessed by comparing the maximum principal stresses with the predicted tensile strength of the concrete at each instant of time.

The results obtained from analyses using this procedure, with and without creep, are presented in the following sections.

6.3 Predicted Thermal Stresses in Large Concrete Columns

6.3.1 Predicted Strength and Stiffness

In order to demonstrate the analysis techniques, three 1m by 1m by 2m high concrete columns (Cook et al (1992)) will be studied. To predict the thermally induced stresses during hydration, it is necessary to first predict the variations of temperature with time and the changing properties of the concrete. The temperature histories were predicted by performing two-dimensional thermal analyses across the cross section, by assuming that there was no temperature gradient over the height of the column. These predictions were made for all three columns, that is, the 35, 90 and 120 MPa concrete columns (see Section 5.5.1). Figure 6.4a shows the finite element idealization used to model the mid-height quadrant of a concrete column. Due to symmetry, only one quarter of the horizontal slice was modeled for predicting both the temperatures and induced stresses during hydration. Wood formwork of 20 mm thickness was modeled by defining the corresponding thermal properties in the modified version of program "DETECT". For these predictions the measured ambient temperature-time data was used (see Fig. 5.26). Figure 6.4b illustrates the predicted time-wise variations of the mechanical properties during hydration, for the centre and corner elements of 120 MPa concrete column. These properties were predicted by tracking the conditions of the different elements and accounting for the history of temperatures using the maturity concept. These changing material properties were used in predicting the induced stresses and to assess the potential for cracking in each column. As can be seen from Fig. 6.4b there is a substantially higher rate of strength and stiffness gain during the first 24 hours after casting. As expected, due to the differences in maturity, the centre achieves higher strengths and stiffnesses than the corner element, particularly during the first 24 hours. Concrete compressive strengths of 78 MPa and 64 MPa are predicted at the centre and at the corner of column,

respectively, at 24 hours (see Fig. 6.4b). Thirteen days after casting, there is a levelling off of the strength gain, with predicted compressive strengths of 98 MPa and 95 MPa at the centre and corner of the 120 MPa column. Miao et al (1993) conducted core tests on the 120 MPa column at 91 days, which resulted in an average compressive strength of 98.7 MPa for the interior and 98.6 MPa for cores taken near the corner.

Figure 6.5 shows the predicted compressive strength contours at the mid-height quadrant of the 35, 90 and 120 MPa concrete columns at 24 hours. This figure illustrates that there is a significant difference (about 21%) in the strength at the centre and corner of the column, due to the difference in maturity. In order to accurately predict the induced thermal stresses during hydration this variation must be accounted for.

6.3.2 Thermal Stresses Without Accounting for Creep

Three-dimensional transient stress analyses were carried out for the three columns made of different concretes. In these analyses, it was assumed that the material exhibits linear stress-strain responses and that the principle of superposition is applicable. To simulate the conditions on the mid-height slice, the deformations in the Z-direction were constrained to be the same, since plane sections were assumed to remain plane. Since the material properties of the concrete change rapidly during the early period of hydration, incremental analyses were carried out in the time domain, using small time steps. As described in Section 6.2 subroutines were developed to track the rapidly changing material properties in each time step and to provide the data necessary for linear elastic analyses. The resulting incremental stresses are then added to determine the total stress-time history for each element.

It must be pointed out that the measured initial and ambient temperature values were used during these analyses and the same concrete thermal properties given in Table 5.4 were assumed. Wood formwork was removed from the boundaries at 120 hours after casting (actual case). Figures 6.6, 6.7, and 6.8 show the predicted temperatures, and maximum principal stresses developed at the centre and corner of the 35, 90 and 120 MPa concrete columns during hydration. The variations of the predicted tensile strengths of the corner elements are also presented. As expected, the

corner experienced a sudden drop of temperature at 120 hours, due to the removal of the formwork. Whereas, the centre of the column did not experience any significant drop due to the large column dimensions and low diffusivity of the concrete. The maximum compressive stresses are developed at the centre and the maximum tensile stresses are developed at the corner of these columns, as expected. During the cooling phase, reversal of stresses is predicted, that is, tension at the centre and compressive stresses near the surface. It must be pointed out that the effect of creep, on the developed thermal stresses, has not been accounted for in these analyses and hence the predicted stresses are overestimated. Figure 6.9 shows the variation of the predicted temperature differentials between the centre and the corner elements for each of the three columns. As can be seen from this figure the 35 and 90 MPa concrete columns have experienced maximum temperature differentials of 25.5°C at 32 hours and 24.5°C at 30 hours, respectively. The 120 MPa concrete column showed a maximum temperature differential of 20°C at 41 hours. It must be pointed out that these columns had different initial concrete temperatures and were subjected to different ambient conditions. The potential for cracking at any time can be assessed by comparing the maximum principal tensile stress with the tensile strength at that instant. Machida and Uehara (1987) presented the cracking potential in terms of a cracking index, that is, the ratio of the tensile strength to the tensile stress. It has been suggested that the probability of cracking is 50% for a cracking index of 1.0, whereas, there is a 95% probability of no cracking for a cracking index of 1.5 or greater for massive concrete members. It has been suggested by the Japan Concrete Institute (1986) that the possibility of cracking can be considered negligible, if the maximum principal tensile stress is less than 50% of the tensile strength. Figure 6.10 compares the variations in the ratios of the predicted maximum principal tensile stress to the tensile strengths for the three columns. As can be seen from this figure all of these ratios are less than 1.0. The 35 and 90 MPa concretes show about the same values of these ratios (i.e., 0.6), whereas the 120 MPa concrete shows a value of 0.42. The lower risk of cracking in the 120 MPa concrete column can be attributed due to lower thermal gradient and higher rate of tensile strength gain. This smaller potential for cracking of the 120 MPa concrete column is also due to the fact that the column had a lower initial placing temperature and a lower ambient temperature than

the other two columns. Because of the different placing temperatures and the different ambient conditions it is not prudent to make general conclusions from these analyses about the influence of concrete strength on the risk of cracking. No cracks were observed on the surface of any of the columns at a time of 120 hours (i.e., time of form removal).

6.4 Influence of Concrete Strength and Creep on Thermal Stresses in Large Columns

In this section, some of the key parameters influencing the risk of cracking of large concrete columns will be studied. In Chapter 1, several measures taken by engineers and contractors to control the temperature differential in structural members were discussed. One rule-of-thumb is to limit the temperature differential across a section to about 20°C (Fitzgibbon (1976)) in order to prevent surface cracking. For high-strength concrete, it has been suggested that the maximum temperature be limited to 70°C (CSA Standard A23.1 (1994)) and that the initial temperature be limited to 25°C (Ryell and Bickley (1987)). Special measures to control cracking in young concrete include using insulation, cooling and special curing techniques. Early removal of formwork or insulation in structural members and abruptly discontinued cooling of mass concrete may result in thermal shock. The effect of initial concrete temperature and the ambient temperature can have a vital impact on the very early-age restraint stresses and therefore the susceptibility of surface cracking due to temperature differentials. In massive concrete structures (e.g., dams), the degree of restraint imposed by existing hardened concrete on the newly cast concrete, and the temperature differential between the successive casts are of the prime concern.

A parametric study was conducted to study the influence of early form removal, the effect of concrete strength and the influence of concrete creep on the thermal gradients and the development of thermal stresses in large columns. In order to compare the results and observe the influence of concrete strength and early form removal on the stresses, the same concrete thermal properties given in Table 5.4 were assumed except that the initial and ambient concrete temperatures were assumed to be constant (i.e., 20°C) for the 35, 90 and 120 MPa concrete columns. Figure 6.11 illustrates the shape of the predicted temperature distribution for the 35 MPa concrete

column at 24 hours. Maximum temperatures of 62°C and 37°C are predicted at the centre and at the corner, respectively, whereas midside of the cross-section developed a temperature of 48°C. It must be pointed out that all of these columns were cast in wood formwork, having a thickness of 20 mm. In all of these cases, the boundary elements (i.e., wood formwork) were removed at 24 hours and the convection elements were shifted to the surfaces. Figures 6.12, 6.13 and 6.14 show the predicted temperatures and maximum principal thermal stresses at two locations of the cross section (i.e., centre and corner) for the three columns. These predictions were made with and without accounting for creep. As expected, there is a sudden drop of temperature at the surface upon form removal, while the centre of the column does not experience such a drop in temperature due to its large size. This early removal of formwork resulted in a large thermal gradient (thermal shock) across the cross section during this early period of hydration. This large temperature differential resulted in significantly increased thermal stresses (see Fig's 6.12, 6.13 and 6.14). It must be pointed out that form removal at very early ages, particularly at the peak temperatures, will increase the induced stresses resulting from the higher thermal gradient as well as from the differential shrinkage. Early form removal also will result in lower tensile strengths near the surface due to both lower temperatures and drying effects. Figures 6.12, 6.13 and 6.14 also show the effect of creep on the induced stresses during hydration. In these analyses, a relative humidity of 90% was assumed during the first 24 hours for the whole cross-section and a value of 50% was assumed for the surface elements after the form removal. For each of the time steps account was taken of the changing concrete strengths and moduli for the three different concretes by using the CEB-FIP Code Equations (1990) for the creep coefficient and using the effective modulus approach given in Section 6.2. As expected, the creep has relieved both the compressive and tensile stresses and has lowered the risk of cracking.

Figures 6.15 and 6.16 show the predicted temperature differentials and ratios of maximum principal tensile stress to tensile strength. Creep was accounted for in the predictions shown in Fig. 6.16. Maximum temperature differentials of 34°C, 33°C and 33°C occurred for the 35, 90 and 120 MPa concrete columns by removing the formwork at 24 hours. As can be seen from Fig. 6.16 the risk of cracking has substantially increased due to the early stripping of the formwork. Although the 90

MPa concrete column shows the maximum potential for cracking, the maximum principal tensile stress to tensile strength ratios are all below 1.0. These ratios are given in Table 6.1 for the cases with and without creep. The predicted stress to strength ratios, including creep, are 0.75, 0.87 and 0.78 for the 35, 90, and 120 MPa concretes, respectively. Although the temperature differentials are similar for the three columns, the higher strength concrete develops larger tensile stresses due to its higher modulus. However, these higher stresses can be compensated for by the higher tensile strength gain for the higher strength concretes. This is particularly evident for the 120 MPa concrete which has about the same risk of cracking as the 35 MPa concrete column.

6.5 Predicted Thermal Stresses in a Large Precast I-Girder

In this section, the thermal stresses induced in the large precast pretensioned I-girder described in Section 5.5.2 are determined. This CPCI 2300 I-girder was cast in an outdoor precast plant. In order to demonstrate the thermal and stress analysis, the stresses will be predicted in the member following form stripping and immediately following prestress release. The variation of temperatures during hydration and the corresponding concrete strengths in the cross-section of I-girder were predicted using the modified version of program "DETECT". In this analysis, the following assumptions were made:

i. The formwork was removed 20 hours after casting.

ii. A constant ambient temperature of 20°C was assumed up until form stripping at time of 20 hours. From this time, the member was subjected to a constant ambient temperature of 5°C to simulate the possible conditions at the site.

iii. The initial placing temperature was assumed to be 18°C.

Figure 6.17a shows the predicted temperature contours just before form removal. In order to carry out a plane-sections stress analysis using program "RESPONSE" (Collins and Mitchell (1991)) the cross section was discretized into six layers as shown in Fig. 6.17b. The strands were included in the idealization of the cross section by lumping the area of the strand (36 x 99 = 3564 mm^2) at their centroid for the midspan section. The average predicted compressive strengths just

after removal of the formwork are shown in Fig. 6.17b. Figure 6.17c shows the drop in predicted temperature expressed as an average value of temperature drop across the width of each element, for the case where the maximum thermal gradient occurs (within one hour after stripping). As can be seen at this stage the temperature drops of 3°C, 19°C and 5.2°C have occurred at the top, near the centre of the web and at the bottom, respectively, of the I-girder. Figure 6.17d shows an elevation view of the 30 m long girder in the stressing bed. The member is pretensioned with 36- 13 mm diameter strands with harping points at the third points of the span.

Figure 6.18a illustrates the results of the plane-sections analysis for the case where the precast beam has been stripped and the maximum thermal differential of 19°C has occurred about one hour after form removal. Because the pretensioning has not been released, the temperature drop results in a axial load restraint force, N, in the longitudinal direction due to the cooling of the pretensioned strands which are fixed at the end abutments. The restraint force, N, was calculated from equilibrium and compatibility considering a shortening strain of 0.076×10^{-3} at the centroid of the section due to thermal loading on an unrestrained member. The resultant force of 497 kN which was combined with the non-linear thermal strain variation over the cross section. The resulting strains in the cross section are given in Fig. 6.18a with the strain causing stress calculated from the linear strain distribution of the total strain and the non-linear thermal strain distribution (i.e., $\epsilon_{cb} = \epsilon_c - \epsilon_{th}$). The stresses in the concrete, f_c, were calculated assuming linear elastic, uncracked concrete with the appropriate moduli, E_c, being used for each layer. As can be seen from Fig. 6.18a the top and bottom flanges have very small compressive stresses, while the web experiences tensile stresses. The peak tensile stress predicted is 3.89 MPa near the centre of the web. This figure also shows the variation of the modulus of rupture of the flange and web concrete. As can be seen the predicted tensile stress exceeds the predicted modulus of rupture, f_r, at the centre of the web, and would result in cracking of the web starting at about mid height. In order to assess the extent of cracking at this stage a non-linear analysis was carried out with program "RESPONSE" setting the cracking stress in the different layers to the correct value of the modulus of rupture. This analysis indicated that cracking will extend over a total height of about 1000 mm. This significant cracking in the web is due to the combined effect of the non-linear

thermal strain distribution due to rapid cooling, together with the external restraint from the anchored pretensioning strands. This type of thermal cracking actually occurred on a high-strength CPCI 2300 I-girder just after the removal of the formwork, as described in Chapter 5.

Figure 6.18b shows the similar analysis just after release of the two harping points. The release of the harping points produces a net negative moment of 140 kN-m at midspan. As can be seen from this figure, the tensile stresses have increased slightly from the elastic analysis. Figure 6.19 shows the predicted concrete stresses after release of the strands from the end abutments. This condition combined with the non-linear thermal strain distribution results in compressive stresses over the height of the section, which would close the crack in the web. These analyses were carried out neglecting creep because the thermal loading due to removal of the formwork was applied very rapidly. Figure 6.20 shows four 2300 mm deep CPCI high-strength I-girders after prestress release that had been produced in an outdoor precasting plant during winter. Cracking was observed in the web at midspan of the first girder cast, just after form removal when the ambient temperature was 5°C. Upon prestress release, the crack closed. These observations together with the predicted response of the stresses in the concrete illustrate the need to consider the effect of thermal stresses and external restraint during the production of precast elements.

Table 6.1 - Comparisons between the maximum principal tensile stresses and the tensile strengths for the three types of concrete with and without creep

Concrete Column	35 MPa	90 MPa	120 MPa
$\sigma_{c1,\,max}$, no creep (with creep), MPa	2.12 (1.87)	5.50 (4.88)	5.54 (5.01)
$f_r(t)$, MPa	2.48	5.61	6.4
$\sigma_{c1,\,max}/f_r(t)$, (with creep)	0.85 (0.75)	0.98 (0.87)	0.86 (0.78)

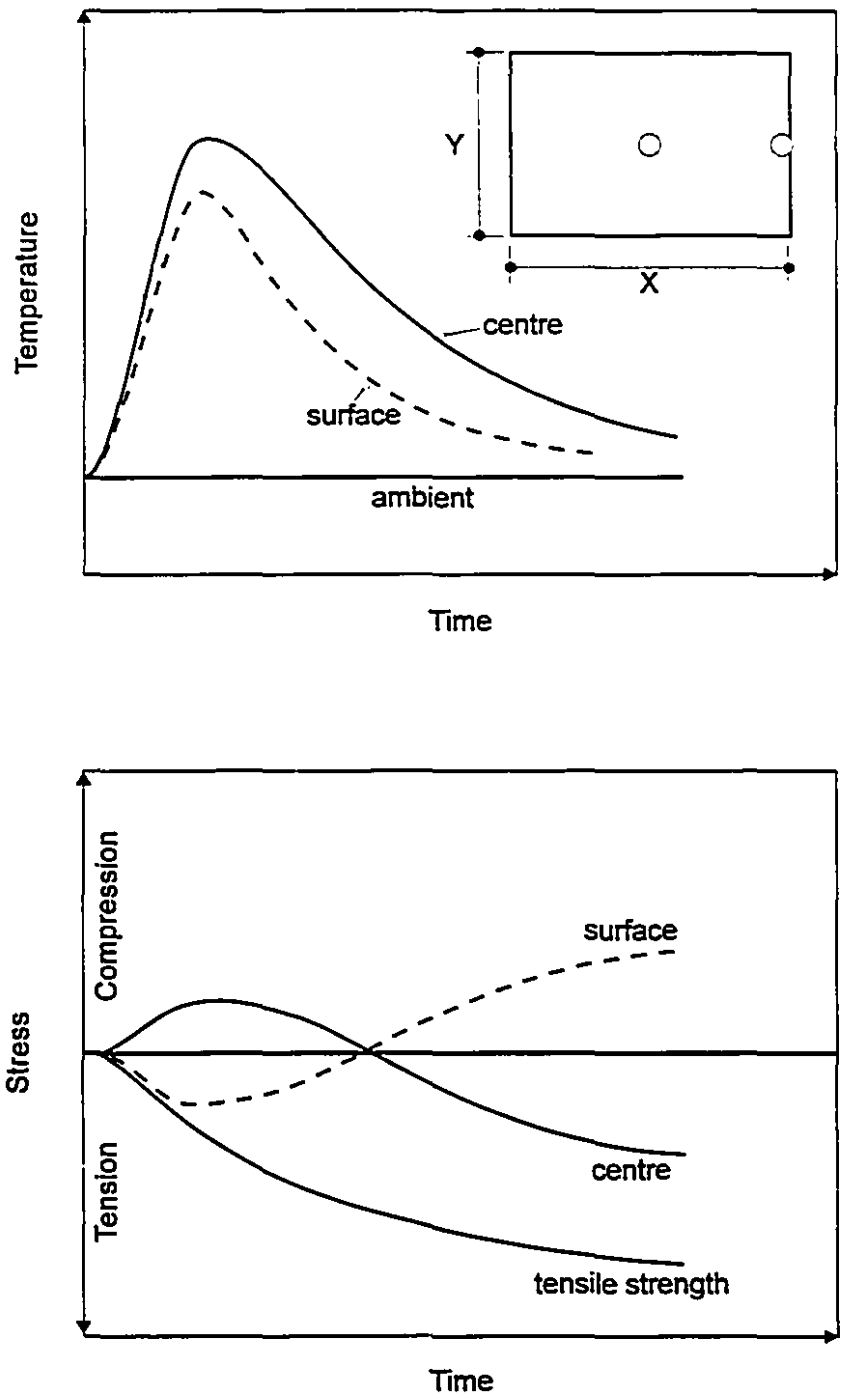

Figure 6.1 - Schematic presentation of the development of stresses at the centre and surface of a cross-section during early ages

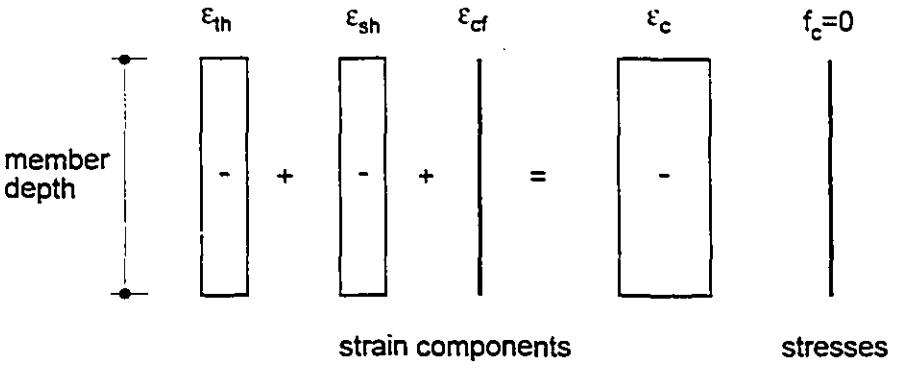

(a) Uniform distribution of thermal and shrinkage strains

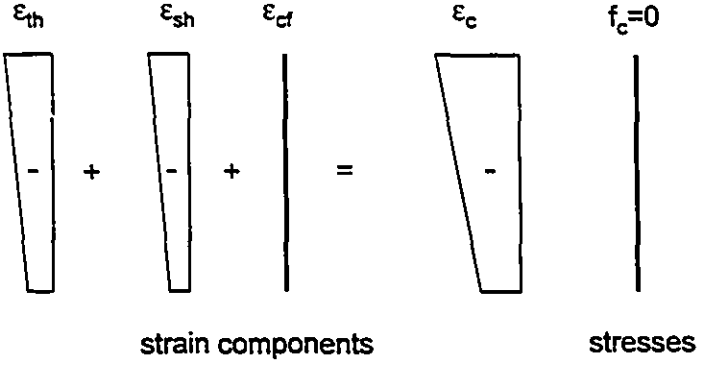

(b) Linear distribution of thermal and shrinkage strains

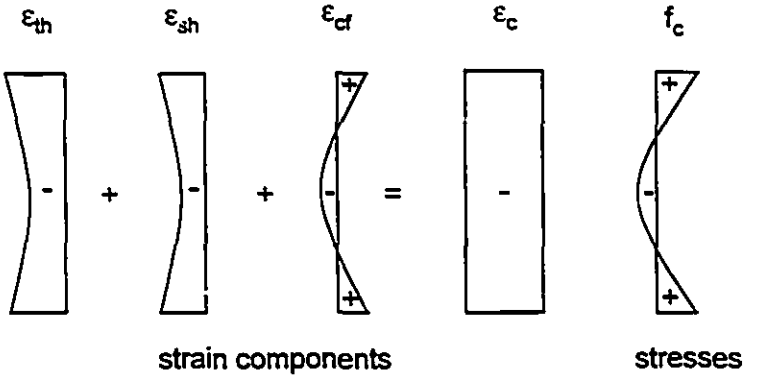

(c) Non-linear distribution of thermal and shrinkage strains

Figure 6.2 - Illustration of strain and stress distributions in a member without external restraint

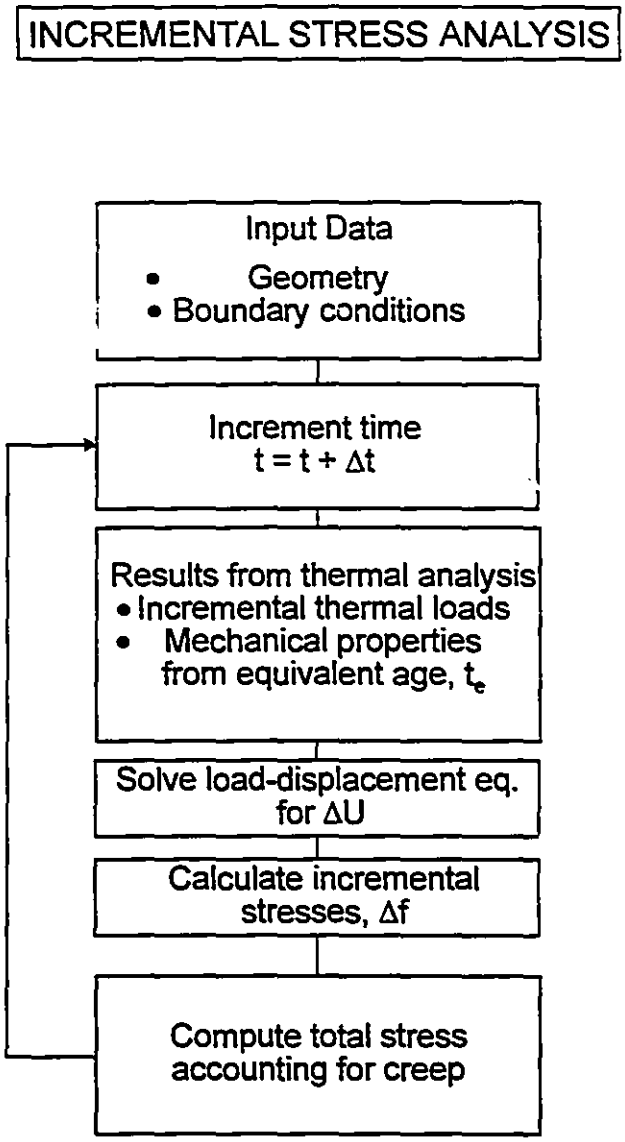

Figure 6.3 - Flow chart for the incremental stress analysis

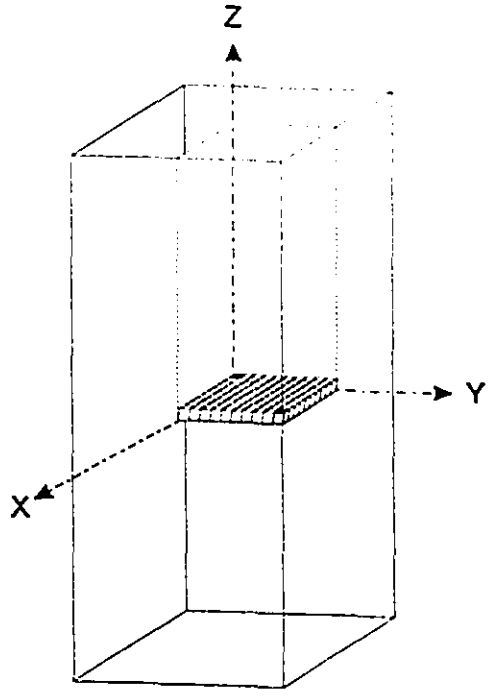

(a) finite element idealization

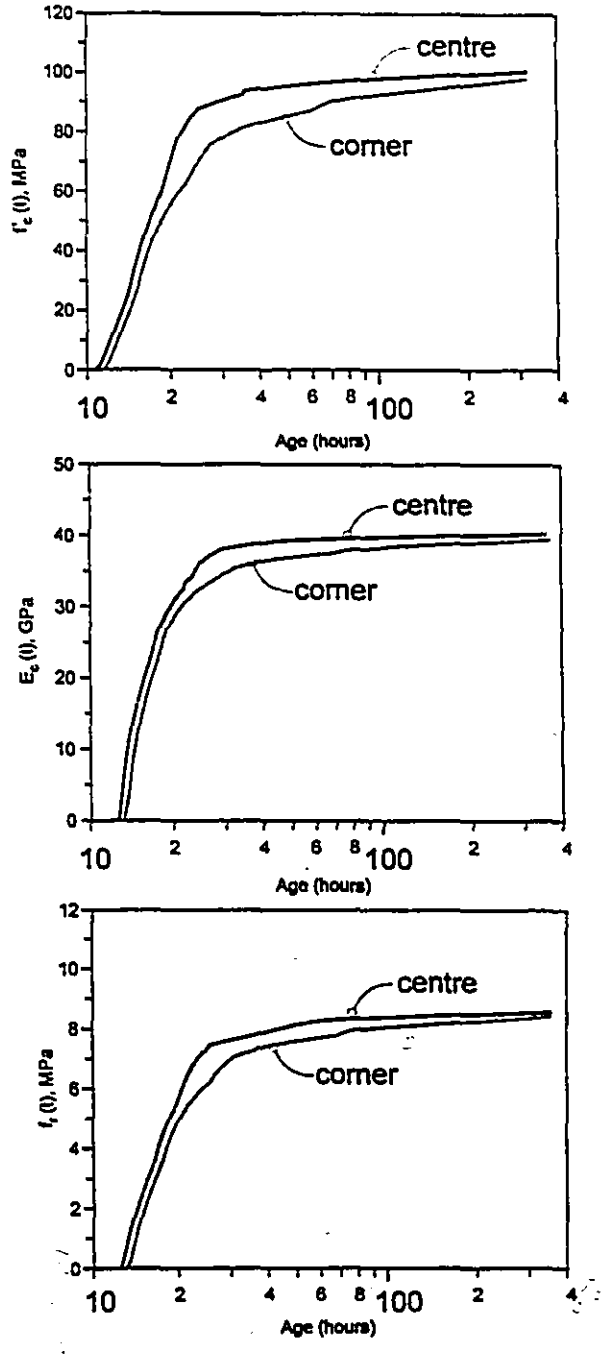

(b) changing mechanical properties at two locations

Figure 6.4 - Tracking of changing mechanical properties for 120 MPa concrete during hydration

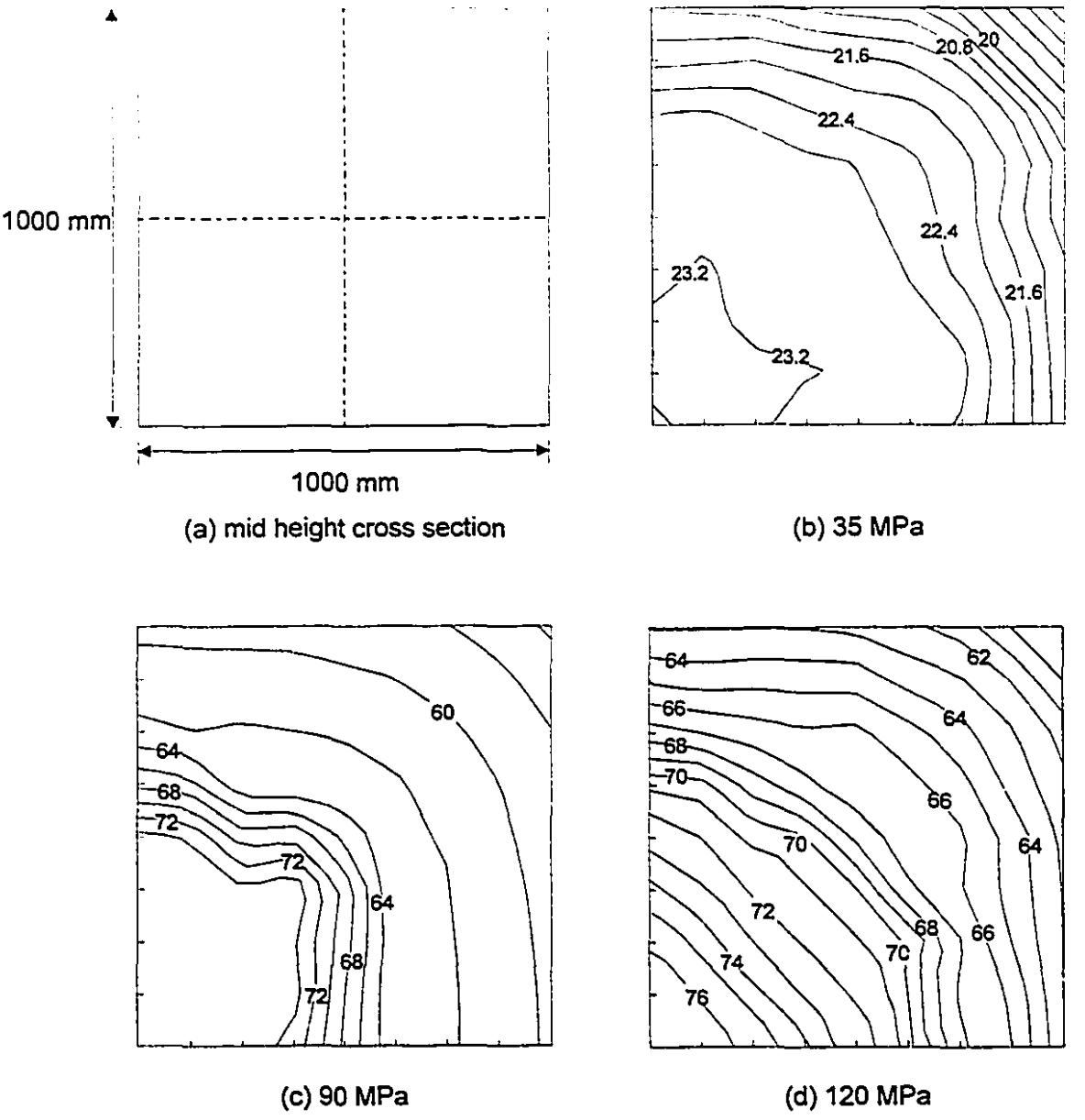

Figure 6.5 - Predicted compressive strength contours in a quadrant of 1 x 1 m concrete columns at 24 hours (in MPa)

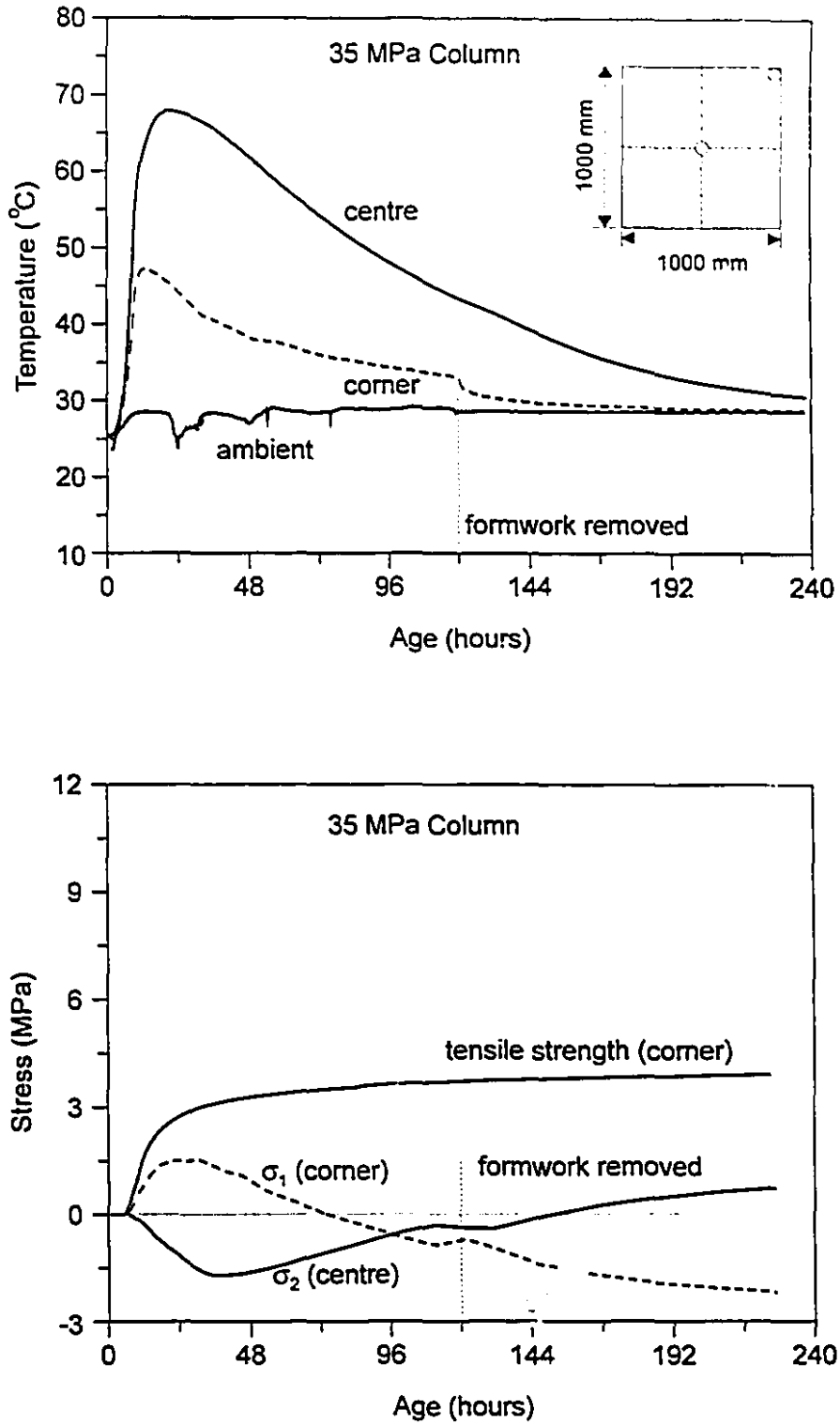

Figure 6.6 - Predicted temperatures, maximum principal stresses and tensile strength in 35 MPa concrete column (tension +ve; compression -ve)

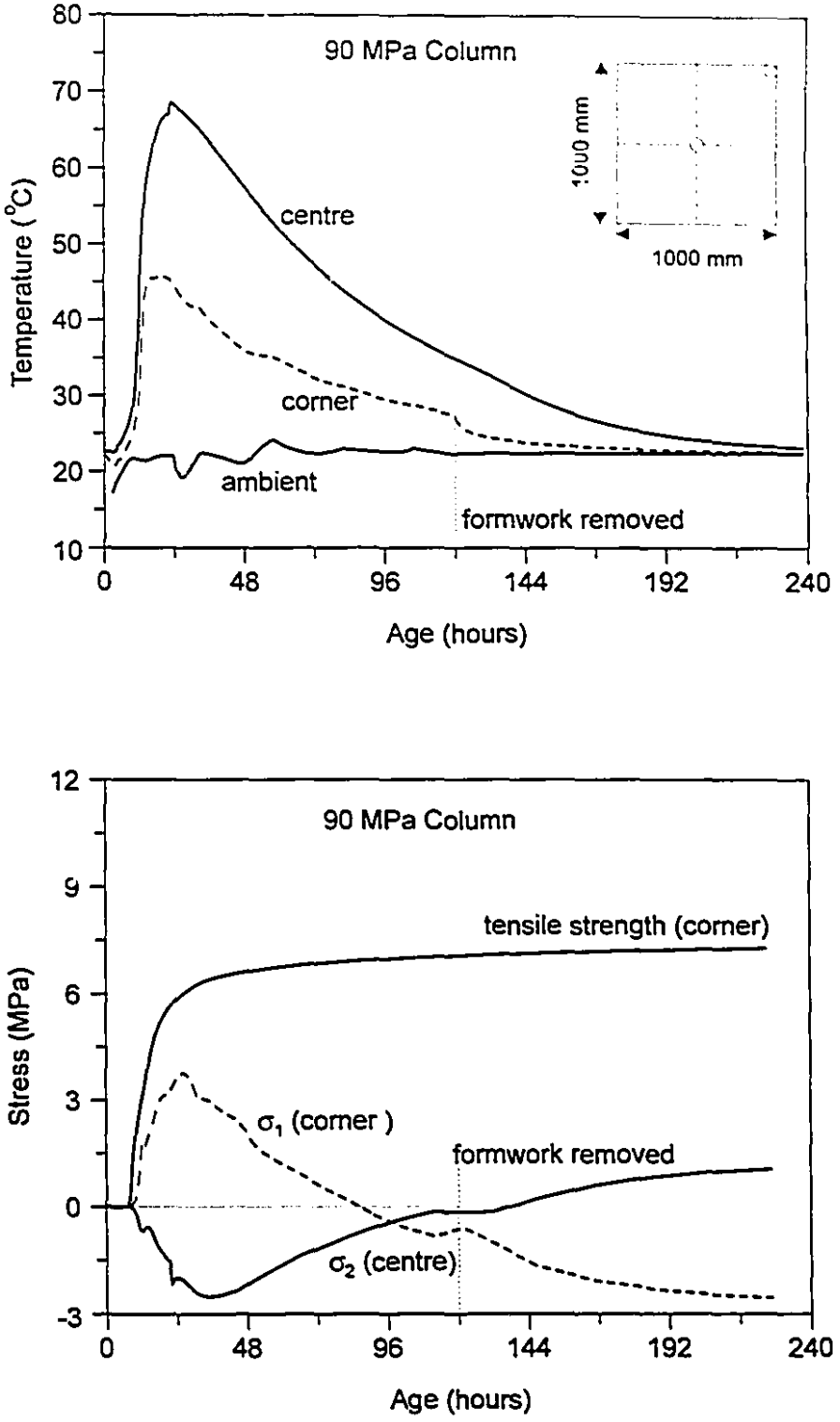

Figure 6.7 - Predicted temperatures, maximum principal stresses and tensile strength in 90 MPa concrete column (tension +ve; compression -ve)

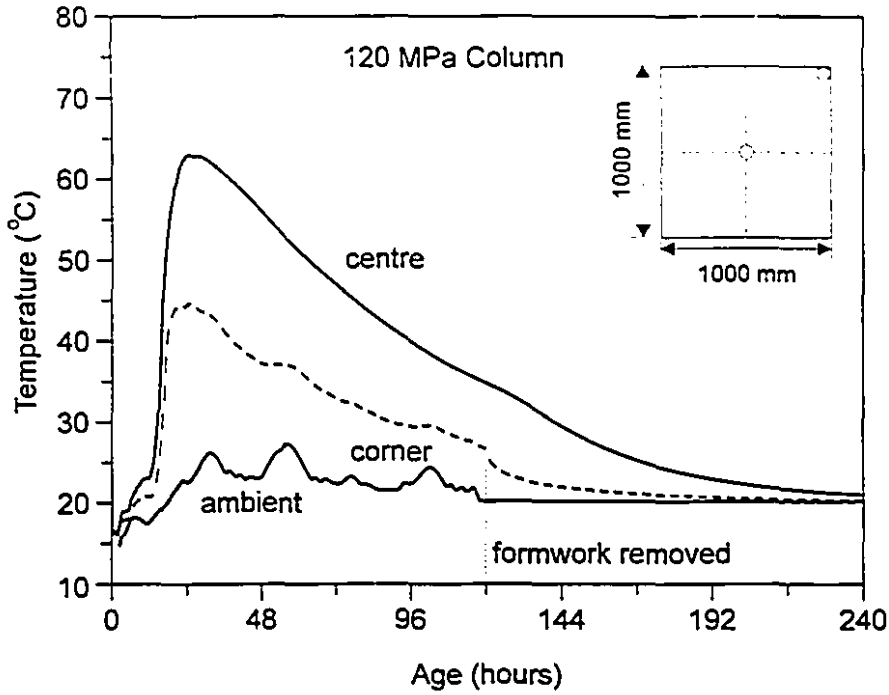

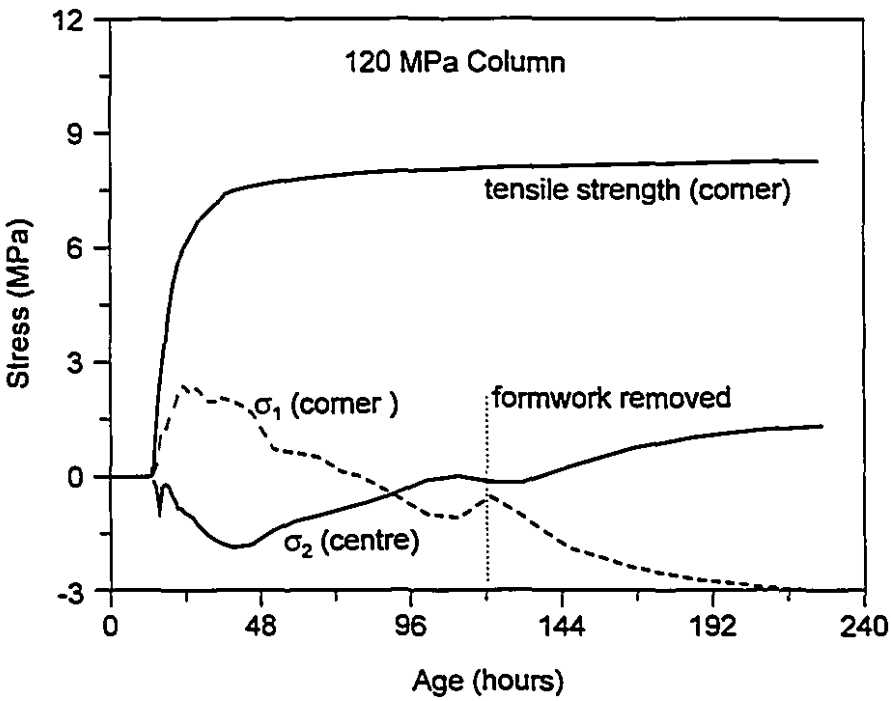

Figure 6.8 - Predicted temperatures, maximum principal stresses and tensile strength in 120 MPa concrete column (tension +ve; compression -ve)

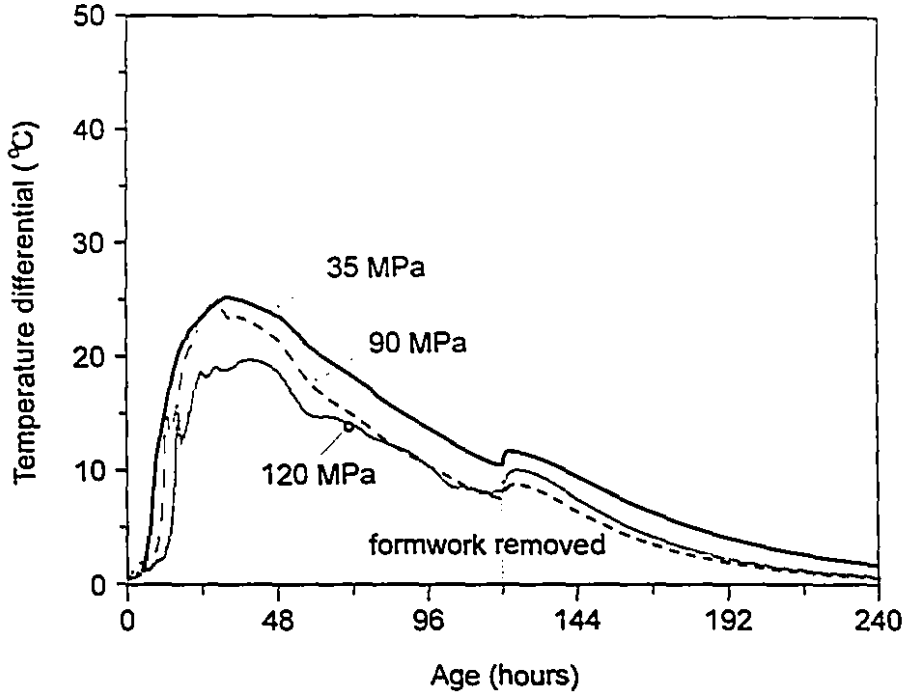

Figure 6.9 - Predicted temperature differentials between the centre and corner for the three columns

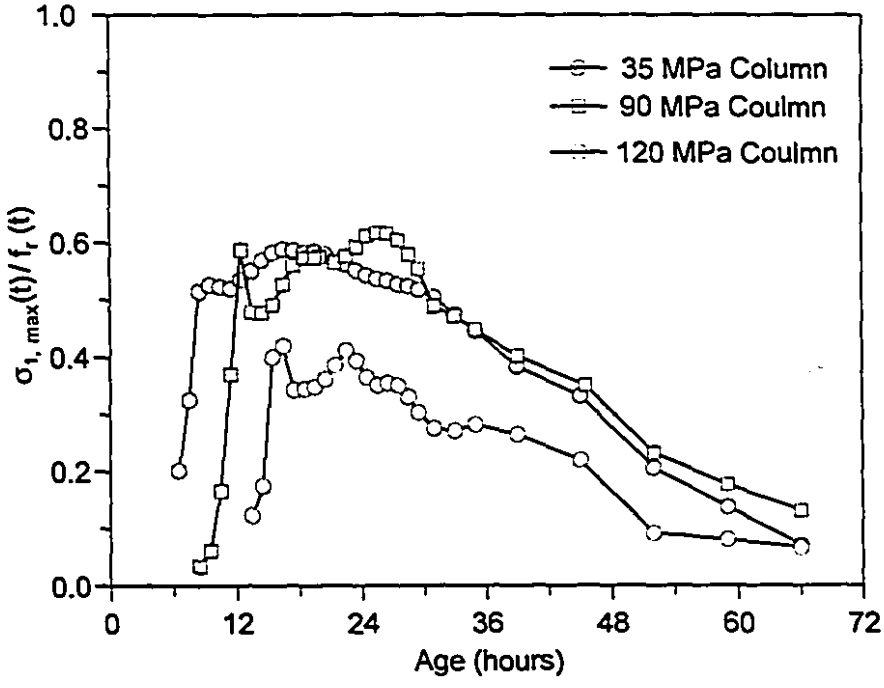

Figure 6.10 - Comparison of maximum principal tensile stresses to tensile strengths at the corner for the three columns

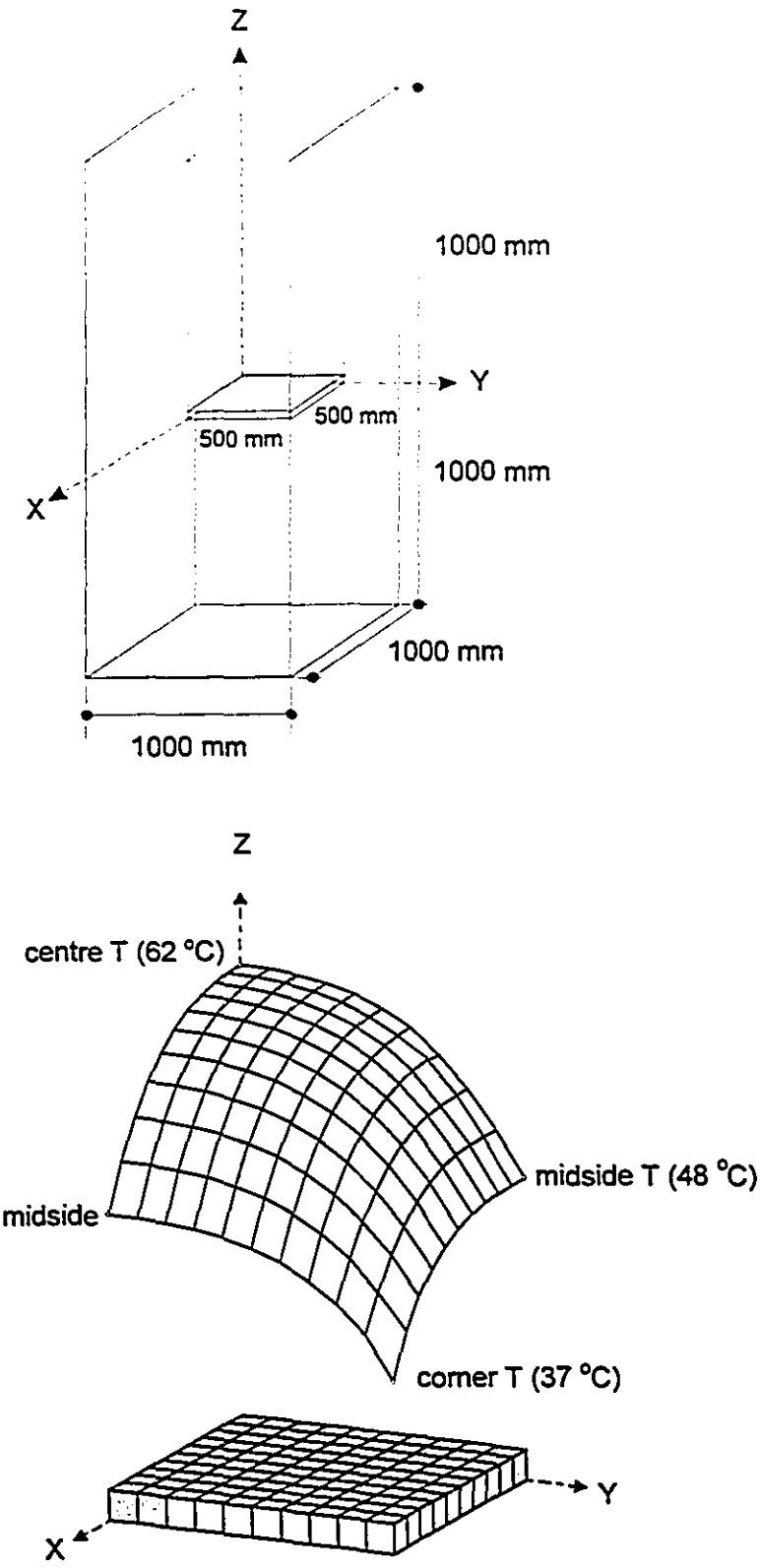

Figure 6.11 - Finite element idealization and predicted temperature at 24 hours for 35 MPa concrete column

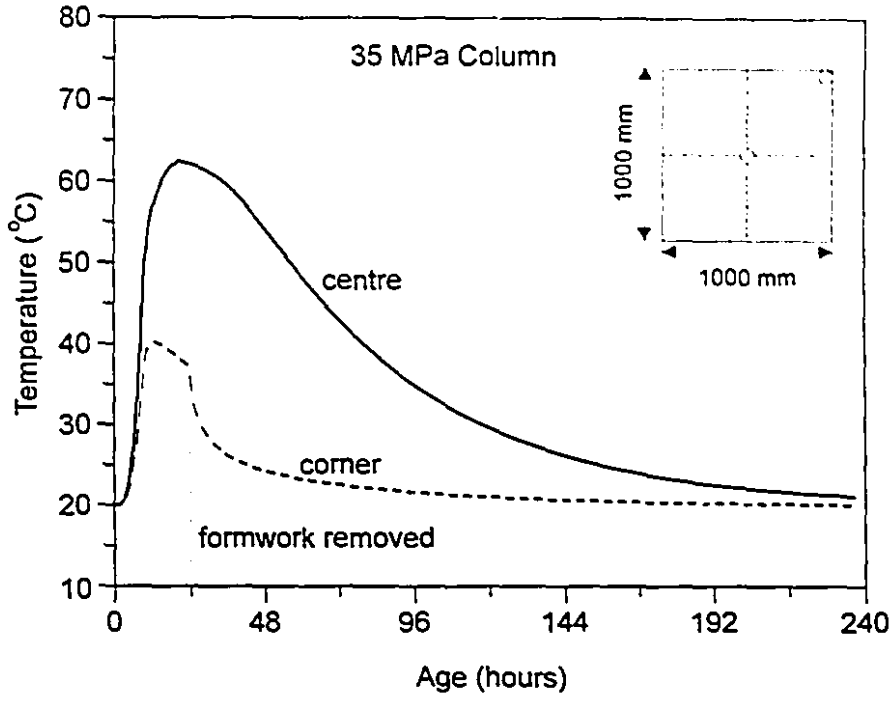

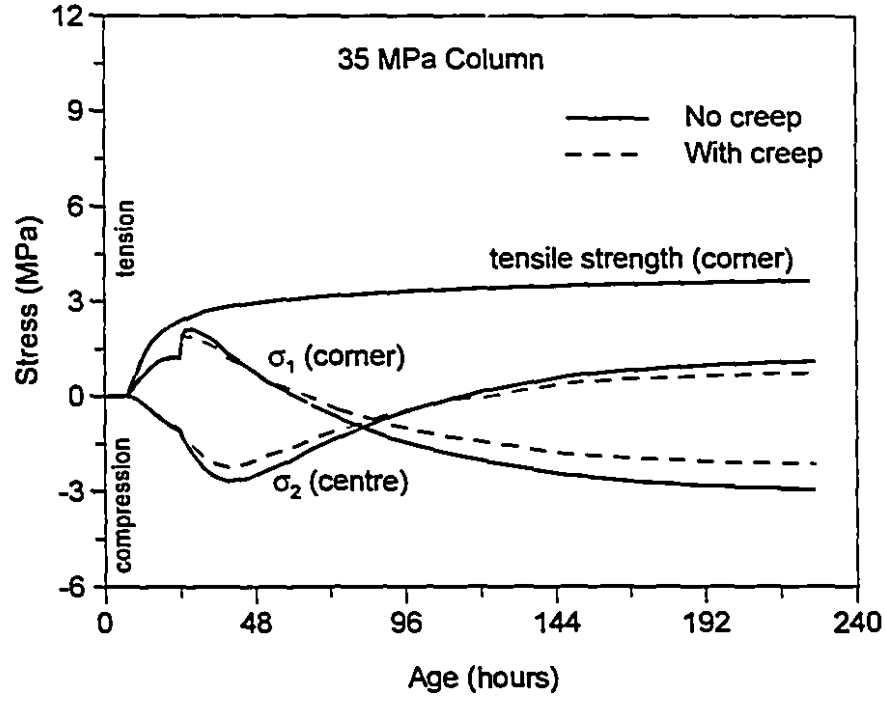

Figure 6.12 - Predicted temperatures, maximum principal stresses and tensile strength in 35 MPa concrete column (wood formwork removed at 24 hours)

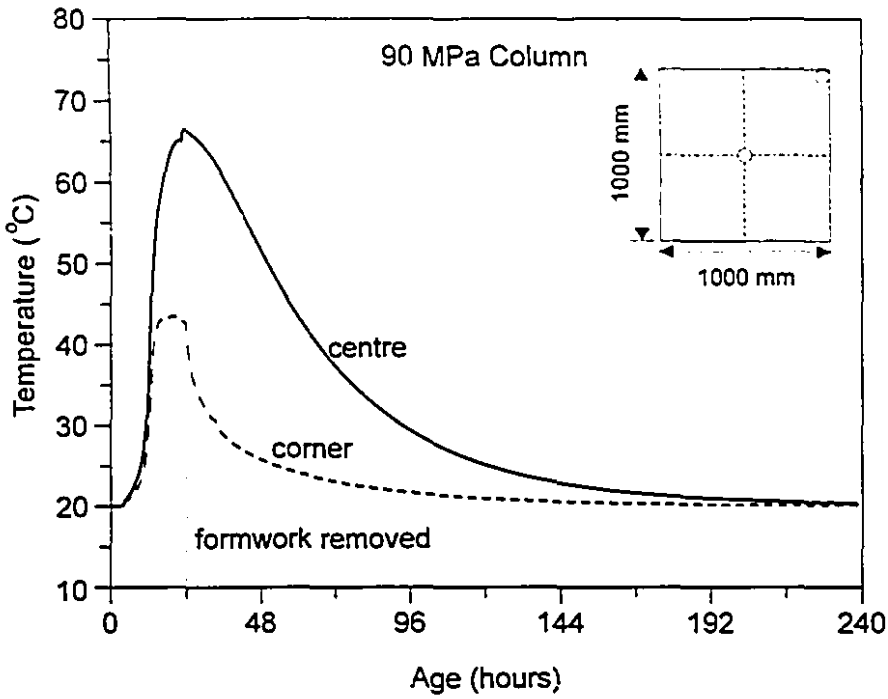

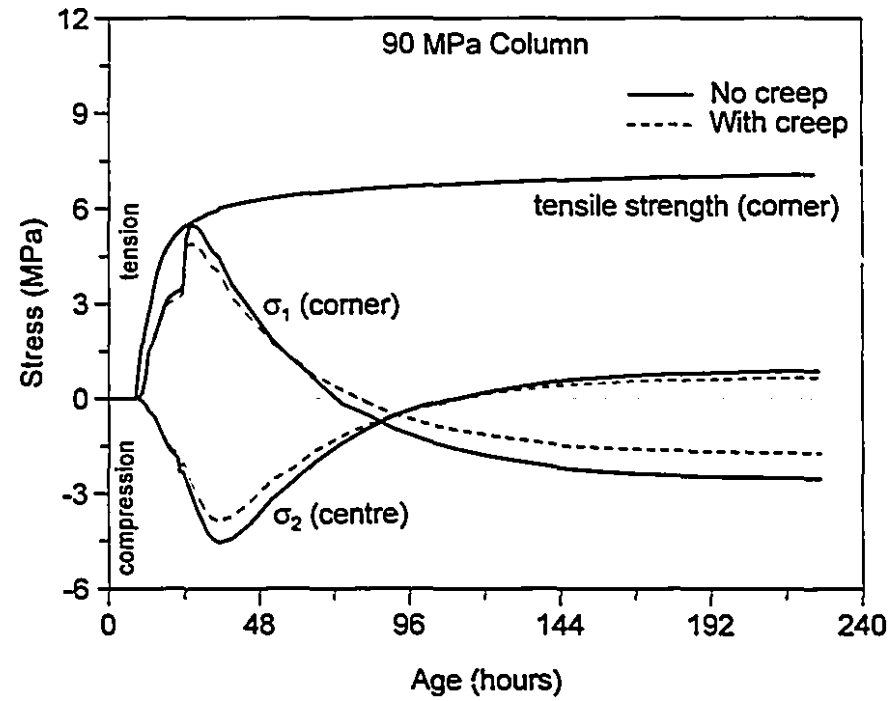

Figure 6.13 - Predicted temperatures, maximum principal stresses and tensile strength for 90 MPa concrete column (wood formwork removed at 24 hours)

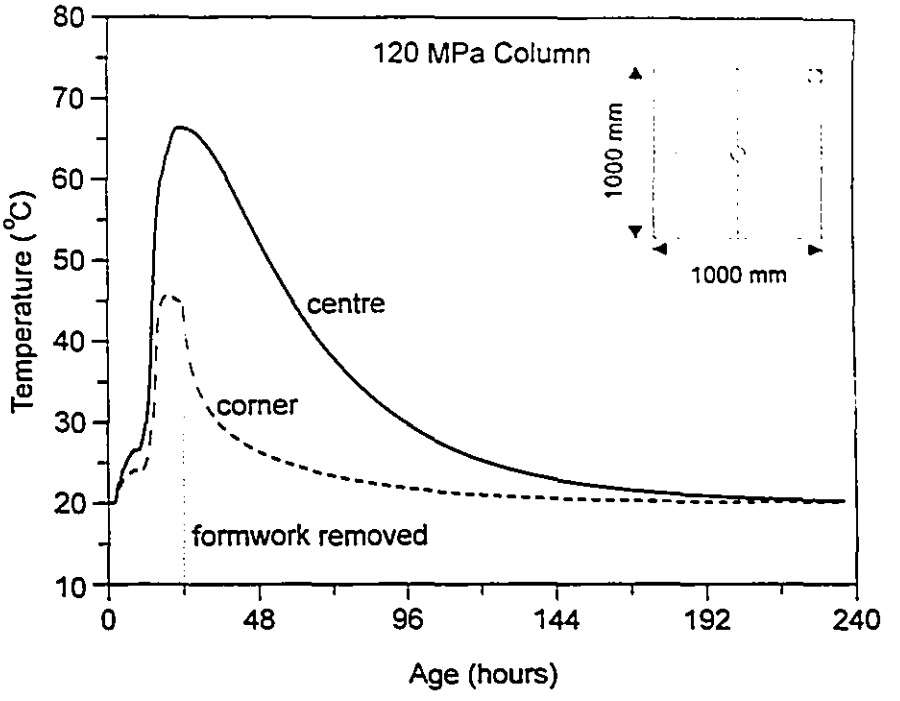

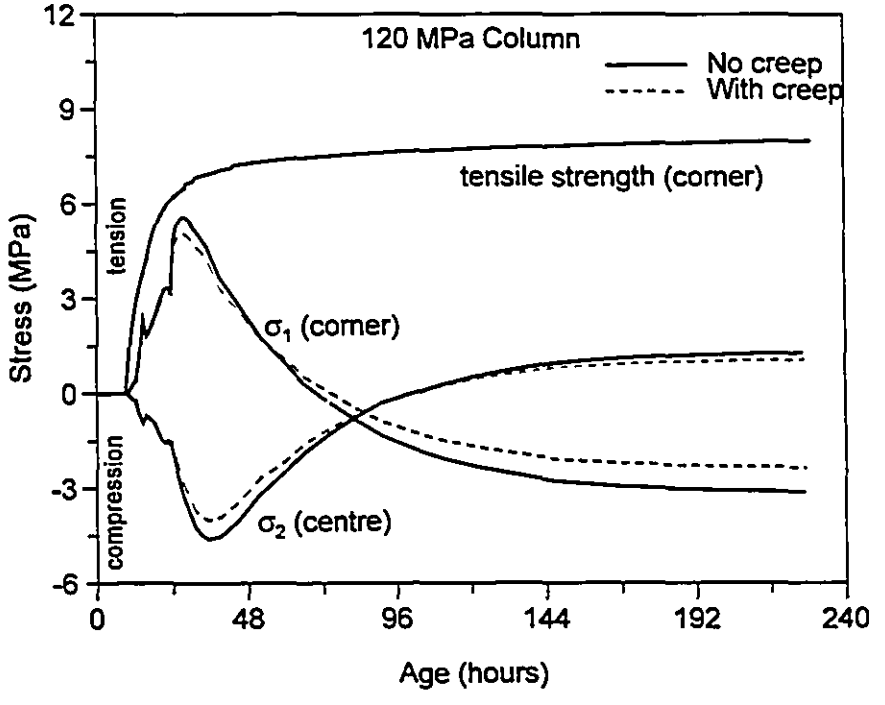

Figure 6.14 - Predicted temperatures, maximum principal stresses and tensile strength in 120 MPa concrete column (wood formwork removed at 24 hours)

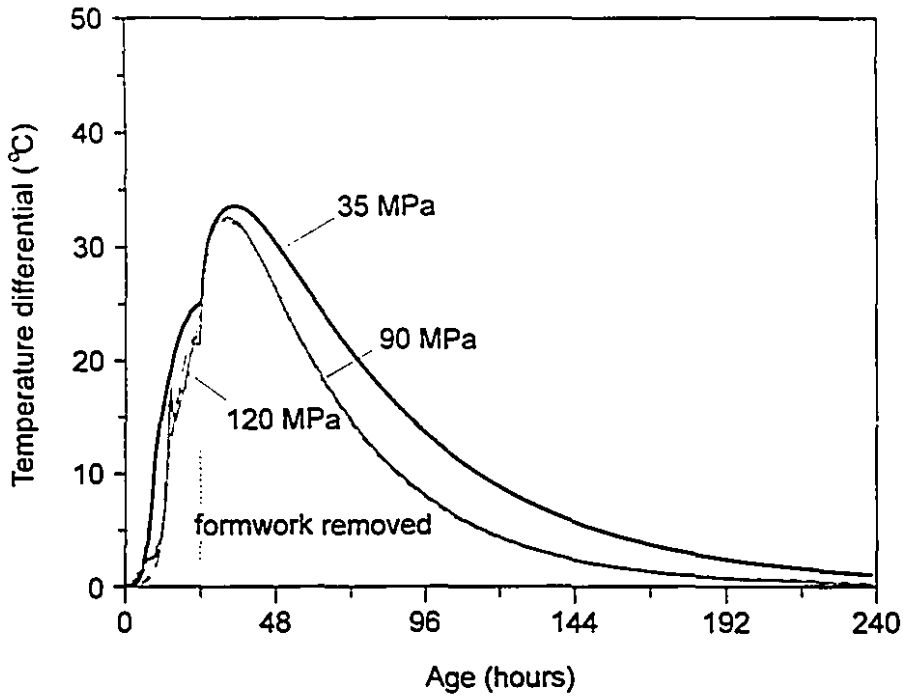

Figure 6.15 - Predicted temperature differentials between the centre and corner for the three columns (wood formwork removed at 24 hours)

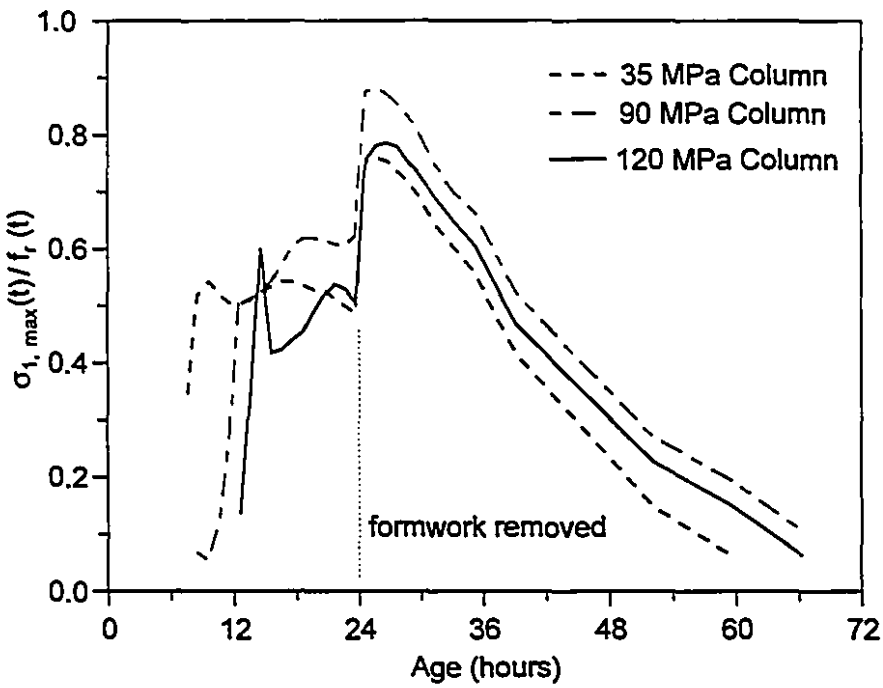

Figure 6.16 - Comparison of maximum principal tensile stresses to tensile strengths for the three columns (wood formwork removed at 24 hours)

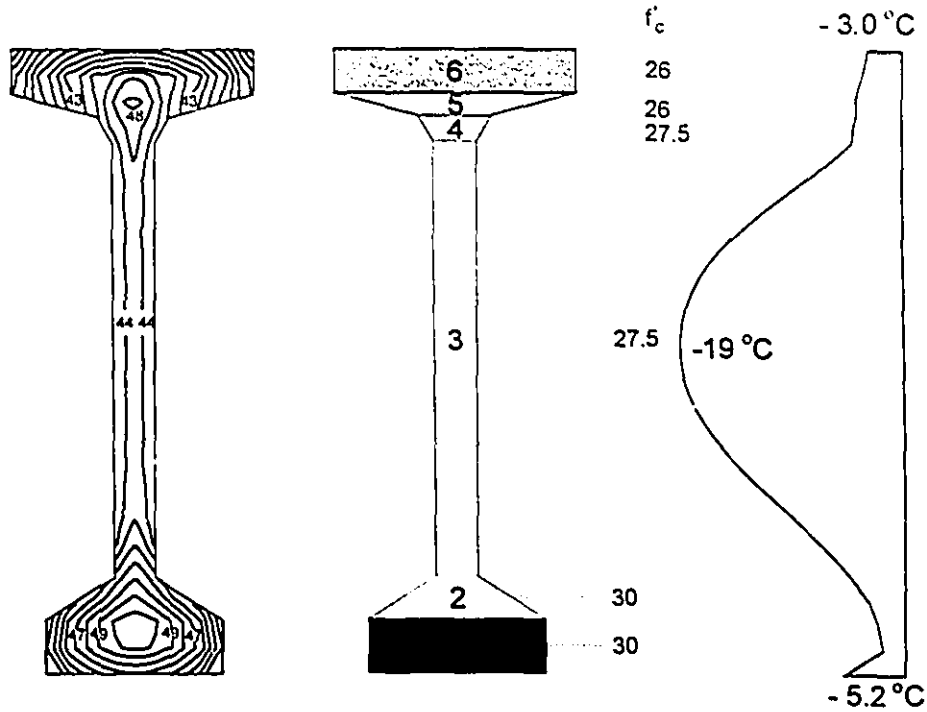

(a) Predicted temperature before form removal

(b) Idealization of cross-section and predicted strength after formwork removal

(c) ΔT after formwork removal

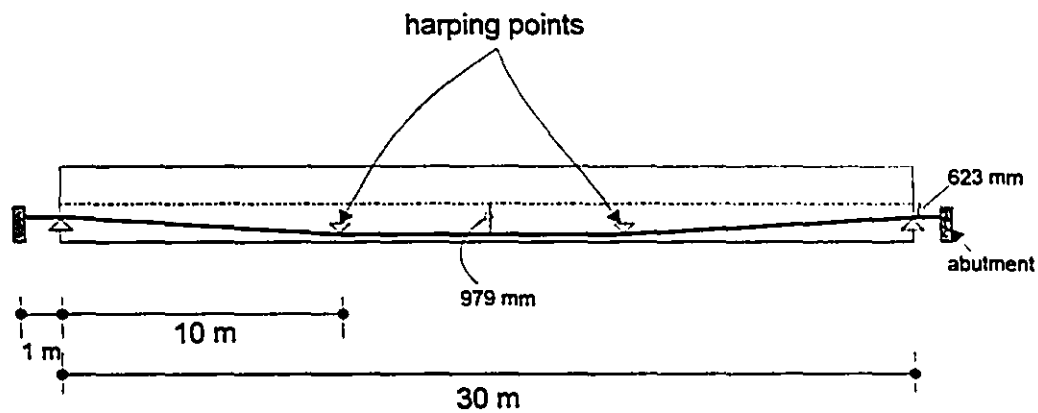

(d) Elevation view of 30 m long CPCI 2300 in pretensioning bed

Figure 6.17 - Temperature development and details of pretensioned bridge I-girder

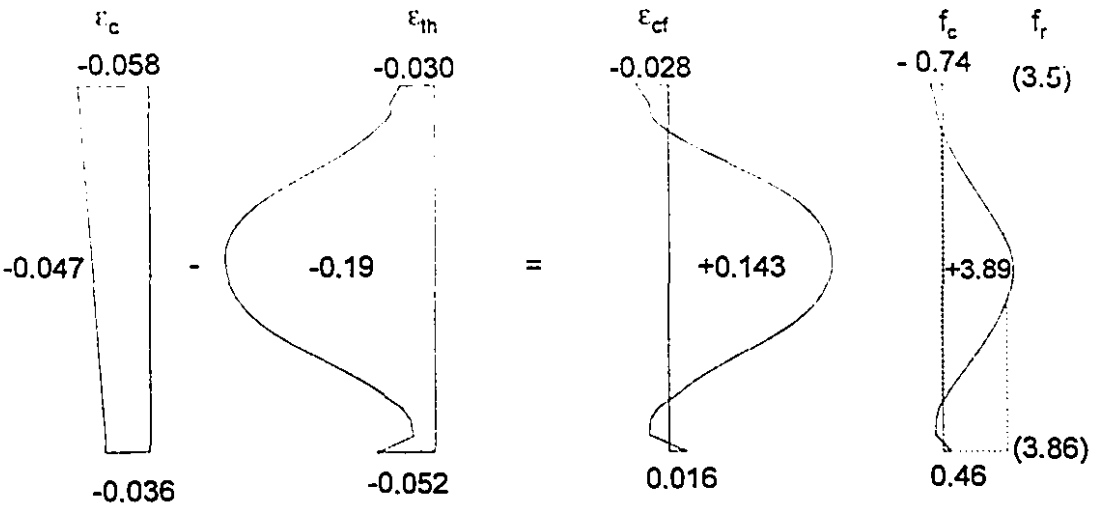

(a) After formwork removal, N=497 kN

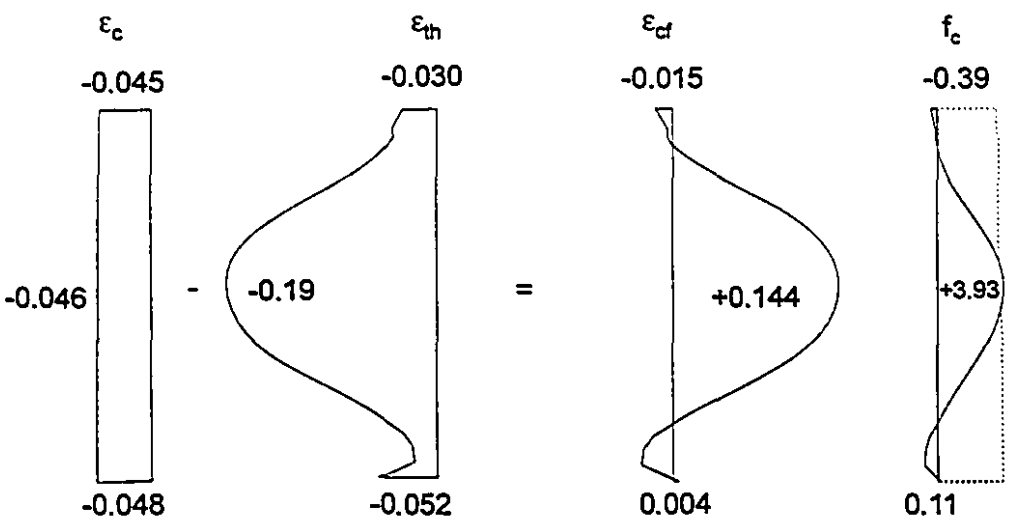

(b) After release of harping point loads, N=497 kN, M=-140 kN-m

Figure 6.18 - Strain and stress distributions in CPCI 2300 girder in stressing bed

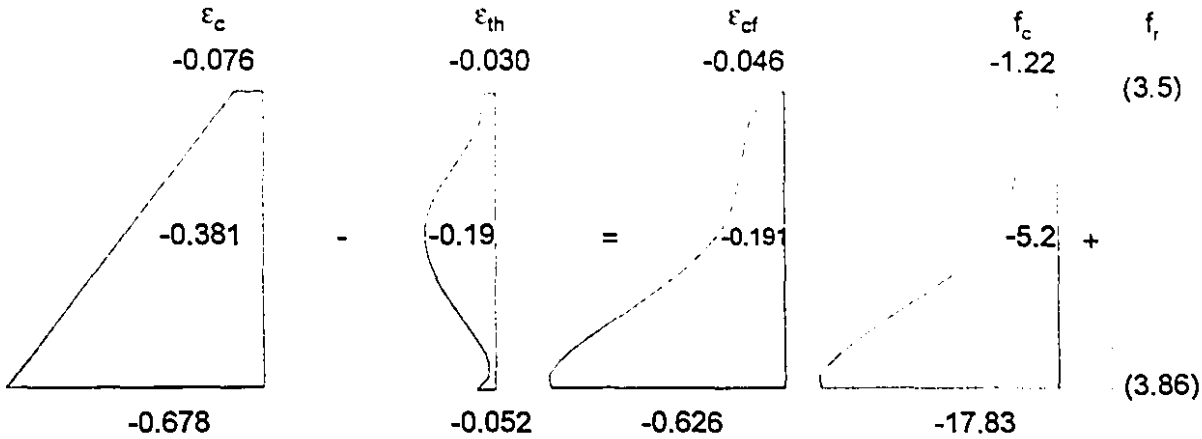

After release of prestress, N=0, M=1630 kN-m

Figure 6.19 - Strain and stress distributions in CPCI 2300 girder immediately after release

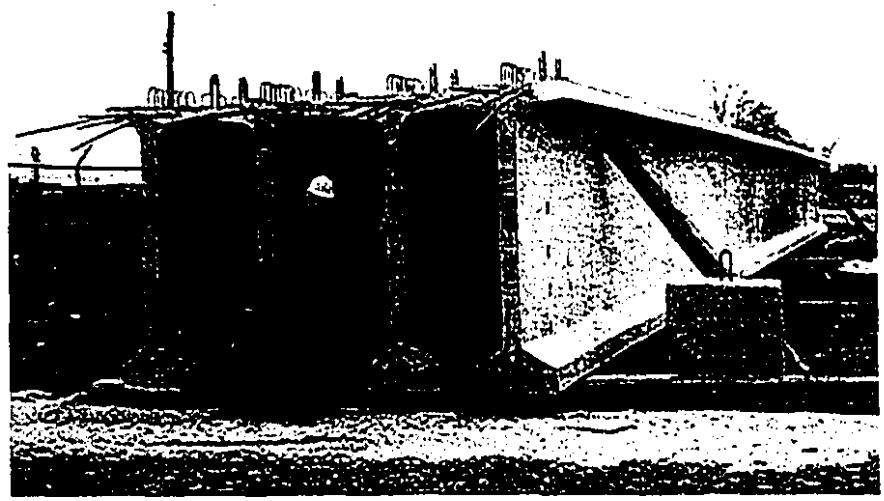

Figure 6.20 - CPCI 2300 high-strength concrete I-girders after removal from pretensioning bed

Chapter 7

Conclusions and Need for Future Research

In this research program, the mechanical and thermal properties of normal (30 MPa), medium (70 MPa) and high-strength (100 MPa) concretes, subjected to different curing conditions were investigated. New techniques and test setups were designed and built to examine these properties at verv early ages. The behavioural aspects of the key mechanical and thermal properties were modelled and were used to perform thermal and stress analyses. The main conclusions drawn from this study are summarised below:

7.1 Mechanical Properties

A large number of samples were tested to examine the mechanical properties of three different types of concretes subjected to three different curing conditions. It was concluded that:

i. As expected, the temperature rise during hydration increases as the cement content and compressive strength increases.

ii. The significant difference in the strength, elastic modulus and the shape of compressive stress-strain responses at very early ages was studied and compared with the values obtained after 24 hours for the normal, medium and high-strength concretes.

iii. The temperature-matched cured specimens (cylinders and flexural beams) gave higher compressive strength and flexural strength than the sealed cylinders, which in turn gave higher values than the air-dried specimens, for a given mix.

iv. The medium and, in particular the high-strength, concretes exhibited

retardation of hydration, which resulted in a time lag in reaching the peak temperatures. This effect is attributed to the high dosages of superplasticizers in these mixes. The slopes of the temperature rise responses increase with increasing cement content and concrete strength. After an initial retardation period, the higher strength concretes (70 and 100 MPa) showed a higher rate of strength and modulus gain than the 30 MPa concrete.

v. After demolding, air-dried curing resulted in lower modulus of rupture values than the specimens subjected to sealed curing. This was particularly evident for the medium and high-strength concretes, which are more sensitive to drying due to their very low water-cement ratios.

vi. The ACI code expression for the modulus of rupture overestimates the modulus of rupture for very early-age concrete and underestimates the modulus of rupture for concrete compressive strengths above 15 MPa. The expression recommended by ACI Committee 363 overestimates the modulus of rupture for the concretes and curing conditions investigated in this study. Expressions are proposed to predict the modulus of rupture for temperature-matched, sealed and air-dried curing.

vii. Expressions are also proposed to predict the compressive strength development of hydrating concretes in terms of equivalent age. These predicted compressive strengths are then used to predict the elastic modulus and the tensile strength.

7.1.1 Creep and Shrinkage

The early-age creep and shrinkage of normal, medium and high-strength concrete was measured for both sealed and air-dried curing. The conclusions from these experimental investigations are as follows:

i. The measured 28-day shrinkage and thermal strains of the specimens subjected to sealed curing was about 33%, 43% and 62% of the shrinkage of the air-dried specimens for the normal, medium and high-strength concretes, respectively.

ii. The high-strength concrete exhibited greater shrinkage and thermal

strains than the medium-strength concrete, which in turn showed greater strains than the normal-strength concrete for both the sealed and air-dried conditions.

iii. The rate of total strain development of the normal-strength concrete, subjected to sealed curing, stabilized more quickly than the medium and high-strength concretes.

iv. The specimens subjected to air-dried curing resulted in higher creep strains than the sealed specimens. This difference is significantly higher for concrete specimens subjected to loading at very early ages.

v. As expected, the creep strains decreased with an increase in the concrete compressive strength at the time of loading.

vi. The creep of high-strength concrete is much more sensitive to the age of loading than the normal and medium-strength concrete investigated, with very early-age loading resulting in significantly higher creep.

vii. Tests were repeated in order to observe the reproducibility of the test results, and very close agreement was observed.

7.2 Thermal Properties

Tests were conducted to measure the thermal properties of three types of concretes. A new testing apparatus was developed to measure the heat of hydration under temperature-matched curing. The conclusions are as follows:

i. The specific heat of the normal, medium and high-strength mature concretes was measured in both saturated and oven-dried conditions. It was observed that the specific heat increased with an increase in temperature and moisture. The specific heat decreased with an increase in density of the concrete.

ii. The thermal conductivity of the maturing normal-strength concrete was found to be about 33% higher than that of hardened concrete, whereas there was only a 2% difference in the thermal conductivity of the early-age and the hardened high-strength concrete. It was also found that the thermal conductivities of the hardened medium and high-strength concretes were 36% and 50% higher, respectively, than that of the

normal-strength concrete at a temperature of 25°C.

iii. The test results on specimens of age 16 hours and greater indicated that the coefficient of thermal expansion is not affected by the age of the concrete.

7.3 Thermal Analyses

A finite element thermal analysis program was modified to properly account for the thermal activation process during hydration as a function of maturity based on Arrhenius' approach. Predicted temperatures were compared with the measured temperature responses in different sizes and shapes of structural concrete elements and very good agreement was found. Additional sub-routines were added to the program to predict the rapidly changing compressive strength, elastic modulus and tensile strength of each element during the hydration period. These changing properties are needed for the subsequent thermal stress analysis. Additional modifications were made to account for important aspects during construction, such as addition or removal of formwork and insulation, by changing the boundary conditions during the analysis.

7.4 Thermal Stress Analyses

Sub-routines were developed to enable incremental stress analysis in the time domain and also to account for the rapidly changing material properties determined from the material property sub-routine used in the thermal analysis. Subroutines were also developed to included the creep of concrete in the incremental stress analyses. The effect of different concrete strengths, early formwork removal and creep of concrete on the risk of cracking were also investigated. It was concluded that the risk of cracking is increased due to early form stripping, whereas creep of concrete reduces the risk of cracking loaded at very early ages.

7.5 Need for Future Research

The following areas should be considered for future research:

i. An experimental study is needed on the early-age behaviour of concrete

containing additives such as fly ash and blast furnace slag.

ii. Shrinkage plays a very important role in the surface cracking of concrete members. Currently there is no rational way of determining the variation of shrinkage strains through the thickness of members, as a function of time. Innovative approaches need to be taken to account for this highly complex phenomenon of shrinkage.

iii. The presence of steel reinforcement on both the thermal and stress analysis needs to be studied. In situations where thermal cracking occurs, the influence of the amount and details of reinforcement on the control of the cracking needs to investigated.

Statement of Originality

The original contributions described in this thesis include:

i. The early-age thermal properties (heat of hydration, conductivity, specific heat and coefficient of thermal expansion) and key mechanical properties (compressive stress-strain responses, compressive strength, elastic modulus, modulus of rupture, creep and shrinkage) of normal, medium and high-strength concretes were investigated. These investigations required the development of some specialised testing setups and involved the study of the effect of three different curing conditions. Such a systematic study of normal, medium and high-strength concretes during the hydration period is not currently available in the literature.

ii. Expressions were proposed to predict the development of key properties such as the compressive strength, elastic modulus, and the modulus of rupture. The CEB-FIP Code expression was found to provide reasonable estimates of creep at early ages.

iii. An experimental study was carried out to investigate the effect of curing and early-form stripping on the temperature and stress development in different shapes and sizes of concrete elements during hydration and to provide measurements for comparing temperature predictions.

iv. Sub-routines were developed for a finite element thermal analysis program to account for the effect of "maturity" during the hydration period and to predict the rapidly changing compressive strength, elastic modulus and tensile strength of each element during hydration.

v. Subroutines, for incremental thermal stress analyses in the time domain were developed. These analyses, which account for the rapidly changing material properties and creep of concrete, were used to predict the risk of thermal cracking in structural elements during hydration.

vi. Parametric analyses were carried out to determine the influence of formwork type, time of formwork removal and strength of concrete and creep on the development of thermal gradients and the risk of cracking.

References

ACI Committee 207, "Mass Concrete for Dams and Other Concrete Structures," ACI Journal, Proceedings, Vol. 67, No. 4, Apr. 1970, pp. 273-309.

ACI Committee 207, "Mass Concrete," ACI 207.1R-87 in ACI Manual of Concrete Practice, Part I, 1992, 27 pp.

ACI Committee 209, "Prediction of Creep, Shrinkage, and Temperature Effects in Concrete Structures," Reported by ACI Committee 209, ACI 209R-92, 1992, 47 pp.

ACI Committee 211.1, "Standard Practice for Selecting Proportions for Normal, Heavyweight, and Mass Concrete," American Manual of Concrete Practice, Part 1, 1988, 34 pp.

ACI Committee 318, "Building Code Requirements for Reinforced Concrete (ACI 318-83)," American Concrete Institute, Detroit, 1983, 118 pp.

ACI Committee 363, "State-of-the-Art Report on High-Strength Concrete," ACI Journal, Proceedings V. 81, No. 4, July-August 1984, pp. 364-411.

ACI Committee 363, "State-of-the-Art Report on High-Strength Concrete," American Concrete Institute. Detroit, Sept. 1992, 55 pp.

ACI Committee 435, "Deflection of Reinforced Concrete Flexural Members," ACI Manual of Concrete Practice, Part 2, 1968, 32 pp.

ACI Committee 517, "Accelerated Curing of Concrete at Atmospheric Pressure," State-of-the-Art, ACI 517.2R-80, ACI Manual of Concrete Practice, Part 5, 1988.

"ADINA-In For ADINA-T Users Manual- A Program for Pre-Processing

and Display of ADINA and ADINA-T Input Data," Report ARD 92-5, ADINA R&D, Inc., Dec. 1992.

Aitcin, P.C., Laplante, P., and Bedard, C., "Development and Experimental Use of a 90 MPa (13,000 psi) Field Concrete," American Concrete Institute, SP-87-5, 1988, pp. 51-70.

Aitcin, P.C., Miao, B., Cook. W.D., and Mitchell, D., "Effects of Size and Curing on Cylinder Compressive Strength of Normal and High-Strength Concretes," ACI Materials Journal, Vol. 91, No. 4, July-August 1994, pp. 349-354.

Alexanderson, J., "Strength Losses in Heat Cured Concrete," Swedish Cement and Concrete Research Institute, No. 43, 1972, 135 pp.

American Society for Testing and Materials, "Standard Test Method for Slump of Portland Cement Concrete," ASTM C 143-78, ASTM Standard, Vol. 04.02, 1988, pp. 85-86.

American Society for Testing and Materials, "Standard Specification for Apparatus for Use in Measurement of Length Change of Hardened Cement Paste, Mortar and Concrete," ASTM C 490-86, ASTM Standard, Vol. 04.02, 1988, pp. 241-244.

American Society for Testing and Materials, "Standard Practice for Making and Curing Concrete Test Specimens in the Field," ASTM C 31-88, ASTM Standard, Vol. 04.02, 1988, pp. 4-8.

American Society for Testing and Materials, "Standard Practice for Capping Cylindrical Concrete Specimens," ASTM C 617-87, ASTM Standard, Vol. 04.02, 1988, pp. 287-290.

American Society for Testing and Materials, "Standard Test Method for Co.npressive Strength of Cylindrical Concrete Specimens," ASTM C 39-86, ASTM Standard, Vol. 04.02, 1988, pp. 19-22.

American Society for Testing and Materials, "Standard Test Method for

Static Modulus of Elasticity and Poisson's Ratio of Concrete in Compression," ASTM C 469-87, ASTM Standard, Vol. 04.02, 1988.

ASHRAE "Ashrae Handbook, Fundamentals," American Society of Heating, Refrigerating and Air Conditioning Engineering, Inc., Atlanta, 1989, Chap. 20&22.

Bakhsh, A.H., Wafa, F.F., and Akhtaruzzaman, A.A., "Torsional Behavior of Plain High-Strength Concrete Beams," ACI Structural Journal, Vol. 87, No. 5, Sept.-Oct. 1990, pp. 583-588.

Bamforth, P.B., "Early Age Thermal Cracking in Concrete," The Institute of Concrete Technology, Technical Note, July 1982, 20 pp.

Bamforth, P.B., "Mass Concrete," Concrete Society Digest No 2, Dec. 12, 1985, 8 pp.

Baron, J., "Fissuration du Béton par Hydratation Localement Différée du Ciment," Laboratoires des Ponts et Chaussées, Rapport de Recherche No. 15, 1971.

Bazant, Z.P., "Mathematical Modelling of Creep and Shrinkage of Concrete," John Wiley and Sons, 1988, 459 pp.

Bazant, Z.P., and Carol, I., "Creep and Shrinkage of Concrete," Proceedings of the Fifth International RILEM Symposium, RILEM Proceedings 22, Barcelona, Spain, Sept. 1993, 934 pp.

Bazant, Z. P., and Chern, Jenn-Chuan., "Stress-Induced Thermal and Shrinkage Strains in Concrete," Journal of Engineering Mechanics, Vol. 113, No. 28, Oct. 1987, pp. 1493-1511.

Bazant, Z.P., and Najjar, L.J., "Non-Linear Water Diffusion in Non-Saturated Concrete," Materials and Structures, Vol. 5, 1972, pp. 3-20.

Bazant, Z.P., and Panula, L., "Practical Prediction of Time Dependant Deformations of Concrete," Materials of Construction, RIELM, Paris, 11,

65, pp. 307-328, and 66, 1978, pp. 415-434, 12, 69, 1979, pp. 169-183.

Bazant, Z.P., and Panula, L., "New Model for Practical Prediction of Creep and Shrinkage," Designing for Creep and Shrinkage in Concrete Structures, ACI SP-76, 1982, pp. 7-23.

Bazant, Z.P., and Wittmann, F.H., "Creep and Shrinkage in Concrete Structures," John Wiley and Sons, 1982, 363 pp.

Bergstrom, S.G., "Curing Temperature, Age and Strength of Concrete," Magazine of Concrete Research, Vol. 4, No. 14, 1953, pp. 61-66.

Bickley, J.A., "Prequalification Requirements for the Supply and Testing of Very High Strength Concrete," High-Performance Concrete, Network of Centres of Excellence on High-Performance Concrete, Feb. 1993, pp. 41-49.

Blick, R.L., "Some Factors Influencing High-Strength Concrete," Modern Concrete, Vol. 36, No. 12, Apr. 1973, pp. 38-41.

Bogue, R.H., "The Chemistry of Portland Cement," Reinhold Publishing Corporation, New York, 1947.

Boulay, C., and Paties, C., "Mesure des déformations du béton au jeune âge," Laboratoire Central des Ponts et Chaussées, Matériaux et Constructions, Vol. 26, 1993, pp. 307-311.

Brown, T.D., and Javaid, M.Y., "The Thermal Conductivity of Fresh Concrete," Materials and Structures, Vol. 3, No. 18, 1970, pp. 411-416.

Burg, R.G. and Ost, B.W., "Engineering Properties of Commercially Available High-Strength Concretes," Research and Development Bulletin RD104T, Portland Cement Association, 1992, 55 pp.

Byfors, J., "Plain concrete at early ages," Swedish Cement and Concrete

Institute, 1980, 465 pp.

Carino, N.J., "Maturity Functions for Concrete," International Conference on Concrete at Early Ages, Ecole Nationale Des Ponts et Chaussées, Vol. 1, 1982, pp. 123-128.

Carino, N.J., and Tank, R.C., "Maturity Functions for Concretes Made with Various Cements and Admixtures," ACI Materials Journal, Vol. 89, No. 2, Mar.-Apr. 1992, pp. 188-196.

Carrasquillo, R.L., Slate, F.O., and Nilson, A.H., "Microcracking and Behavior of High Strength Concrete Subject to Short-Term Loading," ACI Journal, Proceedings Vol. 78, No. 3, May-June 1981, pp. 179-186.

Carrasquillo, R.L., Nilson, A.H., and Slate, F.O., "Properties of High-Strength Concrete Subjected to Short-Term Loads," ACI Journal, Proceedings Vol. 78, No. 3, May-June 1981, pp. 171-178.

Carslaw, H.S., and Jaeger, J.C., "Conduction of Heat in Solids," Clarendon Press, New York, 2nd Edition, 1986, 510 pp.

CEB-FIP Model Code 1978, "Model Code for Concrete Structures," CEB Comité Euro-International Du Béton, 1978.

CEB-FIP Model Code 1990, CEB Comité Euro-International Du Béton, Bulletin D'Information No. 195, Chapters 1-5, 1990.

Collins, M.P. and Mitchell, D., "Prestressed Concrete Structures," Prentice Hall Inc., 1991, 766 pp.

Cook, W.D., Miao, B., Aitcin, P.C. and Mitchell, D., "Thermal Stresses in Large High-Strength Concrete Columns," ACI Materials Journal, Vol. 89, No. 1, Jan.-Feb. 1992, pp. 61-68.

CSA A23.1-94, CSA A23.2-94, "Concrete Materials and Methods of Concrete Construction, Canadian Standards Association (CSA), 1994, 350 pp.

Danielsson, U., "Conduction Calorimeter Studies of the Heat of Hydration of a Portland Cement," Cement och Betong-Institutet, Handlingar nr 38, Stockholm, 1966.

De Larrard, F., and Roy, R., "Relation Entre Formulation et Quelques Propriétés Mécaniques des Bétons à Hautes Performances," Materials of Construction, RILEM, Vol. 25, 1992, pp. 464-475.

De Larrard, F., Acker, P., and Roy, R Le., "Shrinkage Creep and Thermal Properties," Chapter 3, High Performance Concrete: Properties and Applications, Edited by Shah S.P. and Ahmad S.H., McGraw Hill Inc., 1994, pp. 65-114.

Fitzgibbon, M.E., "Large-Pours-2, Heat Generation and Control," Concrete Magazine, Current Practice Sheet, Dec. 1976, pp. 33-35.

Freiesleben Hansen, P. and Pedersen, E.J., "Maleinstrument til Kontrol af Betons Haerding," Norisk Betong, 1977, pp. 21-25.

Ghali, A., and Favre, R., "Concrete Structures: Stresses and Deformations," Chapman and Hall Ltd, New York, NY, 1986, 352 pp.

Gonnerman, H.F., and Shuman, E.C., "Compression, Flexural and Tension Tests of Plain Concrete," Proceedings, ASTM, Vol. 28, Part II, 1928, pp. 527-564.

Grieb, W.E., and Werner, G., "Comparison of Splitting Tensile Strength of Concrete with Flexural and Compressive Strengths," Public Roads, Vol. 32, No. 5, Dec. 1962.

Gunzler, J., "Mechanische Eigenschaften von Jungem Beton im Gleitbau," Bauplanung Bautechnik, 1970, pp. 372-375.

Hansen, P.G., "Physical Properties of Concrete at Early Ages," School of Mines and Metallurgy, University of Missouri, 1956, 140 pp.

Hansen, P.F., Hansen, J.H., Kjaer, U., and Pedersen, E.J., "Thermal

Properties of Hardening Cement Paste," International Conference on Concrete of Early Ages, Paris, April 1982, pp. 23-26.

Holman, J.P., "Heat Transfer," McGraw Hill Publishing Company, Seventh Edition, 1990, 714 pp.

Japan Concrete Institute, "Proposed Recommendation for Control of Cracking in Massive Concrete," Japan Concrete Institute, 1986.

Jawed, I., Skalny, J., and Young, J.F., "Hydration of Portland Cement," Structure and Performance of Cement, Applied Science Publisher, England, 1983, pp. 237-317.

Jerome, M.R., "Tensile Strength of Concrete," ACI Journal, Proceedings Vol. 81, No. 2, March-April 1984, pp. 158-165.

Kaplan, M.F., "Flexural and Compressive Strength Concretes as Affected by the Properties of Coarse Aggregates," ACI Journal, Proceedings V. 55, No. 11, May 1959, pp. 1193-1208.

Kasai, Y., "Initial Strength of Concrete," Japan Cement Engineering Association, 15th General Meeting, 1961, pp. 188-189.

Kasai, Y., Matsui, I., and Yokoyama, K., "Volume Change of Concrete at Early Ages," International Conference on Concrete of Early Ages, Vol. 1, Paris, April 1982, pp. 51-56.

Kasai, Y., Matsui, I., and Yokoyama, K., "Shrinkage and Cracking of Concrete at Early Ages," International Conference on Concrete of Early Ages, Paris, April 1982, Vol. 1, pp. 45-50.

Kjellsen, K.O., and Detwiler, R.J., "Later-Age Strength Prediction by a Modified Maturity Model," ACI Materials Journal, Vol. 90, No. 3, May-June 1993, pp. 220-227.

Klieger, P., "Effect of Mixing and Curing Temperatures on Concrete Strength," ACI Journal, Vol. 12, No. 29, 1958, pp. 1063-1081.

Klink, S.A., "Actual Poisson Ratio of Concrete," ACI Journal, Nov.-Dec. 1985, pp. 813-817.

Klink, S.A., "Axial Strain Variations in Concrete Under Uniform Uniaxial Compressive Stress," Cement and Concrete Research, Vol. 5, 1975, pp. 405-418.

Laplante, P., "Propriétés Mécaniques des Bétons Durcissants:Analyse Comparée des Bétons Classiques et à Très Hautes Performances," Études et Recherches des Laboratoires des Ponts et Chaussées, Décembre 1993, 299 pp.

Lessard, M., Chaallal, O., and Aitcin, P., "Testing High Strength Concrete Compressive Strength," High-Performance Concrete, Network of Centres of Excellence on High-Performance Concrete, Feb. 1993, pp. 50-57.

Lew, H.S., and Reichard, T.W., "Mechanical Properties of Concrete at Early ages," Journal ACI, Oct. 1978, pp. 533-542.

L'Hermite, R., "Volume Change of Concrete," Proceedings of the 4th International Symposium on the Chemistry of Cement, 1960, pp. 659-694.

Lofqvist, B., "Temperature Effekter i Hardnande Betong," Tekniskt Meddelande Fran Kung1. Vatterfallsstyrelsen Nr 22, Stockholm, 1946, 195 pp.

Machida, N., and Uehara, K., "Non-Linear Thermal Stress Analysis of a Massive Concrete Structure," Computers and Structures, Vol. 26, No. 1/2, 1987, pp. 287-296.

Malhotra, V.M., "Maturity Concept and the Estimation of Concrete Strength," A Review. Indian Concrete Journal, Vol. 48, No. 4, 1974, pp. 122-126.

Malhotra, V.M., "Are 4 x 8 Inch Concrete Cylinders as Good as 6 x 12

Inch Cylinders for Quality Control of Concrete?," ACI Journal, Vol. 73, No. 1, Jan. 1976, pp. 33-36.

Mehta, P.K., and Monteiro, P.J.M., "Concrete-Structure, Properties and Materials," Prentice-Hall Inc., Englewood Cliffs, New Jersey, 1993, 548 pp.

CPCI, Metric Design Manual, "Precast and Prestressed Concrete," Canadian Prestressed Concrete Institute, 1987, pp. 1-33.

Meyers, S.L., "Thermal Expansion Characteristics of Hardened Cement Paste and Concrete," Proceedings Highway Research Board, Vol. 30, 1950, pp. 193-203.

Miao, B., Aitcin, P.C., Cook, W.D., and Mitchell, D., "Influence of Concrete Strength on In Situ Properties of Large Columns," ACI Materials Journal, Vol. 90, No. 3, May-June 1993, pp. 214-219.

Miao, B., Chaallal, O., Perraton, D., and Aitcin, P.C., "On-Site Early Age Monitoring of High-performance Concrete Columns," ACI Materials Journal, Vol. 90, No. 5, Sept.-Oct. 1993, pp. 415-420.

Mindess, S and Young, J.F., "Concrete," Prentice-Hall Inc., Englewood Cliffs, New Jersey, 1981, 671 pp.

Mitchell, L.J., "Thermal Expansion Tests on Aggregates, Neat Cement, and Concretes," Proceedings ASTM, Vol. 53, 1953, pp. 963-977.

Mitchell, D., and Bickley, J.,"Code Implications: High-Performance Concrete," Structural Concrete Conference, 1993 CPCA/CSCE Proceedings, 1993, pp. 115-126.

Mukherjee, P.K., and Thomas, M.D.A., "Temperature Rise and Thermal Cracking of Mass Concrete at an Early Age," Proceedings 1993 CPCA/CSCE Structural Concrete Conference, 1993, pp. 308-321.

Muller, H.S., "New Prediction Models for Creep and Shrinkage of

Concrete," Creep and Shrinkage of Concrete: Effect of Materials and Environment, SP-135, April 1992, pp. 1-18.

Nagamatsu, S., and Sato, Y., "Study on the Distribution of Water Loss in Concrete by Non-Linear Diffusion Equation," Review of the 35th General Meeting of the Cement Association of Japan, 1981, pp. 90-92.

Naik, T.K., "Maturity Functions for Concrete Cured During Winter Conditions," ASTM STP 858, Temperature Effects on Concrete, Edited by T.R. Naik, ASTM, Philadelphia, 1985, pp. 107-117.

Neville, A.M., "Properties of Concrete," Pitman Publishing Ltd., London, 1981, 799 pp.

Neville, A.M., and Dilger, W.H., "Creep of Concrete, Plain, Reinforced and Prestressed," North Holland Publishing Company, 1970, 622 pp.

Neville, A.M., Dilger, W.H., and Brooks, J.J., "Creep of Plain and Structural Concrete," Construction Press, Longman Group Limited, 1983, 361 pp.

Nilson, A.H., "Design Implications of Current Research on High-Strength Concrete," American Concrete Institute, SP-87-7, 1988, pp. 85-118.

NRMCA, "High-Strength Concrete," National Ready Mixed Concrete Association of Australasia, Cement and Concrete Association of Australia, 1992, 31 pp.

Nurse, R.W., "Steam Curing of Concrete," Magazine of Concrete Research, Vol. 1, No. 2, 1949, pp. 79-88.

Oluokun, F.A., Burdette, E.G., and Deatherage, J.H., "Elastic Modulus, Poisson's Ratio, and Compressive Strength Relationships at Early Ages," ACI Materials Journal, Jan.-Feb. 1991, pp. 3-10.

Oluokun, F.A., Burdette, E.G., and Deatherage, J.H., "Splitting Tensile Strength and Compressive Strength Relationship at Early ages," ACI

Materials Journal, March-April 1991, pp. 115-121.

Perenchio, W.F., and Klieger, P., "Some Physical Properties of High-Strength Concrete," Research and Development Bulletin, RD056.01T, Portland Cement Association, Skokie, Illinois, 1978.

Pickett , G., "The Effect of Change in Moisture Content on the Creep of Concrete Under a Sustained Load," ACI Journal, Vol. 38, 1942, pp. 333-356.

Pitts, D.R., and Sissom, L.E., "1000 Solved Problems in Heat Transfer," Schaum's Solved Problems Series, McGraw Hill Book Company, 1991, 421 pp.

Polivka, R.M., and Wilson, E.D., "Finite Element Analysis of Nonlinear Heat Transfer Problems," Structural Engineering and Applied Mechanics, Department of Civil Engineering, University of California, Berkeley, June 1976, 98 pp.

Price, W.H., "Control of Cracking in Mass Concrete Dams," Concrete International, Oct. 1982, pp. 36-44.

Rastrup, E., "Heat of Hydration in Concrete," Magazine of Concrete Research, Vol. 6, No. 17, Sept. 1954, pp. 79-92.

Rasmussen, T.H., and Andersen, T., "Haerdeteknologi Beton-Teknik," June 1989.

Regourd, M., and Gautier, E., "Comportement des Ciments Soumis au Durcissement Accéléré," Durcissement Accéléré des Bétons, Annales de l ITBTP, No. 387, 1980, pp. 83-96.

RILEM, "Properties of Set Concrete at Early Ages," State-of-the-Art Report, Materials and Structures, Vol. 14, No. 84, 1981, pp. 399-450.

Ryell, J., and Bickley, J.A., "Scotia Plaza: High Strength Concrete for Tall Buildings," Symposium on the Utilization of High-Strength Concrete,

Stavanger, Proceedings, June 1987, pp. 641-654.

Ryell, J., and Fasullo, C.E.T., "The Characteristics of Commercial High Strength Concrete in the Toronto Area," Proceedings 1993 CPCA/CSCE Structural Concrete Conference, 1993, pp. 278-292.

Sakata, K., "A Study on Moisture Diffusion in Drying Shrinkage of Concrete," Cement and Concrete Research, Vol. 13, No. 2, 1983, pp. 216-224.

SAP90, "A Series of Computer Programs for the Finite Element Analysis of Structures," Heat Transfer Analysis Users Manual, Computer and Structures, Inc., Berkeley, California, 1990.

SAP90, "A Series of Computer Programs for the Static and Dynamic Finite Element Analysis of Structures," Users Manual, Computer and Structures, Inc., Berkeley, California, 1989.

SAS, "Language Guide for Personal Computers," Version 6 edition, 1985, 428 pp.

Shah, S.P. and Ahmad. S.H., "Structural Properties of High Strength Concrete and its Implications for Precast Prestressed Concrete," Journal of the Prestressed Concrete Institute, Vol. 30, No. 6, Nov.-Dec. 1985, pp. 92-119.

Shah, S.P. and Ahmad. S.H., (Editors) "High Performance Concrete: Properties and Applications," McGraw-Hill Inc., 1994, 403 pp.

Sigvaldason, O.T., "The Influence of Testing Machine Characteristics Upon the Cube and Cylinder Strength of Concrete," Magazine of Concrete Research, Vol. 18, No. 57, Dec. 1966, pp. 197-206.

Springenschmid, R., and Breitenbucher, R., "Cement with Low Crack-Susceptibility," Advances in Cementious Materials, Ceramic Transactions, The American Ceramic Society 16, Proceedings of Conference 1990 in Gaithersburg, 1991, pp. 701-713.

Trost, H., "Auswirkungen des Superpositionsprinzips auf Kriech- und Relaxationsprobleme bei Beton und Spannbeton," (Effects of the Principle of Superposition on Creep and Relaxation Problems in Concrete and Prestressed Concrete), Beton- und Stahlbetonbau, Vol. 62, No. 10, Oct. 1967, pp. 230-238; No. 11, Nov. 1967, pp. 261-269.

Troxell,G.E., Raphael, J.M., and Davis, R.E., "Long-Time Creep and Shrinkage Tests of Plain and Reinforced Concrete," Proceedings of ASTM, Vol. 58, 1958, pp. 1101-1120.

Van Breugel, K., "Additional Remarks on the Risk of Cracking in Hardening Concrete," Proceedings of RILEM International Conference on Concrete at Early Ages, Paris, Vol. 2, 1982, pp. 103-108.

Verbeck, and Helmuth., "Structures and Physical Properties of Cement Paste," Chemistry of Cement Paste, The Fifth International Symposium, Tokyo, Part II, 1968, pp. 1-32.

Wafa, F.F., and Ashour, S.A., "Mechanical Properties of High-Strength Fiber Reinforced Concrete," ACI Materials Journal, Vol. 89, No. 5, Sept. - Oct. 1992, pp. 449-455.

Walker, S., Bloem, D.L., and Mullen, W.G., "Effects of Temperatures Changes on Concrete Influenced by Aggregates," ACI Journal, Vol. 48, 1952, pp. 661-679.

Wang, C., and Dilger, W.H., "Shrinkage Prediction for Practical Designs," Proceedings of the CSCE Structural Conference, Montreal, 1989.

Weigler., and Karl., "Junger Beton," Teil 1 + 11, Betonwerk + fertigteil-Technik, 1974, pp. 6-7.

Werner, G., "The Effect of Type of Capping Material on the Compressive Strength of Concrete Cylinders," Proceedings, ASTM, Vol. 58, 1958, pp. 1166-1186.

Whiting, D., Litvin, A., and Goodwin, S., "Specific Heats of Selected Concretes," ACI Journal, Vol. 75, No. 7, 1978, pp. 299-305.

Yuan, R.L., Ragab, M., Hill, R.E., and Cook, J.E., "Evaluation of Core Strength in High-Strength Concrete," Concrete International, May 1991, pp. 30-34.

Zia, P., Leming, M.L., and Ahmad, S.H., "High Performance Concretes," Strategic Highway Research Program, SHRP-C/FR-91-103, Jan. 1991, pp. F-65.

APPENDIX A

Compressive Strength and Elastic Modulus Test Results of Normal (30 MPa), Medium (70 MPa) and High-Strength (100 MPa) Concretes

Age (days)	$f_c'(t)$ (MPa)	$E_c(t)$ (GPa)
	S1	
0.36	2.40	4.29
0.37	3.30	6.72
0.59	11.92	16.47
0.71	13.48	19.29
0.84	13.98	19.20
1.02	16.50	19.80
1.26	19.42	21.22
2.16	21.30	23.04
3	22.20	23.78
7	23.34	24.04

Table A.1 - Compressive strength and elastic modulus test results for normal-strength concrete due to temperature-matched curing

Age (days)	$f_c'(t)$ (MPa)	$E_c(t)$ (GPa)
	S1	
0.33	9.62	11.22
0.38	14.80	21.02
0.7	37.60	27.73
0.72	44.80	29.69
0.83	54.60	34.52
1.12	69.10	37.15
3	74.80	40.20
3	70.00	39.07
3	72.40	39.64

Table A.2 - Compressive strength and elastic modulus test results for medium-strength concrete due to temperature-matched curing

Age (days)	$f_c'(t)$ (MPa)			$E_c(t)$ (GPa)		
	S1	S2	Mean	S1	S2	Mean
0.59	18.75	-	18.75	11.72	-	11.72
0.63	24.60	-	24.60	19.70	-	19.70
0.74	51.40	-	51.40	30.10	-	30.10
0.76	62.80	-	62.80	33.63	-	33.63
0.92	79.30	-	79.30	36.85	-	36.85
1.01	91.00	91.4	91.20	37.92	39.21	38.56
1.75	104.7	-	104.7	41.37	-	41.37
4	111.5	109.1	110.3	42.14	43.03	42.58
7	107.3	109.3	108.3	-	42.69	42.69

Table A.3 - Compressive strength and elastic modulus test results for high-strength concrete due to temperature-matched curing

Age (days)	$f_c'(t)$ (MPa)				$E_c(t)$ (GPa)			
	S1	S2	S3	Mean	S1	S2	S3	Mean
0.29	0.89	-	-	0.89	2.94	-	-	2.94
0.4	2.14	-	-	2.14	5.17	-	-	5.17
0.6	7.79	-	-	7.79	13.68	-	-	13.68
0.74	10.81	-	-	10.81	16.15	-	-	16.15
0.85	10.67	-	-	10.67	16.14	-	-	16.14
1	11.46	-	-	11.46	17.24	-	-	17.24
1.24	15.56	-	-	15.56	19.60	-	-	19.60
2.14	18.45	-	-	18.45	-	-	-	-
3	21.28	19.53	19.31	20.04	21.70	20.77	21.40	21.3
7	22.8	22.90	24.60	23.43	23.35	22.13	24.13	23.21
14	23.8	26.30	26.00	25.40	23.35	25.02	24.71	24.36
21	25.6	27.80	24.70	26.03	24.42	25.62	24.82	24.95
28	28.2	28.00	27.70	27.97	26.17	26.24	25.67	26.02
91	33.58	33.36	34.40	33.70	26.14	27.90	-	27.02

Table A.4 - Compressive strength and elastic modulus test results for normal-strength concrete due to sealed curing

Age (days)	$f_c'(t)$ (MPa)				$E_c(t)$ (GPa)			
	S1	S2	S3	Mean	S1	S2	S3	Mean
0.29	0.53	-	-	0.53	1.65	-	-	1.65
0.40	1.75	-	-	1.75	5.00	-	-	5.00
0.44	2.73	-	-	2.73	6.69	-	-	6.69
0.52	3.86	-	-	3.86	9.86	-	-	9.86
0.64	6.18	-	-	6.18	11.93	-	-	11.93
0.83	8.65	-	-	8.65	13.30	-	-	13.30
0.92	10.40	-	-	10.40	14.84	-	-	14.84
1	10.54	-	-	10.54	15.05	-	-	15.05
2	17.70	14.82	-	16.26	19.55	16.85	-	18.20
3	16.80	17.10	16.30	16.74	18.25	19.18	17.31	18.25
7	18.60	19.30	19.06	18.90	19.27	18.64	19.65	19.19
14	21.80	21.90	-	21.80	20.45	20.02	-	20.23
21	21.70	21.50	22.10	21.80	20.26	19.57	20.95	20.26
29	21.70	22.7	22.10	22.20	19.55	20.18	20.07	19.93
91	23.69	24.17	23.48	23.78	18.87	20.62	18.92	19.47
365	26.60	23.78	25.47	25.30	-	-	-	-

Table A.5 - Compressive strength and elastic modulus test results for normal-strength concrete due to air-dried curing

Age (days)	$f_c'(t)$ (MPa)				$E_c(t)$ (GPa)			
	S1	S2	S3	Mean	S1	S2	S3	Mean
0.27	2.70	-	-	2.70	2.93	-	-	2.93
0.34	6.50	-	-	6.50	11.14	-	-	11.14
0.35	12.25	-	-	12.25	14.05	-	-	14.05
0.45	24.3	-	-	24.30	22.99	-	-	22.99
0.51	28.65	-	-	28.65	25.33	-	-	25.33
0.61	30.53	-	-	30.53	25.60	-	-	25.60
0.68	38.1	-	-	38.10	29.81	-	-	29.81
0.91	41.9	-	-	41.90	31.67	-	-	31.67
1.09	43.6	-	-	43.60	-	-	-	-
2	48.92	-	-	48.92	34.76	-	-	34.76
6	54.72	-	-	54.72	33.03	-	-	33.03
24	71.0	74.6	72.24	72.3	33.76	33.65	36.88	34.77
29	75.7	78.76	-	77.00	38.34	38.61	-	38.47
86	84.93	88.53	86.8	86.75	39.53	39.7	40.36	39.86

Table A.6 - Compressive strength and elastic modulus test results for medium-strength concrete due to sealed curing

Age (days)	$f_c'(t)$ (MPa)				$E_c(t)$ (GPa)			
	S1	S2	S3	Mean	S1	S2	S3	Mean
0.37	1.36	-	-	1.36	1.47	-	-	1.47
0.47	7.40	-	-	7.40	9.76	-	-	9.76
0.55	18.85	-	-	18.85	19.94	-	-	19.94
0.6	26.15	-	-	26.15	24.57	-	-	24.57
0.91	33.90	-	-	33.90	28.78	-	-	28.78
0.96	36.12	-	-	36.12	27.14	-	-	27.14
4	51.87	51.66	52.72	52.08	30.82	30.90	32.28	31.33
7	53.19	56.78	55.79	55.20	33.45	30.78	30.21	31.48
14	61.26	57.84	-	59.50	31.31	29.44	-	30.38
21	64.97	63.68	64.03	64.20	31.57	30.29	30.97	30.95
28	64.73	64.62	66.67	65.40	31.44	31.49	32.63	31.85
91	69.2	65.9	66.8	67.30	29.6	29.5	29.98	29.69

Table A.7 - Compressive strength and elastic modulus test results for medium-strength concrete due to air-dried curing

Age (days)	$f_c'(t)$ (MPa)				$E_c(t)$ (GPa)			
	S1	S2	S3	Mean	S1	S2	S3	Mean
0.64	1.46	-	-	1.46	-	-	-	-
0.69	5.07	-	-	5.07	3.53	-	-	3.53
0.78	13.6	-	-	13.60	-	-	-	-
0.80	20.6	-	-	20.60	19.56	-	-	19.56
0.88	29.4	-	-	29.40	22.38	-	-	22.38
1.03	37.4	-	-	37.40	25.92	-	-	25.92
3	71.06	69.22	69.02	69.77	34.05	34.59	33.27	33.97
7	80.1	76.23	79.3	78.54	36.30	34.74	34.97	35.34
14	90.62	91.67	-	91.14	37.35	38.46	-	37.91
21	90.74	95.4	98.2	94.78	39.59	37.3	39.87	38.92
28	98.16	100.8	98.69	99.23	38.46	38.51	37.69	38.22
76	99.43	101.5	-	100.5	39.51	41.21	-	40.36
91	103.92	99.95	-	101.9	40.03	42.27	-	41.15

Table A.8 - Compressive strength and elastic modulus test results for high-strength concrete due to sealed curing

Age (days)	$f_c'(t)$ (MPa)				$E_c(t)$ (GPa)			
	S1	S2	S3	Mean	S1	S2	S3	Mean
0.73	8.85	-	-	8.85	8.27	-	-	8.27
0.75	16.59	-	-	16.59	15.79	-	-	15.79
0.89	30.20	-	-	30.20	21.58	-	-	21.58
1.04	48.70	-	-	48.70	30.52	-	-	30.52
1.77	65.30	-	-	65.30	-	-	-	-
3	74.10	74.06	-	74.08	33.98	35.16	-	34.57
7	80.7	81.3	82.05	81.35	34.53	35.46	34.55	34.84
14	87.83	85.34	81.85	85	33.5	35.62	-	34.58
21	92.77	94.24	94.03	93.7	36.18	35	36.95	36.04
28	97.29	95.47	94.38	95.7	39.17	36.41	37.02	37.53
78	99.07	96.07	-	97.57	36.17	37.14	-	36.65
104	97.26	98.96	-	98.11	36.98	37.24	-	37.11

Table A.9 - Compressive strength and elastic modulus test results for high-strength concrete due to air-dried curing

Age (days)	$f_c'(t)$ (MPa)			
	S1	S2	S3	Mean
0.25	0.14	-	-	0.14
0.30	0.36	-	-	0.36
0.54	9.05	-	-	9.05
0.85	14.62	-	-	14.62
0.96	16.02	-	-	16.02
1.5	19.06	-	-	19.06
2	19.74	19.56	-	19.65
3	20.57	24.19	22.0	22.26

Table A.10 - Compressive strength test results for normal-strength concrete due to temperature-matched curing (batch 2)

Age (days)	$f_c'(t)$ (MPa)			
	S1	S2	S3	Mean
0.23	0.076	-	-	0.076
0.28	0.2	-	-	0.2
0.31	0.84	-	-	0.84
0.42	2.41	-	-	2.41
0.56	6.06	-	-	6.06
0.83	10.25	-	-	10.25
0.94	12.26	-	-	12.26
1.5	15.98	-	-	15.98
2.02	16.81	-	-	16.81
3	19.9	21.8	19.48	20.40
7	24.33	24.72	23.38	24.15
14	25.24	25.92	25.46	25.54
21	26.03	29.98	26.43	27.48
28	29.75	29.2	27.49	28.81
91	33.0	33.81	32.90	33.24

Table A.11 - Compressive strength test results for normal-strength concrete due to sealed curing (batch 2)

Age (days)	$f_c'(t)$ (MPa)				$E_c(t)$ (GPa)			
	S1	S2	S3	Mean	S1	S2	S3	Mean
0.812	14.59	-	-	14.59	14.07	-	-	14.07
0.934	27.9	-	-	27.9	24.66	-	-	24.66
0.976	33.18	-	-	33.18	25.04	-	-	25.04
1	34.25	-	-	34.25	27.09	-	-	27.09
1.79	60.94	64.75	-	62.84	33.30	32.68	-	32.99
2	65.9	64.4	-	65.15	31.90	33.22	-	32.56
3	70.22	71.08	72.19	71.16	31.78	33.79	33.32	32.96
7	81.68	80.75	80.84	81.09	34.50	35.07	34.82	34.79
15	90.37	90.65	89.61	90.21	35.06	35.33	-	35.19
21	93.37	94.51	95.08	94.32	36.86	36.97	36.56	36.79
28	98.03	94.91	97.08	96.67	35.86	36.94	-	36.40

Table A.12 - Compressive strength and elastic modulus test results for high-strength concrete due to air-dried curing (batch 2)

APPENDIX B

Flexural Strength Test Results of Normal (30 MPa), Medium (70 MPa) and High-Strength (100 MPa) Concretes

Age (days)	f_t (t), MPa Temperature-matched curing
	S1
0.75	1.47
0.81	1.87
0.88	2.03
0.96	2.61
1.08	2.53
2	3.38
3	4.07
6	4.70
7	4.75
14	4.48

Age (days)	f_t (t), MPa Sealed curing		
	S1	S2	Mean
0.38	0.91	-	0.91
0.46	1.50	-	1.50
0.54	1.89	-	1.89
0.71	2.70	-	2.70
0.79	3.11	-	3.11
1.04	3.31	-	3.31
1.89	3.81	-	3.81
1.89	3.50	-	3.5
3	3.44	3.61	3.52
7	4.21	3.65	3.93
14	4.12	4.05	4.08
29	4.28	4.22	4.25
91	4.83	4.62	4.73

Age (days)	f_t (t), MPa Air-dried curing			
	S1	S2	S3	Mean
0.36	0.39	-	-	0.39
0.40	0.66	-	-	0.66
0.54	1.46	-	-	1.46
0.61	1.79	-	-	1.79
0.67	2.19	-	-	2.19
0.88	2.82	-	-	2.82
1	2.96	-	-	2.96
2	3.10	3.17	-	3.13
3	3.34	3.46	-	3.40
7	3.55	3.48	-	3.51
16	3.77	4.14	-	3.95
38	4.28	3.73	-	4 00
91	4.73	4.42	4.77	4.64

Table B.1 - Flexural strength test results for normal-strength concrete due to different curing conditions

Age (days)	f_t (t), MPa Temperature-matched curing			
	S1			
0.38	0.53			
0.44	1.01			
0.48	2.41			
0.52	2.67			
0.56	3.38			
0.61	3.21			
0.87	4.21			
0.98	4.97			
1.11	5.11			
2	5.89			

Age (days)	f_t (t), MPa Sealed curing			
	S1	S2	S3	Mean
0.29	0.084	-	-	0.084
0.39	0.55	-	-	0.55
0.43	0.97	-	-	0.97
0.46	1.42	-	-	1.42
0.51	2.07	-	-	2.07
0.54	2.29	-	-	2.29
0.58	2.7	-	-	2.70
0.92	4.16	-	-	4.16
1.19	4.43	-	-	4.43
7	5.19	4.66	-	4.90
14	5.24	4.91	-	5.07
21	5.13	5.29	-	5.21
28	5.7	5.54	5.93	5.72
91	6.43	-	-	6.43

Age (days)	f_t (t), MPa Air-dried curing			
	S1	S2	S3	Mean
0.44	1.04	-	-	1.04
0.50	1.78	-	-	1.78
0.55	2.44	-	-	2.44
0.60	2.94	-	-	2.94
0.62	3.26	-	-	3.26
0.84	3.74	-	-	3.74
0.91	3.89	-	-	3.89
1	4.00	-	-	4.00
2.07	4.09	-	-	4.09
3	4.2	-	-	4.20
7	4.05	4.69	4.43	4.39
15	4.92	4.73	-	4.82
28	5.94	5.87	-	5.90
91	6.02	6.14	6.42	6.39

Table B.2 - Flexural strength test results for medium-strength concrete due to different curing conditions

Age (days)	f_t (t), MPa Temperature-matched curing
	S1
0.67	2.58
0.73	3.75
0.80	5.56
0.94	7.35
1.03	8.08
1.77	9.83
2.02	10.6
3	11.8

Age (days)	f_t (t), MPa Sealed curing			
	S1	S2	S3	Mean
0.66	0.79	-	-	0.79
0.73	2.6	-	-	2.60
0.78	4.00	-	-	4.00
0.88	4.76	-	-	4.76
1.06	5.18	-	-	5.18
1.07	5.80	-	-	5.80
1.77	6.60	6.99	-	6.80
3	7.24	7.76	7.63	7.54
7	7.19	7.89	7.04	7.37
21	8.24	8.45	8.61	8.43

Age (days)	f_t (t), MPa Air-dried curing			
	S1	S2	S3	Mean
0.71	0.72	-	-	0.72
0.75	1.54	-	-	1.54
0.79	2.39	-	-	2.39
0.88	4.20	-	-	4.20
1	5.50	-	-	5.50
7	6.37	5.73	5.02	5.71
10	6.04	-	-	6.04
14	6.20	6.77	-	6.49
21	8.90	7.47	7.45	7.94
28	7.97	8.07	8.10	8.05
36	8.26	-	-	8.26
118	8.58	-	-	8.58

Table B.3 - Flexural strength test results for high-strength concrete due to different curing conditions